

# Higgs Phenomenology in Warped Extra Dimensions

Nima Pourtolami

A Thesis  
In the Department  
of  
Physics

Presented in Partial Fulfillment of the Requirements  
For the Degree of  
Doctor of Philosophy (Theoretical Particle Physics) at  
Concordia University  
Montreal, Quebec, Canada

March 2015

©Nima Pourtolami, 2015

**CONCORDIA UNIVERSITY  
SCHOOL OF GRADUATE STUDIES**

This is to certify that the thesis prepared

By: **Nima Pourtolami**

Entitled: **Higgs Phenomenology in Warped Extra Dimensions**

and submitted in partial fulfillment of the requirements for the degree of

**DOCTOR OF PHILOSOPHY (Theoretical Particle Physics)**

complies with the regulations of the University and meets the accepted standards with respect to originality and quality.

Signed by the final Examining Committee:

\_\_\_\_\_ Chair  
Judith Kornblatt

\_\_\_\_\_ External Examiner  
Hooman Davoudiasl

\_\_\_\_\_ External to Program  
Dmitry Korotkin

\_\_\_\_\_ Examiner  
Alexandre Champagne

\_\_\_\_\_ Examiner  
S. Twareque Ali

\_\_\_\_\_ Thesis Supervisor  
Mariana Frank

Approved by

\_\_\_\_\_  
Laszlo Kalman, Graduate Program Director

\_\_\_\_\_  
André Roy, Dean, Faculty of Arts & Science

# Abstract

**Higgs Phenomenology in Warped Extra Dimensions**

**Nima Pourtolami, Ph.D.**

**Concordia University, 2015**

This thesis is a study on phenomenology of beyond the Standard Model in the context of warped extra-dimensional (Randall-Sundrum) models. These models, through introducing a large extra space dimension along which the standard model fields can propagate, can address the hierarchy between the Plank and weak scales, provided that the geometry is suitably curved along the fifth dimension and the extra dimension is stabilized. The space-time background that is considered in this thesis is mainly in a more general form which is modified from the usual  $AdS_5$ . This modification can alleviate considerably the bounds coming from precision electroweak tests and flavor physics. Of course, the usual  $AdS_5$  geometry is a special case and can be reproduced by taking the correct limits.

In this thesis, we mainly consider the case where the extra dimension is bounded by two stabilized hard walls (branes) at the TeV (IR brane) and Plank (UV brane) scales. Also our principal consideration will be the case when all the standard model fields propagate in the bulk, although we comment on the case where only the Higgs is localized on the TeV brane.

Within this context, after a broad review of the main concepts, we first address the phenomenology of a bulk scalar Higgs boson, and calculate its production cross section at the LHC as well as its tree-level effects on mediating flavor changing neutral currents. We perform the calculations based on two different approaches. First, we compute our predictions analytically by considering all the degrees of freedom emerging from the dimensional reduc-

tion (the infinite tower of Kaluza-Klein modes (KK)). In the second approach, we perform our calculations numerically by considering only the effects caused by the first few KK modes, present in the 4-dimensional effective theory. In the case of a Higgs leaking far from the brane, both approaches give the same predictions as the effects of the heavier KK modes decouple. However, as the Higgs boson is pushed towards the TeV brane, the two approaches seem to be equivalent only when one includes heavier and heavier degrees of freedom (which do not seem to decouple). To reconcile these results it is necessary to introduce a type of higher derivative operator which essentially encodes the effects of integrating out the heavy KK modes and dresses the brane Higgs so that it looks just like a bulk Higgs.

Secondly we calculate the production rate of the Higgs boson at the LHC in the context of general 5D warped scenarios, and show that it is generically consistent with the current experimental results from the LHC for Kaluza-Klein (KK) masses as low as 2 TeV, unlike in pure  $AdS_5$  scenarios, where for the same masses, the Higgs production typically receives corrections too large to be consistent with LHC data. Thus the new pressure on warped models arising from LHC Higgs data is also alleviated in modified  $AdS_5$  warped scenarios.

And finally we show that in these backgrounds, high energy flavor symmetries are inherent. When these high energy symmetries are broken at lower energies, they produce the Standard Model (SM) structure including the neutrinos. This feature is completely general and depends neither on the details of the background metric, as long as it produces the required hierarchy, nor on the exact form of the symmetry, as long as it produces the required PMNS matrix. The reason for this phenomena is inherent in the structure of the exponential hierarchy factors of warped extra-dimension scenarios with bulk matter fields. While these factors produce the hierarchy of masses in quarks and charged lepton sectors, they flatten in to a plateau at larger  $c$ -parameters to accommodate the neutrinos. In the case of the quark and charged lepton sectors, these exponential hierarchy factors “wash off” the structure of the order one five dimensional Yukawa couplings, and naturally produce the hierarchical masses and the CKM matrix, while for the neutrinos sector, while for the neutrinos, the structure of the high energy symmetries are preserved to attain the SM.

# Acknowledgements

This is a good opportunity for me to express my gratitude to the people who had a great influence to make this work possible.

I would like to thank my supervisor Prof. Mariana Frank not only for her supervision and guidance throughout this research but also for all her supports, insights, encouragements, and above all, the research environment that she created since the beginning of my program at the Concordia University. Her support, care and knowledge made this work possible.

I would like to thank Dr. Manuel Toharia - whose role in this thesis resembles more that of a supervisor - for his valuable suggestions and contributions to both this work and my understanding of phenomenology without which this work would not have been possible.

I would like to express my gratefulness to my supervisor at the University of Oklahoma, Prof. Kimball A. Milton for all his support, patience and supervision. His unique method of teaching research to graduate students, had a key role in my understanding of theoretical high energy physics, divergences and the analytical side of the nature.

I would like to thank Prof. Howard Baer, Prof. Ron Kantowski and Prof. Mohammad Meherafarin, who all had a decisive influence on my understanding of physics and collaborators Prof. Cherif Hamzoui, Dr. E. K. Abalo, Dr. Prachi Parashar and Dr. Jef Wagner.

Above all, I would like to thank my parents and my sister for all their support and love.

# Contribution of the Author

The original research work contained in this thesis is presented in Chapters 3, 4 and 5. The research in Chapters 3 and 4 has been conducted in collaboration with Prof. Mariana Frank and Dr. Manuel Toharia and has been published in [1, 2]. Chapter 5 is prepared in collaboration with Dr. Mariana Frank, Dr. Cherif Hamzaoui and Dr. Manuel Toharia and has been published in [3] and the work on Modified  $AdS_5$  presented in this chapter is going to be published soon [4].

In Chapters 3 and 4, the analytical and computational calculations which lead to the final results of the research as well as the production of the graphs was conducted by the author as a partial the fulfillment of the requirements for the degree of doctor of philosophy in the Concordia Physics Department, Montreal, Quebec.

In Chapter 5, the computational calculations and partial analytical calculations which lead to the final results of the research as well as the production of the graphs was conducted by the author as a partial the fulfillment of the requirements for the degree of doctor of philosophy in the Concordia Physics Department, Montreal, Quebec.

# Contents

<b>List of Figures</b>	<b>viii</b>
<b>List of Tables</b>	<b>ix</b>
<b>1 Introduction</b>	<b>1</b>
<b>2 The Standard Model of Particle Physics</b>	<b>13</b>
2.1 A Brief Overview of SM . . . . .	13
2.2 The Flavor Structure of the SM . . . . .	18
2.3 Higgs Physics . . . . .	21
2.4 Standard Model as an Effective Field Theory . . . . .	24
2.5 Naturalness of the SM . . . . .	26
2.6 Warped Extra Dimensional Models . . . . .	28
<b>3 Higgs Phenomenology From Bulk to Brane</b>	<b>31</b>
3.1 Introduction . . . . .	31
3.2 Warped Extra Dimensions with Higgs in the Bulk . . . . .	33
3.3 Higgs phenomenology: all KK fermions . . . . .	36
3.3.1 Higgs Flavor violating couplings . . . . .	37
3.3.2 Higgs production . . . . .	39
3.4 Higgs phenomenology: individual KK modes . . . . .	43
3.4.1 Higgs Flavor violating couplings . . . . .	44
3.4.2 Higgs production . . . . .	45
3.5 The Effect of Higher Derivative Operators . . . . .	46
3.6 Misalignment between Higgs VEV and Higgs profile . . . . .	49
3.7 Discussion and Outlook . . . . .	51
<b>4 Higgs Phenomenology In Modified <math>AdS_5</math> Geometries</b>	<b>55</b>

4.1	Introduction . . . . .	55
4.2	Soft-wall inspired models . . . . .	57
4.3	Higgs Production through gluon fusion . . . . .	61
4.4	Decoupling of the Heavy KK modes . . . . .	67
4.5	Conclusions . . . . .	68
<b>5</b>	<b>Warped Flavor Symmetry</b>	<b>71</b>
5.1	Introduction . . . . .	71
5.2	Fermion masses in warped space . . . . .	74
5.3	Flavor democracy . . . . .	85
5.4	Conclusion . . . . .	90
<b>6</b>	<b>Conclusions and Outlook</b>	<b>92</b>
<b>A</b>	<b>Analytical Results for Bulk Higgs Gluon Fusion</b>	<b>110</b>
<b>B</b>	<b>Bulk to Brane Limit</b>	<b>112</b>
<b>C</b>	<b>Infinite Sums in Modified <math>AdS_5</math></b>	<b>114</b>
<b>D</b>	<b>Explicit Expressions for the Field Profiles</b>	<b>116</b>
	<b>Additional Works</b>	<b>119</b>

# List of Figures

1.1	Basic QED process. . . . .	9
2.1	The running coupling constants of the SM . . . . .	16
2.2	Integrating out the heavy fields . . . . .	25
3.1	The shift in the top quark Yukawa coupling as a function of the bulk Higgs localization parameter $\beta$ . . . . .	39
3.2	Loop diagram showing the contribution of the quark $Q_i$ to the Higgs-gluon-gluon coupling . . . . .	40
3.3	KK contribution to $c_{hgg}/c_{hgg}^{SM}$ as a function of the bulk Higgs localization parameter $\beta$ . . . . .	44
3.4	Contribution to the coupling $ c_{hgg} $ (relative to the Standard Model) as a function of the Higgs localization parameter $\beta$ . . . . .	47
3.5	Shift of the top quark Yukawa coupling and contribution to $c_{hgg}$ , relative to the Standard Model . . . . .	48
4.1	Loop diagram showing the contribution of the quark $Q_i$ to the Higgs-gluon-gluon coupling. . . . .	61
4.2	Higgs production rate ratio in modified $AdS_5$ compared to the Standard Model	64
4.3	Quark Yukawa couplings relative to their SM values . . . . .	66
4.4	Higgs production rate via gluon fusion in the CGQ scenario . . . . .	69
5.1	The modified- $AdS_5$ warp factor $A(y)$ versus the standard RS warp exponent, $y$	75
5.2	The $\delta = 1$ plots and the neutrino masses in the $\nu - a$ plane . . . . .	78
5.3	Effective 4D Yukawa couplings for fermions . . . . .	80
5.4	The neutrino masses versus the $\nu$ parameter. . . . .	82
5.5	Scan plot of $V_{e3}$ versus $V_{\mu 3}$ . . . . .	87

# List of Tables

- 2.1 List of SM spin  $\frac{1}{2}$  particles and their quantum numbers . . . . . 15
- 2.2 The Higgs quantum numbers in the SM . . . . . 17
  
- 5.1 A point in the 0-th order 5D fermion  $c$ -parameter space for  $\mu$ - $\tau$  symmetry  
symmetry . . . . . 90

# Chapter 1

## Introduction

The Standard Model of Particle Physics, SM for short, is arguably the most successful theory that mankind has ever come up with. It successfully describes three of the four fundamental forces of nature, namely the electromagnetic, weak and strong forces down to unprecedented scales of  $\sim 10^{-18} m$  or, equivalently, up to energies of  $\sim 1 \text{ TeV}$ <sup>1</sup>. This scale is called the weak scale as it is related to the strength of the weak force. The model is very predicting. For example, the amount of deviation of the anomalous magnetic moment of the electron,  $g$ , from the "Dirac magnetic moment of the electron", due to the quantum corrections defined as

$$a = \frac{g - 2}{2},$$

is experimentally given by

$$a = 0.00115965218073(28).$$

This is to be compared with the SM predicted value

$$a = 0.00115965217760(520),$$

which is accurate up to more than 10 decimal places. We should mention that not all the observables are measured or calculated with this level of precision, but this just reveals how precise the SM can be. Another interesting fact about the SM is that, it can be extrapolated up to exponentially higher energies. At some energy scale, the fourth force of nature, gravity,

---

<sup>1</sup>On the other limit, we have Einstein's general relativity which seems to hold up to scales of  $\sim 10^{19} m$  which is about the thickness of the Milky Way. However, if one considers the standard model of cosmology, which includes cold dark matter, CDM, and dark energy,  $\Lambda$ , (therefore, the  $\Lambda$ CDM model for short) then this extends to about the known boundary of the universe,  $\sim 10^{27} m$ .

becomes important and it can not be neglected anymore. The scale at which gravity becomes important is called the Planck scale,  $M_{Pl}$ , which is about  $\sim 10^{18}$  TeV <sup>2</sup>.

The SM is built upon a mathematical framework called Quantum Field Theory (QFT). QFT emerges from the reconciliation of Quantum Mechanics (QM), which describes the physics of small particles, and Einstein's Special Relativity (SR), which provides the correct description of particles at high speeds (*i.e.*, close to the speed of light,  $c$ ). It turns out that each of these theories impose certain constraints on the structure of the theory. As we will try to show in this Introduction, these constraints are much more restraining than what one would naively expect. As a consequence, the structure of QFT is a necessary consequence of these constraints. For example it can be proven that the only way to reconcile QM with SR is to promote physical states into "quantized fields" *cf.* below, and the only way to save causality is to introduce the notion of antiparticles and so on. The fact that this combination matches our experimental results is truly fascinating.

It is worthwhile to mention that the SM within its range of validity is a unique theory, meaning that it has no competition within this range. Furthermore, as we will see here and in Chapter 2, it is a very simple theory when one considers the plethora of experiments that it successfully explains. In the SM, every observable is built out of "elementary particles". This is a good point to give a bit more precise definition of an elementary particle, which is a fundamental concept in high energy physics. An elementary particle is assumed to be point like all the way up to the Planck scale and is the smallest building block of a mathematical structure (called the Hilbert space,  $\mathcal{H}$ , *cf.* below), which falls into an irreducible and unitary representation of the space-time symmetries (the Poincaré group, *cf.* below). We will see that, they are for example labeled by their momentum squared (mass),  $p^\mu p_\mu$ , spin,  $J$ , and a set of other discrete intrinsic quantum numbers depending on the properties of the particle. These labels encode the symmetries of the fields as well the symmetries of the space-time that these fields belong to. Physical states containing a combination of these elementary particles, and the addition of the symmetries of the problem and the strength of their mutual interactions at a given energy scale, accommodate for all the existing particles in nature. As the energy scale and hence the symmetries<sup>3</sup> change, the degrees of freedom of the problem change as well and hence these elementary particles might not be a good set of degrees of freedom for a certain problem. In the following we give a very crude definition to the Hilbert

---

<sup>2</sup>This is what is known as the *reduced Planck mass*,  $\sqrt{\frac{\hbar c}{8\pi G}}$ .

<sup>3</sup>In low energy physics, these symmetries are almost always determined by the effective potential functions of the problem.

space as well as an extremely brief review of the main concepts in QM and SR in order to better explain these concepts.

Let's start with a basic definition of the Hilbert space: The Hilbert space is a complex vector space with an inner product,  $\langle \Phi | \Psi \rangle: \mathcal{H} \times \mathcal{H} \rightarrow \mathbb{C}$ , such that the norm,  $\langle \Psi | \Psi \rangle$ , turns  $\mathcal{H}$  into a metric space in which every Cauchy sequence is convergent. Any general physical state in this space is represented by a state<sup>4</sup>,  $|\Psi\rangle$ , which is a normalized vector, *i.e.*,  $\langle \Psi | \Psi \rangle = 1$ .

Now that we have defined the Hilbert space, we can state a very rough version of the principles of QM [5, 6]:

1. All physical states are represented by states,  $|\Psi\rangle$  in  $\mathcal{H}$ .
2. For a physical system in the state  $|\Psi\rangle$ , which can be decomposed into an orthogonal basis as in  $|\Psi\rangle = \sum_n a_n |\psi_n\rangle$ , the result of an experimental measurement is given by the probability of finding it in a certain state  $\psi_n$  which is given by

$$|\langle \Psi | \psi_n \rangle|^2.$$

3. Physical observables are given by a map of the Hilbert space onto itself

$$|\Psi\rangle \rightarrow \mathcal{O}|\Psi\rangle,$$

where the operators  $\mathcal{O}$  are linear and Hermitian<sup>5</sup>, meaning that  $\mathcal{O} = \mathcal{O}^\dagger$ , as physical observables must be real in the sense that the eigenvalues,  $\lambda$ , of the equation

$$\mathcal{O}|\Psi\rangle = \lambda|\Psi\rangle$$

must be real. The adjoint operator,  $\mathcal{O}^\dagger$  is defined via  $\langle \mathcal{O}^\dagger \Phi | \Psi \rangle = \langle \Phi | \mathcal{O} \Psi \rangle$ .

A key concept in theoretical physics is the notion of symmetries. Intuitively, one expects that if a physical theory is to be useful, it must be that two different observers measuring the same physical event come up with the same results. In terms of the second postulate of QM mentioned above, one needs to ensure that measurements of observers  $O$  and  $O'$ , given by  $|\langle \Psi | \psi_n \rangle|^2$  and  $|\langle \Psi' | \psi'_n \rangle|^2$  respectively, which are performed within two different systems of coordinates  $S$  and  $S'$ , must agree

$$|\langle \Psi | \psi_n \rangle|^2 = |\langle \Psi' | \psi'_n \rangle|^2.$$

---

<sup>4</sup>Strictly speaking, this is a "ray",  $\mathcal{R}$ , and not a state. States and rays are equal up to a phase.

<sup>5</sup>This condition might be too restrictive as it has been suggested that being only symmetric under parity and time, P-T symmetry, which is less restrictive than Hermiticity, can be enough [7, 8, 9, 10, 11, 12, 13]. Generalization to QFT has not been yet as successful [14, 15].

This very simple but logical constraint, when combined with the space-time symmetries imposed by SR, is indeed very constraining and determines most of the structure of QFT. First one notes that the operators that transform one state into another, which must preserve the outcomes (symmetry transformations)<sup>6</sup>, must be unitary,  $U^\dagger = U^{-1}$ , (such that  $\langle U\Psi|U\Phi\rangle = \langle\Psi|U^\dagger U\Phi\rangle = \langle\Psi|\Phi\rangle$ ) and linear, (*i.e.*,  $U|\eta\Psi + \xi\Phi\rangle = \eta U|\Psi\rangle + \xi U|\Phi\rangle$ )<sup>7</sup> [16].

Now we give a brief review of the concepts needed from SR. It is important to distinguish between external symmetries and internal symmetries. We have already talked about the external symmetries that are imposed by the space-time and its geometry. It is a well experimentally established fact that the speed of light,  $c$ , can not be surpassed. This ties space and time together with a Minkowski metric<sup>8</sup>

$$\eta_{\mu\nu} = \text{diag}(-1, +1, +1, +1)$$

and imposes the so called Poincare transformations on coordinate transformation of vectors, which consist of Lorentz transformations,  $\Lambda$ , and translations,  $a^\mu$

$$x^\mu \rightarrow \Lambda^\mu_\nu x^\nu + a^\mu, \quad (1.1)$$

where the Greek indices  $\mu, \nu$  assume values 0, 1, 2, 3, for  $t, x, y$ , and  $z$  coordinates respectively, and,  $x^\mu$  are the components of the position vector  $\mathbf{x} = (x^0, x^1, x^2, x^3)$ . Throughout this thesis the Einstein summation rule is in place, meaning that whenever an index is repeated, once down and once up, as  $\nu$  in the Eq. 1.1, a summation over that index is assumed (*i.e.*, an inner product). The transformation matrices,  $\Lambda$ , are  $4 \times 4$  matrices consisting of angles of rotations and boosts which are transformation to systems which have some velocity,  $v$ , with respect to the original system. These matrices must have the property that they preserve the length of the vectors<sup>9</sup>. This, in addition to the two constraints,  $\text{Det}\Lambda = +1$  and  $\Lambda_0^0 \geq 1$ , imposes that they must belong to the proper, orthochronous Lorentz group,  $\text{SO}(1,3)$ . This is exactly in the same manner as the rotations of coordinates in 3 dimensions are described

---

<sup>6</sup>Note that in this example the symmetry we considered was the symmetry under the change of the system of coordinates. Nature does not care about the system of coordinates we choose, so any physical results must be independent of it.

<sup>7</sup>It is possible that the symmetry transformation be anti-unitary and anti-linear, but the use of this possibility is far less in physics.

<sup>8</sup>As far as the space-time is flat. Also note that in this chapter we have used the mostly + metric while in the following chapters we will use the mostly negative metric,  $\eta_{\mu\nu} = \text{diag}(+1, -1, -1, -1)$  to be consistent with our published papers.

<sup>9</sup>In the sense that  $\eta_{\mu\nu}\Lambda^\mu_\rho\Lambda^\nu_\sigma = \eta_{\rho\sigma}$ .

by  $3 \times 3$  rotation matrices  $R_{ij}$  and belong to  $\text{SO}(3)$ , where in contrast to the Greek indices, the italic indices run from 1 to 3.  $\text{SO}(1,3)$  has 6 generators, 3 rotations and 3 boosts.

Combining the two discussions on QM and SR, the Poincare external symmetry transformations on physical states must take the form

$$|\Psi\rangle \rightarrow U(\mathbf{\Lambda}, \mathbf{a})|\Psi\rangle \quad (1.2)$$

where  $U(\mathbf{\Lambda}, \mathbf{a})$  is the unitary representation of the Lorentz transformation,  $\mathbf{\Lambda}$ , and translation,  $\mathbf{a}$ . In the following we will use this transformation law for the one-particle states as well as for the many particle states in order to be able to systematically categorize them.

It is important to note that all symmetries lead to conservation laws. This can be formally proven, but for our purposes it suffices to justify it intuitively, by remembering the fact that the symmetry transformations are concocted in a way that certain symmetries are manifest and conserved, (*e.g.*, The length of our four vectors under space-time translations). For example the symmetry under coordinate translations (rotations), lead to the conservation of energy and momentum (angular momentum). Conservation laws in physics are a direct consequence of the symmetries.

In order to define elementary particles we want to find one-particle states for which as many symmetries as possible are manifest. Wigner [16] in 1931, classified one-particle states. These states are defined as states with definite energy momentum vector,  $P^\mu$  with  $P^0 = E$ , energy, and  $P^i = p^i$ , momentum as

$$P^\mu |\Psi_{p,\sigma}\rangle = p^\mu |\Psi_{p,\sigma}\rangle, \quad (1.3)$$

where the  $p^\mu$  are the eigenvalues, the label  $p$ , emphasizes that the state has a definite momentum, and the particle label  $\sigma$  corresponds to all other *discrete* degrees of freedom of the state. For elementary particles all of these labels are discrete. This is not true for several particles, as in that case some of the  $\sigma$ s as well as  $p$  must be continuous. As mentioned before, elementary particles are states with definite momentum  $p$ , (*i.e.*, an eigenstate of the momentum operator as in Eq. 1.3) for which all labels, except for  $p$ , must be discrete. It was first shown by Wigner that group theoretical constraints on the transformation of one particle states with definite momentum fall under the transformations of the so called "little group"<sup>10</sup> of  $p$  under Lorentz symmetries. By this we mean that a Lorentz transformation of

---

<sup>10</sup>It is possible to show that the set of all transformations that leave the momentum of the state invariant form a group which is indeed a subgroup of the Lorentz group. This group is called the little group.

these states (*cf.* 1.2) is of the following form

$$U(\Lambda)|p, \sigma\rangle \propto \mathcal{D}_{\sigma\sigma'}(W)|\Lambda p, \sigma'\rangle, \quad (1.4)$$

where summation over the repeated group label  $\sigma'$  is assumed and  $\mathcal{D}_{\sigma\sigma'}(W)$  furnishes the little group representation. We have also used the common short hand,  $|\Psi_{p,\sigma}\rangle = |p, \sigma\rangle$ . These states must then be normalized, which fixes the proportionality constant. These are classifications of the one particle states, the most important of which (*i.e.*, the ones that occur in nature) are massive particles with  $P^2 = m^2 > 0$  with little group  $\text{SO}(3)$ , the ordinary group of rotations in three dimensions, and massless particles with  $P^2 = 0$  that transform under  $\text{ISO}(2)$ , which is the group of rotations and translations in two dimensions. This leads to the observed phenomena that massive particles transform under spin representations, while massless particles under helicity or polarization representations. An example is the easiest way that can clarify the previous statement; a massive spin 1 particle has 3 degrees of freedom:  $s = -1, 0, 1$  but a massless spin 1 (of helicity 1) particle has only 2 degrees of freedom:  $h = -1, 1$ . At this place it is worthwhile to mention that this simple consequence of symmetries is the main reason behind the existence of gauge theories on which QFT and the SM are built upon. As we shall see in Chapter 2, in these theories, this discontinuous difference between massive and massless degrees of freedom, will force us to introduce an extra symmetry called the gauge symmetry, to remove (or gauge away) an extra degree of freedom to be able to describe the physics of massless particles<sup>11</sup>.

There are also symmetries under the non-connected part of the Lorentz group. The statement of a theory being described by Hermitian operators is equivalent to the statement of invariance under  $CPT$ , *i.e.*, parity,  $P$ , time reversal,  $T$ , and charge conjugation,  $C$ . Up until now, we have both experimental and theoretical reasons to believe that  $CPT$  is conserved. But how about  $CP$  (or  $T$ ) individually? Out of the three forces which are described by the SM, the electromagnetic force preserves  $CP$  and the weak force violates it. Theoretically, there is no reason why the strong force should not violate  $CP$ , but experimentally this violation has not been observed. This is one of the few remaining puzzles of modern physics which we will list at the end of this introduction.

In addition to the external space-time symmetries mentioned above, the physical fields that are defined on top of this manifold also might exhibit certain symmetries. These symmetries

---

<sup>11</sup>For example, if one enforces the transformation property,  $A_\mu(x) \rightarrow A'_\mu(x) + \frac{1}{g}D_\mu\theta(x)$  with the gauge covariant derivative  $D_\mu = \partial_\mu - ig\tau.A_\mu$ , then, under the local symmetry transformation  $\psi(x) \rightarrow \psi'(x) = e^{-i\tau.\theta(x)}\psi(x)$ , the Lagrangian  $\mathcal{L} = \bar{\psi}i\gamma^\mu D_\mu\psi - m\bar{\psi}\psi$  is invariant.

are called internal symmetries and are special features of the specific field that one considers. These are in general called the "charge(s)" of the field. A famous example would be the conservation of the electric charge in electromagnetic interactions<sup>12</sup>.

Now that we have given a basic definition of the elementary particles, lets see how the multi particle states are formed and what constraints are introduced when we consider them. These states are a superposition of the one particle states. Under Lorentz transformations these multi-particle states transform as (*cf.* Eq. 1.4)

$$U(\Lambda)|p_1, \sigma_1, p_2, \sigma_2, \dots, p_N, \sigma_N\rangle = \sum_{\sigma'_1, \sigma'_2, \dots} |\Lambda p_1, \sigma'_1, \Lambda p_2, \sigma'_2, \dots, \Lambda p_N, \sigma'_N\rangle \times \mathcal{D}_{\sigma_1 \sigma'_1}(W_1) \mathcal{D}_{\sigma_2 \sigma'_2}(W_2) \dots \mathcal{D}_{\sigma_N \sigma'_N}(W_N). \quad (1.5)$$

If we further consider two states with the same particle content but with two particles permuted, as in the following

$$|p_1, \sigma_1, p_2, \sigma_2, \dots, p_N, \sigma_N\rangle \propto |p_2, \sigma_2, p_1, \sigma_1, \dots, p_N, \sigma_N\rangle, \quad (1.6)$$

we can see that as these states describe the same particle content. Also because if we interchange twice we should get back to the original state, the two sides of the Eq. 1.6 should be at most related by a phase,  $e^{i\phi}$ , with  $\phi$  scalar and dimensionless. As long as one considers only elementary particle interchanges, and not a combination of them, one can show that this phase can only be  $\pm 1$  and nothing else:

$$|p_1, \sigma_1, p_2, \sigma_2, \dots, p_N, \sigma_N\rangle = \pm |p_2, \sigma_2, p_1, \sigma_1, \dots, p_N, \sigma_N\rangle. \quad (1.7)$$

One can then introduce a particle creation operator,  $a_{p,\sigma}^\dagger$  which creates a particle acting on the vacuum,  $|0\rangle$ , and an annihilation operator,  $a_{p,\sigma}$ , which destroys it

$$|p, \sigma\rangle = a_{p,\sigma}^\dagger |0\rangle \quad |0\rangle = a_{p,\sigma} |p, \sigma\rangle.$$

With proper (Lorentz invariant) normalization, one can then summarize this paragraph into

$$[a_{p,\sigma}, a_{p',\sigma'}^\dagger]_{\pm} = (2\pi)^3 p^0 \delta^{(3)}(p - p') \delta_{\sigma,\sigma'}, \quad (1.8)$$

---

<sup>12</sup>These symmetries are more interrelated than presented here. For example, certain symmetries of a field are imposed due to its spin, which itself imposes the space-time transformations of the field. The electric charge is an example of such interconnection. It turns out that this conservation is a direct consequence of the photon being spin 1.

where the minus sign stands for commutator, and the plus sign for the anticommutator. All particles in the SM can be classified according to the property shown in Eq. 1.8. The particles which obey the commutator relation are called bosons, and the particles satisfying the anticommutator relation are called fermions. By considering the types of interactions and the spin of particles it turns out that all bosons are spin integer and fermions have half integer spin. Statistical behavior of bosonic and fermionic states are very different, which is a direct consequence of Eq. 1.7.

It is important to note that all of these came from the symmetries which were imposed by the general principles of QM and SR. As we mentioned before, QFT derives its structure from the fact that the combination of QM and SR is very restrictive. Now we are ready to summarize the particle content of the SM. In the SM, all the matter particles are the following fermions (all with spin 1/2)

1. 6 quarks in 3 generations (in total 36 after one considers 3 colors for each flavor as well as antiquarks)

$$u, d, c, s, t, b.$$

2. 6 leptons in 3 generations (in total 12, considering anti leptons)

$$e, \nu_e, \mu, \nu_\mu, \tau, \nu_\tau.$$

The force carriers in the SM are all bosons with spin 1 (called gauge vector bosons):

1. The photon,  $\gamma$ , that carries the force of electromagnetism.
2. The  $W^+$ ,  $W^-$  and the  $Z$  vector bosons, that are massive and carry the weak force.
3. The 8 gluons,  $g$ , which mediate the strong nuclear force.

There is also the Higgs boson,  $H$ , which has spin 0 and is responsible for the generation of mass for the elementary particles<sup>13</sup>.

The Higgs boson was discovered on July 4th 2012, at the Large Hadron Collider (LHC) [17, 18]. It was a very significant discovery as the Higgs boson was predicted by the SM<sup>14</sup>

---

<sup>13</sup>As explained in Chapter 2, to be slightly more precise, at high energies, the SM Higgs field is a complex doublet field with 4 degrees of freedom. At low energies, the  $W$  fields, which are massless at high energies and hence have only 2 degrees of freedom, acquire 3 of these degrees of freedom to become massive and the last degree of freedom constitutes for the Higgs particle, while also acquiring a vacuum expectation value which is responsible for the mass of all elementary particles in the SM.

<sup>14</sup>*cf.* Chapter 2.

but had been experimentally elusive for decades. Its discovery completed the SM picture of particle physics. Of course one needs to wait for the results of the next run of the LHC in the upcoming months to see whether there are deviations from the SM Higgs or not. We will discuss the properties of the Higgs boson in more depth in Chapter 2.

In addition to the particle content mentioned above, the SM also determines the interactions among these particles. The way the SM does that is again through the symmetries. The three fundamental forces of nature that are part of the SM, namely, electromagnetic, weak, and strong forces interact with matter particles (or among themselves except for the photon) that carry their corresponding charges. These charges stem from the symmetries that these fields preserve. The gauge symmetry group of the SM is  $SU(3) \times SU(2) \times U(1)$ , where the  $SU(3)$  is for the strong interactions and the  $SU(2) \times U(1)$  is for the weak and electromagnetic forces (collectively called the electroweak forces). Each interaction in the SM is visualized by a diagram called a Feynman diagram. All diagrams are made out of basic diagrams. For example the basic diagram for all quantum electrodynamic, QED, processes is shown in Fig. 1.1. It shows an interaction between a charged matter particle, either a quark or a lepton with a photon.

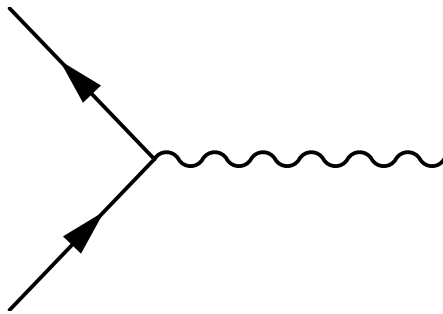


Figure 1.1: Basic QED process.

The SM interactions are as follows:

1. The quarks,  $q$ , interact with all the gauge vector bosons, (*i.e.*,  $\gamma$ ,  $W^+$ ,  $W^-$ ,  $Z$  and  $g_s$ ) and the Higgs.
2. The leptons,  $l$ , do not interact with the gluons. Other than that, they are similar to quarks.
3. The photon,  $\gamma$ , interacts with only  $W^\pm$ , charged leptons and quarks.
4. The  $Z$  interacts with the  $W^\pm$ ,  $l$ ,  $q$  and the  $H$ .

5. The  $W^\pm$  interact with the  $Z$ ,  $\gamma$ ,  $l$ ,  $q$ ,  $H$  and themselves.
6. The  $g$ 's interact with only the  $q$  and themselves.
7. The Higgs interacts with all massive particles. This means every particle (including itself) except the  $\gamma$  and the  $g$ 's.

The interaction of the quarks with the gauge weak bosons,  $W^+$ ,  $W^-$  and  $Z$ , is very interesting as it causes the quark fields to mix with each other. The amount of this mixing is encrypted in the Cabibbo-Kobayashi-Maskawa (CKM) matrix. The CKM matrix is a  $3 \times 3$  unitary matrix which encodes the degree of mixing between quarks of different generations and is measured to be very close to the identity matrix, which means that the mixing between the first generation quarks,  $u, d$ , with the second generation  $c, s$  is much stronger than with the third generation,  $t, b$ .

At the end of this section, we mention some of the issues and shortcomings of the SM (phenomena which we still do not understand). These problems can be categorized as the following:

- Hierarchies of the parameters within the SM
  - The cosmological constant problem: if our vacuum is to be effectively described by a field theory all the way up to the Planck scale, from simple dimensional analysis, one would expect that the energy density of the vacuum to be of order  $M_{Pl}^4 \sim (10^{19})^4 \text{ GeV}^4$ , which is drastically off from the observed value,  $10^{-47} \text{ GeV}^4$ . This is perhaps the most difficult and most drastic problem and as far as the author to this thesis knows, non of the beyond the SM theories, except for maybe anthropic principle arguments, address this issue.
  - The hierarchy between the electroweak scale (the Higgs,  $W$ ,  $Z$  masses) and the Planck scale: why is there about 16 orders of magnitude difference between these scales?
  - There is about 5 orders of magnitude hierarchy between the lightest (the electron) and heaviest (the top quark) Dirac fermions<sup>15</sup> in the SM, and 11 orders of magnitude if one considers Dirac neutrinos.
  - The hierarchy between the angles of the CKM matrix: there are several orders of magnitude differences between neighboring generations and far generations.

---

<sup>15</sup>Or in other words the hierarchy between the Yukawa couplings of the Higgs boson with these particles.

- The strong  $CP$  problem: why is doesn't the strong force violate  $CP$ ?
- Particles missing from the SM, which concern the incompleteness of the SM
  - There is no Dark Matter (DM) fields in the SM, although we know<sup>16</sup> that around 27% of the matter in the universe is made out of Dark Matter particles.
  - Neutrinos and their mixing angles, and also why are the neutrino mixing angles so different from the CKM mixing angles?
- Ontological problems
  - Why is the gauge group of the SM  $SU(3) \times SU(2) \times U(1)$ ? After all, this not the first group that comes to mind.
  - Where does the spectrum of particles and their quantum numbers come from?

The level of importance of these problems is to some extent a matter of taste and not all physicists agree on whether some of them are issues or not. But perhaps the most important of these it the Planck-weak hierarchy problem. The SM in its current formulation is highly sensitive to UV physics as any new physics at energies higher than the current experimental limits can bring about huge corrections to the SM. Therefore, from early on there have been may efforts to solve this problem. Technicolor, supersymmetry, and warped extra dimensions are all examples of these attempts. In this thesis our emphasis is on the warped extra dimensional models. In these scenarios one assumes the existence of an extra spacial dimension along which the geometry is warped down from the Planck scale down to the TeV relegating the hierarchy problem to a higher energy scale. This is in contrast to supersymmetrical extensions of the SM, which in general provide a UV stable theory. Nevertheless, these models provide a very interesting alternative to the solution of the hierarchy problem at energies accessible to the current experiments at the LHC.

The general structure of this thesis is as follows: In Chapter 2, we provide a brief and general overview of the SM and some related topics. The tone of this chapter is very pedagogic and is aimed at the general reader. The topics presented are merely touched upon with the aim of providing a background for the rest of the chapters. Each section covers a separate topic and is independent of the other sections. We also consider the hierarchy problem of the SM and the Randall-Sundrum (RS) solution to the hierarchy problem.

Chapters 3, 4 and 5 are reproduced from [1], [2], and [3, 4] respectively. In Chapter 3,

---

<sup>16</sup>This is of course, if we leave modified gravity theories aside.

within the RS scenario, we consider the phenomenology of the Higgs in the bulk<sup>17</sup> of the extra dimension. Specifically we compare the effect of the infinite tower of the particle states appearing in the extra dimension (Kaluza-Klein, or KK modes ) versus only the first several modes to the Higgs production rate and we show that, while the heavy KK fields tend to decouple at heavier and heavier scales as the Higgs is located more and more towards the IR brane<sup>18</sup>, one needs to include the contributions of an additional operator to get consistent results.

Chapter 4, after a brief introduction to modified warped geometries and their consequences, we calculate the bulk Higgs production rate in these models and we show that these models are specifically interesting for the current LHC physics as they can accommodate KK modes as light as  $\sim 1$  TeV, well within the range of the current experiments at the LHC, while still being safe from the dangerous inconsistencies of the pure RS models.

Finally in Chapter 5, we use these models to explain the flavor sector of the SM. Namely we address the differences between the mixing angles in the quark and the lepton sectors and show that these could be explained within the context of warped extra dimensions.

---

<sup>17</sup>By a "bulk field" we mean that the field can leak into the extra dimension. This is in contrary to a "brane field" which is a field is localized with a Dirac delta function on one of the boundaries.

<sup>18</sup>An  $n$ -brane is a generalization of a membrane with  $n$  spacial dimensions and 1 time dimension.

# Chapter 2

## The Standard Model of Particle Physics

As mentioned in the introduction, the Standard Model of Particle Physics (SM) is arguably the most successful theory of mankind. Combined with Einstein's gravity, it is valid with an astonishingly precision within huge scales from about  $\sim 10^{19}m$  down to the weak scale,  $\sim 10^{-18}m$  (*cf.* also the first footnote in Chapter 1). This section provides a brief overview of the main topics in SM.

### 2.1 A Brief Overview of SM

In the Introduction, we indicated that the SM is basically a list of particles, their quantum numbers and a certain number of parameters which describe the strength of their coupling and their interactions. The degrees of freedom of the SM (its particles content and their corresponding quantum numbers) change with the energy scale through phase transitions. This is the reason why the SM is valid for such large range of energies. Above the weak scale (roughly about 1 TeV), the whole SM picture is unified under the gauge group  $SU(3)_c \times SU(2)_W \times U(1)_Y$ . The gauge vector bosons which are the mediators of forces consist of spin 1 particle fields in the adjoint representation of these gauge groups. Therefore, there are  $N^2 - 1 = 8$  gauge bosons (*gluons*) that mediate the strong interactions and there are  $3 + 1$  bosons,  $B_\mu$ , for the electroweak interactions. In this first section, we introduce the SM field content in more detail, as well as the parameters of the SM. The general Lagrangian of the

SM is written as a sum over contributions from the following sectors

$$\mathcal{L}^{SM} = \mathcal{L}_{Gauge} + \mathcal{L}_{Matter} + \mathcal{L}_{Mass}. \quad (2.1)$$

The first term in the above equation contains the Yang-Mills kinetic terms for the gauge boson force carriers. It looks like the following

$$\mathcal{L}_{Gauge} = -\frac{1}{4}G_{\mu\nu}^a G^{\mu\nu a} - \frac{1}{4}W_{\mu\nu}^a W^{\mu\nu a} - \frac{1}{4}B_{\mu\nu} B^{\mu\nu}, \quad (2.2)$$

where we are assuming a flat Lorenz geometry and the Greek indices  $\mu$  and  $\nu$  are the Lorenz (space-time) indices that run over 0 to 3. The index  $a$  on the other hand, is the gauge group index<sup>1</sup>, and runs from 1 to 8 for the  $SU(3)_{color}$  group of the strong interactions, and from 1 to 3 for the  $SU(2)_W$  of the electroweak. The last term in the  $\mathcal{L}_{Gauge}$  corresponds to the gauge group  $U(1)$ . The field strengths,  $G_{\mu\nu}$ ,  $W_{\mu\nu}$  and  $B_{\mu\nu}$ , are gauge invariant and are defined in terms of commutations of gauge covariant derivatives

$$D_\mu = \partial_\mu + ig_{1,2,3}B_\mu \quad (2.3)$$

$$F_{\mu\nu} = i[D_\mu, D_\nu], \quad (2.4)$$

where for the non-Abelian gauge fields we have defined  $B_\mu(x) \equiv B_\mu^a(x)T^a$ . As an aside, one can easily check that under a local gauge transformation,  $U(\omega(x)) = e^{i\omega(x)T^a}$  with  $T^a$  the generators of the gauge group, if one requires that the gauge fields (or connections in geometrical sense) to transform as  $B_\mu \rightarrow UB_\mu U^\dagger - i\partial_\mu U U^\dagger$ , then the Lagrangian would be gauge invariant as required. Note that at these energies the electromagnetic and weak forces are unified, and the matter fields (spin  $\frac{1}{2}$  particles) are also massless. Using only left handed fields, the list of spin  $\frac{1}{2}$  particles in the SM with their respective quantum numbers is given in Table 2.1. From the table 2.1, one can easily deduce the kinetic terms of the SM fields which are contained in the matter section of the SM Lagrangian as

$$\mathcal{L}_{Matter} = L_i^\dagger \bar{\sigma}^\mu D_\mu L_i + \bar{e}_i^\dagger \bar{\sigma}^\mu D_\mu \bar{e}_i + Q_i^\dagger \bar{\sigma}^\mu D_\mu Q_i + \bar{u}_i^\dagger \bar{\sigma}^\mu D_\mu \bar{u}_i + \bar{d}_i^\dagger \bar{\sigma}^\mu D_\mu \bar{d}_i \quad (2.5)$$

where the index  $i$  runs over the 3 flavors and as suggested in table 2.1, we have used  $L_i$  and  $Q_i$  for the lepton and quark  $SU(2)_W$  doublets. Here, we are using the two component notation such that  $\sigma^\mu = (\sigma^0, \sigma^1, \sigma^2, \sigma^3)$ , and  $\bar{\sigma}^\mu = (\sigma^0, -\sigma^1, -\sigma^2, -\sigma^3)$ . The Dirac spinors can be written in term of these spinors as

$$\psi_D = \begin{pmatrix} \psi \\ \xi^\dagger \end{pmatrix}. \quad (2.6)$$

---

<sup>1</sup>Note that the gauge fields are in the adjoint representation of the connected part of the group, while as we will see later, the matter fields are in the fundamental representation.

		$SU(3)_C$	$SU(2)_W$	$U(1)_Y$
$L_i$	$\nu_e, \nu_\mu, \nu_\tau$	1	2	$-\frac{1}{2}$
	$e, \mu, \tau$			
$\bar{e}, \bar{\mu}, \bar{\tau}$		1	1	+1
$Q_i$	$u, c, t$	3	2	$+\frac{1}{6}$
	$d, s, b$			
$\bar{u}, \bar{c}, \bar{t}$		$\bar{3}$	1	$-\frac{2}{3}$
$\bar{d}, \bar{s}, \bar{b}$		$\bar{3}$	1	$+\frac{1}{3}$

Table 2.1: List of SM spin- $\frac{1}{2}$  particles and their quantum numbers.

One important point that is apparent from Table 2.1 is that matter fields interact with the gauge bosons according to their representation, and hence the covariant derivatives in Eq. 2.5 are different depending on which field they are acting on. For example for the left handed particles we have

$$D_\mu L_i = \left( \partial_\mu - \frac{ig_1}{2} B_\mu + \frac{ig_2}{2} W_\mu^a T^a \right) L_i \quad (2.7)$$

$$D_\mu Q_i = \left( \partial_\mu + \frac{ig_1}{6} B_\mu + \frac{ig_2}{2} W_\mu^a T^a + ig_3 G_\mu^a T^a \right) Q_i, \quad (2.8)$$

while the singlets of  $SU(2)$  (right handed fields) do not interact with the weak gauge bosons, and therefore for the singlets the middle terms in the right hand side of the above definitions of the covariant derivative are absent, for example

$$D_\mu e_R = \left( \partial_\mu - ig_1 B_\mu \right) e_R \quad (2.9)$$

$$D_\mu u_R = \left( \partial_\mu + \frac{2ig_1}{3} B_\mu + ig_3 G_\mu^a T^a \right) u_R. \quad (2.10)$$

In addition to these, the SM prescribes the coupling constants of each of these forces (*i.e.*, their strength). Despite their name, these couplings constants change (run) with energy. Fig. 2.1 shows the SM couplings and their dependence on energy, obtained using the following equations<sup>2</sup>

$$\frac{1}{\alpha_1}(\mu) \simeq 59 - \frac{41}{20\pi} \log\left[\frac{\mu}{M_Z}\right] \quad (2.11)$$

$$\frac{1}{\alpha_2}(\mu) \simeq 30 - \frac{19}{12\pi} \log\left[\frac{\mu}{M_Z}\right] \quad (2.12)$$

$$\frac{1}{\alpha_3}(\mu) \simeq 8.5 - \frac{7}{2\pi} \log\left[\frac{\mu}{M_Z}\right], \quad (2.13)$$

<sup>2</sup>These equations are quoted here only for the sake of completeness. They are called 1-loop renormalization group (RG) equations.

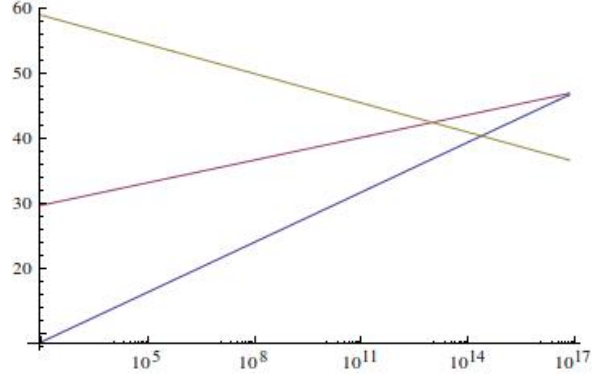


Figure 2.1: The running coupling constants of the SM. The horizontal axis is the energy in GeV, and the plots from top to bottom are  $\frac{1}{\alpha}$  (khaki) for the electromagnetic force,  $\frac{1}{\alpha_w}$  (red) for the weak force and  $\frac{1}{\alpha_s}$  (blue) for the strong force.

where the  $\alpha$ 's are defined as  $\alpha_i \equiv \frac{g_i^2}{4\pi}$ .

To these, one must also add parameters associated with the Yukawa matrix. The Yukawa terms in the SM enter through the last part in the Lagrangian given in Eq. 2.1, which itself consists of two parts:

$$\mathcal{L}_{Mass} = \mathcal{L}_{Yukawa} + \mathcal{L}_{Higgs}. \quad (2.14)$$

The Yukawa sector describes the interaction of the SM fermionic fields with the Higgs boson field

$$\mathcal{L}_{Yukawa} = Y_{ij}^e \bar{e}_j (L_i H^\dagger) + Y_{ij}^d \bar{d}_j (Q_j H^\dagger) + Y_{ij}^u \bar{u}_j (Q_i H) + c.c. \quad (2.15)$$

In addition, the Higgs sector of the SM Lagrangian which consists of the kinetic and the potential terms

$$\mathcal{L}_{Higgs} = (D_\mu H)^\dagger (D_\mu H) - V(H), \quad (2.16)$$

with  $V(H)$  being the Higgs potential. At this stage we have not yet included the neutrino mass terms, which depend on whether one considers Dirac neutrinos or Majorana ones. Ignoring the neutrinos, there are in total 13 physical parameters in the Yukawa matrices. At this stage the Yukawa couplings are in the so-called gauge basis and not in the mass basis, which is obtained when we diagonalize the Yukawa matrices and redefine the fermion fields. This is done after the electroweak phase transition which we discuss next. These physical parameters are the masses for the fermions,  $m_e, m_\mu, m_\tau, m_u, m_d, m_c, m_s, m_t, m_b$  (ignoring the

neutrino masses), 3 angles in the CKM matrix,  $\theta_{12}, \theta_{23}, \theta_{13}$  and one CP violating phase,  $\delta_{CP}$ .

We now turn to weak scale phase transition, namely the Higgs mechanism. This mechanism is responsible for separating the weak force and the electromagnetism by breaking the  $SU(2) \times U(1)$  part of the gauge group into a single  $U(1)$  symmetry, which corresponds to the charge conservation of the electromagnetic force. It also renders the fermions massive. From the Higgs Lagrangian, Eq. 2.16, if we further require that the SM be renormalizable, which is essential if want to extrapolate the model to exponentially higher energies, the most general potential for the Higgs field,  $V(H)$ , that one can write is given by

$$V(H) = -m^2 H^\dagger H + \lambda (H^\dagger H)^2. \quad (2.17)$$

For  $m^2 > 0$  this potential has the famous Mexican hat profile, and its minimum is given by

$$v = \left( \frac{m^2}{\lambda} \right)^{\frac{1}{2}}. \quad (2.18)$$

The SM Higgs itself is a complex scalar  $SU(2)_W$  doublet field with four degrees of freedom,

$$H = \begin{pmatrix} H^+ \\ H^0 \end{pmatrix}. \quad (2.19)$$

Its quantum numbers are given in Table (2.2), from which we can write down the Higgs interaction with other bosons

$$D_\mu H = (\partial_\mu - ig_1 W_\mu^a T^a - i \frac{g_2}{2} B_\mu) H. \quad (2.20)$$

At low energies one must minimize the Higgs potential,  $\frac{\partial V(H)}{\partial H} = 0$ , while the Higgs kinetic

		$SU(3)_C$	$SU(2)_W$	$U(1)_Y$
$H$	$H^+$	1	2	$+\frac{1}{2}$
	$H^0$			

Table 2.2: The Higgs quantum numbers in the SM.

term can be set to zero,  $D_\mu H \rightarrow 0$ , which is equivalent to having a constant Higgs field with

a vacuum expectation value (VEV). It is customary to break the  $SU(2)$  gauge invariance by letting the Higgs field VEV to acquire the following form

$$H_{vac} \equiv \langle H \rangle = \begin{pmatrix} 0 \\ v \end{pmatrix}, \quad (2.21)$$

but any global transformation on the above field would give the same physics. Furthermore, if we parametrize the excitations around the vacuum in the direction of the generators that break the symmetry by  $\xi(x)$ , and the perturbations around the VEV by  $h(x)$ , we have

$$H(x) = e^{i\xi^a(x)T^a} \begin{pmatrix} 0 \\ v + h(x) \end{pmatrix}. \quad (2.22)$$

It is the resonance of these perturbations around the VEV that is called the Higgs particle. Here is how the Higgs mechanism works: at low energies the Higgs field acquires the expectation value given in Eq. 2.21, *i.e.*, the Higgs potential through the phase transition process acquires a minimum different from zero. To reflect this insert the above Higgs field, Eq. 2.22 and Higgs covariant derivative, Eq. 2.20 into the Higgs Lagrangian, Eq. 2.16. This results in mass terms for the following field combinations, "the weak gauge bosons":

$$W_\mu^\pm = \frac{1}{\sqrt{2}}(W_\mu^1 \mp iW_\mu^2) \quad (2.23)$$

$$Z_\mu^0 = \cos(\theta_W)W_\mu^3 - \sin(\theta_W)B_\mu \quad (2.24)$$

while the following combination remains massless, "the electromagnetic photon":

$$A_\mu = \sin(\theta_W)W_\mu^3 + \cos(\theta_W)B_\mu, \quad (2.25)$$

where the Weinberg angle is defined as

$$\cos(\theta_W) \equiv \frac{g_2}{\sqrt{g_1^2 + g_2^2}} \quad (2.26)$$

With these conventions, we can introduce two more parameters of the SM, the Higgs VEV,  $v = 174$  GeV and the Higgs mass,  $m_H \simeq 125$  GeV. There is only one parameter left, namely the Quantum Chromodynamics (QCD) vacuum parameter,  $\theta_{QCD} \sim 0$  about which we will talk later.

## 2.2 The Flavor Structure of the SM

As mentioned in the previous section the fermion interactions arise from the Yukawa interactions given by the Lagrangian

$$\mathcal{L}_{Yukawa} = -Y_{ij}^e \bar{e}_j (L_i H^\dagger) - Y_{ij}^d \bar{d}_j (Q_i H^\dagger) + Y_{ij}^u \bar{u}_j (Q_i H) + h.c., \quad (2.27)$$

where by  $H$  is given in Eq. 2.19 while  $Q_i$ ,  $L_i$  and  $H^\dagger$  are

$$Q_i = \begin{pmatrix} u_i \\ d_i \end{pmatrix}, \quad L_i = \begin{pmatrix} \nu_i \\ e_i \end{pmatrix}, \quad H^\dagger = \begin{pmatrix} H^{0*} \\ -H^- \end{pmatrix}. \quad (2.28)$$

Expanding the  $SU(2)$  group indices one obtains

$$\mathcal{L}_{Yukawa} = Y_{ij}^e \bar{e}_j (\nu_i H^- + e_i H^{0*}) + Y_{ij}^d \bar{d}_j (u_i H^- + d_i H^{0*}) + Y_{ij}^u \bar{u}_j (u_i H^0 - d_i H^+) + h.c.. \quad (2.29)$$

After the  $SU(2) \times U(1)$  symmetry breaking, the Higgs acquires a VEV ( $v \simeq 174$  GeV) which generates the mass matrices

$$M^u = vY^u, \quad (2.30)$$

and similarly for  $M^d$  and  $M^e$ . While in the gauge basis the  $SU(2) \times U(1)$  symmetry of the Lagrangian was apparent, the physical masses of the fermions are acquired only after the electroweak symmetry breaking. The mass basis is given after a bi-unitary diagonalization of these matrices as the following

$$V_u(M^u)V_{\bar{u}}^\dagger = \begin{pmatrix} m_u & 0 & 0 \\ 0 & m_c & 0 \\ 0 & 0 & m_t \end{pmatrix}, \quad (2.31)$$

and similarly for the  $M^d$  and  $M^e$ . Here  $V_u$  and  $V_{\bar{u}}$  are different eigenvector matrices acting from the left and right of the mass matrix respectively. Therefore, in the mass basis one needs to redefine the fermion fields as

$$u \rightarrow V_u u, \quad \bar{u} \rightarrow V_{\bar{u}} \bar{u}. \quad (2.32)$$

This field redefinition in turn affects the gauge terms through the covariant derivatives in the kinetic terms (*cf.* Eq. 2.7 and 2.8). As a result of this rotation, while the neutral current interactions remain intact, the charged current will involve interactions the following matrix

$$V_{CKM} = V_u V_d^\dagger = \begin{pmatrix} V_{ud} & V_{us} & V_{ub} \\ V_{cd} & V_{cs} & V_{cb} \\ V_{td} & V_{ts} & V_{tb} \end{pmatrix}, \quad (2.33)$$

which is the Cabibbo-Kobayashi-Maskawa matrix [19, 20]. A standard parametrization of the CKM matrix is the Wolfenstein form [21, 22, 23, 24]

$$V_{CKM} = \begin{pmatrix} 1 - \lambda^2 & \lambda & A\lambda^3(\rho - i\eta) \\ -\lambda & 1 - \lambda^2 & A\lambda^2 \\ A\lambda^3(1 - \rho - i\eta) & -A\lambda^2 & 1 \end{pmatrix},$$

where  $\lambda$ ,  $A$ ,  $\rho$  and  $\eta$  are the Wolfenstein parameters. Not all of these parameters are independent. The unitarity of the CKM matrix imposes

$$\sum_i V_{ij}V_{ik}^* = \delta_{jk} \quad \text{and} \quad \sum_j V_{ij}V_{kj}^* = \delta_{ik}. \quad (2.34)$$

Let's take a look at how the symmetries were broken and how many free parameters are left. The original classical flavor symmetry of a Lagrangian with all the couplings and Yukawa couplings equal to zero in the quark sector was  $U(3)_u \times U(3)_d \times U(3)_{\bar{u}} \times U(3)_{\bar{d}}$ . First, turning on the Yukawa couplings  $Y_u$  and  $Y_d$  breaks this down to  $U(1)_u^3 \times U(1)_{\bar{d}}^3$  as manifest in the field redefinitions, Eq. 2.32, where we changed the basis from the gauge basis to the mass basis. Adding the weak coupling,  $g_2$  means that the left handed quarks cannot rotate separately, so from these six symmetries, one remains unbroken,  $U(1)_B$  which corresponds to the rotation of all quarks by the same amount. This is the baryon number conservation symmetry. The CKM matrix is unitary so it has nine parameters: six phases and three real numbers. Using the five broken  $U(1)$ 's we can remove five of these phases and therefore we are finally left with one phase, three mixing angles and six invariant masses.

Note that until now the neutrinos are massless, as there are no neutrino singlet interaction terms in the Lagrangian. There are several ways for the neutrinos to acquire mass, and while the simplest way is to assume that they are Majorana fermions and the mass is given through a dimension five operator, in this thesis we assume that the neutrinos are Dirac particles, and hence there is an additional term in the Lagrangian, Eq. 2.27, coupling the singlet right-handed neutrino to the left-handed lepton doublet

$$\mathcal{L}_{Yukawa} \supset Y_{ij}^\nu \bar{\nu}_j (L_i H). \quad (2.35)$$

Following the exact same procedure as for the CKM matrix one arrives at the Pontecorvo-Maki-Nakagawa-Sakata (PMNS) matrix

$$V_{PMNS} = V_\nu V_e^\dagger, \quad (2.36)$$

which is usually written in the following form

$$U = \begin{pmatrix} U_{e1} & U_{e2} & U_{e3} \\ U_{\mu1} & U_{\mu2} & U_{\mu3} \\ U_{\tau1} & U_{\tau2} & U_{\tau3} \end{pmatrix}. \quad (2.37)$$

Similar to the CKM matrix, the PMNS matrix has three angles and one phase which can be parametrized in many different ways. A general parametrization [25] is  $U_{PMNS} = U \cdot P$  where  $P$  and  $U$  are given by the following matrices

$$U = \begin{pmatrix} c_{12}c_{13} & s_{12}c_{13} & s_{13}e^{-i\delta} \\ -s_{12}c_{23} - c_{12}s_{23}s_{13}e^{i\delta} & c_{12}c_{23} - s_{12}s_{23}s_{13}e^{i\delta} & s_{23}c_{13} \\ s_{12}s_{23} - c_{12}s_{23}s_{13}e^{i\delta} & -c_{12}s_{23} - s_{12}c_{23}s_{13}e^{i\delta} & c_{23}c_{13} \end{pmatrix}, \quad P = \begin{pmatrix} 1 & 0 & 0 \\ 0 & e^{i\alpha} & 0 \\ 0 & 0 & e^{i\beta} \end{pmatrix}, \quad (2.38)$$

where the phase  $\delta$  is the Dirac CP violation phase and  $\alpha$  and  $\beta$  are the Majorana CP violation phases. The mixing angles  $c_{ij} = \cos \theta_{ij}$  and  $s_{ij} = \sin \theta_{ij}$  are given by [24] ( $3\sigma$  allowed ranges consistent with both  $\Delta m^2 > 0$  and  $\Delta m^2 < 0$ )

$$\sin^2 \theta_{1,2} = 0.259 - 0.359 \quad \sin^2 \theta_{23} = 0.374 - 0.641 \quad \sin^2 \theta_{13} = 0.0176 - 0.0298 \quad (2.39)$$

Interestingly this is approximately consistent (except for  $\theta_{13} \neq 0$ ) with the tri-bi-maximal texture

$$U = \begin{pmatrix} \sqrt{\frac{2}{3}} & \frac{1}{\sqrt{3}} & 0 \\ \frac{-1}{\sqrt{6}} & \frac{1}{\sqrt{3}} & \frac{-1}{\sqrt{2}} \\ \frac{-1}{\sqrt{6}} & \frac{1}{\sqrt{3}} & \frac{1}{\sqrt{2}} \end{pmatrix} P. \quad (2.40)$$

We will use this texture in Chapter 5 to address the neutrino phenomenology in the warped extra dimensions.

## 2.3 Higgs Physics

The historical discovery of the Higgs boson gave experimental access to the Higgs sector of the SM. It was for the first time that access to the level of energies enabled to probe the Higgs sector. In this section we give an argument [26, 27, 28, 29] based on unitarity of why the Higgs sector had to be introduced. As mentioned in section 2.1, the Higgs mechanism breaks the  $SU(2) \times U(1)$  symmetry of the SM and hence it is closely related to the weak scale. The weak

gauge bosons below the weak energy scale are  $W^+$ ,  $W^-$ ,  $Z$ ,  $\gamma$ , as in Eqs 2.23, 2.24 and 2.25. The gauge symmetry of the Lagrangian is not really a symmetry. It is merely a consequence of the fact of an added redundancy to the description of the gauge fields, in order to make Lorenz invariance manifest, and therefore the fields that live on the same gauge manifold, *i.e.*, fields that differ from each other only by a gauge transformation, must be physically equivalent. The gauge symmetry of the Lagrangian enforces this equivalence. Bearing this fact in mind, we now add a gauge violating mass term to the Lagrangian. This is motivated by the fact that we know that experimentally there are three massive gauge bosons in nature and a term in the Lagrangian is needed to describe them as follows

$$\mathcal{L} \supset \frac{1}{2} m_W^2 W_\mu^a W^{a\mu}. \quad (2.41)$$

It is possible to show that in order for this theory to be valid up to high energies with  $E \gg M_W$ , it must have the features of a Higgs theory for consistency with the unitarity bounds. Through this demonstration we will see that the key issue here is the redundancy in the description of the massive spin 1 gauge bosons. Consider a massive spin 1 particle at rest with momentum vector,  $k^\mu = (M_W, 0, 0, 0)$ , longitudinal polarization vector,  $\epsilon_L = (0, 0, 0, 1)$  and transverse polarization vectors  $\epsilon_{T1} = (0, 0, 1, 0)$  and  $\epsilon_{T2} = (0, 1, 0, 0)$ . They satisfy  $\epsilon_\lambda \cdot \epsilon_\lambda^* = -1$  and

$$\epsilon_\lambda^\mu k_\mu = 0. \quad (2.42)$$

Now if we boost in one direction, say  $\hat{z}$ , then  $k^\mu = (E_k, 0, 0, k)$  which means that the longitudinal polarization vector does not satisfy Eq. 2.42 any more. Rather the vector  $\epsilon_L = (\frac{k}{m_W}, 0, 0, \frac{E_k}{m_W})$  would be orthogonal to the momentum vector,  $k^\mu$ . In the limit of very high energies, this will translate into

$$\epsilon_L \rightarrow \frac{k^\mu}{m_W} + \mathcal{O}\left(\frac{m_W}{E_k}\right) \quad E_k \gg m_W. \quad (2.43)$$

Thus, as the momentum vector,  $k^\mu$ , approaches being a null vector, in order for the longitudinal polarization to stay orthogonal to the momentum vector, it needs to be more and more lined up with the momentum,  $\epsilon_L \propto k^\mu$ . This is exactly what one would expect from the Lorentz geometry. This tells us that the longitudinal polarization of the vector bosons grows with energy and that this component might cause problems for the theory.

Looking at the gauge boson propagator is also insightful. The quantum field operator of a spin 1 particle is given by

$$\phi^\mu(x) = \phi^{\mu+}(x) + \phi^{\mu-}(x), \quad (2.44)$$

where  $\phi^{\mu-}(x) = (\phi^{\mu+}(x))^\dagger$  and

$$\phi^{\mu+}(x) = \int \frac{d^3p}{(2\pi)^{3/2} \sqrt{E_p}} e^{i\mathbf{p}\cdot x} \sum_{\lambda} a_{p,\lambda} \epsilon_{\lambda}^{\mu}(p). \quad (2.45)$$

Here, the operator  $a_{p,\lambda}$  has particle labels of the little group, (in this case, being a massive spin 1, the group is  $SO(3)$ ) and the  $\epsilon_{\lambda}^{\mu}(p)$  map the little group labels into the Lorentz space-time labels. From this we can find the propagator,  $[\phi^{\mu+}(x), \phi^{\nu-}(x)]$

$$\frac{-i}{p^2 - m_W^2} - \eta^{\mu\nu} - \frac{p^{\mu}p^{\nu}}{m_W^2}. \quad (2.46)$$

Note that at large energies this propagator does not die off, and yet again this is the longitudinal polarization that causes problems as it grows with energy.

Let us examine the behavior of the  $t$  channel of the process,  $e_R^+ e_L^- \rightarrow W_L^+ W_L^-$ , at high energies. We can see that the amplitude,  $|\mathcal{M}|^2$ , and hence the cross section grow with energy:

$$|\mathcal{M}|^2 \propto \frac{g^4}{M_W^4} t \cdot u \quad (2.47)$$

where  $t \equiv (p_1 - p_3)^2$  and  $u \equiv (p_1 - p_4)^2$  are called the Mandelstam variables. This conflicts with unitarity as the cross section,  $\sigma$ , must be bounded by  $\frac{1}{s}$ , where  $s \equiv (p_1 + p_2)^2$  is also called a Mandelstam variable.

The argument is as follows. The scattering matrix,  $S$ , that relates the "in" to the "out" states,  $\psi_{out} = S\psi_{in}$  must be unitary and therefore satisfy  $S^\dagger S = 1$ . Writing  $S = 1 + iT$ , one arrives at  $2 \text{Im } T = T^\dagger T$  from which the optical theorem for  $2 \rightarrow 2$  scattering is derived

$$\text{Im } A(2 \rightarrow 2) = s \sum_{\text{all final states}} \sigma(2 \rightarrow \text{final}) \geq s \sigma(2 \rightarrow 2). \quad (2.48)$$

Now the partial wave expansions of a  $2 \rightarrow 2$  scattering amplitude and of its cross section are given by

$$A(2 \rightarrow 2) = 16\pi \sum_{\ell} (2\ell + 1) P_{\ell}(\cos \theta) a_{\ell}, \quad \sigma(2 \rightarrow 2) = \frac{16\pi}{s} \sum_{\ell} (2\ell + 1) P_{\ell}(\cos \theta) |a_{\ell}|^2 \quad (2.49)$$

which yields the following unitary bound:

$$|a_{\ell}|^2 \leq \text{Im}(a_{\ell}). \quad (2.50)$$

This means that for the real part of the partial wave amplitude,  $|\text{Re}(a_{\ell})| \leq \frac{1}{2}$ . For any process to have a unitary scattering matrix, it must satisfy this bound. Comparing with Eq. 2.49,

one arrives at the original claim, that  $\sigma \lesssim \frac{1}{s}$ . The energy scales at which problems occurs is  $E \sim 4\pi \frac{M_W}{g_2} \sim 4\pi v$ , with  $v$  being the VEV of the Higgs.

If one now calculates the  $s$  channel of the same process,  $e_R^+ e_L^- \rightarrow W_L^+ W_L^-$ , that too grows at high energies, and since the weak coupling,  $g$ , is the same in both processes the two diagrams exactly cancel. This is due to the fact that this is a non-Abelian gauge theory. Had we considered a random interaction between the massive vector bosons, where one of the strength of interaction vertex for the vector bosons was not  $g$ , then the violation of unitarity at high energies would be unavoidable. This means that the theory in its current form does not satisfy unitarity and hence does not make sense.

Therefore, both from this and from the discussion about the longitudinal polarization vector, we see that the main issue is the longitudinal modes in three gauge boson interactions. The cancellation that occurred in our example gives a clue on how to solve the problem: the three gauge boson interactions must have a gauge theory structure. The simplest way to resolve this is to introduce the Higgs boson with a vertex strength of  $vg^2 = M_W g$  coming from the term  $|h|^2 W^2$  in the Lagrangian. Then, after the electroweak symmetry breaking, the term  $vg^2 h W^2$  with  $h$  being the physical Higgs, exactly cancels the three gauge boson vertices.

## 2.4 Standard Model as an Effective Field Theory

Given a set of interacting particles constrained by some symmetry, even if the high energy degrees of freedom are not known, one can always write down a low energy effective field theory to describe the interactions between our set of particles. For that we simply need to represent the particles, or the relevant degrees of freedom in our theory, by fields, and then construct the interaction Lagrangian so that it is compatible with the symmetries. Whether or not the degrees of freedom in the theory are relevant or not depends on the energy scale of validity of the theory. Particles heavy enough that they can not be produced on shell at these available energies are assumed to have been integrated out, Fig. 2.2. Essentially, this is replacing the heavy degrees of freedom of the theory with their equations of motion. There could very well exist different equivalent field theories having the same degrees of freedom and hence describing the same physics.

Depending on the needed precision of the calculation one might have to include higher order operators up to order  $\frac{E}{\Lambda}$  where  $\Lambda$  is the mass scale of the fields that are integrated out, or in

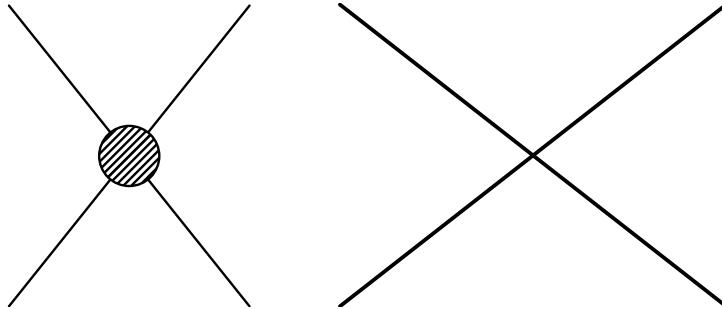


Figure 2.2: Integrating out the heavy fields for a  $2 \rightarrow 2$  scattering for a renormalizable theory; the diagram in the left is replaced by the diagram in the right.

other words, the cutoff of the theory.

In general this procedure does not produce a renormalizable quantum field theory, as the degrees of freedom often change as one approaches higher energies. Therefore one needs to include counter-terms for unknown ultraviolet (UV) sensitive physics. For higher precisions one needs higher and higher order counter-terms, but always a finite number of them for a finite precision. The general rule of thumb in the procedure is that after including *all* operators consistent with the symmetries of the theory up to mass dimension  $N$ , we can renormalize the theory using the same operators. The higher mass dimension operators of  $\dim(\mathcal{O})$  are suppressed by  $(\frac{E}{\Lambda})^{\dim(\mathcal{O})-4}$ . This theory then needs to be “matched” with the experimental data by fixing the coefficients of each operator.

This general framework can be used to probe both low energy physics when the high energy Lagrangian is known (by integrating out the heavy degrees of freedom *e.g.*, the Fermi model), or to probe new physics by considering the SM as a low energy effective field theory. Experimentally we have probed the theory up to scales of  $\sim \text{TeV}$ , therefore every interaction we measure arises in an effective Lagrangian. To proceed to higher energies, one needs to include higher mass dimension operators in the Lagrangian. All of these operators are built out of the same SM fields mentioned before. Here we mention the most famous of these operators. Operators with dimension less than or equal to 4 are already included in Eq. 2.1 with one exception:

$$\mathcal{L} \supset g' \epsilon^{\mu\nu\rho\sigma} G_{\mu\nu} G_{\rho\sigma}. \quad (2.51)$$

This operator leads to the strong CP problem, because the experimental bounds on the coefficient,  $g' < 10^{-10}$ , have not yet been understood theoretically.

There is only one possible dimension 5 operator which is consistent with the symmetries of

the theory in the SM

$$\mathcal{L} \supset \frac{c_{ij}}{\Lambda} (L_\alpha^{ia} h^b \epsilon_{ab}) (L_\beta^{jc} h^d \epsilon_{cd}) \epsilon^{\alpha\beta}, \quad (2.52)$$

where Greek letters denote the  $SU(2)$  spinor indices, Latin letters  $a, b, c$  and  $d$  are for  $SU(2)$  weak indices and Latin letters starting from  $i$  denote flavor indices. This operator gives rise to the Majorana neutrino masses. After the electroweak symmetry breaking:

$$\rightarrow \frac{c_{ij} v^2}{\Lambda} \nu_L^i \nu_L^j. \quad (2.53)$$

Interestingly, the  $\Lambda$  suppression also explains why the neutrino masses are so small.

There are about 80 possible operators with mass dimension 6. These operators are suppressed by  $\Lambda^2$ . Discuss all these operators is beyond the scope of this introduction, but we mention that the best known of these operators are the ones with four interacting fermion fields (*e.g.*,  $\frac{qqq\ell}{\lambda^2}$ ) responsible for proton decay and also for rare muon decays into three electrons.

A very efficient way to probe high energy physics is to look for SM operator coefficients which are zero or very small and for approximate symmetries that these terms violate. Through this method we can impose bounds on any new physics that violates that symmetry. In other words, any physics below those bounds must respect the same approximate symmetry as the SM (causing the coefficient to be small), otherwise the beyond the SM (BSM) model will yield a much larger contribution through quantum corrections. We will show how to use the effective field theory view in warped extra dimensions in Chapter 3.

## 2.5 Naturalness of the SM

It is a fact, strongly supported by experiments, that the value of physical observables are typically given by the scales enforced by the dimensional analysis multiplied by a factor of  $\mathcal{O}(1)$ . Historically it has been very fruitful to spot the cases where this dimensional analysis does not work, and look for an explanation. As an example, Dirac was baffled by the fact that the mass of the proton is much smaller than the Planck mass. This problem has as a solution the chiral symmetry that protects the proton mass from receiving large quantum corrections,. However the hierarchy between the weak scale and the Planck scale is still an one of the most important (unsolved) problems of modern physics, which could be an invaluable hint to the structure of physics at higher energies. As we mentioned in the Introduction,

there are also some other hierarchies in the theory that, although perhaps not as important as the weak-Planck hierarchy, are also outstanding problems. For example, why is the top quark so much heavier than the electron? There could be a deep reason for that which may become clear within the framework of a theory in the future, but this problem does not have an explanation within the SM. Also, how do we differentiate between different hierarchies in a theory?

Through the work of lots of physicists, including Dirac, Weisskopf, Wilson, Weinberg and t'Hooft, we now have a clear understanding of the core of this problem. The same problem has been stated differently through out the history of modern physics. Very briefly some of these formulations are:

- Power divergences are bad, logarithmic divergences one can deal with. This humble sentence has a deep meaning. Logarithmic divergences receive corrections from *all* scales, while power divergences receive all of their corrections from the highest energies and smallest length scales, exactly where our theory fails to be valid and this is why they are bad.
- A small *scalar* mass in your theory is unnatural. This means being very close to a second order phase transition which requires a lot of fine tuning and is unstable. Also scalar mass terms receive quadratic corrections from the highest scales and are sensitive to any new physics at high energies, which connects to the next point.
- A theory is unnatural if it is sensitive to high energy physics, that is, if small changes in the parameters of the theory at high energy results in huge corrections to the low energy physics. These corrections are due to the quantum fluctuations. Even if at the classical level one imposes a combination of cancelations that yield the small scalar mass in question, the quantum fluctuations of the full theory restore the dimensional analysis.
- t'Hooft's technical naturalness: A dimensionless parameter is naturally small only if the theory is more symmetric when it is exactly zero. This explains why the proton can be naturally light, but a scalar field can not. Without the fermion mass term, the Lagrangian is more symmetric, and therefore the fermion masses can be small. This is not true for the scalar mass term.

## 2.6 Warped Extra Dimensional Models<sup>3</sup>

Introduction of additional dimensions to the 4D space time has been abundant in the literature. The incentive to do so has always been force unification, in recent times, the unification of gravity and the rest of the SM forces. The modern view of the certain class of theories named "large extra dimensions" was first developed by Arkani-Hamed *et al.* in 1998 [31]. They showed that the weak-Planck scale hierarchy problem could be explained if gravity could propagate in the bulk of extra dimensions. Interestingly the size of these extra dimensions could be roughly between a millimeter and a  $\text{TeV}^{-1}$ , well within the possible range of detection of our current detectors. The next breakthrough was due to Lisa Randal and Raman Sundrum [32, 33] who postulated a warped geometry with a five dimensional Anti-de Sitter ( $AdS_5$ ) background space time metric given by

$$ds^2 = e^{-2ky} \eta_{\mu\nu} dx^\mu dx^\nu - dy^2 \equiv g_{MN} dx^M dx^N, \quad (2.54)$$

where  $\eta_{\mu\nu}$  is the flat four dimensional Minkowski metric with mostly minus signs,  $k$  is the momentum (or curvature scale) along the fifth dimension and  $x^M = (x^\mu, y)$  are the 5D space-time coordinates with  $M = (\mu, 5)$ . The 5D metric,  $g_{MN}$  is defined via the above equation. We might use the conformal coordinates in which the above metric takes the form

$$ds^2 = \frac{1}{(kz)^2} (\eta_{\mu\nu} dx^\mu dx^\nu - dz^2), \quad (2.55)$$

where the new coordinate,  $z$  is related to  $y$  by  $z = e^{ky}/k$ . To accommodate experimental observations, this extra dimension must have a finite length. Originally it was assumed that one must compactify the geometry on a circle through the identification  $y \leftrightarrow y + 2\pi R$ , with two 3-branes placed at the orbifold fixed points. Later, it was realized that the chiral representation of fermions in the SM can be nicely incorporated in this model with the fifth dimension being compactified on a  $Z_2$  orbifold,  $S_1/Z_2$ , which identifies  $y \leftrightarrow -y$ . In the original Randall Sundrum setup, this extra dimension was bounded by two branes (hard walls) at the locations  $y = 0$  for the UV (or Planck) brane and  $y = y_1$  for the infrared (IR), or TeV brane<sup>4</sup>. In the original RS scenario it was assumed that all the SM fields are localized in the TeV brane [32, 33], but this was soon replaced by a scenario in which all of these fields were allowed to propagate within the bulk, except for the Higgs field, which was still localized in the TeV brane [34, 35, 36, 37, 38, 39, 40, 41, 42, 43, 44, 45, 46]<sup>5</sup>. The second scenario had

<sup>3</sup>A very nice and pedagogical review of extra dimensional models is given by Tony Gherghetta [30].

<sup>4</sup>For the conformal coordinates the location of the branes is  $z = R = 1/k$  and  $z = R' = e^{ky_1}/k$ .

<sup>5</sup>These scenarios are named RS1 and RS2 respectively.

the advantage that, depending on the localization of the SM field inside the bulk of the extra dimension, and on how much this geographical position overlaps with the Higgs field still localized on the TeV brane, particles would acquire different masses, and hence the model could address another hierarchy problem, namely the flavor hierarchy within the SM.

We now show how the Planck-Weak hierarchy problem is solved in the RS1 model. For an IR localized Higgs the action is given by

$$S_H = \int d^4 dy \sqrt{-g} \delta(y - y_1) (g^{\mu\nu} \overline{D}_\mu H D_\nu H - M_{5D}^2 (H^\dagger H) + \lambda (H^\dagger H)^2) \quad (2.56)$$

where the determinant of the metric,  $\sqrt{-g} = e^{-4ky}$ . Due to the appearance of the metric  $g^{\mu\nu}$  in front of the kinetic term, one needs to normalize the kinetic term through the redefinition of the Higgs field,  $H \rightarrow e^{ky_1} H$ . This "warps" down the physical Higgs mass as

$$m_H = M_{5D} e^{-ky_1}. \quad (2.57)$$

This process is generic to all mass scales in this RS1 model, as all the SM fields confined to the IR brane can lead to dangerous FCNC and proton decays. As mentioned before, RS2 solves this problem by allowing the SM fields to propagate in the bulk. This leaves five dimensional bulk fields in a slice of  $AdS_5$ . One then needs to go through the one century old procedure of Kaluza-Klein dimensional reduction, which essentially means solving the equation of motion for the fields along the fifth dimension and reduce the 5D Lagrangian to a 4D effective one, which includes a tower of infinite KK modes for each of these 5D fields. The mass scale of the first KK mode is given by

$$m_1 \sim k e^{-ky_1}, \quad (2.58)$$

and the mass of higher order KK modes is given by the momentum of the standing quantum wave along the fifth dimension within the boundaries. For the RS metric, these turn out to be Bessel functions  $J_n$  and  $Y_n$ , satisfying the appropriate boundary conditions, and the mass is given approximately by

$$m_n \sim n m_1. \quad (2.59)$$

The only subtlety involved in this procedure is the fermion field boundary conditions. In odd number of space-time dimensions, the spinor representations require the  $\gamma_5$  matrix to carry a space-time index, and hence one loses the chirality present in four dimensions. The model might become useless unless, except for the fact that boundary conditions on the 5D fermion fields require that

$$\delta \bar{\Psi}_R \Psi_L|_{y=0, y_1} = \delta \bar{\Psi}_L \Psi_R|_{y=0, y_1} = 0, \quad (2.60)$$

where  $\Psi_L$  and  $\Psi_R$  are the left handed and right handed fields respectively. This means that one of the left handed or right handed fields must satisfy Dirichlet boundary conditions, a result perfectly consistent with SM (*cf.* Table 2.1). In the following chapters, we study specific aspects of warped extra dimensions.

# Chapter 3

## Higgs Phenomenology From Bulk to Brane

### 3.1 Introduction

Warped extra dimensional models have become very popular because they are able to address simultaneously two intriguing issues within the Standard Model (SM): the hierarchy problem and the mass/flavor problem. They were originally introduced to treat the first issue [32, 33] in a setup where the SM fields were all localized at one boundary of the extra dimension. Later it was realized that by allowing fields to propagate into the bulk, different geographical localization of fields along the extra dimension could help explain the observed masses and flavor mixing among quarks and leptons [34, 35, 36, 37, 38, 39, 40, 41, 42, 43, 44, 45, 46]. Flavor bounds and precision electroweak tests put pressure on the mass scale of new physics in these models [47, 48, 49, 50, 51, 52, 53], but extending the gauge groups and/or matter content (e.g. [54, 48, 55, 56, 57, 58, 59, 60, 61, 62]) or by slightly modifying the spacetime warping of the metric (e.g [63, 64, 65, 66]), it is possible to keep the new physics scale at the TeV level at the reach of the Large Hadron Collider (LHC).

Electroweak symmetry breaking can still happen via a standard Higgs mechanism in these scenarios (although it can also be implemented as as Pseudo-Nambu-Goldstone boson (PNGB) [67, 68] or described within the effective theory formalism [69, 70]). As the LHC announced the discovery of a light Higgs-like particle of a mass around 125 GeV [17, 18], it becomes crucial to have a detailed prediction of the properties of the physical Higgs particle in these

models. The Higgs boson itself must be located near the TeV boundary of the extra dimension in order to solve the hierarchy problem, and so typically it is assumed to be exactly localized on that boundary (brane Higgs scenario). Nevertheless, it is possible that it leaks out into the bulk (bulk Higgs scenario), and in doing so indirectly alleviate some of the bounds plaguing these models [71].

The calculation of the production cross section of the brane Higgs in these scenarios has been addressed before [72, 73, 74, 75, 76, 77, 78, 53, 79] but we will pay close attention to the more recent works of [75, 77, 78, 53, 79]. The towers of fermion Kaluza-Klein (KK) modes will affect significantly the SM prediction and in [77] it was found that the Higgs boson production rate can receive important corrections, either enhancing or suppressing the Standard Model prediction. The suppression or enhancement depends on the model parameters considered, in particular on the phases appearing in the different Yukawa-type operators present in the 5D action. Previously, the analysis of [75], in which only the first few modes were considered, gave no contribution to the rate from the towers of KK fermions. Finally, the analysis of [78, 53, 79] seems to indicate that with just a few KK modes a substantial effect is obtained, but of opposite sign as the one predicted from summing the infinite tower [77].

In this chapter we consider the effects of allowing the Higgs boson to propagate in the bulk, with its profile more or less localized towards the IR brane depending on the value of the mass parameter  $\beta$ , related to the bulk mass of the 5D Higgs field.

To keep matters as simple as possible we will set up a model containing a single family of up-type 5D fermions along with a bulk Higgs scalar. Generalization to a more realistic scenario is straight forward but we prefer to stay as transparent as possible due to the many subtleties involved in the calculation.

We first compute the contribution of the complete tower of KK fermions to the Higgs production cross section as well as to the tree-level shift happening between the light fermion mass and its Yukawa coupling (leading to flavor violating couplings when considering three fermion families). These calculations, as outlined in [80, 77], are analytically straightforward and allow us to obtain simple and compact results. We then repeat the same analysis numerically from the point of view of an effective theory in which only the first few KK fermions contribute. We show that for a bulk Higgs with a thickness of the order of inverse TeV scale, the results obtained are the same as the results obtained by summing the complete KK tower (i.e. heavier modes decouple). Moreover, these results are consistent with the predictions obtained in [80, 77] for the specific case of a brane localized Higgs. The two approaches out-

lined seem to give different predictions as the bulk Higgs is continuously pushed towards the brane. It turns out that in order to maintain the consistency of both approaches we need to include in the analysis the effects of a special type of higher order operators. After these effects are included, we will come back and address in the discussion section the differences among the existing calculations in the literature and stress the importance of including the mentioned higher order operators in the analysis.

This chapter is organized as follows. In Sec. 3.2 we summarize the simple 5D warped space model used in the calculation. In Sec. 3.3 we present analytical results for the Higgs flavor-changing effects (3.3.1) and production (3.3.2), using the full tower of KK fermions. We use numerical methods to calculate the effects of including just a few KK modes in Sec. 3.4, both for flavor-changing neutral currents effects (3.4.1) and Higgs boson production (3.4.2). We include the effect of the higher order operator in Sec. 3.5 and discuss the misalignment between the Higgs boson profile and its vacuum expectation value (VEV) in Sec. 3.6. We discuss the significance of our results, compare them to previous analyses and conclude in Sec. 3.7. We leave some of the details for the Appendices A and B.

## 3.2 Warped Extra Dimensions with Higgs in the Bulk

We consider the simplest 5D warped extension of the SM, in which we keep the SM local gauge groups and just extend the space-time by one warped extra dimension.

The spacetime metric is the usual Randall-Sundrum form [32, 33]:

$$ds^2 = \frac{R^2}{z^2} (\eta_{\mu\nu} dx^\mu dx^\nu - dz^2), \quad (3.1)$$

with the UV (IR) branes localized at  $z = R$  ( $z = R'$ ). We denote the  $SU(2)_L$  doublets by  $\mathcal{Q}^i(x, z)$  and the  $SU(2)_L$  singlets by  $\mathcal{U}^j(x, z)$  where  $i, j$  are flavor indices and  $x$  represents the 4D spacetime coordinates while  $z$  represents the extra dimension coordinate. The fermions are expected to propagate in the bulk [34, 35, 36, 37, 38, 39, 40, 41, 42, 43, 44, 45, 46].

The up-sector fermion action that we consider is therefore

$$S_{fermion} = \int d^4x dz \sqrt{g} \left[ \frac{i}{2} (\bar{\mathcal{Q}}_i \Gamma^A \mathcal{D}_A \mathcal{Q}_i - \mathcal{D}_A \bar{\mathcal{Q}}_i \Gamma^A \mathcal{Q}_i) + \frac{c_{q_i}}{R} \bar{\mathcal{Q}}_i \mathcal{Q}_i + \frac{i}{2} (\bar{\mathcal{U}}_j \Gamma^A \mathcal{D}_A \mathcal{U}_j - \mathcal{D}_A \bar{\mathcal{U}}_j \Gamma^A \mathcal{U}_j) + \frac{c_{u_j}}{R} \bar{\mathcal{U}}_j \mathcal{U}_j + (Y_{ij}^* \bar{\mathcal{Q}}_i H \mathcal{U}_j + h.c.) \right], \quad (3.2)$$

with  $\mathcal{D}_A$  being the covariant derivative, and we have added a Yukawa interaction with a Higgs field  $H$  which in principle can be either brane or bulk localized. From the 5D fermion mass terms one defines dimensionless parameters  $c_{u_i}, c_{q_i}$  which are *a priori* quantities of  $\mathcal{O}(1)$ . The coefficients  $Y_{ij}^*$  have inverse energy units ( $1/\sqrt{\Lambda}$ ) since Yukawa couplings in 5D are higher dimensional operators.

After separating 5D fields into left and right chiralities we impose a mixed ansatz for separation of variables

$$q_L(x, z) = q_L^0(z)q_L^0(x) + Q_L^1(z)\Psi_L^1(x) + \dots, \quad (3.3)$$

$$q_R(x, z) = q_R^0(z)u_R^0(x) + Q_R^1(z)\Psi_R^1(x) + \dots, \quad (3.4)$$

$$u_L(x, z) = u_L^0(z)q_L^0(x) + U_L^1(z)\Psi_L^1(x) + \dots, \quad (3.5)$$

$$u_R(x, z) = u_R^0(z)u_R^0(x) + U_R^1(z)\Psi_R^1(x) + \dots, \quad (3.6)$$

where  $q_L^0(x)$  and  $u_L^0(x)$  are the SM fermions and  $\Psi_{L,R}^n(x)$  are the heavier KK modes. In order to obtain a chiral spectrum, we choose boundary conditions for the fermion wavefunctions

$$q_L(++), \quad q_R(--), \quad u_L(--), \quad u_R(++), \quad (3.7)$$

so that before electroweak symmetry breaking only  $q_L^0$  and  $u_R^0$  will be massless (zero modes) with wavefunctions:

$$q_L^0(z) = f(c_q) \frac{R'^{-\frac{1}{2}+c_q}}{R^2} z^{2-c_q}, \quad (3.8)$$

$$u_R^0(z) = f(-c_u) \frac{R'^{-\frac{1}{2}-c_u}}{R^2} z^{2+c_u}, \quad (3.9)$$

where we have defined  $f(c) \equiv \sqrt{\frac{1-2c}{1-\epsilon^{1-2c}}}$  and the hierarchically small parameter  $\epsilon = R/R' \approx 10^{-15}$ . Thus, if we choose  $c_q(-c_u) > 1/2$ , the zero mode wavefunctions are localized towards the UV brane; if  $c_q(-c_u) < 1/2$ , they are localized towards the IR brane.

In order to implement minimally the Higgs sector out of a 5D scalar we use the following action [81]

$$\mathcal{S}_{\text{Higgs}} = \int dz d^4x \left(\frac{R}{z}\right)^3 \left[ \text{Tr}|\mathcal{D}_M H|^2 - \frac{\mu^2}{z^2} \text{Tr}|H|^2 \right] - V_{UV}(H)\delta(z-R) - V_{IR}(H)\delta(z-R'), \quad (3.10)$$

where  $\mu$  is the 5D mass for the Higgs boson. The boundary potentials  $V_{UV}(H)$  and  $V_{IR}(H)$  yield boundary conditions that can accommodate electroweak symmetry breaking, so that

one obtains a Higgs VEV with a non-trivial profile along the extra-dimension. Around that VEV, one should then add perturbations and obtain the spectrum of physical modes, i.e. a SM-like Higgs boson and a tower of KK Higgs fields. The expansion should look like

$$H(x, z) = v_\beta(z) + h_\beta(z)h(x) + \dots, \quad (3.11)$$

and we can choose the boundary conditions such that the profile of the Higgs VEV  $v_\beta(z)$  takes the simple form

$$v_\beta(z) = V(\beta) z^{2+\beta}, \quad (3.12)$$

where  $\beta = \sqrt{4 + \mu^2}$  and

$$V(\beta) = \sqrt{\frac{2(1 + \beta)}{R^3(1 - (R'/R)^{2+2\beta})}} \frac{v_4}{(R')^{1+\beta}}, \quad (3.13)$$

where  $v_4$  is the SM Higgs boson VEV. One should note that the wave function  $h_\beta(z)$  of the light physical Higgs (lightest KK Higgs field) will have the form

$$h_\beta(z) = \frac{v_\beta(z)}{v_4} \left( 1 + \mathcal{O} \left( \frac{m_h^2 z^2}{1 + \beta} \right) \right), \quad (3.14)$$

so that for a light enough Higgs boson mass both profiles  $h_\beta(z)$  and  $v_\beta(z)$  are aligned (i.e. proportional to each other).

The previous bulk Higgs sector is capable of reproducing the brane Higgs limit, since the wavefunction of the light Higgs (and its VEV) both depend exponentially on the parameter  $\beta$ . As this parameter is increased, the wavefunctions are pushed more and more towards the IR brane mimicking a perfectly localized Higgs sector.<sup>1</sup> Indeed, the wave function of the Higgs can act as a brane localizer since

$$\lim_{\beta \rightarrow \infty} h^2(z) = \lim_{\beta \rightarrow \infty} v^2(z) = \delta(z - R'), \quad (3.15)$$

where the Dirac delta function is defined as the limit of a sequence of functions with increasing value of  $\beta$ . One can easily prove that for any wavefunction  $f(z)$  (or a product of wavefunctions) we have

$$\lim_{\beta \rightarrow \infty} \int_R^{R'+} h^2(z) f(z) dz = f(R'). \quad (3.16)$$

There is however an issue about localizing the whole Higgs sector towards the brane since we just showed that only quadratic Higgs operators will “become” brane localizers. When a

---

<sup>1</sup>Moreover the masses of the heavier KK Higgs fields depend linearly on the  $\beta$  parameter and so these fields will decouple from the theory for very large  $\beta$ .

5D action operator contains more than two (or less than two) Higgs fields, the (successful) localization of such operators is not guaranteed. In fact in order to ensure that the 5D bulk Higgs scenario correctly tends smoothly to a fully localized Higgs sector, one should implement a prescription enforcing a precise  $\beta$  dependence on the coefficients of all operators containing Higgs fields. More precisely, the coefficient  $Y^N(\beta)$  of an operator containing  $N$  Higgs fields (before electroweak symmetry breaking) should behave as

$$Y^N(\beta) = Y_1^N \times \beta^{\frac{2-N}{2}}, \quad (3.17)$$

where  $Y_1^N = Y^N(1)$ . This is the only way to ensure that we can have

$$\lim_{\beta \rightarrow \infty} \int_R^{R'+} Y^N(\beta) h^N(z) f(z) dz = \lim_{\beta \rightarrow \infty} \int_R^{R'+} Y_1^N \beta^{\frac{2-N}{2}} h^N(z) f(z) dz = Y_1^N f(R'), \quad (3.18)$$

or in other words

$$\lim_{\beta \rightarrow \infty} Y^N(\beta) h^N(z) = Y_1^N \delta(z - R'). \quad (3.19)$$

In particular for 5D Yukawa type couplings this prescription implies that the 5D Yukawa coupling will have to carry a  $\sqrt{\beta}$  dependence in order to ensure that the brane limit Yukawa coupling is non-vanishing [82] (see also [80]). But it also means that any other 5D action operator containing a single Higgs field would need to carry the same  $\sqrt{\beta}$  dependence. On the other hand, 5D action operators containing 3 Higgs fields (like the operator  $H^2 HQU$ ) would have a diverging limit for  $\beta$  large unless its action coefficient  $Y^3(\beta)$  is itself suppressed by  $1/\sqrt{\beta}$ .

The previous prescription makes it technically possible to define a localized Higgs sector from a 5D bulk Higgs field, but it certainly seems quite contrived to appropriately fix all operator coefficients such that they all can give non-zero and finite contributions when the Higgs is localized. A brane localized Higgs sector could seem “un-generic” or “un-natural” if it is to be seen as a limiting case of a bulk Higgs. More details about the complete prescription for operators containing Higgs fields are presented in Appendix B.

### 3.3 Higgs phenomenology: all KK fermions

For completeness and consistency, we present first a result previously obtained in [80], namely the computation of the shift between the light SM fermion mass term and its Yukawa coupling with the Higgs field (leading to Higgs mediated FCNC when more than one fermion family

is considered). We then calculate the coupling between the physical Higgs and two gluons for the 5D bulk Higgs case.<sup>2</sup>

We can follow two routes to obtain our predictions. The computation of the flavor violating couplings of the Higgs scalar with fermions will be obtained in an approach based on considering *first* electroweak symmetry breaking and *then* solving the 5D equations of motion for the fermions (i.e. the effect of the Higgs VEV is directly taken into account in the equations of motion and during the dimensional reduction procedure). The alternative (and equivalent) approach would be to consider *first* the dimensional reduction (i.e. obtain the 4D effective theory in the gauge basis), and *then* consider the electroweak symmetry breaking in the presence of the infinite tower of KK fermions. After performing the diagonalization of the infinite fermion mass matrix (as well as canonical normalization of the fermion kinetic terms) we should recover the same results. We use the first approach in the first subsection, and the second approach in the computation of the Higgs coupling to gluons and also in the following sections where we will truncate the infinite mass matrix in order to consider only the effect of the first few KK modes.

### 3.3.1 Higgs Flavor violating couplings

After imposing electroweak symmetry breaking in the Higgs sector, the four profiles  $q_{L,R}(z)$  and  $u_{L,R}(z)$  introduced in eqs. (3.3) to (3.6) must obey the coupled equations coming from the equations of motion:

$$-m_u q_L - q'_R + \frac{c_q + 2}{z} q_R + \left(\frac{R}{z}\right) v_\beta(z) Y_u u_R = 0, \quad (3.20)$$

$$-m_u^* q_R + q'_L + \frac{c_q - 2}{z} q_L + \left(\frac{R}{z}\right) v_\beta(z) Y_u u_L = 0, \quad (3.21)$$

$$-m_u u_L - u'_R + \frac{c_u + 2}{z} u_R + \left(\frac{R}{z}\right) v_\beta(z) Y_u^* q_R = 0, \quad (3.22)$$

$$-m_u^* u_R + u'_L + \frac{c_u - 2}{z} u_L + \left(\frac{R}{z}\right) v_\beta(z) Y_u^* q_L = 0, \quad (3.23)$$

where the ' denotes derivative with respect to the extra coordinate  $z$  and  $Y_u$  is 5D Yukawa coupling.

---

<sup>2</sup>We follow very closely the general procedure outlined in [77] and explicitly compute the prediction for the bulk Higgs case and then compare it with the brane localized Higgs limit that was presented there. For the sake of simplicity here we assume the matter fields belong to the usual SM gauge group.

It is simple to deduce from these equations an exact expression for the mass eigenvalue  $m_u$  in terms of the fermion profiles [80]

$$m_u = R^4 \int_R^{R'} dz \left( \frac{m_u}{z^4} (|u_L|^2 + |q_R|^2) + \frac{Rv_\beta(z)}{z^5} (Y_u u_R q_L^* - Y_u^* q_R u_L^*) \right), \quad (3.24)$$

and compare it to the expression of the fermion Yukawa coupling, i.e

$$y_4^u = R^5 \int_R^{R'} dz \frac{h_\beta(z)}{z^5} (Y_u u_R q_L^* + Y_u^* q_R u_L^*), \quad (3.25)$$

where  $h_\beta(z)$  is the profile of the physical Higgs field.

With these two expressions we compute the shift (or misalignment) between the fermion mass  $m_u$  and the Yukawa coupling  $y_4^u$  as

$$\Delta^u = m_u - v_4 y_4^u, \quad (3.26)$$

which becomes simply

$$\Delta^u = R^4 \int_R^{R'} dz \left( \frac{m_u}{z^4} (|u_L|^2 + |q_R|^2) - 2Y_u^* \frac{Rv_\beta(z)}{z^5} q_R u_L^* \right). \quad (3.27)$$

In order to proceed further, a perturbative approach is used, such that we assume that  $(\tilde{Y}_u v_4 R') \ll 1$  where  $v_4$  is the SM Higgs VEV. Knowing the analytical form of the VEV profile  $v_\beta(z)$  and using the  $(\tilde{Y}_u v_4 R')$  small parameter it is possible to solve perturbatively the system of coupled equations (Eq. 3.20) to (Eq. 3.23) to any order in  $(\tilde{Y}_u v_4 R')$  (see [80] for details). The result for the shift in the top quark Yukawa coupling is

$$\begin{aligned} \frac{\Delta_1^t}{mv_4} &= \frac{2m_t^2}{v_4} R'^2 \frac{2 + c_u - c_q + \beta}{(1 - 2c_q)(1 + 2c_u)} \left[ \frac{1}{6 + c_u - c_q + 3\beta} - \frac{1}{5 + 2c_u + 2\beta} \right. \\ &\quad \left. - \frac{1}{5 - 2c_q + 2\beta} + \frac{1}{4 + c_u - c_q + \beta} \right], \end{aligned} \quad (3.28)$$

where we have only included the contribution from the third term in eq. (3.27), as the other terms are subdominant for light quarks, although not necessarily for the top quark. For clarity we omit their analytical expression here, but the complete analytical result can be found in [80] and in the Appendix A of this work. The shift in the Yukawa coupling has some dependence on the Higgs localization parameter  $\beta$  and it is shown in Figure 3.1 as the “infinite sum” result, as the procedure we followed is equivalent to diagonalizing the infinite fermion mass matrix in the gauge eigenbasis.

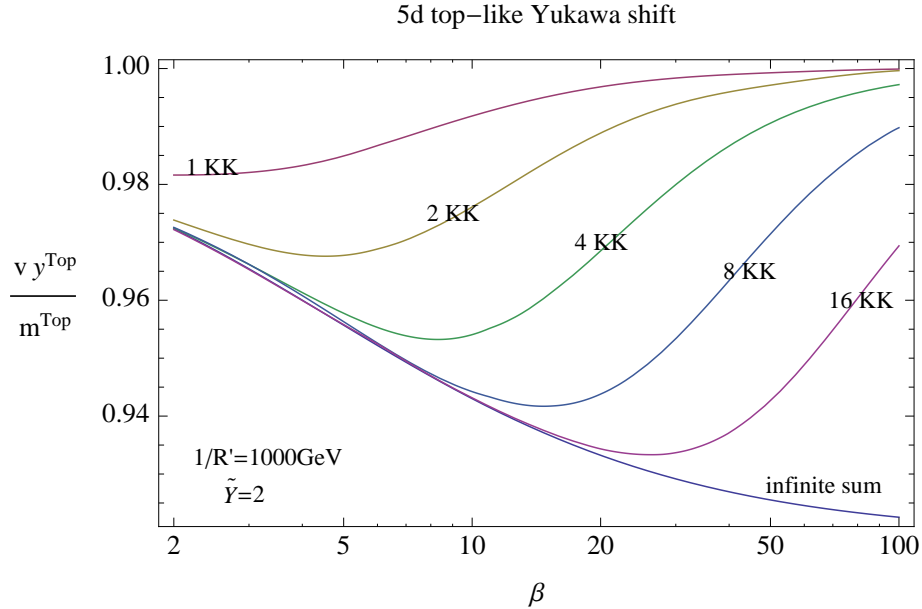


Figure 3.1: The shift in the top quark Yukawa coupling as a function of the bulk Higgs localization parameter  $\beta$ . Each line represents an effective theory containing the given amount of KK fermions. The lower line (blue) represents the contribution from the infinite tower of KK modes. Apart from the direct phenomenological impact of this result, this term also affects the  $hgg$  coupling, as discussed in the text. The dimensionless 5D Yukawa couplings are fixed at  $\tilde{Y} = 2$  and the KK scale is set at  $\frac{1}{R'} = 1000$  GeV (the overall effect scales as  $\tilde{Y}^2 v^2 R'^2$ ).

### 3.3.2 Higgs production

In this section we follow the approach of working with the infinite fermion KK modes with wavefunctions in the gauge basis. This is not the physical basis after electroweak symmetry breaking since Yukawa couplings will introduce off-diagonal terms in the infinite fermion mass matrix, which should be properly diagonalized in order to obtain the physical basis.

Since the Higgs field is not charged under QCD the main contribution to its coupling to gluons comes from a top quark loop, as shown in Figure 3.2; if the model contains many heavy quarks the resulting cross section for the process is  $gg \rightarrow h$  is [83]

$$\sigma_{gg \rightarrow h}^{SM} = \frac{\alpha_s m_h^2}{576\pi} \left| \sum_Q \frac{y_Q}{m_Q} A_{1/2}(\tau_Q) \right|^2 \delta(\hat{s} - m_h^2), \quad (3.29)$$

with  $\tau_Q \equiv m_h^2/4m_Q^2$ ,  $\hat{s}$  being the  $gg$  invariant mass squared and  $Q$  representing the physical fermions with physical Yukawa couplings  $Y_Q$  and masses  $m_Q$ . The form factor is given

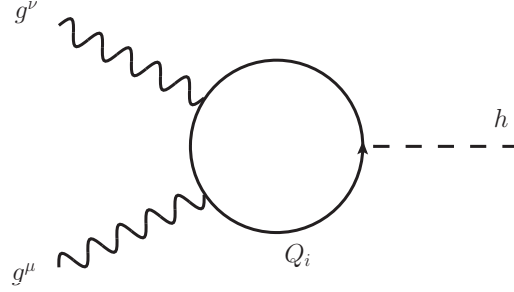


Figure 3.2: Loop diagram showing the contribution of the quark  $Q_i$  to the Higgs-gluon-gluon coupling. In the SM, the dominant contribution is through the top quark due to its large Yukawa coupling with the Higgs boson. In RS the heavier KK fermions contribute to the coupling with potentially large effects, either suppressing or enhancing the SM coupling, depending on the phases present in the different Yukawa-type operators present in the 5D action, and on the localization of the Higgs (see text for details).

by

$$A_{1/2}(\tau) = \frac{3}{2}[\tau + (\tau - 1)f(\tau)]\tau^{-2}, \quad (3.30)$$

with

$$f(\tau) = \begin{cases} [\arcsin\sqrt{\tau}]^2 & \tau \leq 0 \\ -\frac{1}{4} \left[ \ln \left( \frac{1+\sqrt{1-\tau^{-1}}}{1-\sqrt{1-\tau^{-1}}} \right) - i\pi \right]^2 & \tau > 1. \end{cases} \quad (3.31)$$

Here we want to figure out the contribution to the  $hgg$  coupling coming from 5D quark doublets and a singlets, i.e. containing the SM quarks (which includes doublets and singlets  $(q_L, u_R)$ ), along with the associated towers of vector-like KK fermions,  $(Q_L, U_R)$ . The relevant quantity to calculate is

$$c_{hgg} = \sum_Q \frac{y_Q}{m_Q} A_{1/2}(\tau_Q), \quad (3.32)$$

where  $y_Q$  is the physical Yukawa coupling of the physical Dirac fermion  $Q$  and  $m_Q$  is its mass. As stated before, it will prove useful to work in the gauge basis, and so we represent the Yukawa couplings between the KK fermions  $Q_L(x)$  and  $U_R(x)$  in the gauge basis as  $Y_{Q_L U_R}^u$ . Its values will be obtained by performing the overlap integral of the Higgs profile and the corresponding bulk fermionic wave functions, i.e.

$$Y_{Q_L U_R}^u = Y^u \int_R^{R'} dz \left( \frac{R}{z} \right)^5 \frac{v_\beta(z)}{v_4} Q_L^{u(i)}(z) U_R^{(k)}(z), \quad (3.33)$$

where we have assumed that the nontrivial Higgs VEV and the physical Higgs profile are perfectly aligned<sup>3</sup>. The Yukawa couplings between different chirality KK fermions and also between zero modes and heavy KK fermions are obtained and written in a similar way so that we can write the infinite dimensional fermion mass matrix as

$$\begin{pmatrix} \bar{q}_L^{u(0)} & \bar{Q}_L^{u(i)} & \bar{U}_L^{(j)} \end{pmatrix} \begin{pmatrix} Y_{q_L u_R}^u v_4 & 0 & Y_{q_L U_R}^u v_4 \\ Y_{Q_L u_R}^u v_4 & M_Q & Y_{Q_L U_R}^u v_4 \\ 0 & Y_{U_L Q_R}^{u*} v_4 & M_U \end{pmatrix} \begin{pmatrix} u_R^{(0)} \\ Q_R^{u(k)} \\ U_R^{(l)} \end{pmatrix}, \quad (3.34)$$

where  $M_Q = \text{diag}(M_{Q_1}, M_{Q_2}, \dots)$  and  $M_U = \text{diag}(M_{U_1}, M_{U_2}, \dots)$  are the KK mass matrices for the corresponding fermion fields in the gauge basis, and we have suppressed fermion family indices to simplify notation. From eqs. (3.30) and (3.31), we notice that in eq. (3.29) the form factors,  $A_{1/2} \approx 0$  for light fermions, and  $A_{1/2} \approx 1$  for the much heavier KK modes and the top quark. Therefore, separating the contribution of the light fermions from the heavy ones we write

$$c_{hgg} = \sum_{\text{light}} \frac{y_Q}{m_Q} A_{1/2}(\tau_Q) + \sum_{\text{heavy}} \frac{Y_Q}{M_Q}, \quad (3.35)$$

where in the first (second) term the sum is only over light (heavy) fermion generations. Noting that

$$\sum_{\text{heavy}} \frac{Y_Q}{M_Q} + \sum_{\text{light}} \frac{y_Q}{m_Q} = \text{Tr}(\mathbf{Y}\mathbf{M}^{-1}), \quad (3.36)$$

where  $\mathbf{M}$  is the fermion mass matrix given in (3.34), while  $\mathbf{Y}$  is the Yukawa matrix, we have

$$c_{hgg} = \text{Tr}(\mathbf{Y}\mathbf{M}^{-1}) + \sum_{\text{light}} \frac{y_Q}{m_Q} (A_{1/2}(\tau_Q) - 1). \quad (3.37)$$

We also note that  $Y = \frac{\partial M}{\partial v_4}$  and since the trace is invariant under unitary transformations, we can compute it in the gauge basis (so we can use the fermion mass matrix in that basis).

Up to first order in  $v_4$  one finds

$$\text{Tr}(\mathbf{Y}\mathbf{M}^{-1}) = \frac{\partial \ln \text{Det}(\mathbf{M})}{\partial v_4} \approx \frac{1}{v_4} - v_4 \sum_{i,j} \frac{2}{M_{Q_i} M_{U_j}} \left( Y_{Q_L i U_R j}^u Y_{U_L j Q_R i}^{u*} - \frac{Y_{q_L U_R j}^u Y_{U_L j Q_R i}^{u*} Y_{Q_L i u_R}^u}{Y_{q_L u_R}^u} \right). \quad (3.38)$$

---

<sup>3</sup>We address the case where  $h_\beta(z) \neq v_\beta(z)/v_4$  in Section 3.6.

Noting that the SM masses and Yukawa couplings are also modified (shifted) as [80]

$$\frac{y_Q}{m_Q}\Big|_{\text{light}} \approx \frac{1}{v_4} \left( 1 + 2 \frac{v_4^2}{Y_{qL^u R}^u} \sum_{i,j} \frac{Y_{qL^u R_j}^u Y_{U_{L_j}^{u*} Q_{R_i}} Y_{Q_{L_i}^{u R}}^u}{M_{Q_i} M_{U_j}} \right), \quad (3.39)$$

we can write the total  $hgg$  coupling as

$$c_{hgg} = -2v_4 \sum_{i,j} \frac{Y_{Q_{L_i}^{u R_j}}^u Y_{U_{L_j}^{u*} Q_{R_i}}}{M_{Q_i} M_{U_j}} + \frac{y_Q}{m_Q}\Big|_{\text{light}} A_{1/2}(\tau_{Q_{\text{light}}}). \quad (3.40)$$

where we have used equations (3.37), (3.38) and (3.39). As we mentioned before, the form factor is negligible for the light fermion generations. Therefore neglecting the last term above, and using (3.33) we have

$$c_{hgg} = -2v_4 Y^u Y^{u*} R \sum_{i,j} \int dz dz' \left(\frac{R}{z}\right)^5 \left(\frac{R}{z'}\right)^5 \frac{Q_L^{(i)}(z) Q_R^{(i)}(z') U_R^{(j)}(z) U_L^{(j)}(z')}{M_{Q_i} M_{U_j}} h_\beta(z) h(z'), \quad (3.41)$$

where the 5D bulk physical Higgs profiles can be normalized as [81]

$$h_\beta(z) = \sqrt{\frac{2(1+\beta)}{R^3(1-\epsilon^{2+2\beta})}} R' \left(\frac{z}{R'}\right)^{2+\beta}, \quad (3.42)$$

with  $\epsilon \equiv R/R' \sim 10^{-15}$  being the warp factor. The sums in eq. (3.40) are given by [77]

$$\sum_{i=1}^{\infty} \frac{Q_L^{(i)}(z) Q_R^{(i)}(z')}{M_{Q_i}} = -\frac{z'^{2+c_q} z^{2-c_q}}{R^4} \left[ \theta(z' - z) - \frac{(z'/R)^{1-2c_q} - 1}{\epsilon^{2c_q-1} - 1} \right], \quad (3.43)$$

and

$$\sum_{j=1}^{\infty} \frac{U_R^{(j)}(z) U_L^{(j)}(z')}{M_{U_j}} = \frac{z^{2+c_u} z'^{2-c_u}}{R^4} \left[ \theta(z' - z) - \frac{(z'/R)^{1+2c_u} - 1}{\epsilon^{-2c_u-1} - 1} \right]. \quad (3.44)$$

Substitution of these sums and of the Higgs profile in Eq. (3.41) and assuming <sup>4</sup>  $\beta \geq 2$  will finally give the total Higgs coupling for the light fermions which is given in Appendix A. If we assume that  $c_q > 1/2$  and  $c_u < -1/2$ , which is the case for light fermions (up-like fermion), the expression for  $c_{hgg}$  can be simplified as

$$c_{hgg}^{Up} \approx v_4 Y^u Y^{u*} R'^2 \frac{2(1+\beta)}{(2+\beta+c_q-c_u)} \frac{1}{4+2\beta}. \quad (3.45)$$

In the case of the top quark, we have to add the contribution due to the last term in Eq. (3.40), since  $A_{1/2}(\tau_{top}) \sim 1$ . Following the notation in [80], we write the additional contribution as

$$\frac{y_Q}{m_Q}\Big|_{\text{light}} A_{1/2}(\tau_{Q_{\text{light}}}) + \frac{\Delta_2^{\text{top}}}{m_t v_4}, \quad (3.46)$$

---

<sup>4</sup>For a completely flat bulk Higgs,  $\beta = 2$ . For any physically acceptable model  $\beta > 2$ .

where the first term is given by eq. (3.39) multiplied by the form factor,  $A_{1/2}$  and last term, is the result of kinetic term corrections due to the shift in Yukawa couplings, which are also not negligible for the heavy fermions. The shift is given by

$$\Delta_2^{top} = R^4 \int_R^{R'} dz \left( \frac{m_t}{z^4} (|u_L|^2 + |q_R|^2) \right). \quad (3.47)$$

For a complete discussion on this, we refer the reader to [80].

So finally for IR localized fermions with  $c_q < 1/2$  and  $c_u > -1/2$  (top-like) we have

$$c_{hgg}^{Top} \approx \frac{y_Q}{m_Q} \Big|_{\text{light}} A_{1/2}(\tau_{Q_{\text{light}}}) + \frac{\Delta_2^{top}}{m_t v_4} - v_4 Y^u Y^{u*} R'^2 \left[ -\frac{1}{4+2\beta} + \frac{1}{2\beta+5-2c_q} + \frac{1}{2\beta+5+2c_u} - \frac{1}{\beta+4-c_q+c_u} \right]. \quad (3.48)$$

Following our ansatz for localizing the Higgs sector, and in order to compare with previous brane Higgs results, we need to replace the 5D Yukawa couplings with the dimensionless and  $\beta$ -independent couplings

$$\tilde{Y} = \frac{\sqrt{2(1+\beta)}}{(2-c_q+c_u+\beta)} Y^{5D}. \quad (3.49)$$

The results obtained in this section, of the contribution of a 5D top-like quark and a 5D up-like quark to the  $hgg$  coupling are shown in both panels of Figure 3.3 as the “infinite sum” result.

### 3.4 Higgs phenomenology: individual KK modes

In this section we take a different approach and compute the effects on Higgs phenomenology (FCNC and production cross section) due to only the first few KK fermions in the model. That is, we consider a 4-dimensional effective theory which contains the SM matter content, augmented by a few levels of KK fields. This procedure is better fitted within the framework we work in (low cut-off effective theories), the drawback being that it is not possible to obtain general analytical predictions in a close form. Our strategy will be to assign some generic values to the parameters of the model and perform the computations numerically. In particular we will fix the bulk mass parameters of the 5D fermions  $Q$  and  $U$  to be  $c_u = -0.6$  and  $c_q = 0.6$  (for an up-type quark) and  $c_u = 0$  and  $c_q = 0.4$  (for a top quark). The value of the dimensionless 5D Yukawa coupling will be taken to be  $\tilde{Y}_1^{5D} = 2$ .

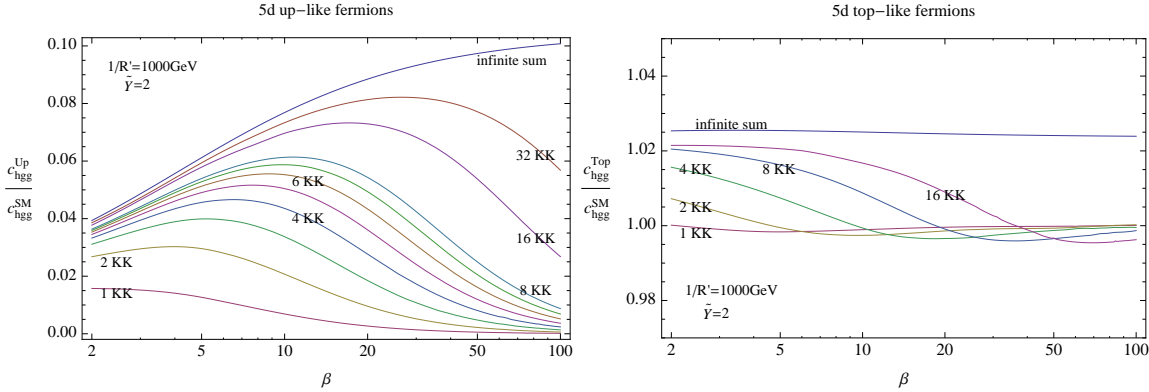


Figure 3.3: Contribution to  $c_{hgg}/c_{hgg}^{SM}$  coming from the KK partners of the “up” quark (left panel) and from the full top quark sector (right panel) as a function of the bulk Higgs localization parameter  $\beta$ . Each line represents the numerical result obtained in an effective theory containing the amount of KK fermions indicated. The upper line (blue) represents the contribution of the infinite tower of KK modes (computed in the text analytically). The dimensionless 5D Yukawas are fixed at  $\tilde{Y} = 2$  and the KK scale is set at  $\frac{1}{R'} = 1000$  GeV (the overall effect scales as  $\tilde{Y}^2 v^2 R'^2$ ).

### 3.4.1 Higgs Flavor violating couplings

In order to evaluate the shift in the Yukawa coupling of the SM fermion (the zero mode) due to the presence of a finite number of KK fermions, we can simply use Eq. (3.39), with the understanding that now the sum is finite, and so we shall sum up to the maximum number of KK modes chosen. We are interested in computing the top quark Yukawa shift as it is the most interesting for direct phenomenology, and also because it will also enter in the calculation of the  $hgg$  coupling. We perform the sum numerically and stop the summation at different maximum numbers of KK fermions. The results are shown in Figure 3.1 in which we focus on the variation of the Yukawa coupling shift with respect to the bulk Higgs localization parameter  $\beta$  and we compare these to the results obtained in the previous section for the infinite KK degrees of freedom. The main observation is that for small  $\beta$ , the finite sums are in good agreement with the infinite sum result. On the other hand for large values of  $\beta$  the Yukawa shift obtained from the finite sums becomes more and more irrelevant and is clearly at odds with the infinite sum prediction.

### 3.4.2 Higgs production

To evaluate the contribution to the  $hgg$  coupling coming from the individual KK fermion modes we proceed as in the previous subsection. We now use Eq. (3.41), and sum up to the maximum number of KK modes desired. We perform the sum numerically and show the results in Figure 3.3. Again we are interested in the variation of the couplings with  $\beta$  and compare them to the result for the  $c_{hgg}$  obtained by calculating the infinite sum, as shown in the previous section.

The two panels of the figure show the contribution to the  $hgg$  coupling coming from a 5D up-like quark (left panel) and the contribution coming from a 5D top-like quark (right panel) for  $\beta$  values up to 100. We can see how the sums over different maximum number of KK modes converge to the infinite sum limit as we vary  $\beta$ . The approximation obtained by considering just a few KK modes is much better for low values of  $\beta$ . For example, from the left panel of Figure 3.3, for  $\beta = 2 \rightarrow 5$ , 8 KK modes saturate some 90% of the infinite sum, while for  $\beta = 20$ , 8 KK modes saturate some 60% of the infinite sum. For  $\beta = 100$  (corresponding to a Higgs highly localized towards the brane), 8 KK modes represent only some 10% of the total KK contribution. This dependence on  $\beta$  is in agreement with the results found in [75], in which a brane localized Higgs was considered (i.e.  $\beta = \infty$ ) and the first few KK fermions considered were found to give a negligible contribution to the  $hgg$  coupling.

We conclude that in all the previous calculations (the top quark Yukawa shift and the contributions to the  $hgg$  coupling coming from up-type and top-like 5D quarks) we have observed the same feature, namely that in the case of a bulk Higgs (small  $\beta$ ), the effect of the heavier KK modes decouples (i.e. performing the infinite sum is equivalent to sum only over the first few KK modes). On the other hand, when  $\beta$  is very large, the heavier degrees of freedom do not seem to decouple hinting towards some type of UV sensitivity of the brane Higgs case. This is not that surprising since the thickness of a Higgs being crushed against the brane is becoming smaller and smaller, and the scale associated with the Higgs localization eventually becomes much larger than the cut-off of the scenario. We will now see how adding a type of higher derivative operators will be sufficient to make the finite sums consistent with the infinite sum results obtained earlier.

### 3.5 The Effect of Higher Derivative Operators

We have just seen how the results obtained in the previous section (3.4), where we sum over a few KK modes agree with the complete KK tower summation of section 3.3 only in the case of a bulk Higgs boson. When the Higgs is on the brane, or very much pushed towards the brane, the results for the two approaches do not seem to agree (see Figure 3.3 when  $\beta \rightarrow 100$ ). We will reconcile the two methods by including, in the effective theory calculation, the contribution of higher derivative operators.

In particular we consider the effect of the following operator in the action with a dimensionful coupling constant  $Y_R$  (flavor indices are suppressed),

$$S \supset \int d^4x dz \sqrt{g} \left[ Y_R \overline{\Gamma^M \mathcal{D}_M \mathcal{Q}} \mathcal{H} \Gamma^N \mathcal{D}_N \mathcal{U} + h.c. \right]. \quad (3.50)$$

The operator is of Yukawa-type as it couples two fermions with the Higgs, but it involves derivatives of fields. The coupling  $Y_R$  should be in units of  $\Lambda$ , the cut-off of the theory, and so obviously this operator is cut-off suppressed (we note that the standard 5D Yukawa  $Y_u$  coupling is also dimensionfull and cut-off suppressed, but by two units less than  $Y_R$ ). Since  $Q_R(z)$  and  $U_L(z)$  satisfy Dirichlet boundary conditions on the IR brane, their derivatives along the extra dimension can be large after electroweak symmetry breaking and so we focus on the operator

$$S \supset \int d^4x dz \left( \frac{R}{z} \right)^3 \left[ Y_R \overline{\partial_z q_R} H \partial_z u_L + h.c. \right], \quad (3.51)$$

which includes only the *wrong* chirality fermion components  $Q_R(z)$  and  $U_L(z)$  as it could lead to potentially large effects.

As explained in the previous sections we can proceed in two ways in order to compute the effects of this operator. We could study the effect of the operator into the 5D equations of motion *after* electroweak symmetry breaking (ESB) and calculate its effects from these. Alternatively, we could solve the equations of motion and perform the dimensional reduction *before* ESB, and then consider the effects produced by the operator by working in this gauge eigenbasis. Both methods should be equivalent, but we will follow the second one. In this approach, we obtain the effective 4D theory and since it is non-renormalizable, we cut-off its spectrum at the cut-off scale thus effectively we only allow a few physical KK modes into the calculation. The effects from higher modes are integrated out and encoded in all higher order operators of the theory with their effects under control by the cut-off suppression. In

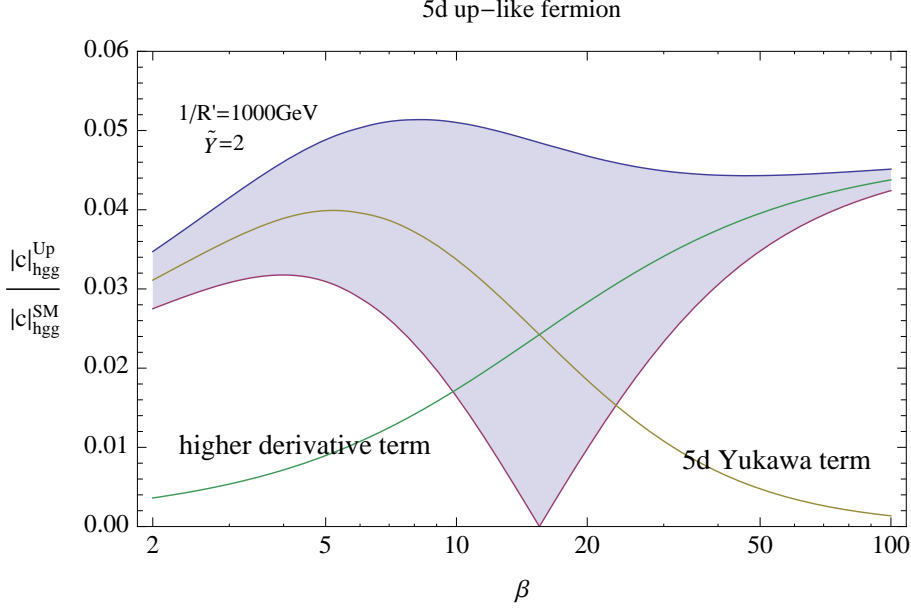


Figure 3.4: Contribution to the coupling  $|c_{hgg}|$  (relative to the Standard Model) as a function of the Higgs localization parameter  $\beta$  when considering *only* a five-dimensional up-type quark, and computed with the higher derivative term discussed in the text in addition to the standard 5D Yukawa coupling term. Since both contributions have independent phases we add and subtract their generic size to obtain the shaded region of possible values. These results are calculated by using only the first 3 KK modes (i.e. considering an effective theory with a cut-off of the order the the fourth KK mass). The dimensionless 5D Yukawas are fixed at  $\tilde{Y} = 2$  and the KK scale is set at  $\frac{1}{R'} = 1000$  GeV (the overall effect scales as  $\tilde{Y}^2 v^2 R'^2$ ).

the case of the  $Y_R$  operator the potentially large derivatives of  $Q_R(z)$  and  $U_L(z)$  can offset the cut-off suppression and so we should keep this operator in the calculations.

In the approach in which the KK modes are in the gauge basis, the  $Y_R$  operator will affect the fermion mass matrix from eq. (3.34), and in particular it will contribute to the  $Y_{U_L Q_R}^u$  terms. Its effects can therefore be tracked into the effects of these *wrong* chirality terms, as was already noted in the appendix of [80]. We can thus formally treat the situation as before, where a truncated version of the infinite mass matrix of eq. (3.34) is considered (with just a few KK levels), but now we redefine the terms  $Y_{U_L Q_R}^u$  to include the contributions from  $Y_R$  as

$$Y_{U_L Q_R}^u = \int_R^{R'} dz \left( \frac{R}{z} \right)^5 \frac{v_\beta(z)}{v_4} \left( Y^u U_L(z) Q_R(z) + Y_R^u \frac{z^2}{R^2} \partial_z U_L(z) \partial_z Q_R(z) \right). \quad (3.52)$$

It is now easy to compute numerically the new effects since from here we just have to repeat

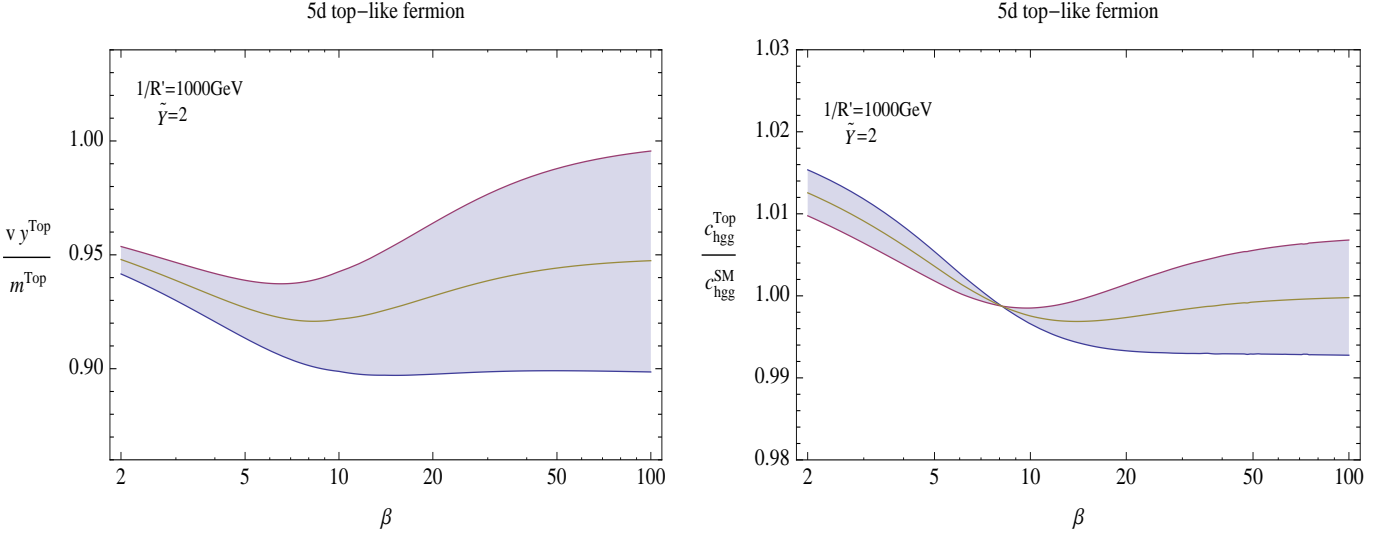


Figure 3.5: Shift of the top quark Yukawa coupling (left) and contribution to the coupling  $c_{hgg}$  (right), relative to the Standard Model, as a function of the Higgs localization parameter  $\beta$ , when considering only a five-dimensional KK top quark, and including in the computation the higher derivative term discussed in the text, in addition to the standard 5D Yukawa coupling term. The contributions from each term have independent phases and so we add and subtract their absolute value to obtain the shaded region of possible values. These results are calculated by using only the first 3 KK modes (i.e. considering an effective theory with a cut-off of the order the the fourth KK mass). The values of the 5D Yukawa  $Y^u$  and of  $Y_R$  are fixed at  $\tilde{Y} = 2$  and the KK scale is set at  $\frac{1}{R'} = 1000$  GeV (the overall effect scales as  $\tilde{Y}^2 v^2 R'^2$ ).

the previous procedure. The results are shown in Figures 3.4 and 3.5. In both figures we show the individual contributions coming from the normal Yukawa coupling  $Y^u$ , from the new  $Y_R^u$  coupling, as well as the combined effect. This combined effect is represented by the shaded region, the reason being that the two types of couplings  $Y^u$  and  $Y_R^u$  have independent phases and so can add up constructively or destructively, or in between. In Figure 3.4 we focus on the contribution to  $hgg$  due to an up-like 5D quark. In Figure 3.5 we show the predictions for the both shift in the SM top quark Yukawa coupling as well as the prediction for the contribution to the  $hgg$  coupling coming from a 5D top-like quark. As we can see, the shift in the top quark Yukawa coupling can be quite large, and for low values of the Higgs localization parameter  $\beta$  the shift obtained always results in a suppression in the Yukawa coupling. For large values of  $\beta$  the shift can be in either direction (suppression or enhancement). In the case of the  $hgg$  coupling, we see that the contribution represents an

enhancement with respect to the SM prediction for small values of  $\beta$ , and again for large values of  $\beta$  the  $c_{hgg}$  coupling can be either enhanced or suppressed depending on the relative phases between  $Y_R$  and  $Y^u$ . For this comparison we have taken the absolute value of both couplings  $Y_R$  and  $Y^u$  to be the same, i.e.  $\tilde{Y} = 2$ , in appropriate units of the cutoff. The main feature to remember is that the effects of the higher derivative operator  $Y_R$  are subdominant for small  $\beta$  but become dominant for large  $\beta$ . The large contribution obtained at large  $\beta$  is precisely what makes these new predictions consistent with the results obtained with the original infinite sum, and so the higher derivative operators that we have considered here somewhat encode the UV sensitivity found in the previous section.

### 3.6 Misalignment between Higgs VEV and Higgs profile

In this section we present a discussion on how to treat the case where the Higgs profile is different from its VEV profile. This is equivalent to consider the mixing effects between the massless zero mode Higgs boson, and the heavy KK Higgs modes and its effects on the Higgs observables computed in this chapter.

We follow closely an argument by Azatov [84] and for simplicity we will discuss a simple situation in which the 4D effective theory contains only two new heavy vector-like fermions,  $Q$  and  $U$ , doublet and singlet of  $SU(2)_L$  respectively. This is the situation one would have when the KK fermion towers are truncated after the first KK excitation.

Let's first define our notation for the following quantities

$$\begin{aligned} Y_{ij}^\beta &\equiv \int dz \left(\frac{R}{z}\right)^5 \psi_i \psi_j \frac{v_\beta(z)}{v_4} \\ X_{ij}^\beta &\equiv \int dz \left(\frac{R}{z}\right)^5 \psi_i \psi_j h_\beta(z), \end{aligned} \quad (3.53)$$

where  $v_4$  is the SM Higgs VEV and  $v_\beta(z), h_\beta(z)$  are the 5D profiles of the Higgs VEV and the Higgs physical field, which are generically different. That is, after EWSB, the Higgs field is expanded around the nontrivial VEV  $v_\beta(z)$  as

$$H(x, z) = v_\beta(z) + h(x)h_\beta(z) + \dots \quad (3.54)$$

In the case of the bulk Higgs sector considered here, both profiles  $v_\beta(z), h_\beta(z)$  are almost

the same, (see eq. (3.14)), the order of the misalignment between them being controlled by powers of  $(m_h R')^2$  (a small quantity).

We consider all the possible couplings between the Higgs and the fermions of the effective theory which after EWSB can be written as the matrix  $\mathcal{M}(v_4, h)$  as

$$(\bar{q}_L, \bar{Q}_L, \bar{U}_L) \begin{pmatrix} Y_{q_L u_R}^\beta v_4 + X_{q_L u_R}^\beta h(x) & 0 & Y_{q_L U_R}^\beta v_4 + X_{q_L U_R}^\beta h(x) \\ Y_{Q_L u_R}^\beta v_4 + X_{Q_L u_R}^\beta h(x) & M_Q & Y_{Q_L U_R}^\beta v_4 + X_{Q_L U_R}^\beta h(x) \\ 0 & Y_{U_L Q_R}^\beta v_4 + X_{U_L Q_R}^\beta h(x) & M_U \end{pmatrix} \begin{pmatrix} u_R \\ Q_R \\ U_R \end{pmatrix}, \quad (3.55)$$

The coupling between the physical Higgs and the two gluons is controlled by the physical Yukawa couplings  $Y_i^{\text{phys}}$  and masses  $M_i^{\text{phys}}$  of the heavier physical fermions running in the loop (top quark and KK modes), i.e.

$$\sum_{\text{heavy}} \frac{Y_i^{\text{phys}}}{M_i^{\text{phys}}} = \text{Tr}(\mathbf{Y}_{\text{phys}} \mathbf{M}_{\text{phys}}^{-1}) - \sum_{\text{light}} \frac{y_i}{m_i}, \quad (3.56)$$

where  $\mathbf{Y}_{\text{phys}}$  is the physical Yukawa coupling and  $\mathbf{M}_{\text{phys}}$  is the physical fermion mass matrix of the setup. Because the trace is invariant under unitary transformations, we can rotate to the gauge basis and write

$$\text{Tr}(\mathbf{Y}_{\text{phys}} \mathbf{M}_{\text{phys}}^{-1}) = \text{Tr}(\mathbf{Y}_{\text{gauge}} \mathbf{M}_{\text{gauge}}^{-1}), \quad (3.57)$$

and note that we can now relate this to the matrix  $\mathcal{M}(v_4, h)$  as

$$\text{Tr}(\mathbf{Y}_{\text{gauge}} \mathbf{M}_{\text{gauge}}^{-1}) = \partial_h \log(\text{Det} \mathcal{M}(v_4, h))|_{h=0}. \quad (3.58)$$

The procedure is the same as was followed in Section 3.3, i.e. we compute the the determinant by expanding in powers of  $v^2/M_i^2$  and after combining everything we obtain

$$\begin{aligned} \sum_{\text{heavy}} \frac{Y_i^{\text{phys}}}{M_i^{\text{phys}}} &= \partial_h \log \text{Det} \mathcal{M}(v_4, h) - \frac{y^{\text{light}}}{m^{\text{light}}} \\ &= v_4 \left( -\frac{X_{Q_L U_R}^\beta Y_{U_L Q_R}^\beta}{M_Q M_U} - \frac{X_{U_L Q_R}^\beta Y_{Q_L U_R}^\beta}{M_Q M_U} \right). \end{aligned} \quad (3.59)$$

This result is the equivalent to eq. (3.40) with the effect of the misalignment between  $v_\beta(z)$  and  $h_\beta(z)$ . One sees that the difference lies in the substitution of one of the  $Y$  terms by an  $X$  term, and so the correction to the result of eq. (3.40) is

$$\delta c_{hgg} = v_4 \left( -\frac{(X_{Q_L U_R}^\beta - Y_{Q_L U_R}^\beta) Y_{U_L Q_R}^\beta}{M_Q M_U} - \frac{(X_{U_L Q_R}^\beta - Y_{U_L Q_R}^\beta) Y_{Q_L U_R}^\beta}{M_Q M_U} \right), \quad (3.60)$$

which is controlled by

$$\left(X_{U_L Q_R}^\beta - Y_{U_L Q_R}^\beta\right) = \int dz \left(\frac{R}{z}\right)^5 U_L(z) Q_R(z) \left(h_\beta(z) - \frac{v_\beta(z)}{v_4}\right), \quad (3.61)$$

and

$$\left(X_{Q_L U_R}^\beta - Y_{Q_L U_R}^\beta\right) = \int dz \left(\frac{R}{z}\right)^5 Q_L(z) U_R(z) \left(h_\beta(z) - \frac{v_\beta(z)}{v_4}\right), \quad (3.62)$$

and since the misalignment between  $v_\beta(z)$  and  $h_\beta(z)$  can be computed perturbatively [80] as

$$h_\beta(z) - \frac{v_\beta(z)}{v_4} = \frac{v_\beta(z)}{v_4} \left(\frac{m_h^2 R'^2}{2(4+\beta)} + \frac{m_h^2 z^2}{4(1+\beta)} + \mathcal{O}(m_h^4 R'^4)\right), \quad (3.63)$$

we obtain

$$\left(X_{U_L Q_R}^\beta - Y_{U_L Q_R}^\beta\right) = m_h^2 R'^2 \left(\frac{Y_{U_L Q_R}^\beta}{2(4+\beta)} + \frac{Y_{U_L Q_R}^{\beta+2}}{4\sqrt{(1+\beta)(3+\beta)}}\right) + \mathcal{O}(m_h^4 R'^4). \quad (3.64)$$

In other words, the effect of considering the misalignment between  $v_\beta(z)$  and  $h_\beta(z)$  is to add a correction with the same structure as the result of eq. (3.40), but with a suppression of  $(m_h R')^2$ , i.e. the correction is at most  $\mathcal{O}(1\%)$ , and becomes much smaller for increasing values of  $\beta$ .<sup>5</sup>

### 3.7 Discussion and Outlook

In this chapter we have presented the results for the predictions of Higgs phenomenology in a toy-model RS setup in which the Higgs field is allowed to propagate in the bulk and with a single 5D fermion field. Our results can be extended to three families to include full flavor effects, but the generic predictions that we would obtain are expected to be basically the same as the ones presented in [80, 77]. That is, that in the context of flavor anarchy, where the action parameters are all of the same order but with more or less random values and phases (with the constraint of obtaining correct SM predictions) the couplings of the Higgs with fermions and gluons and photons can receive important corrections, either enhancing or suppressing the SM predictions. However, the two references mentioned present calculations performed by including the effect of all the KK fermions, technically assuming an infinite

---

<sup>5</sup>The dependence on  $\beta$  of the integrals  $Y_{U_L Q_R}^\beta$  and  $Y_{Q_L U_R}^\beta$  is quite mild and so, in terms of order of magnitude, we have  $Y_{U_L Q_R}^\beta \sim Y_{U_L Q_R}^{\beta+2}$ .

cut-off for the model (where a brane Higgs is considered). In general, all these scenarios break down at a low cut-off, becoming strongly coupled for both gauge and Yukawa interactions. The implicit assumption made in [80, 77] was that the effects of the heavier modes should decouple quickly, at least for the case of a bulk Higgs field. The main motivation to perform the calculations by considering the full infinite fermion KK tower, as well as pushing the Higgs into the brane was mainly of technical nature. Indeed both the flavor structure of the Higgs Yukawa couplings as well as the coupling to gluons and photons can be computed analytically with those ingredients. In [80], the authors checked analytically that the corrections to the Higgs Yukawa couplings were actually of the same order for a bulk Higgs and a brane Higgs.

However it was pointed out in [78, 53, 79] that in the brane Higgs case, the effects of the heavier KK fermion modes do not decouple and that they all contribute evenly in the computation of the Higgs couplings in the model. On the other hand, we showed in sections 3.3 and 3.4 of this chapter that the heavier KK modes in the case of a bulk Higgs do decouple very quickly, so that the analytical result obtained by using the infinite KK tower approaches with great precision the numerical result obtained by considering an effective theory with only a few KK fermion modes. Moreover, when considering the effective theory with only a few KK modes, one should include in the action all possible operators and in particular the higher derivative ones introduced in Section 3.5. These effects were omitted in [78, 53, 79], and as we showed in this work, the importance of these operators increases as the Higgs is more and more localized towards the brane. In [75], the authors considered an RS setup with a highly localized Higgs and the presence of only a few KK fermions and studied the effects on the Higgs couplings to gluons and photons, among other observables. In the limit of the SM gauge group (they did consider an extended gauge group) they found no significant deviations from the SM predictions. Indeed this result is consistent with our findings of Section 3.4 (no higher derivative operators invoked yet), since as it can be seen on Figures 3.5 and 3.4, the shift in Higgs Yukawa couplings and the new effects to Higgs-gluon-gluon coupling vanish in the limit of highly localized Higgs (large  $\beta$  parameter). On the other hand, in [78, 53, 79] it is claimed that large effects should be present in the case of a brane Higgs and with only a few KK modes present in the effective theory (and no higher derivative operators), a result inconsistent with both our findings and those found in [75]. We can trace the origin of the disagreement in their calculation of the Higgs Yukawa couplings. Those are computed by using the full 5D equations of motion, which as we have said earlier is equivalent to considering the complete tower of KK modes. Then, using these couplings, they calculate the  $hgg$  radiative

coupling but now including only a finite amount of KK fermions. This treatment leads to a highly suppressed top quark Yukawa coupling (due to effects from the infinite KK tower) and a vanishing contribution to  $hgg$  from the loops of KK fermions considered (one would need the whole tower to obtain a finite effect). Their end result is a suppressed top quark Yukawa coupling and a suppressed  $hgg$  coupling (due to the smaller top quark Yukawa), predictions which are at odds with the findings of [75, 77] and of this chapter.

The procedure of [78, 53, 79] seems inconsistent because essentially the authors use infinite KK degrees of freedom in one part of their calculation (the SM quark Yukawa couplings computation via equations of motion) but then they truncate the KK degrees of freedom in order to compute the  $hgg$  coupling. In any case, had they included the higher derivative operators introduced in this chapter, their results would have changed dramatically since then, the effect to  $hgg$  coming from the top quark Yukawa loop would remain basically the same, but the effects due to loops of a few KK fermions would dominate the overall effect (and thus the result would start to become consistent with the findings of [77]).

Also, the predictions of [75] should change if one considers the effects of the higher derivative operators introduced in Section 3.5. In that situation, the Higgs couplings can receive large corrections, and can be of any sign (suppression or enhancement) due to the different phases present in the couplings  $Y$  and  $Y_R$ . In fact we have found here that for a Higgs field in the bulk, our results are more predictive than for a brane Higgs field, because the effect of the higher derivative operators is subdominant for a bulk Higgs field.<sup>6</sup> The effects from only the 5D Yukawa operators are aligned [80], and thus all the KK quarks add up in phase. In that situation we can have definite predictions for the effects caused by a single family of fermions, i.e. it will produce a suppression in the light quark Yukawa coupling and an enhancement in Higgs boson production (as well as suppression in the Higgs to photons coupling) [77], with the caveat of taking the dimensionless couplings of both Yukawa terms and higher derivative operators to be the same (consistent with the usual assumption that all 5D coefficients have to be of the same order). Taking into account the three fermion families in conjunction with a bulk Higgs field might weaken this prediction due to complicated flavor mixings and structure, but still one should be able to draw a correlation between Yukawa couplings and Higgs production (and  $h \rightarrow \gamma\gamma$ ) for the case of a bulk Higgs field. The parameter space of

---

<sup>6</sup>Again, the reason for this is that the value of the derivatives of the bulk fermions is suppressed by the higher value of the 5D cutoff. When the Higgs boson is pushed towards the brane, the derivatives of these fermions fields (with the “wrong” chirality) becomes larger and larger, and the 5D cutoff does not suppress anymore the effect of these operators.

the bulk Higgs scenario can therefore be under a tighter pressure as more and more precise experimental measurements in Higgs observables at the LHC become available. In particular if the predicted and correlated deviations of Higgs couplings is not clearly observed this should put bounds on the KK scale of the bulk Higgs scenario.

The situation for a Higgs on the brane is different. The higher order derivative terms are now important. Each KK tower of light quarks and the top will contribute to the  $hgg$  coupling, but their effect depends on arbitrary relative phases (between  $Y_R$  and  $Y_{5d}$ ), and so one cannot make a firm statement about the magnitude and phase of the overall contribution: it can be a suppression or an enhancement, or in between.

Finally we comment again on the apparent problem of a highly localized Higgs scenario (brane Higgs) in which predictions made from a truncated fermion KK tower are very different from predictions made from an infinite fermion KK tower. This apparent UV-sensitivity can actually be lifted by considering the higher derivative operators described here (first introduced in [80]). When these are included, the predictions made with a finite KK fermion tower become consistent with the original predictions obtained with an infinite fermion tower. A more esthetic problem with the brane Higgs scenario remains, since the definition of the Higgs operators seems highly unnatural, if one understands a brane Higgs field as a limit of a bulk Higgs field. All operators involving Higgs fields will have to have a precise and definite dependence on  $\beta$  (a large number), which seems quite contrived, specially in a framework in which no big numerical hierarchies should arise from fundamental 5D coefficients. In any case, with the ansatz outlined in the text and reviewed in Appendix B, one can still work consistently with a brane Higgs field as a limit case of a bulk Higgs field.

# Chapter 4

## Higgs Phenomenology In Modified $AdS_5$ Geometries

### 4.1 Introduction

While the recent discovery of a Standard Model (SM)-like Higgs boson at the LHC completes the particle spectrum of the Standard Model (SM), from the theoretical standpoint, the SM still seems incomplete. Among other things, no explanation is offered for the hierarchy puzzles, one of which concerns the large mass gap between the electroweak scale ( $M_{\text{ew}} \sim 200$  GeV) and the Planck scale ( $M_{\text{Pl}} \sim 10^{18}$  GeV). Another hierarchy is the one in the observed masses of the fermions, from the very light neutrinos ( $m_\nu \sim 5 \times 10^{-2}$  eV) to the top quark ( $m_t \sim 175$  GeV). A popular modification to the SM that tries to address these issues is to modify the space-time symmetries by extending the number of space dimensions. If the additional dimension, extending between two branes, one at the TeV scale (IR brane) and the other at Planck scale (UV brane), with gravity propagating in the bulk, is warped, the resulting geometry generates naturally the Planck-electroweak scale hierarchy, with a large  $M_{\text{Pl}}$  generated from a small length of the extra dimension [32, 33]. While in the original Randall-Sundrum (RS) model the SM fields were located on the IR brane, it was later shown that if one lets the SM fields - except for the Higgs - to propagate in the bulk of the fifth dimension, fermion masses can be naturally hierarchical, with masses determined by their localization with respect to the two branes: the lighter fermions are localized near the Planck brane, while the heavier ones are localized near the TeV brane. The mass is determined by the overlap integrals with the TeV localized Higgs profile. This new framework was able

to address issues of the original RS model associated with flavor-changing neutral currents (FCNC), proton decay and neutrino masses [34, 35, 85, 36, 86, 87].

However, generic models with warped extra dimensions are still very constrained by electroweak and flavor precision tests [88, 89, 90, 91, 92, 60] so that the scale of the lightest KK modes should be set to  $\mathcal{O}(10 \text{ TeV})$  or more. Various methods can be implemented to avoid some of these tensions. To reduce pressure from electroweak precision tests, one can enlarge the gauge symmetry of the SM by introducing a custodial symmetry that limits the corrections to various precision observables [93, 92]. Even with custodial protection, very strong flavor constraints (specifically coming from  $K^0 - \bar{K}^0$  mixing) must still be addressed [47]; in the absence of any flavor symmetry<sup>1</sup> it was noted that when the Higgs is allowed to leak out of the TeV brane and its 5D Yukawa couplings enhanced, there is a general reduction of flavor bounds, but still keeping the KK masses at some 3 – 5 TeV or more [71].

Another interesting alternative to address tensions from precision electroweak and flavor tests is to modify the space-time metric, so that close to the TeV brane, the background deviates from pure five-dimensional anti-de Sitter space ( $AdS_5$ ). This modification suppresses large corrections to the electroweak and flavor observables and makes it possible to reduce the constraints to  $M_{KK} \gtrsim 1 \text{ TeV}$ , without the need to invoke custodial symmetry [94, 63, 65, 95, 64, 66, 96, 97]. A comprehensive analysis of the implications of these models at the LHC, analyzing the production of both electroweak and strong KK gauge bosons, has been performed in [98].

However, it has also been pointed out that a new source of potential tension in  $AdS_5$  scenarios can arise from the Higgs sector itself [99, 77]. The towers of fermion KK modes can affect significantly the Higgs boson production rate by either enhancing or suppressing the Standard Model prediction. The predicted suppression or enhancement depends on the model parameters considered, such as the nature of the Higgs (bulk or brane localized), or the phases of the Yukawa operators and other higher dimensional operators [77, 1]<sup>2</sup>. It is interesting to note that in the case of a bulk Higgs the importance of higher dimensional operators is reduced [100], as well as the effect of the phases in brane localized Yukawa operators. In that situation, one obtains a more specific prediction for the effects on the Higgs production rate, namely that there should be a general enhancement with respect to the SM prediction [77, 1]. In this same scenario of bulk Higgs, the physical Yukawa couplings between Higgs

---

<sup>1</sup>See for example [55, 62] for minimal flavor proposals managing to lift importantly the flavor bounds.

<sup>2</sup>Also *cf.* Chapter 3.

and fermions are overall suppressed [80, 1], both effects (enhancement in Higgs production and suppression in fermion Yukawa couplings), being intimately correlated<sup>3</sup>.

Motivated by these considerations, we investigate what is the situation for Higgs production in more general warped models with a modified  $AdS_5$  metric. Since some of these models manage to avoid all precision tests for quite low KK scales (2 TeV) we ask the question of whether, for such low KK masses, they can also limit the potential enhancements in Higgs production, present in RS scenarios.

This chapter is organized as follows. In the next section, Sec. 4.2, we present a brief description of standard RS scenarios and of two more general warped space scenarios. In Sec. 4.3 we give the results for Higgs production through gluon fusion in the two models with generalized warped space metrics and compare them with the RS predictions. We then discuss the decoupling of the heavier modes in Sec. 4.4 and finally we summarize our findings and conclude in Sec. 4.5. Some explicit formula are left for the Appendix C.

## 4.2 Soft-wall inspired models

The setup of warped extra-dimensional models consists of a slice of a five-dimensional anti-de Sitter space  $AdS_5$ , where the effective 4D scale is dependent of the position of the extra dimension. In the standard RS formulation, the metric is given by

$$ds^2 = e^{-2A(y)} \eta_{\mu\nu} dx^\mu dx^\nu - dy^2, \text{ with } A(y) = ky, \quad (4.1)$$

where the two branes are localized at  $y = 0$  and  $y = y_1$ ,  $k \sim M_{Pl}$  is the curvature scale of the  $AdS_5$ , and we are using the mostly positive metric for  $\eta_{\mu\nu}$ . Solving the gauge hierarchy problem requires that the warping exponent,  $ky_1$ , to be around  $\sim 35$ , which can be stabilized with a modest fined-tuning of the parameters [102, 103]. The TeV scale is generated from  $\bar{M}_{Pl} e^{-ky_1}$ , with  $\bar{M}_{Pl}$  the reduced 4D Planck scale. The KK excitations of the gauge bosons contributions to the electroweak precision observables - especially the  $T$  parameter - introduce a lower bound on the masses of these KK excitations of about  $\sim 10$  TeV, making them unobservable at LHC.

It was then observed that one way to address this issue was to consider a stabilized solution to the 5D scalar-gravity system, in which the  $AdS_5$  behaviour near the UV brane was

---

<sup>3</sup>See [101] for a description of the same effect in the Yukawa couplings from the CFT dual picture.

maintained, but a deformation of conformality near the IR brane was apparent [94, 63, 65, 95, 64, 66]. These scenarios assume a bulk Higgs and allow for a softening of electroweak constraints through suppressed couplings of the electroweak KK modes. In turn, this lowers the bounds on the KK masses, yielding a model within the reach of the LHC in the near future. Assuming the following superpotential with real arbitrary parameters  $\nu$  and  $b$

$$W = 6k(1 + be^{\nu\phi/\sqrt{6}}),$$

the stabilizing scalar field,  $\phi$ , and the modified metric warp factor,  $A(y)$  can be found, and are given by [104]

$$\phi(y) = -\frac{\sqrt{6}}{\nu} \log(\nu^2 bk(y_s - y)) \quad (4.2)$$

$$A(y) = ky + \frac{1}{\nu^2} \ln \left( 1 - \frac{y}{y_s} \right), \quad (4.3)$$

where  $y_s = y_1 + \Delta$  ( $\Delta > 0$ ) is the position of the singularity imposed by the scalar field, and is *outside* of the physical dimension, so the logarithm is always single valued and positive within the physical distance  $y = 0$  and  $y = y_1$ . The RS limit is obtained in either of the limits  $\nu \rightarrow \infty$ , or  $y_s \rightarrow \infty$ . The curvature radius along the extra dimension is given by

$$L(y) = \frac{\nu^2(y_s - y)}{\sqrt{1 - 2\nu^2/5 + 2\nu^2k(y_s - y) + \nu^4k^2(y_s - y)^2}}. \quad (4.4)$$

The requirement that the gravitational expansion remains perturbative, yields the following bound on this radius

$$kL_1 \equiv kL(y_1) \geq 0.2. \quad (4.5)$$

The bulk 5D Higgs profile along the extra dimension can be given by

$$h(y) = h_0(y)e^{aky}, \quad h_0(y) = \alpha_1 \left( 1 + \alpha_2 \int_0^y e^{4A(y') - 2aky'} dy' \right), \quad (4.6)$$

where  $a$  is a parameter that determines the localization of the Higgs profile along the extra dimension, which holographically can be viewed as the dimension of the Higgs condensate operator. In order to solve the hierarchy problem (Higgs localized near the IR brane) we must have  $a \geq a_{min}$ . Following [94, 63, 65, 95, 64] we introduce the following measure

$$\delta \equiv \left| e^{-2(a-2)ky_s} ky_s (-2(a-2)ky_s)^{\frac{4}{\nu^2}-1} \Gamma\left(1 - \frac{4}{\nu^2}, -2(a-2)k(y_s - y_1)\right) \right|$$

which is an estimate of the amount of fine tuning needed in order to save the RS solution to survive the hierarchy problem. To determine  $a_{min}$  throughout this chapter we have set

$\delta = 0.1^4$  in the above equation and solved for  $a$ . The profile  $h_0$  in equation (4.6) is given by the normalization condition

$$\int_0^{y_1} dy h(y)^2 e^{-2A(y)} = 1,$$

and obtained explicitly as

$$h_0 = \left\{ e^{2(a-1)ky_s} (2(a-1)ky_s)^{-(1+\frac{2}{\nu^2})} \left( \Gamma \left[ \left(1 + \frac{2}{\nu^2}\right), 2(a-1)k(y_s - y_1) \right] - \Gamma \left[ \left(1 + \frac{2}{\nu^2}\right), 2(a-1)ky_s \right] \right) y_s \right\}^{-\frac{1}{2}}. \quad (4.7)$$

The matter action of the SM fields in Dirac spinor notation is given by

$$S_{mat} = \int d^5x \sqrt{-g} \mathcal{L}_{mat} = \int d^5x \sqrt{-g} \left( \frac{1}{2} (i\bar{\Psi} \Gamma^M D_M \Psi - iD_M \bar{\Psi} \Gamma^M \Psi) + M_\Psi(y) \bar{\Psi} \Psi \right), \quad (4.8)$$

where  $\Psi = (\psi_L, \psi_R)^T$  are the 5D fields and the capital index,  $M$ , runs over the five space time dimensions with the spinor fiber indices being summed over as  $\Gamma^M \equiv E_a^M \gamma^a$ , with  $\gamma^a \equiv (\gamma^\mu, \gamma^5)$ . The covariant derivative is  $D_M = \partial_M + \omega_M$  with the spin connection given by  $\omega_M = \frac{1}{8} \omega_{MAB} [\gamma^A, \gamma^B]$ . The funfbein and the inverse funfbein are given by

$$e_M^a = (e^{-A(y)} \delta_\mu^\alpha, 1), \quad E_a^M = (e^{A(y)} \delta_\alpha^\mu, 1).$$

The mass term coefficient,  $M_\Psi(y)$  in general depends on the extra dimension coordinate and  $\sqrt{-g} = e^{-4A(y)}$ . Following the standard ansatz, we decompose the fields into an extra dimensional profile field and SM 4D fields. The equations of motion of the profiles can be decoupled and written in the following convenient form

$$\partial_y (e^{-A-2Q} \partial_y (e^{Q-2A} \psi_L)) + m_n^2 e^{-Q-A} \psi_L = 0, \quad (4.9)$$

$$\partial_y (e^{-A+2Q} \partial_y (e^{-Q-2A} \psi_R)) + m_n^2 e^{Q-A} \psi_R = 0, \quad (4.10)$$

where we defined

$$Q(y) \equiv \int_0^y M_\psi(y') dy'. \quad (4.11)$$

We are going to consider two different choices for the above fermion bulk mass,  $M_\psi$ :

---

<sup>4</sup>We obtain, approximately,  $a_{min} \simeq 2 \frac{A(y_1)}{ky_1}$ , and for a physically acceptable model we usually require  $a \geq 2 \frac{A(y_1)}{ky_1}$ . The  $\delta$  criterion given above usually corresponds to an  $a_{min}$  smaller than this estimation which in turn leads to some fine tuning of the 5D parameters.

- Inspired by the standard RS choice  $Q_\psi^{RS}(y) = c_\psi k y$  one can chose a  $y$ -dependent bulk mass proportional to the warp factor  $A(y)$ . We call this the CGQ scenario [94, 63, 65, 95, 64]

$$Q_\psi(y) = c_\psi A(y) \quad (4.12)$$

- Alternatively one can consider a constant mass, and we denote this choice as the CPS scenario [66], (see also [96, 97])

$$Q_\psi(y) = c_\psi k. \quad (4.13)$$

As usual, imposing the proper boundary conditions on either left or right handed fields will ensure the existence of normalized chiral massless zero modes. Their expressions are:

$$[\text{CGQ}] \quad \begin{cases} u_R^0 &= f(-c_u) e^{(2+c_u)A(y)} \\ q_L^0 &= f(c_q) e^{(2-c_q)A(y)} \end{cases} \quad (4.14)$$

$$[\text{CPS}] \quad \begin{cases} u_R^0 &= f(-c_u) e^{(2+c_u)ky} \left(1 - \frac{y}{y_s}\right)^{-\frac{2}{\nu^2}} \\ q_L^0 &= f(c_q) e^{(2-c_q)ky} \left(1 - \frac{y}{y_s}\right)^{-\frac{2}{\nu^2}} \end{cases} \quad (4.15)$$

and we have defined<sup>5</sup>

$$f(c) \equiv \left\{ y_s \left( (1-2c)ky_s \right)^{\frac{1-2c}{\nu^2}-1} e^{(1-2c)ky_s} \times \left[ \Gamma \left( 1 - \frac{1-2c}{\nu^2}, (1-2c)k(y_s - y_1) \right) - \Gamma \left( 1 - \frac{1-2c}{\nu^2}, (1-2c)ky_s \right) \right] \right\}^{-\frac{1}{2}} \quad (4.16)$$

for the CGQ scenario. For the case of the CPS scenario one just needs to set  $c = 0$  *inside* the gamma functions, and leave everything else as is.

For generic values of  $\nu$  and  $y_s$  the eigenvalues and eigenfunctions (masses and profiles) of the KK fermion modes can be obtained by solving numerically equations (4.9) and (4.10).

It is useful to mention here an intuitive reason behind better lower bounds on the KK modes in this model. The electroweak relevant oblique parameters,  $S$  and  $T$  are proportional to the following dimension 6 operators [65, 93]:

$$|H \dagger D_\mu H|^2, \quad H^\dagger W_{\mu\nu} H B^{\mu\nu}.$$

Intuitively, due to the deviations of the metric from  $AdS_5$  near the IR brane, and more acute warping near that brane, all the KK modes, including the gauge boson KK modes, become

---

<sup>5</sup>In analogy with the usual RS profiles  $f(c) \equiv \sqrt{\frac{1-2c}{1-e^{(1-2c)ky_1}}}$ .

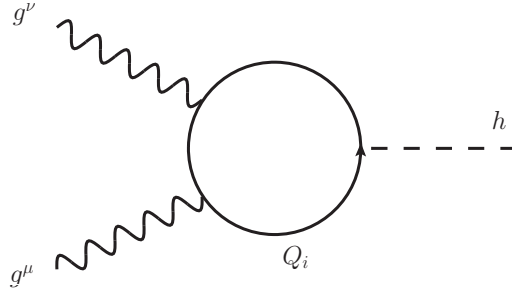


Figure 4.1: Loop diagram showing the contribution of the quark  $Q_i$  to the Higgs-gluon-gluon coupling. In the SM, the dominant contribution is through the top quark due to its large Yukawa coupling with the Higgs boson. In warped space models the heavier KK fermions contribute to the coupling with potentially large effects, either suppressing or enhancing the SM coupling, depending on the phases present in the different Yukawa-type operators present in the 5D action, and on the localization of the Higgs (see text for details).

more localized near the IR brane. As a result, for a Higgs field that is delocalized sufficiently from the IR brane, its couplings to these KK modes are suppressed, which results in lower bounds for the KK mode masses in these models. Obviously, as the Higgs field becomes more localized near the IR brane, these couplings become large (even larger than in the pure  $AdS_5$  case) and the bounds become worse. Therefore the success of this model is crucially dependent on the localization of the Higgs field along the 5th dimension.

### 4.3 Higgs Production through gluon fusion

In this section we solve numerically for the eigenvalues and eigenfunctions of Eqs. (4.9) and (4.10) with the goal of calculating the Higgs production rate through gluon fusion. (Analytic solutions are unfortunately not available).

In the SM, the main contribution to the Higgs coupling to gluons comes from a top quark loop correction. In warped extra dimensional models there are many heavy KK quarks with important couplings with the Higgs, and thus one needs to add all of their contributions to the loop (see Figure 4.1), so that the resulting cross section for the process  $gg \rightarrow h$  is

$$\sigma_{gg \rightarrow h}^{SM} = \frac{\alpha_s m_h^2}{576\pi} \left| \sum_Q \frac{y_Q}{m_Q} A_{1/2}(\tau_Q) \right|^2 \delta(\hat{s} - m_h^2), \quad (4.17)$$

with  $\tau_Q \equiv m_h^2/4m_Q^2$ ,  $\hat{s}$  being the  $gg$  invariant mass squared and  $Q$  representing the physical

fermions with physical Yukawa couplings  $Y_Q$  and masses  $m_Q$ . The form factor is given by

$$A_{1/2}(\tau) = \frac{3}{2}[\tau + (\tau - 1)f(\tau)]\tau^{-2}, \quad (4.18)$$

with

$$f(\tau) = \begin{cases} [\arcsin\sqrt{\tau}]^2 & \tau \leq 0 \\ -\frac{1}{4} \left[ \ln \left( \frac{1+\sqrt{1-\tau^{-1}}}{1-\sqrt{1-\tau^{-1}}} \right) - i\pi \right]^2 & \tau > 1. \end{cases} \quad (4.19)$$

The relevant quantity that we wish to evaluate is the effective coupling

$$c_{hgg} = \sum_Q \frac{y_Q}{m_Q} A_{1/2}(\tau_Q), \quad (4.20)$$

where  $y_Q$  is the 4D Yukawa coupling of fermion  $Q$ , in the mass eigenbasis, and  $m_Q$  is its mass. In the gauge basis (the basis *before* spontaneous EW symmetry breaking) the Yukawa couplings are given by the following overlap integral along the fifth dimension,

$$Y_{Q_i U_k}^u = Y^u \int_0^{y_1} dy e^{-4A(y)} h(y) Q_L^{u,(i)}(y) U_R^{(k)}(y), \quad (4.21)$$

and can be written as the following infinite dimensional Yukawa matrix,  $\mathbf{Y}$

$$\begin{pmatrix} q_L^0, & Q_L^i, & U_L^j \end{pmatrix} \begin{pmatrix} Y_{q_L u_R}^u & 0 & Y_{q_L U_R^b}^u \\ Y_{Q_L^i u_R}^u & 0 & Y_{Q_L^i U_R^b}^u \\ 0 & Y_{U_L^j Q_R^a}^{u*} & 0 \end{pmatrix} \begin{pmatrix} u_R^0 \\ Q_R^a \\ U_R^b \end{pmatrix}. \quad (4.22)$$

In the same gauge basis we can also write down the infinite dimensional fermion mass matrix

$$\mathbf{M} = \begin{pmatrix} Y_{q_L u_R}^u v_4 & 0 & Y_{q_L U_R^b}^u v_4 \\ Y_{Q_L^i u_R}^u v_4 & M_Q & Y_{Q_L^i U_R^b}^u v_4 \\ 0 & Y_{U_L^j Q_R^a}^{u*} v_4 & M_U \end{pmatrix}. \quad (4.23)$$

where  $v_4 = 174$  GeV is the Higgs vacuum expectation valued (VEV), and  $M_Q$  and  $M_U$  are the  $n$ -dimensional diagonal matrices of the tower of  $n$  KK modes mass eigenvalues.

We proceed here by considering an effective field theory with only 3 KK levels, but we refer the reader to Section IV for a discussion involving the use of the full tower of KK fields. In our effective approach here, the previous matrices  $\mathbf{M}$  and  $\mathbf{Y}$  become  $7 \times 7$  truncated mass and Yukawa matrices. In order to use Eq. (4.20), we diagonalize numerically the mass

matrix  $\mathbf{M}$  above by a bi-unitary transformation. Performing the same transformation on the Yukawa matrix,  $\mathbf{Y}$ , one can finally use Eq. (4.20) to calculate the Higgs production cross section<sup>6</sup>.

In all our numerical analysis we took  $k = 10^{18}$  GeV fixed, and then tuned all other parameters in such a way that all of the scenarios yield approximately the same zero mode masses (the SM quark masses) and the same lightest KK mode mass ( $\simeq 2.1$  TeV). While this value for the lightest KK mass is already dangerously low for RS scenarios, in general warped models with modified  $AdS_5$  metrics (like the CGQ and CPS scenarios considered here), such low KK masses can be safe from electroweak precision constraints as well as flavor constraints [94, 63, 65, 95, 64, 66]. The regime in which this happens is such that  $kL_1 \simeq 0.2$ , and so we restrict ourselves to that region of parameter space when considering the modified models.

It is important to note that the zero mode masses are sensitive to the values of the Higgs localization parameter  $a$  through Yukawa couplings

$$y = \frac{Y^{5D}}{\sqrt{k}} \int_0^{y_1} dy e^{-4A(y)} h(y) q_L^0(y) u_R^0(y). \quad (4.24)$$

Using equations (4.6), (4.14) and (4.15) the above integral can be evaluated

$$y = -\frac{h_0}{f(c_q)f(c_u)} y_s ((a - c_q + c_u)(ky_s))^{\frac{c_u - c_q}{\nu^2} - 1} e^{ky_s(a - c_q + c_u)} \times \left( \Gamma \left[ \left( \frac{c_q - c_u}{\nu^2} + 1 \right), (a - c_q + c_u)ky_s \right] - \Gamma \left[ \left( \frac{c_q - c_u}{\nu^2} + 1 \right), (a - c_q + c_u)k(y_s - y_1) \right] \right).$$

In order to keep the 5D Yukawa couplings  $Y^{5D}$  fixed for all of these models<sup>7</sup> while requiring the correct SM quark masses, we have to set the values of  $c_q$  and  $c_u$  separately for each value of  $a$ , and for each different scenario. On a technical level, to be able to produce a correct top quark mass we had to set  $Y_{top}^{5D} \simeq 3$  in all cases (so that even when we write  $Y^{5D} \simeq 1$  in the left panel of Figure 4.2 we are still using  $Y_{top}^{5D} \simeq 3$ ).

To proceed further we need to include the flavor families of the SM, and to do so we will consider a simplified version of the SM model, that is, we take a *SM-like* setup in which the 5D Yukawa couplings are diagonal, and thus we will ignore flavor inter-mixings in our loop

---

<sup>6</sup>If flavor families are included, this transformation in general will not diagonalize the full Yukawa matrix  $\mathbf{Y}$  leading thus to tree-level Higgs mediated flavor changing currents [101, 80].

<sup>7</sup>For a fair comparison among scenarios, we maintain the value of  $Y^{5D}$  fixed in all of them, given that the production cross section is proportional to  $(Y^{5D})^2$ .

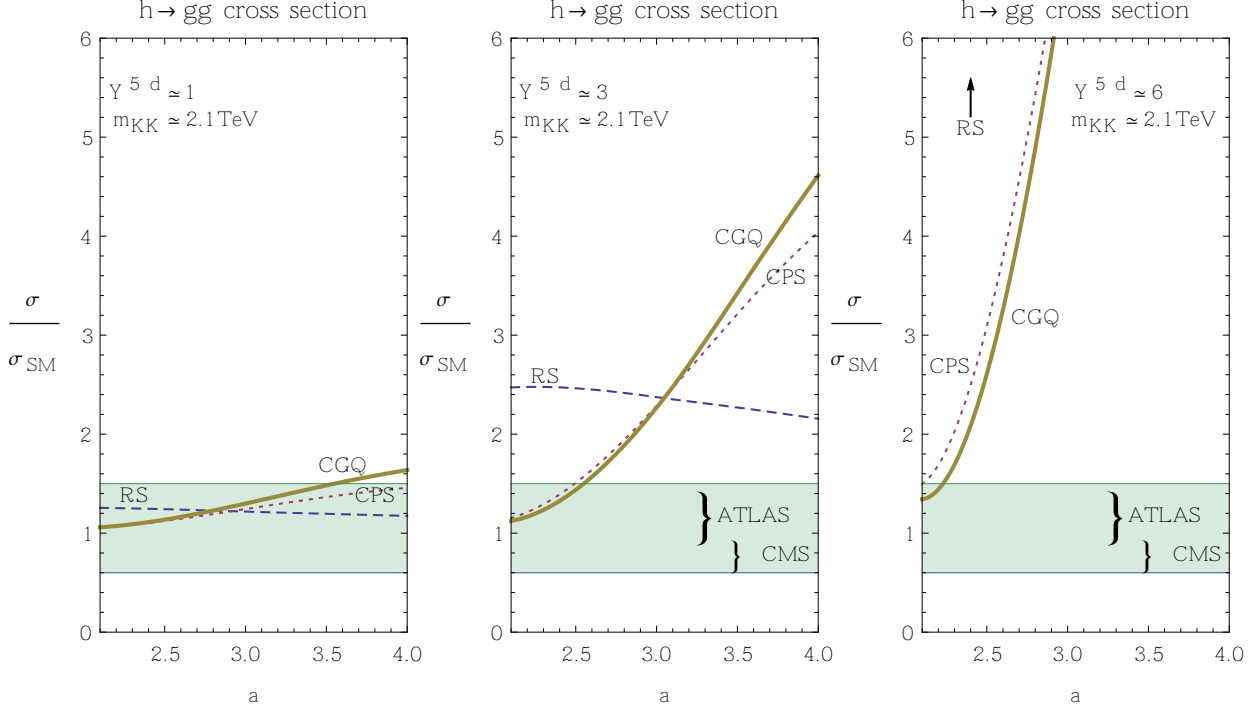


Figure 4.2: Higgs production rate ratio to Standard Model prediction as a function of the Higgs localization parameter,  $a$ . In all scenarios we consider an effective field theory consisting of a tower of 3 KK modes. The dashed line (blue) corresponds to the RS scenario with bulk Higgs. The solid and dotted lines correspond to the modified  $AdS_5$  scenarios CGQ ( $\nu = 0.5$ ,  $kL_1 \simeq 0.27$ ) and CPS ( $\nu = 0.5$ ,  $kL_1 \simeq 0.29$ ) and the lightest KK mass is about 2.1 TeV in all models. The 5D Yukawa coupling is varied between  $Y^{5D} \sim 1$  (left panel),  $Y^{5D} \sim 3$  (middle panel) and  $Y^{5D} \sim 6$  (right panel). The shaded regions show the experimental bounds from CMS and ATLAS.

calculation. With this simplifying assumption, it is straightforward to add the contributions of all the fermions running in the loop. This is of course not a viable scenario of flavor, but it does illustrate fairly the effects on Higgs production. Thus we consider the presence in the loop of five light quarks (which have negligible effect) and their associated KK quarks (which yield the main new contributions), as well as one SM top quark and its associated KK top quarks (the overall contribution from the top sector is actually very close to the SM top contribution). This simplified flavor structure for fermions is used in the three scenarios we consider, i.e. bulk-Higgs-RS, CGQ and CPS, and so we can obtain fair comparisons between the different predictions for Higgs production cross section generated by each model.

In the case of the CGQ scenario, the fermion bulk mass term is  $M_i = c_i A'(y)$  (see Eqs. (4.11)

and (4.12)) and we used the values  $\nu = 0.5$ , and  $kL_1 \equiv kL(y_1) = 0.27$  for the curvature radius as defined in equation (4.4). The  $\delta = 0.1$  criterion yields  $a_{min} \simeq 2.09$  and the values for  $c_q$  ( $\simeq -c_u$ ) are being slightly decreased as  $a$  becomes larger in order to keep the  $Y^{5D}$  constant (as explained above). The CPS case is essentially the same model but with a constant fermionic bulk mass of  $M_i = c_i k$  (see Eqs. (4.11) and 4.13)). We have again used the value  $\nu = 0.5$ , but in order to keep the lightest KK mass fixed at the same value as the other models we set  $kL_1 \equiv kL(y_1) = 0.29$  for the curvature radius. The  $\delta = 0.1$  criterion this time yields  $a_{min} \simeq 2.06$ . Finally the RS scenario (with a bulk Higgs) is obtained in the limit  $\nu \gg 1$  and  $kL_1 \rightarrow 1$ . The numerical results obtained in this limit match the results obtained using the analytical RS formulae [77, 1], providing thus a nontrivial consistency check of the procedure.

The results are shown in Figure 4.2, in which we plot the ratio of Higgs production cross section relative to the SM one, as a function of the Higgs localization parameter  $a$  for the three models. The solid and dotted lines correspond to predictions from the CGQ and CPS models, respectively, while the dashed line represents the prediction of the RS scenario (with fermions and Higgs in the bulk). For each model, the numerical calculation involves the contributions from light quarks and 3 KK modes in the loop. The three panels correspond to different values for the 5D Yukawa coupling:  $Y^{5D} \sim 1$  on the left side,  $Y^{5D} \sim 3$  in the middle, and  $Y^{5D} \sim 6$  on the right side. The shaded regions represent experimental restrictions on cross sections from CMS ( $\mu \equiv \frac{\sigma}{\sigma_{SM}} = 0.8 \pm 0.22$ ) and ATLAS ( $\mu \equiv \frac{\sigma}{\sigma_{SM}} = 1.2 \pm 0.3$ ) results [25].

From all panels, it is clear that the behaviour of the CGQ and CPS models is very similar. In particular, both are very sensitive to the Higgs localization parameter  $a$ , while the RS model is much more stable against variations in  $a$ . Second, one can see that both modified warped models alleviate the enhancements in Higgs production present in RS models, but only for a small region of  $a$ , fortuitously the same region for which the electroweak constraints are satisfied [94, 63, 65, 95, 64]. The restriction becomes more stringent with increased  $Y^{5D}$ , so that for  $Y^{5D} \sim 1$ , the  $a$  parameter can be anywhere between its minimal value  $a_{min}$  and about 3 – 4 (depending on the CGQ model or the CPS model), while for  $Y^{5D} \sim 6$  the parameter  $a$  is constrained to be in a really small region around  $a_{min}$ . By comparison, the RS model seems “safe” when  $Y^{5D} \sim 1$ <sup>8</sup>, but then is completely disfavoured for  $Y^{5D} \sim 3$  and  $Y^{5D} \sim 6$

---

<sup>8</sup>Of course, for such low KK masses the minimal RS scenario without custodial protection is already excluded due to precision electroweak tests and flavor bounds. In fact the smaller the value of  $Y^{5D}$  the worse the flavor bounds become [62, 71].

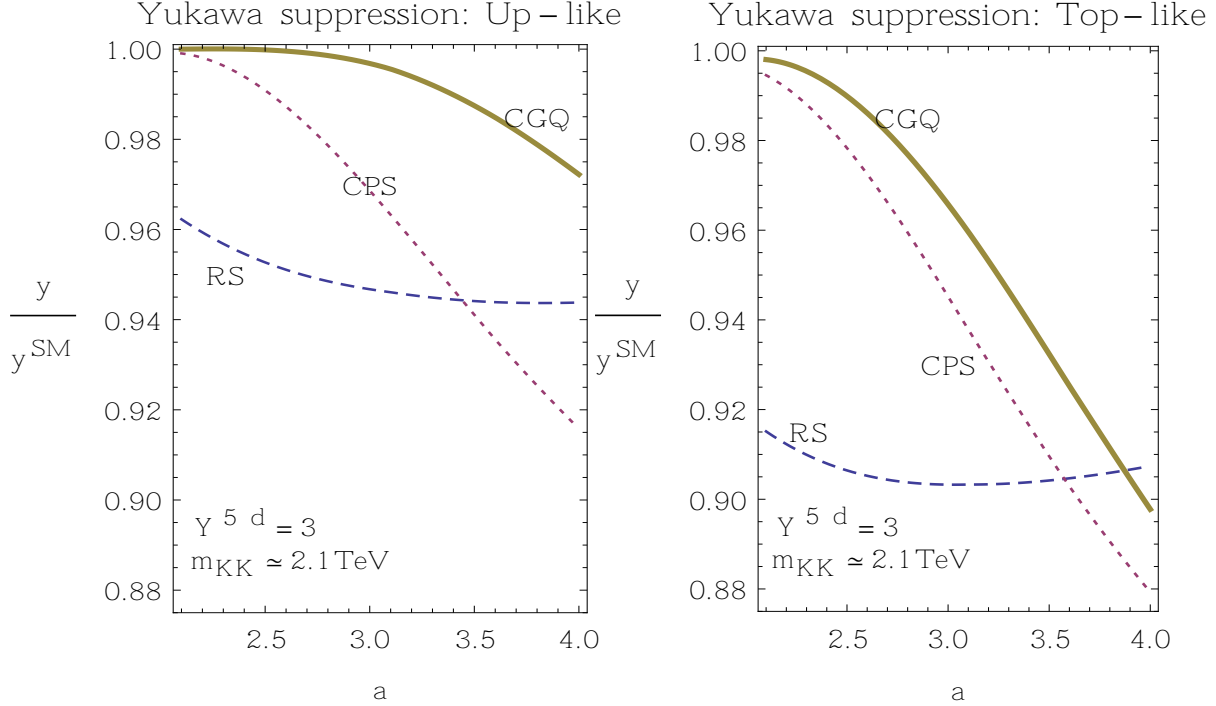


Figure 4.3: Quark Yukawa couplings relative to their SM values, of a light quark (left panel) and the top quark (right panel) as a function of the Higgs localization parameter,  $a$ . In all scenarios we consider an effective field theory consisting of a tower of 3 KK levels with  $Y^{5D} \sim 3$  and with the lightest KK mass at about 2.1 TeV. The dashed line (blue) corresponds to RS with bulk Higgs. The solid and dotted lines correspond to the CGQ ( $\nu = 0.5$ ,  $kL_1 \simeq 0.27$ ) and CPS ( $\nu = 0.5$ ,  $kL_1 \simeq 0.29$ ) models of general metrics respectively.

(where it lies outside the range of the figure).

The main message from these plots is that in the modified warped scenarios, the Higgs should be as de-localized as possible otherwise, if the Higgs is pushed towards the IR, the bounds become even worse than in RS (or at least the bounds we have considered here, namely those coming from LHC Higgs production). The reason for this behaviour with the parameter  $a$  is that in the CGQ and CPS scenarios, the warp factor grows faster than in RS near the IR boundary. The effect of this is to actually concentrate the KK modes closer to the IR brane, and if one de-localizes sufficiently the Higgs profile away from the IR, the overlap integral between Higgs and KK fermions is suppressed with respect to the RS case. This leads to suppressed corrections to Higgs production, and we believe that this is also the origin for the suppressed contributions to electroweak and flavor observables.

As a further check, in Figure 4.3 we plot the relative size of light quarks Yukawa couplings (left

panel) and top quark Yukawa coupling (right panel) as a function of the Higgs localization parameter  $a$ , where both effects are computed by considering a truncated tower of just 3 KK fermion modes for each scenario. We choose  $Y^{5D} \sim 3$  in all plots and here again we observe that the suppressed Yukawa couplings in the RS model are relatively independent of the Higgs de-localization, while in both the CPS and the CGQ scenarios, the suppression in these couplings depends dramatically on the localization parameter  $a$ . These effects confirm the findings of the previous figure, namely that for small  $a$  (Higgs very de-localized) the modified warped scenarios produce very little effects in the Higgs sector, but these effects grow very quickly as the Higgs is pushed towards the TeV brane. The RS dependence on Higgs localization is much milder, but the effects are quantitatively quite large for the low KK masses considered here. We note here that even though the top Yukawa coupling can be quite suppressed, the scenarios still predict an enhancement in Higgs production. The reason is that the reduction produced by suppressed top couplings is balanced by the positive contribution due to the top KK tower. To this contribution, one must add the positive contributions of the other 5 towers of KK fermions (associated to the 5 other SM quarks) [77].

Finally let us comment again that we have focused on a simplified version of the SM in which we ignored the flavor mixing between families, in order to simplify the sums in the loop calculation. Our main goal was to compare Higgs production among different models and study the general effects of the metric modification relative to the usual RS setup. A realistic scenario including the full flavor structure is underway, but the results should not be much different from the ones presented here, since flavor inter-mixings are not expected to produce big changes in the contributions to the loops generating the  $hgg$  coupling.

## 4.4 Decoupling of the Heavy KK modes

In this section, we consider the effect of including the full tower of the KK modes on the evaluation of the Higgs production cross section, by performing the infinite sums analytically. Following the procedure given in [1, 77] we obtain the following expression for  $c_{hgg}$ , Eq. (4.20),

$$c_{hgg} = \text{Tr}(\mathbf{Y}\mathbf{M}^{-1}) + \sum_{\text{light}} \frac{y_Q}{m_Q} (A_{1/2}(\tau_Q) - 1) \quad (4.25)$$

$$= -2v_4 \sum_{i,j} \frac{Y_{Q_L i U_R j}^u Y_{U_L j Q_R i}^{u*}}{M_{Q_i} M_{U_j}} + \frac{y_Q}{m_Q} \Big|_{\text{light}} A_{1/2}(\tau_{Q_{\text{light}}}). \quad (4.26)$$

Here the couplings are the elements of the Yukawa matrix  $\mathbf{Y}$  given in Eq. (4.22) and  $\mathbf{M}$  is the fermion mass matrix in the gauge basis given by Eq. (4.23). We have also used the fact that  $\mathbf{Y} = \frac{\partial \mathbf{M}}{\partial v_4}$  and therefore  $\text{Tr}(\mathbf{Y}\mathbf{M}^{-1}) = \text{Tr}(\frac{\partial \mathbf{M}}{\partial v_4} \mathbf{M}^{-1}) = \frac{\partial \ln \text{Det}(\mathbf{M})}{\partial v_4}$ .

Since the form factor,  $A_{1/2}$  is negligible for the light fermion generations, we can neglect the last term in Eq. (4.25), and using Eq. (4.21) we have

$$c_{hgg} = -2v_4 Y^u Y^{u*} \sum_{i,j} \int dy dy' e^{-4A(y)} e^{-4A(y')} \frac{Q_L^{(i)}(y) Q_R^{(i)}(y')}{M_{Q_i}} \frac{U_R^{(j)}(y) U_L^{(j)}(y')}{M_{U_j}} h(y) h(y'), \quad (4.27)$$

where the Higgs profile is given in Eq. (4.6). The infinite sums in this equation can be performed using the completeness of the Sturm-Liouville system. We have (see the Appendix C)

$$\sum_{n=1}^{\infty} \frac{\hat{U}_R^{(n)}(y) \hat{U}_L^{(n)}(y')}{m_n} = e^{Q(y)-Q(y')} \left[ \theta(y' - y) - \frac{\int_0^{y'} e^{A-2Q}}{\int_0^{y_1} e^{A-2Q}} \right] \quad (4.28)$$

$$\sum_{n=1}^{\infty} \frac{\hat{Q}_L^{(n)}(y) \hat{Q}_R^{(n)}(y')}{m_n} = -e^{Q(y')-Q(y)} \left[ \theta(y' - y) - \frac{\int_0^{y'} e^{A+2Q}}{\int_0^{y_1} e^{A+2Q}} \right]. \quad (4.29)$$

Inserting this back into Eq. (4.27) for  $c_{hgg}$  we can finally calculate the  $hgg$  cross section. Figure 4.4 shows the result of evaluating the Higgs production cross section using the infinite KK tower, compared to the result obtained using effective field theories with one, two and three KK modes. As we can see, the result obtained using a very small number of modes converge quickly to the result using infinite sum, which means that the heavy KK modes decouple from the evaluation of the cross section. The decoupling of heavy modes is particularly true in the region where the Higgs production cross section is safe from large enhancements from the presence of KK modes in the loop. This observation seems to imply that at least for the observable considered here, the Higgs production rate, the 5D warped models with bulk Higgs, which are essentially valid only up to  $\Lambda_{UV} \sim \mathcal{O}(10 \text{ TeV})$ , are calculable and the effects of higher order operators should be suppressed (see also [1]).

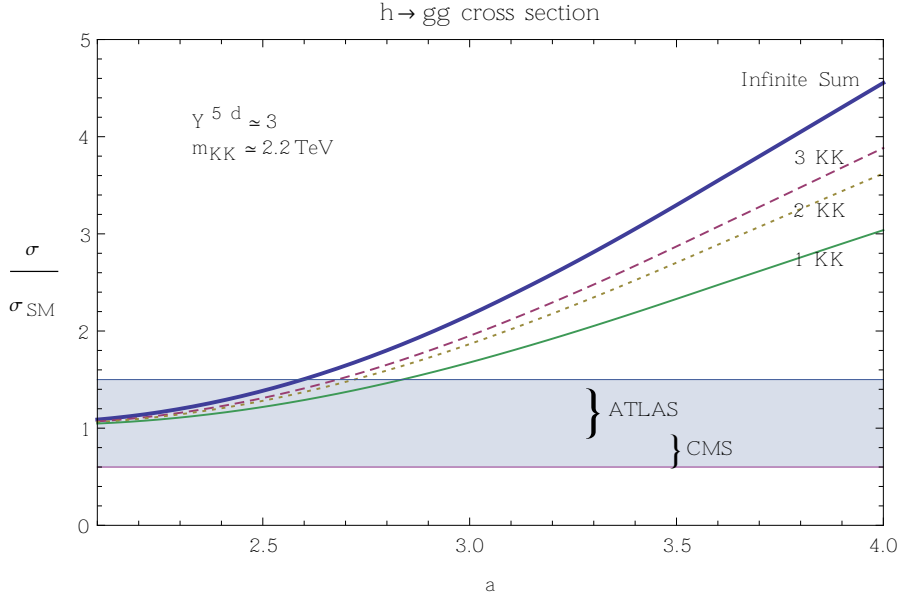


Figure 4.4: Higgs production rate via gluon fusion in the CGQ scenario. The solid thick line (blue) shows the contribution due to the full tower of KK modes. The dashed (red), dotted (khaki) and thin solid (green) lines show the contribution due to a tower of 3, 2 and 1 KK modes respectively. The shaded region shows the experimental bounds from CMS and ATLAS.

## 4.5 Conclusions

In this chapter we calculated the Higgs production rate via gluon fusion in 5D scenarios with modified  $AdS_5$  metrics. In the SM, the Higgs production cross section is determined by the coupling of the top quark to the Higgs field. Just like in RS, the deviations from the SM in modified  $AdS_5$  models are caused by the presence of extra KK fermion towers, associated to each of the six SM quarks, and their couplings to the Higgs field. These KK fermions circulate through the loop responsible for the Higgs production through gluon fusion, and they can lead to large enhancements in the Higgs production cross section. In RS models with fermions and Higgs fields propagating in the bulk, depending on the values of the 5D Yukawa couplings, the enhancements can reach 50% if the lightest KK mass is  $\sim 2$  TeV (at odds with ATLAS and CMS data). In fact the new data from LHC Higgs searches have become a stringent bound on warped scenarios, to be considered together with flavor and electroweak precision tests.

The couplings with the KK fields are generated by the overlap of the KK fermions wave

functions and the Higgs profiles along the fifth dimension, thus the localization of these fields is crucial to the calculation. In the general warped scenarios, the KK fermions are pushed *towards* the IR brane compared to the RS model due to the metric growth near that boundary. On the other hand the localization of the Higgs profile along the 5th dimension is controlled by a free parameter  $a$ : the smaller the values for  $a$ , the less localized the Higgs profile<sup>9</sup>. Our results show that a more de-localized Higgs field leads to a more SM-like Higgs production, due to suppressed overlap integrals between Higgs and KK fermions. Moreover, this seems to happen in the parameter region which is also safe from electroweak and flavor precision tests. We have also shown, by comparing the results obtained using a small number of modes with the effects of the whole KK tower, that the former converges quickly to the latter in the same region, leading further support to the validity of our calculation.

Thus we have shown that, based on results from Higgs production, the modified  $AdS_5$  scenarios considered here are consistent with the experimental results for light KK masses of  $\sim 2$  TeV (unlike RS models). This was a non-trivial check, and necessary, since while these scenarios had proved to be safer in terms of precision tests (electroweak and flavor) compared to RS, the new Higgs production data from the LHC might have been in conflict with the effects from the models. Our results confirm the viability of these scenarios, which allow for new physics at lower scales than conventional RS models and thus could yield signals at the LHC in the near future.

---

<sup>9</sup>As we mentioned before, holographically this parameter corresponds to the dimension of the Higgs condensate operator and therefore its value is crucial in obtaining the correlation functions in the strongly coupled *modified*-CFT theory.

# Chapter 5

## Warped Flavor Symmetry

### 5.1 Introduction

The discovery at the LHC of a SM-like Higgs boson with a mass of 125 GeV was a huge step forward in confirming the validity of the Standard Model (SM) and probing the electroweak symmetry breaking mechanism. But despite its experimental success, the SM still fails to provide an explanation for the origin and observed pattern of fermion masses and mixings.

In the quark sector, the masses are extremely hierarchical, with the top much heavier than the rest of the quarks and with a strong ordering. In the up sector, the masses are separated by three orders of magnitude, while in the down sector the mass ratios are separated by two orders of magnitude. The quarks also exhibit mixing patterns given by three small mixing angles and a large (CP) phase. In the lepton sector, the charged lepton masses obey a similar hierarchical pattern as the down-type quarks. On the other hand, neutrino masses are known to be very small (though not known exactly) and their square mass differences imply a closer mass pattern,  $\Delta m_{31(32)}^2 : \Delta m_{21}^2 \sim 10^2 : 1$ . Leptons appear to mix maximally and given the special characteristics of neutrinos this has been long-seen as pointing towards a different flavor origin between quarks and leptons, and also to the necessity of introducing new physics. After the successful measurement of the neutrino mixing angle  $\theta_{13}$  by the Daya Bay [105, 106], T2K [107, 108], MINOS [109, 110], RENO [111] and Double Chooz [112, 113] Collaborations, the determination of the neutrino mass hierarchy has become a priority for theoretical studies and future neutrino experiments. A great deal of theoretical work in

this area has been trying to provide answers, based on such diverse frameworks as see-saw mechanisms [114, 115, 116, 117, 118, 119, 120], Abelian [121, 122, 123] and non-Abelian [124, 125, 126, 127, 128, 129, 130, 131, 132, 133, 134, 135, 136, 137, 138, 139, 140, 141] symmetries imposed on the leptonic sector (both charged and neutral), and many texture structures for leptonic mass matrices, including modifications of accepted paradigms, such as tri-bi-maximal [142, 143, 144, 145, 146, 147], bi-maximal [148, 149, 150, 151, 152, 153] and democratic [154, 155, 156] neutrino mixing matrices. While various attempts to unify the description of quarks and leptons already exist (mostly based on quark-lepton complementarity [157, 158, 159, 160, 161, 162, 163, 164, 165, 166, 167, 168, 169, 170]), an attractive possibility would be that quarks and leptons obey the same symmetry at a higher scale, which is then slightly broken at lower scales, yielding different patterns for masses and mixing for the quarks/leptons than for the neutrinos. This is the scenario we plan to investigate here in which small symmetry breaking terms have very different effects on quark and leptons due to the geometry of the scenario.

The confirmed existence of a Higgs-like boson at CERN still requires a mechanism to stabilize its mass against large radiative corrections. One elegant way to address both the hierarchy problem and the fermion flavor hierarchy problem relies on introducing a warped extra dimension. Warped extra dimensional models were first introduced to deal with the hierarchy problem of the SM [32, 33] by introducing an extra dimension to produce a five dimensional anti-de Sitter ( $AdS_5$ ) geometry bounded by two hard walls (branes) along the extra dimension, referred to as the Planck (or UV) brane and the TeV (or IR) brane. Allowing for exponential modulation along this compact extra dimension, from the gravity scale down to the weak scale [32, 33], then produces naturally the well known weak-Planck mass hierarchy. The original Randall-Sundrum (RS) model localized all SM fields on the IR brane, leading to severe flavor violation bounds on the new physics scale.

It was later shown that if the fermions were allowed to propagate in the bulk of the extra dimension [86, 34, 99, 91], the same model could address the flavor hierarchy problem of the SM as well. The model thus emerges as a geometric theory of flavor. Localizing the Higgs on the IR brane with anarchic order-one couplings to the bulk fermions, the profiles of the fermion zero-modes can be adjusted to reproduce the observed Yukawa couplings in the low energy theory. Since the first and second generation fermions are localized towards the UV brane, they inherit substantial flavor protection from the “RS-GIM mechanism” [37]. However, allowing the SM fields to propagate in the bulk means that, from an effective 4D point of view, a tower of KK fermions exists for all the SM fields, yielding enhanced

contributions to electroweak and flavor observables in the SM [93, 171, 172, 91, 89, 88, 90, 37]. This effect imposes a stringent bound on the scale of new physics of some  $\sim 10$  TeV [47, 71] and hence renders these models completely out of the reach of current experiments. Some solutions can be proposed to relieve these restrictions. One way would be to extend the gauge symmetry of the model by introducing an  $SU(2)_R$  gauge sector with custodial protection [92, 91, 93]. The basic idea is to align the down-type Yukawa couplings using the additional symmetry, so that the primary sources of intergenerational mixing are the up-type Yukawa couplings. Since the dominant constraints on FCNCs come from the down-type sector, the constraint on KK masses is substantially relaxed. A different approach to address the issue is through a slight modification of the warping factor along the extra dimension allowing it to deviate slightly from the  $AdS_5$  metric [63, 94, 65]. This deviation is such that the warping is more drastic near the TeV brane, while the background becomes more  $AdS_5$ -like near the Planck brane. These type of metric solutions can help suppress dangerous contributions to the electroweak and flavor observables reducing the constraints on new physics down to about  $\sim 1$  TeV.

Another source of interesting new contributions in these models has been shown to originate in the Higgs production rate through gluon fusion [80, 1, 2].

Interestingly, in the modified 5D metric scenarios the region of parameter space in which the dangerous contributions to flavor and electroweak precision observables are small is the same as the region in which the new contributions to the Higgs production cross section are also small (and thus safe). Moreover, this is achievable only when the Higgs field in these models is allowed to leak considerably into the bulk.

In the context of warped extra dimensional models with  $\mathcal{O}(1)$  5D Yukawa couplings and with no structure a priori (*i.e.*, flavor anarchy), one can easily generate the hierarchical structure of the quark and charged lepton sectors while, due to large mixing angles, the neutrino sector must be treated differently. In particular, in [173], it was shown that if the Higgs leaks sufficiently into the bulk it is possible that the (exponentially small) neutrino wave functions become independent on the flavor structure of the 5D neutrino mass parameters ( $c_\nu^i$ ) and thus the 4D neutrino flavor structure depends directly on the flavor structure of the 5D neutrino Yukawa couplings.

In this chapter, we propose [3, 4] a unified picture of fermion masses and mixings in the context of a warped extra dimensional model with pure  $AdS_5$  and modified  $AdS_5$  background metrics, and with all the SM fields in the bulk, including the Higgs. In this picture, the same

flavor symmetric structure is imposed on all the fermions of the SM, including neutrinos. Small flavor breaking effects are exponentially enhanced in the quark and charged lepton sectors, thus producing hierarchical masses and mixings. With a sufficiently leaked Higgs, the neutrino wave functions are flavor-blind and the flavor structure is governed by the 5D neutrino Yukawa flavor structure.

As expected, the results are similar in both type of metrics indicating that the precise nature of the flavor symmetry or the precise nature of the metric solution is not crucial for the main property of the scenarios, namely that in the neutrino sector, flavor observables are directly linked to the fundamental flavor symmetry, while in the quark and charged lepton sectors, the flavor symmetry is washed-out and the observed hierarchies depend on the small flavor symmetry breaking terms.

This chapter is organized as follows. We summarize the features of the model in Section 5.2, with particular emphasis on fermion mass generation. We explore an implementation of a democratic flavor symmetry in Section 5.3. We summarize our results and conclude in Section 5.4. We leave the details of some of the calculation for the Appendix D.

## 5.2 Fermion masses in warped space

We consider a 5D warped space with the extra dimension compactified and allow all SM fields to propagate in the following generalized warped space-time metric:

$$ds^2 = e^{-2A(y)} \eta_{\mu\nu} dx^\mu dx^\nu - dy^2, \quad (5.1)$$

$\eta_{\mu\nu} = \text{diag}(1, -1, -1, -1)$  being the flat metric. The 5-th dimension,  $y$ , is bounded by two branes localized at  $y = 0$  and  $y = y_1$  and  $A(y)$  is a model-dependent function. As mentioned in the introduction, some generalized warped models can be safe from precision electroweak tests and flavor bounds for very low KK masses. With this advantage in mind, we consider the modified- $AdS_5$  scenario with the following warp exponent [94, 174]:

$$A(y) = ky + \frac{1}{\nu^2} \ln \left( 1 - \frac{y}{y_s} \right), \quad (5.2)$$

where  $k \sim M_{Pl}$  is the  $AdS_5$  curvature, expected to be of the order of the Planck mass scale,  $y_s$  is the position of the metric singularity, always chosen to be outside of the physical region,  $y_s > y_1$ , and  $\nu > 0$  is a model parameter taken to be real. This parameter, alongside with  $\Delta = y_s - y_1$ , the distance between the location of the metric singularity and the IR brane,

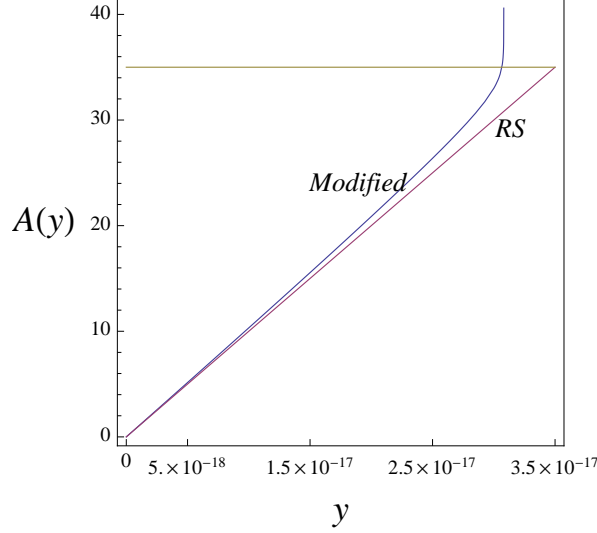


Figure 5.1: The modified- $AdS_5$  warp factor  $A(y)$  versus the standard RS warp exponent,  $y$ . The horizontal line corresponds to  $ky = 35$ . For the same amount of warping, the modified scenario requires a shorter length scale along the 5-th dimension.

measures the departure of the metric from the pure  $AdS_5$  background. The smaller the values of  $\Delta$  and  $\nu$ , the more modified the metric; intuitively, the singularity has a larger effect on the physics at the IR brane as it gets closer to it. One can calculate the curvature along the 5th dimension and arrive at

$$R(y) = 8A''(y) - 20(A'(y))^2. \quad (5.3)$$

The curvature radius,  $L(y) = \sqrt{-20/R}$ , in units of  $k$  along the fifth dimension is then given by

$$kL(y) = \frac{k\Delta}{\sqrt{1 - 2\nu^2/5 + 2\nu^2k\Delta + (\nu^2k\Delta)^2}}. \quad (5.4)$$

One can see that for values of  $\nu > \sqrt{5/2}$ , this function has a minimum before the singularity and therefore, the curvature can change sign within the physical region. For simplicity, following [65], we impose that this minimum is located outside of the physical region and hence the curvature radius is a monotonically decreasing function between the UV and the IR branes.

The more familiar RS metric is recovered by taking the limits  $\nu \rightarrow \infty$  and  $y_s \rightarrow \infty$ , obtaining  $A(y) = ky$ , with the curvature radius being constant,  $kL = 1$ . In Figure 5.1, we compare the two metrics and plot the warp exponent function  $A(y)$  for the  $AdS_5$  and the modified- $AdS_5$  cases. We can see that the amount of warping near the IR brane at around  $ky = 35$  is larger

for the modified- $AdS_5$ . Thus, as the figure indicates, the same amount of warping from the UV brane to the IR brane in the modified scenario requires a slightly smaller length of the 5-th dimension and hence an IR brane slightly closer to the UV brane. The curvature radius (Eq. 5.4) at the UV brane is approximately equal for the pure and modified  $AdS_5$  spaces with,  $ky(y) \simeq 1$ . In contrary, at the IR brane, as  $kL(y)$  is a monotonically decreasing function,  $ky(y)$  assumes its minimal value for the modified  $AdS_5$  space and hence  $kL_1 \equiv kL(y_1)$  is a good measure of the amount of deviation from the pure  $AdS_5$  space with constant curvature radius.

The 5D fermion Lagrangian density with Dirac neutrinos is

$$\begin{aligned} \mathcal{L}_q = & \mathcal{L}_{kinetic} + M_{q_i} \bar{Q}_i Q_i + M_{u_i} \bar{U}_i U_i + M_{d_i} \bar{D}_i D_i + (Y_{ij}^{u5D} H \bar{Q}_i U_j + h.c.) \\ & +(Y_{ij}^{d5D} H \bar{Q}_i D_j + h.c.) + (Q_i \rightarrow L_i, U_i \rightarrow N_i, D_i \rightarrow E_i) \end{aligned} \quad (5.5)$$

where,  $i, j$  are flavor indices and the 5D Yukawa parameters,  $Y_{ij}^{5D}$ , are dimension-full quantities of  $\mathcal{O}(1) \times \sqrt{k}$ .  $Q_i$  ( $L_i$ ) are 5D quark (lepton) fields for  $SU(2)$  doublets while  $U_i$  ( $N_i$ ) and  $D_i$  ( $E_i$ ) are  $SU(2)$  singlet quark (lepton) fields. The bulk mass,  $M_i$ , originating from the momentum along the 5-th dimension, can be taken in general to be  $y$ -dependent. To be able to compare, we choose it such that it coincides with its usual definition in RS models, and express it in units of the 5-th dimension curvature,  $k$ , as  $M_{\psi_i} = c_{\psi}^i k$ , where  $c_{\psi}^i$  are localization parameters, dimensionless quantities of  $\mathcal{O}(1)$ , and  $\psi_i$  runs over all SM quarks and leptons<sup>1 2</sup>. Dimensional reduction then yields the normalized profile for the fermion and the Higgs fields along the bulk of the extra dimension,  $q_L^{0,i}(y)$ ,  $u_R^{0,i}(y)$  and  $h(y)$ , which are given by

$$q_L^{0,i}(y) = q_0^i e^{(2-c_q^i)A(y)} \quad (5.6)$$

$$u_R^{0,i}(y) = u_0^i e^{(c_u^i+2)A(y)} \quad (5.7)$$

$$h(y) = h_0 e^{aky} \quad (5.8)$$

with  $q_0^i = f(c_q^i)$ ,  $u_0^i = f(-c_u^i)$  and  $h_0 = e^{-(a-1)ky_s} \mathfrak{h}_0$ , and where  $f(c)$  and  $\mathfrak{h}_0$  are normalization factors depending on  $c$ ,  $\nu$  and  $y_s$  and are given in Appendix D, along with their limiting expressions for the usual RS (AdS5) metric background. From these profiles, one can check that the localization of the fields in the bulk of the extra dimension is determined by the values of the  $c_q^i$  for the fermion fields, such that a value of  $c_q^i > 1/2$  indicates a UV

<sup>1</sup> We use throughout  $c_q$  for the doublets ( $c_q$  and  $c_l$ ) and  $c_u$  for the singlets ( $c_u$ ,  $c_d$ ,  $c_\nu$  and  $c_e$ ).

<sup>2</sup> Alternative fermion and Higgs profiles can be found in [174, 2] where different bulk mass conventions are adopted.

localized field, while a value of  $c_\psi^i < 1/2$  localizes the field near the IR brane<sup>3</sup>. The Higgs field localization along the 5-th dimension is given by the parameter  $a$ , the dimension of the Higgs condensate operator. A completely IR brane localized field corresponds to the limit  $a \rightarrow \infty$ , while for a delocalized Higgs field,  $a$  is small. However, in order to maintain the original Randall-Sundrum solution to the hierarchy problem without fine-tuning, the Higgs field localization should be such that  $a \gtrsim 2$  (for an  $AdS_5$  metric background). If the 5D Higgs potential is of the form  $V_{bulk}(H) = M_{5d}^2 H^2$ , with associated brane potentials at each boundary, the Higgs profile has two solutions, one growing towards the IR and another one which is decaying at the IR brane. This last one is proportional to  $e^{(4-a)ky}$  in the  $AdS_5$  background. In order to maintain the RS solution to the hierarchy problem the decaying solution has to be subdominant, and this happens naturally for  $a > 2$ . For  $a < 2$ , however, some fine-tuning between the parameters of the bulk scalar potential and the brane potentials is necessary in order to suppress the unwanted solution. In the modified- $AdS_5$  scenario the lowest value of  $a$  that does not require fine-tuning depends on the various new metric parameters [175]. In this case, the Higgs profile is given by

$$h(y) = h_0 e^{aky} \left[ 1 + (M_0/k - a) [F(y) - F(0)] \right], \quad (5.9)$$

where  $M_0$  is the brane Higgs mass term (coefficient of the  $|H|^2 \delta(y - y_1)$  term at the IR brane) and the function  $F(y)$  is given by

$$F(y) = e^{-2(a-2)ky_s} k y_s [-2(a-2)ky_s]^{-1+4/\nu^2} \Gamma \left[ 1 - \frac{4}{\nu^2}, -2(a-2)k(y_s - y) \right]. \quad (5.10)$$

The decaying term at the IR brane is the second term in Eq. (5.9) and one can see that by forcing  $M_0/k \simeq a$  (fine-tuning parameters) the solution can become sub-dominant. In order to avoid this fine-tuning of parameters, we note that as  $F(y)$  is a monotonically increasing function, if one has  $\delta \equiv |F(y_1)| \sim \mathcal{O}(1)$  no fine tuning is needed to guarantee that the increasing solution for the Higgs profile dominates. When the parameter  $\delta = F(y_1)$  becomes larger, this signals a need of fine-tuning of parameters to suppress its large value. Fig. 5.2 shows the no-fine-tuning region (above the red (solid)  $\delta = 1$  curve) in the plane  $(a, \nu)$ , where  $a$  is the Higgs localization parameter and  $\nu$  is the metric parameter of the modified metric solution. In the region below, the ‘‘fine-tuned’’ region, one requires a fine-tuning of Lagrangian parameters with a tuning precision growing exponentially (the very close by dashed curve locates the points where  $\delta = 10$ , i.e. where the tuning is already 10 %).

---

<sup>3</sup>This convention is for left handed doublets. For right handed singlet fields, our convention is such that  $c_u^i > -1/2$  for a UV localized field and  $c_u^i < -1/2$  for an IR localized field.

In producing these graphs, in each case we have first set the value of the IR brane position,  $ky_1$ , which in turn fixes the value of  $y_s$ , the position of the singularity. Then for each value of the parameter  $\nu$  we solve for  $a$  in  $\delta(a, \nu, y_1, y_s) = 1$ .

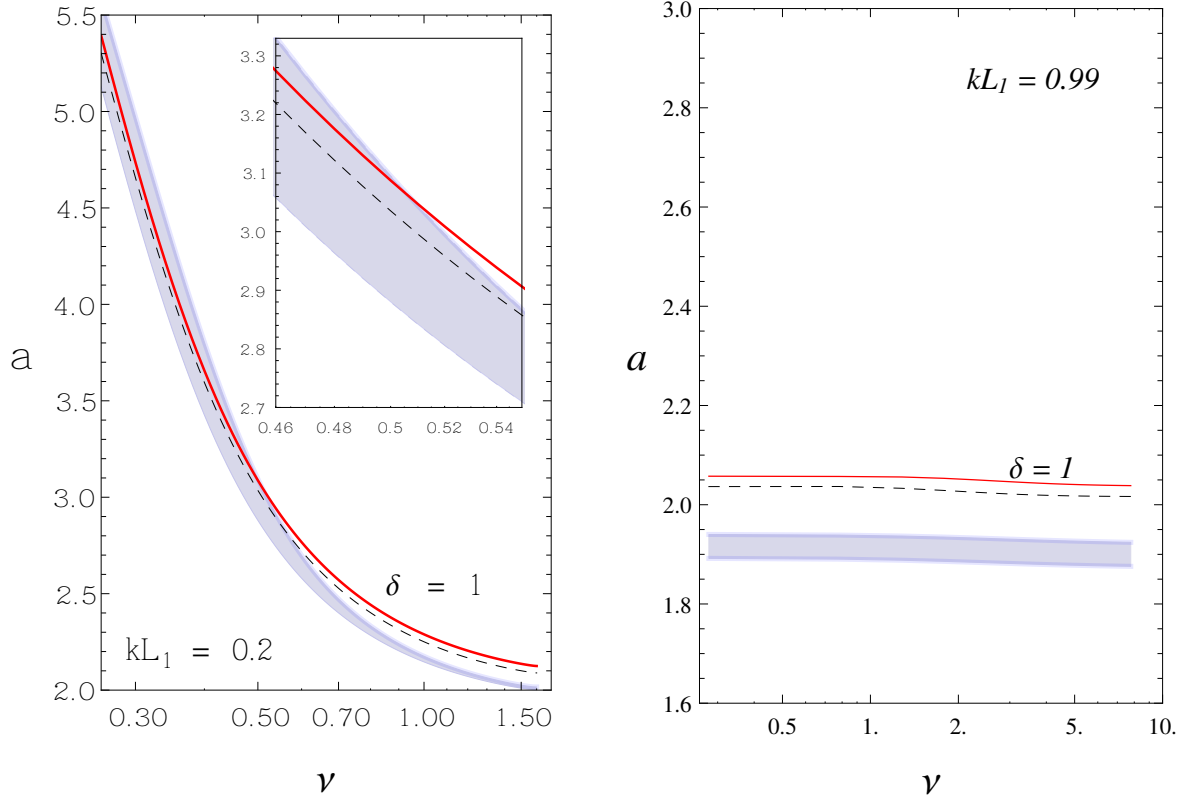


Figure 5.2: The  $\delta = 1$  plots and the neutrino masses in the  $\nu - a$  plane for  $kL_1 = 0.2$  (big AdS5 deviation) and  $kL_1 = 0.99$  (more RS-like). The red (solid) curve locates the no-fine-tuning threshold in which  $\delta = 1$ . Above this curve  $\delta < 1$  and below the curve  $\delta > 1$  (and hence this is the unwanted fine-tuned region). The shaded area corresponds to a heavy neutrino mass ( $m_3$  in *normal* ordering),  $m_\nu \sim 5 \times 10^{-11}$  GeV for different values of the  $c$ -parameters, but such that the mass expression has no exponential sensitivity to the  $c$ -parameters. Note that in the RS-like case, with  $kL_1 = 0.99$  and  $\nu$  large, it is not possible to obtain neutrino masses without fine-tuning or without quitting the neutrino plateau region. On the other hand, for large deviations from AdS5 (left panel) and small enough  $\nu$ , it is possible to find non-tuned points with neutrino masses in the plateau (i.e no exponential  $c$ -dependence).

To first order, the effective SM Yukawa couplings are obtained from the overlap integral

$$y_{ij}^u = \frac{Y_{ij}^u}{\sqrt{k}} \int_0^{y_1} dy e^{-4A(y)} h(y) q_L^{0,i}(y) u_R^{0,j}(y) \quad (5.11)$$

where the super index  $u$  denotes the four types of Yukawa couplings of the SM, i.e.  $u = u, d, e, N$  and we have defined the *dimensionless* 5D Yukawa couplings as  $Y_{ij}^u = Y_{ij}^{5D}/\sqrt{k} \sim \mathcal{O}(1)$ . Given the profiles (5.6), (5.7) and (5.8) and the metric (5.2), the integral above can be performed analytically and written as

$$y_{ij}^u = \tilde{Y}_{ij}^u h_0 f(c_q^i) f(-c_u^j), \quad (5.12)$$

where the factor  $\tilde{Y}_{ij}^u$ , defined in Appendix D, has very mild  $c^i$  dependence. The function  $f(c)$  is such that depending on the value of  $c$ , the Yukawa couplings can present an exponential sensitivity to  $c$  or a mild dependence. Finally  $h_0$  is the bulk Higgs normalization factor and does not depend on the fermion mass parameters  $c^i$ . Also note that although throughout the paper we have suppressed the explicit dependence of the fields on the metric parameters,  $\nu, y_s, y_1$  and  $k$  and in particular all of the factors of Eq. (5.12) are metric dependent. As shown in Appendix D, one can always retrieve the RS limit for these terms by taking the limit  $\nu, y_s \rightarrow \infty$ .

The fermion masses are given, to first order, by the eigenvalues of the  $3 \times 3$  Yukawa matrices of the form

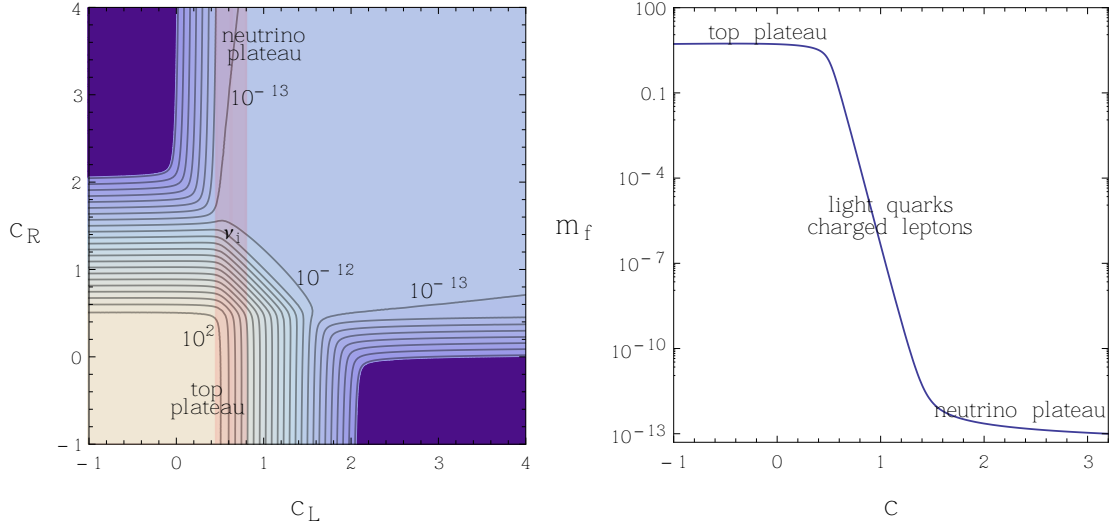
$$v y^u = v \begin{pmatrix} y_{11}^u & y_{12}^u & y_{13}^u \\ y_{21}^u & y_{22}^u & y_{23}^u \\ y_{31}^u & y_{32}^u & y_{33}^u \end{pmatrix}. \quad (5.13)$$

In general, in order to get the correct SM masses, no exponential  $c$ -dependence is needed for the top quark, which corresponds to  $c_q^t \lesssim 1/2$  and  $c_u^t > -1/2$  (this region of parameter space corresponds to the top plateau shown in Fig. 5.3). For the rest of the SM particles  $c_q^i \gtrsim 1/2$  and  $c_u^i < -1/2$ , which implies that the Yukawa couplings will depend exponentially on the values of the  $c_i$ . In the case of neutrinos however, in order to accommodate their tiny masses, one needs localization parameters  $c_\nu < -1$ . It was shown [173] that for a delocalized Higgs with  $a$ -parameter small compared to the localization parameter  $c_i$ , the 4D effective neutrino masses depend exponentially on  $a$  but loose their dependence on the  $c_i$ 's. This region of parameter space corresponds to the neutrino plateau shown in Fig. 5.3. In other words the limit of the function in Eq. (5.12) for large  $c_\nu$ -s is given by

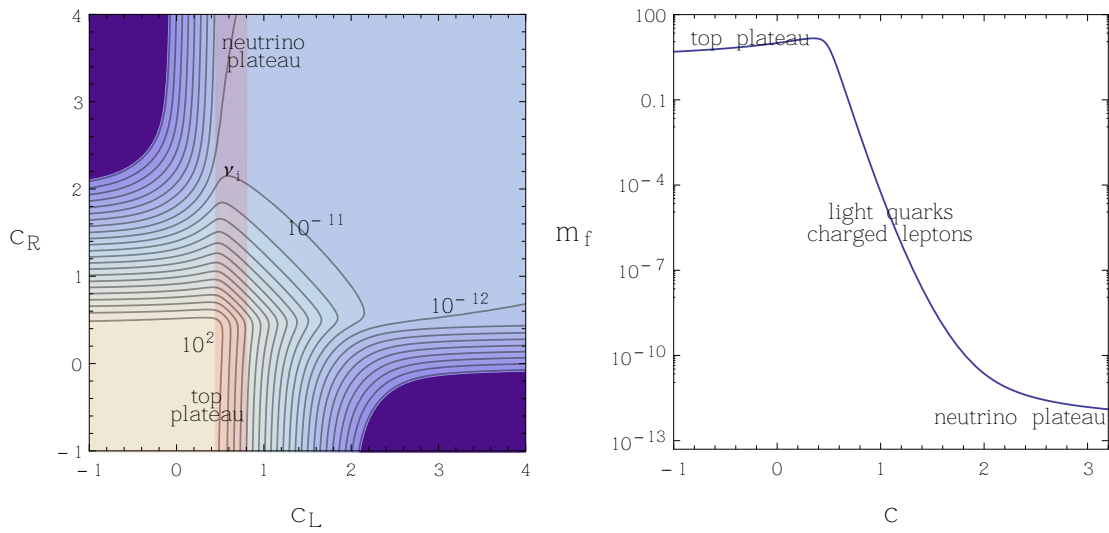
$$y_{ij}^u \sim \tilde{Y}_{ij}^u h_0. \quad (5.14)$$

To make this more transparent, in the formula for fermion masses given by (cf. Eq.(5.12))

$$(M_f)_{ij} = v \tilde{Y}_{ij}^u h_0 f(c_q^i) f(-c_u^j), \quad (5.15)$$



(a) RS with all SM fields including the Higgs in the bulk,  $a = 2.04$  and  $\delta = 1$ .



(b) Modified- $AdS_5$  with  $\nu = 0.32$ ,  $kL(y_1) = 0.2$ ,  $A(y_1) = 35$ ,  $a = 4.46$  and  $\delta = 1$ .

Figure 5.3: Effective 4D Yukawa couplings for fermions as a function of the fermion bulk mass parameter  $c$  for the RS (a) and general warped space-time metric (b). The plots in the right hand side are produced by taking the  $c$ -parameters for the doublet and the singlet to be equal. In the contour plots, each contour depicts one order of magnitude difference with respect to its adjacent contour. A typical region for the neutrino masses with  $m_3 \sim 5 \times 10^{-11}$  GeV and  $m_2 \sim 5 \times 10^{-12}$  are shown on with black dots. The overlap between the shaded regions show a realistic region for the plateau.

we factor the exponential behaviors and write them in the following two distinct limits

$$\begin{aligned} (M_f)_{ij} &\sim v Y_{ij}^f \epsilon^{(c_q^i - \frac{1}{2})} \epsilon^{-(c_u^j + \frac{1}{2})} \quad \text{for} \quad c_q > 1/2, c_u < -1/2 \\ (M_\nu)_{ij} &\sim v Y_{ij}^N e^{-ky_1(a-1)} \quad \text{for} \quad c_q - c_u > a \end{aligned} \quad (5.16)$$

where  $\epsilon = e^{-A(y)}$  (see Appendix D for details).<sup>4</sup>

The limits described in Eq. (5.16) imply that, as the quark and charged lepton mass matrix elements are exponentially dependent on the  $c_i$  parameters, the structure in the 5D Yukawa matrix elements  $Y_{ij}^f$  will be somehow washed-out and always generically hierarchical fermion masses as well as small mixing angles. For the neutrinos on the other hand, since there is no exponential sensitivity on the flavorful  $c_i$  parameters, any structure inherent in the 5D Yukawa matrix elements will survive in the 4D effective theory. This is the region of neutrino parameter space we are interested in and is shown in 5.3 as the neutrino plateau. In RS models, the actual height of the neutrino plateau is determined exclusively by the value of the  $a$  parameter. Moreover, by a numerical misfortune, for the value of the warp factor required to solve the hierarchy problem, the highest possible neutrino masses in the plateau, and without fine-tuning ( $a > 2$ ), are too small to be phenomenologically viable by 1-2 orders of magnitude (see upper panels in Fig. 5.3). A bit of tuning, some enhancement of the 5D Yukawas and/or trespassing the edge of the plateau would then be required, making the scenario less attractive for our purposes. On the other hand, in modified- $AdS_5$  scenarios, although the level of the plateau is still highly sensitive to the value of  $a$ , it could actually be increased by some two orders of magnitude and thus allow for phenomenologically acceptable neutrino masses in the desired region of the model (see Fig. 5.2 and lower panels in Fig. 5.3). This feature occurs because the modified AdS5 metric (see Eq. (5.2)) exhibits a richer parameter space. In the RS metric, in order to produce the correct neutrino masses, we need  $a \sim 1.85$ . This value amounts to about 1% fine tuning of parameters in the 5D Higgs potential. For modified- $AdS_5$  scenarios however, one can produce a neutrino plateau within the experimental bounds for a large range of values of the  $a$  parameter since there are two new independent parameters that can be scanned, namely  $\nu$  and  $kL_1$ . It is quite interesting that the parameter space for which the neutrino plateau is most favorable, is also the region where small KK masses do satisfy bounds coming from flavor and electroweak precision measurements [95, 98] and also from Higgs phenomenology [1].

In order to further illustrate this issue, we show in Fig. 5.4 the resulting neutrino masses in

---

<sup>4</sup>For modified- $AdS_5$ ,  $\epsilon_{mod} = e^{-ky_1} \left(1 - \frac{y_1}{y_s}\right)^{\frac{1}{\nu^2}} \sim 10^{-15}$  while for RS  $\epsilon_{RS} = e^{-ky_1} \sim 10^{-15}$ .

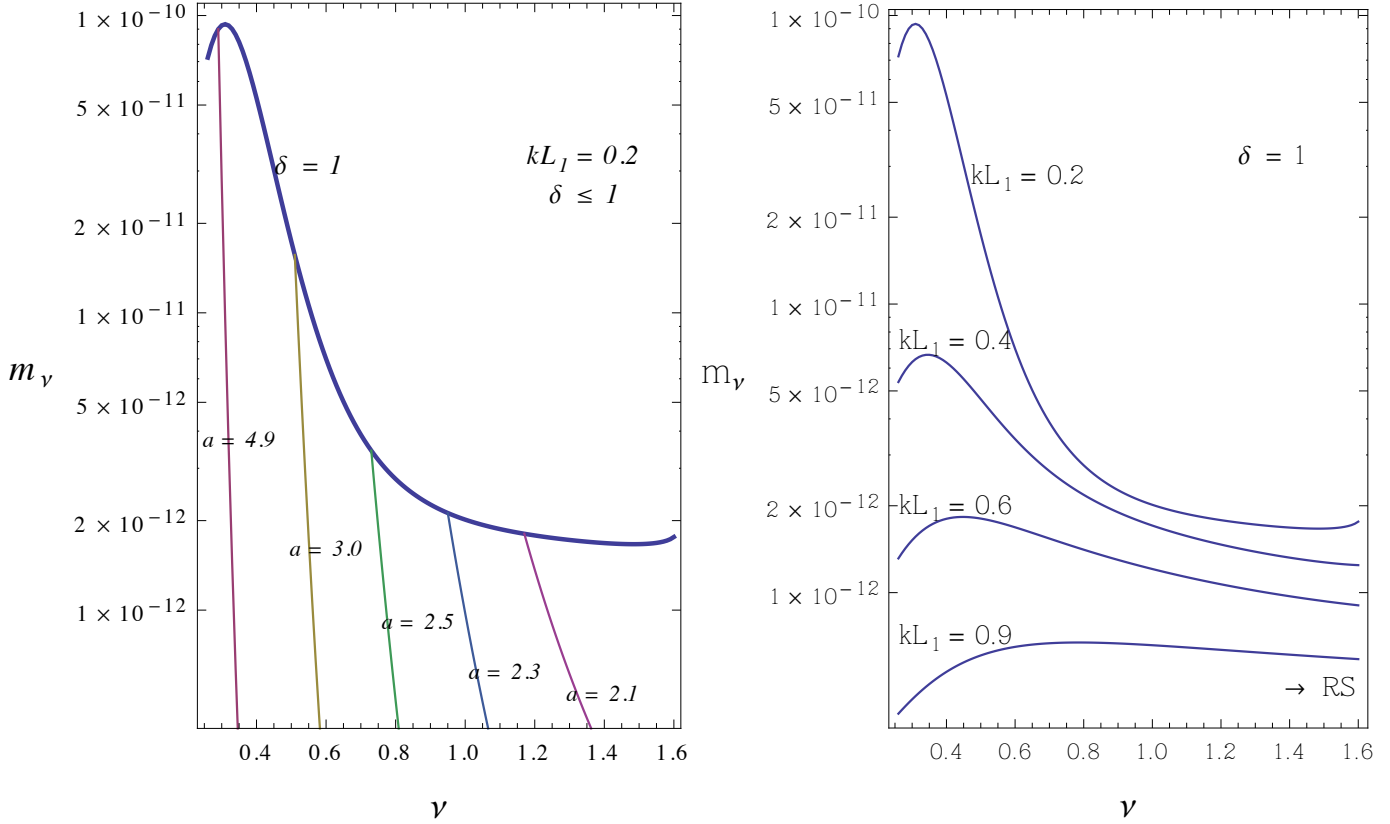


Figure 5.4: On the left we have plotted the neutrino masses as a function of the metric parameter  $\nu$  for different values of the Higgs localization parameter  $a$  and fixed  $ky_1 = 0.2$ . The fermion mass parameters ( $c$ 's) are fixed such that we are in a region where there is no exponential dependence on them (the neutrino “plateau”). The curves end whenever the fine-tuning threshold ( $\delta = 1$ ) is reached (thick overlapping curve). Note that for small values of  $\nu$  the neutrino masses become larger while still remaining in the non-tuned regime and in the “neutrino” plateau. On the right hand we have the same plot for different values of  $ky_1$  and fixed  $\delta = 1$ . The graph corresponding to  $kL_1 = 0.9$  at larger values of  $\nu$  remains constant and (approximately) coincides with the RS limit.

the plateau region as a function of the parameter  $\nu$ , and for different values of  $a$  (left panel) and  $kL_1$  (right panel). The area below the curves is the no-fine-tuning region, and one can see that the largest neutrino masses (in the plateau) happen for  $\nu \sim 0.3$  for  $kL_1 = 0.2$ , whereas in the RS limit, i.e.  $kL_1 \sim 1$  and  $\nu$  large, the masses are some two orders of magnitude lower (a bit too low). This makes the extended metric scenarios a more natural framework for the flavor mechanism investigated here, and adds to the main advantage of these scenarios (i.e. a much lower KK scale consistent with electroweak and flavor bounds).

In any case, qualitatively the general features of the flavor structure of these modified- $AdS_5$  models are very similar to these features in the pure  $AdS_5$  models for the bulk mass  $c^i$  parameters. Therefore, in order to illustrate our flavor setup, it will be useful to consider the simpler case of the RS metric. In this case the fermion mass formulas (5.16), can be simplified dramatically. As usual, we consider the mass matrix for the neutrino sector separately from the case of quarks and charged leptons mass matrices. Consider the case with  $c_{q,u}^i > \frac{1}{2}$ . In this case we have,

$$\begin{aligned} (M_f)_{ij} &\simeq v\epsilon^{(c_q^i - \frac{1}{2})}\epsilon^{-(c_u^j + \frac{1}{2})}\sqrt{2(a-1)|1-2c_q^i||1+2c_u^j|}\tilde{Y}_{ij}^f \\ (M_\nu)_{ij} &\simeq v\epsilon^{a-1}\frac{\sqrt{2(a-1)|1-2c_l^i||1+2c_\nu^j|}}{\sqrt{\epsilon^{(1-2c_l^i)}-1}\sqrt{\epsilon^{(1+2c_\nu^j)}-1}}\tilde{Y}_{ij}^\nu, \end{aligned} \quad (5.17)$$

where the 5D Yukawa couplings are given by,<sup>5</sup>

$$\tilde{Y}_{ij}^u \simeq \frac{1}{a - c_q^i + c_u^j} Y_{ij}^u. \quad (5.18)$$

From Eq. (5.6), (5.7) and (5.11) one can see that there are two sources of flavor structure: the 5D dimensionless Yukawa couplings,  $Y_{ij}^u$  and the bulk mass coefficients  $c_\psi^i$ . We are interested in scenarios in which all Yukawa matrices ( $Y_F = Y_{ij}^u, Y_{ij}^d, Y_{ij}^\nu$ , and  $Y_{ij}^e$ ) and fermion bulk mass matrices from the 5D Lagrangian ( $\mathbf{c}_f = \mathbf{c}_q, \mathbf{c}_u, \mathbf{c}_d, \mathbf{c}_l, \mathbf{c}_\nu$ , and  $\mathbf{c}_e$ ) share the same symmetry structure, which is then slightly broken through some high energy mechanism according to

$$Y_F = Y_F^0 + \delta Y_F, \quad (5.19)$$

$$\mathbf{c}_f = \mathbf{c}_f^0 + \delta \mathbf{c}_f, \quad (5.20)$$

where the matrices  $Y_F^0$  and  $\mathbf{c}_f^0$  are flavor symmetric while the perturbation matrices  $\delta Y_F$  and  $\delta \mathbf{c}_f$  are random. Inserting these perturbations in Eqs. (5.17), the fermion masses receive corrections to leading order as follows

$$\begin{aligned} m_t &= m_t^0 + \delta m_t & c_q^3, c_u^3 &< 1/2 \\ (m_f)_{ij} &= (m_f)_{ij}^0 f(\delta c_q^i) f(\delta c_u^j) \sim (m_f)_{ij}^0 \epsilon^{(\delta c_q^i + \delta c_u^j)} & a &> c_l^i + c_\nu^j \\ (m_\nu)_{ij} &= (m_\nu)_{ij}^0 + \delta(m_\nu)_{ij} & a &< c_l^i + c_\nu^j. \end{aligned} \quad (5.21)$$

Therefore the same exponential sensitivity on the bulk mass  $c^i$  parameters,  $\epsilon \sim 10^{-15}$ , responsible for producing the SM hierarchy in standard RS, is now translated into exponential

<sup>5</sup>For the exact formulas see Appendix D.

sensitivity of the symmetry breaking terms. As a consequence, small symmetry breaking terms ( $|\delta c_i| \sim 0.1$ ) can produce mass corrections of order  $10^{-15(\delta c^i + \delta c^j)}$  (*i.e.*, a hierarchy of order  $\sim 10^6$ ) to the quark and charged lepton mass matrices. This is in complete agreement with the observed hierarchy in these sectors. As mentioned before, the neutrinos and the top quark fields live in the two plateaus (see Fig. 5.3) with mild  $c_i$  sensitivity.

For the mixing angles, the eigenvector matrix that diagonalizes the neutrino sector should be very close to the eigenvector matrix of the 5D Yukawa matrix. However, in the quark and charged lepton sectors the mixing matrices are generically close to the unit matrix with their off-diagonal entries hierarchically small as <sup>6</sup>:

$$V_L^u \simeq \begin{pmatrix} 1 & \frac{f_q^1(\tilde{M}_u)_{21}}{f_q^2(\tilde{M}_u)_{11}} & \frac{f_q^1(\tilde{Y}_u)_{13}}{f_q^3(\tilde{Y}_u)_{33}} \\ -\frac{f_q^1(\tilde{M}_u^*)_{21}}{f_q^2(\tilde{M}_u^*)_{11}} & 1 & \frac{f_q^2(\tilde{Y}_u)_{23}}{f_q^3(\tilde{Y}_u)_{33}} \\ \frac{f_q^1(\tilde{M}_u^*)_{31}}{f_q^3(\tilde{M}_u^*)_{11}} & -\frac{f_q^2(\tilde{Y}_u^*)_{23}}{f_q^3(\tilde{Y}_u^*)_{33}} & 1 \end{pmatrix}, \quad (5.22)$$

where  $f_q^i$  is shorthand for the profile functions  $f(c_q^i)$ ,  $(\tilde{M}_u)_{ij}$  is the  $ij$  minor of the matrix in parenthesis and  $(\tilde{Y}_u)_{ij}$  is the  $ij$  element of the Yukawa matrix. We define the CKM and the PMNS matrices as the following

$$V_{CKM} \equiv V_L^u V_L^{d\dagger} \quad \text{and} \quad V_{PMNS} \equiv V_L^e V_L^{\nu\dagger}. \quad (5.23)$$

As mentioned after Eq. (5.16), for the quarks and charged leptons, the off-diagonal mixing angles are also exponentially sensitive to the  $c^i$  parameters and hence to the small symmetry breaking terms. The matrix elements of the  $V_L^f$  in Eq. (5.22) can then be written as

$$(V_L^{u,d,e})_{ij} \sim (V_L^{u,d,e})_{ij}^0 \epsilon^{(\delta c_q^i - \delta c_q^j)} \quad (\text{for } u, d \text{ and } e) \quad (5.24)$$

where  $(V_L^{u,d,e})_{ij}^0$  are the elements before the flavor symmetry breaking and  $\{i, j\}$  can be  $\{1, 2\}$ ,  $\{1, 3\}$  and  $\{2, 3\}$ . We see again that, due to exponential warping, all original symmetries present in the high energy theory are washed out in the quark and charged lepton sectors. Contrary to this, in the Dirac neutrino sector the terms in the  $V_L^\nu$  much less sensitive to the symmetry breaking terms since their own dependence on the  $c_i$  is mild in the region of parameters we are interested. If we define the eigenvectors of the 5D neutrino Yukawa matrix as

$$Y_\nu^{diag} = V_{Y_L} Y_\nu V_{Y_R}, \quad (5.25)$$

---

<sup>6</sup>Similar expressions are obtained for  $V_L^d$  and  $V_L^q$ .

then the matrix diagonalizing the 4D effective neutrino mass matrix

$$(V_L^\nu)_{ij} \sim (V_{Y_L})_{ij}. \quad (5.26)$$

We have not specified so far the type of symmetry imposed since the framework is pretty general. In the next section we will consider a concrete implementation of the idea, one within flavor democracy. The background metric considered will be the modified AdS5 solution, in the most favorable region of parameter space.

### 5.3 Flavor democracy

In this section we assume a democratic structure [176, 177, 178, 179, 180] for all the flavor parameters, meaning in our case that the 5D Yukawa couplings,  $Y_F^0$  are invariant under  $S_3 \times S_3$  while the 5D fermion bulk mass matrices,  $\mathbf{c}_f^0$  are invariant under  $S_3$  permutations. Explicitly, the democratic 5D Yukawa couplings and 5D fermion bulk mass matrices are given by

$$Y_F^{Dem} \propto \begin{pmatrix} 1 & 1 & 1 \\ 1 & 1 & 1 \\ 1 & 1 & 1 \end{pmatrix} \quad \text{and} \quad \mathbf{c}_f^{Dem} = \begin{pmatrix} A_f & B_f & B_f \\ B_f & A_f & B_f \\ B_f & B_f & A_f \end{pmatrix}. \quad (5.27)$$

Overall, there are four Yukawa matrices,  $Y_u^{Dem}$ ,  $Y_d^{Dem}$ ,  $Y_e^{Dem}$  and  $Y_\nu^{Dem}$ , corresponding to the up-quark sector, the down-quark sector, the charged leptons and the neutrinos. There are six fermion bulk c-matrices, namely  $\mathbf{c}_q^{Dem}$ ,  $\mathbf{c}_u^{Dem}$ ,  $\mathbf{c}_d^{Dem}$ ,  $\mathbf{c}_l^{Dem}$ ,  $\mathbf{c}_e^{Dem}$  and  $\mathbf{c}_\nu^{Dem}$ .

They can all be diagonalized simultaneously with the same unitary transformation

$$V_{Dem} = \begin{pmatrix} \sqrt{\frac{2}{3}} & 0 & \frac{1}{\sqrt{3}} \\ -\frac{1}{\sqrt{6}} & \frac{1}{\sqrt{2}} & \frac{1}{\sqrt{3}} \\ -\frac{1}{\sqrt{6}} & -\frac{1}{\sqrt{2}} & \frac{1}{\sqrt{3}} \end{pmatrix} U, \quad \text{with} \quad U = \begin{pmatrix} \cos(\theta_\nu) & \sin(\theta_\nu) & 0 \\ -\sin(\theta_\nu) & \cos(\theta_\nu) & 0 \\ 0 & 0 & 1 \end{pmatrix}, \quad (5.28)$$

which results in two zero eigenvalues for the Yukawa matrices, while the bulk mass matrices,  $\mathbf{c}_f^{Dem}$  acquire two degenerate eigenvalues. The 5D Yukawa and bulk mass matrices become in their diagonal basis

$$Y_F^0 = y_F^0 \begin{pmatrix} 0 & 0 & 0 \\ 0 & 0 & 0 \\ 0 & 0 & 1 \end{pmatrix} \quad \text{and} \quad \mathbf{c}_f^0 = \begin{pmatrix} c_f^{1^0} & 0 & 0 \\ 0 & c_f^{1^0} & 0 \\ 0 & 0 & c_f^{3^0} \end{pmatrix}, \quad (5.29)$$

where  $y_F^0$  are complex Yukawa couplings and the index  $F$  runs over  $u, d, e$ , and  $\nu$ . The elements  $c_f^{i0}$  are real and the index  $f_i$  runs over doublets  $q_i, l_i$  as well as singlets  $u_i, d_i, \nu_i$  and  $e_i$ , with  $i$  being the flavor index. Note that in this flavor symmetric limit, all fermions except for the  $t$  quark,  $b$  quark  $\tau$  lepton and  $\nu_\tau$  lepton end-up massless. The 5D flavor structure of Eq. (5.29) yields the 0-th order CKM and PMNS matrices of this scenario

$$V_i^0 = \begin{pmatrix} \cos \theta_i^0 & \sin \theta_i^0 & 0 \\ -\sin \theta_i^0 & \cos \theta_i^0 & 0 \\ 0 & 0 & 1 \end{pmatrix}, \quad (5.30)$$

where  $i = \text{CKM, PMNS}$ . The angle  $\theta_i^0$ , depends on the detailed structure of the symmetry breaking terms,  $\delta Y_F$  and  $\delta \mathbf{c}_f$  in Eqs. (5.20) and (5.19), and is not fixed by the underlying  $S_3 \times S_3$  symmetry. The structure so far is completely democratic but also quite far from the experimental observations.

Adding generic small perturbations as in Eqs. (5.19) and (5.20) will break the flavor symmetry and lift the degeneracies to produce SM-like masses and mixing angles. In the neutrino sector, the two level degeneracy is lifted by a small amount  $(\delta Y_F)_{ij}$ . This suggests a *normal* hierarchy ordering with a heavier eigenstate and two lighter ones with similar masses. Using Eq. (5.16) and taking only the generic size of the perturbations as  $(\delta Y_F)_{ij} \simeq \delta Y^\nu$  for simplicity, yields the following relations for the neutrino masses

$$m_1 \sim \delta Y^\nu v e^{-ky_1(a-1)}, \quad m_2 \sim \delta Y^\nu v e^{-ky_1(a-1)}, \quad m_3 \sim (1 + \delta Y^\nu)v e^{-ky_1(a)} \quad (5.31)$$

Neutrino mass data requires  $v e^{-ky_1(a-1)} \simeq 0.3$  eV and in order to solve the hierarchy problem we need  $ky_1 \simeq 35$ , which means that the value of the Higgs localization parameter should be about  $a \simeq 1.8$ . As explained in the previous section this value of  $a$  requires some fine-tuning of parameters in the 5D Higgs potential. As observed then, with modified- $AdS_5$  metrics it is possible to remain in a non-tuned region, and in particular we find that the best region is for  $\nu \sim 0.2$  and  $kL_1 \sim 0.3$  where the parameter  $a$  can have a value of 4.5.<sup>7</sup> In order to obtain the observed neutrino mass hierarchy ratio  $r$ , given by  $r = (|m_2|^2 - |m_1|^2) / (|m_3|^2 - |m_1|^2) \simeq 0.03$ , the size of the Yukawa perturbations  $\delta Y$  must be fixed to  $\delta Y^\nu \lesssim \sqrt{r} \simeq 0.17$ , since there are no restrictions on the values of bulk mass parameters,  $c_i$ -s (as long as they are within the bounds  $a < c_\nu + c_l$ ).

Consider the elements  $V_{e2}, V_{e3}$  and  $V_{\mu 3}$  of the PMNS matrix. As mentioned before, due to the plateau in the neutrino sector for small  $a$  parameter, the 5D Yukawa matrix structure

---

<sup>7</sup>In the modified- $AdS_5$  case Eq. 5.31 will be slightly modified and higher values of the  $a$ -parameter become acceptable.

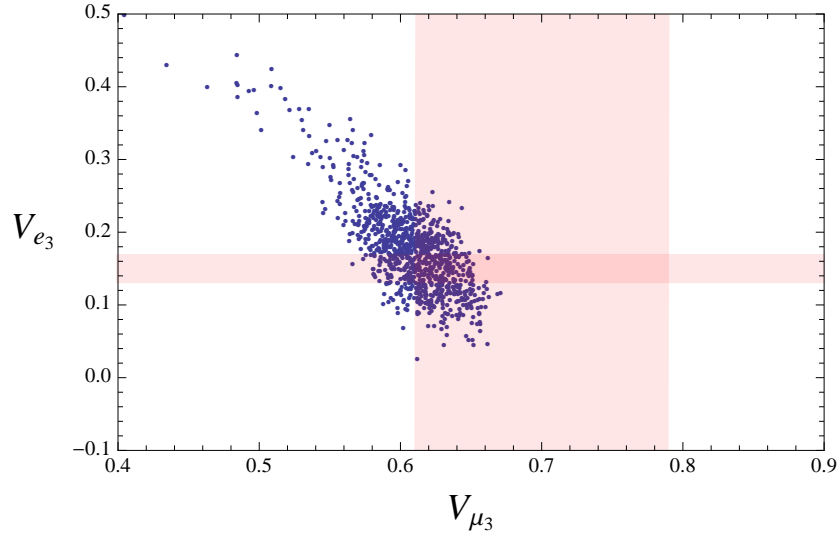


Figure 5.5: Scan plot of  $V_{e3}$  versus  $V_{\mu3}$  with random values of  $\delta Y_\nu$ ,  $\delta Y_e$ ,  $c_l$  and  $c_\nu$ . On the other we have fixed  $c_l^3 = 0.41$ ,  $(\delta Y^\nu)_{13} = 0.008$  and  $(\delta Y^\nu)_{23} = 0.13$ . The concentration of points in a precise region shows that the mixing angles  $V_{e3}$  and  $V_{\mu3}$  are highly sensitive to only these three parameters. If the flavor violating terms  $\delta Y$ 's are to be kept in the 10% level,  $V_{\mu3}$  is expected to be at the lower end of its experimental uncertainty, whereas the smallness of  $V_{e3}$  is exclusively due to a small ratio of Yukawa perturbations  $(\delta Y^\nu)_{13}/(\delta Y^\nu)_{23}$ .

is preserved and therefore the eigenvectors are solely given by a tri-bi-maximal matrix, Eq. (5.28) (which diagonalizes the  $Y_F^0$ ) plus some perturbation which diagonalize  $\delta Y_F$ . This is already very much like the PMNS matrix and, since in the charged lepton sector the eigenvectors matrix,  $V_L^e$ , is close to the identity, *cf.* Eq. (5.22), in general we have  $V_{\mu3} \simeq (V_L^{\nu\dagger})_{23}$  and  $V_{e3} \simeq (V_L^{\nu\dagger})_{13}$ , (*cf.* Eq. (5.23)). The value of  $V_{e2}$  on the other hand, from Eq. (5.30), is fixed by  $\theta_i$ , which depends on the structure of the neutrino Yukawa flavor violating matrix  $\delta Y_{ij}^\nu$ . Therefore we have

$$\begin{aligned}
 V_{e2} &\sim \sin \theta_\nu^0, \\
 V_{e3} &\propto \delta Y_{13}^\nu f(c_l^3), \\
 V_{\mu3} &\propto \delta Y_{23}^\nu f(c_l^3).
 \end{aligned}
 \tag{5.32}$$

Note that these features are specific to the case  $a < c_l^3 + c_\nu^j$  and  $c_l^3 < 1/2$ , and are not generic in usual warped extra dimension scenarios.

In Fig. 5.5 we present a scan of the model parameters to verify the validity of Eq. (5.32). In this scan we randomly perturbed the values of the 5D parameters  $Y_\nu$ ,  $Y_e$ ,  $c_l$  and  $c_\nu$ , but kept the values of the three relevant parameters  $c_l^3$ ,  $(Y^\nu)_{13}$  and  $(Y^\nu)_{23}$  fixed. We see from the

figure that the obtained values of the matrix elements  $V_{\mu 3}$  and  $V_{e 3}$  can be made to lie within the experimental bounds, by fixing only three parameters, with all other terms randomly perturbed. In particular the formulas show the sensitivity of these two PMNS mixing angles to the flavor structure of the neutrino Yukawa matrix  $\delta Y^\nu$ , but not to the charged lepton Yukawa matrix  $\delta Y^l$  or to the bulk masses  $\delta c^i$ , except for  $\delta c_l^3$ . Knowing that experimentally  $V_{\mu 3}^{\text{exp}} \simeq 0.65$  and  $V_{e 3}^{\text{exp}} \simeq 0.15$ , for the numerical evaluations we took the bulk mass parameter of the third family lepton doublet  $c_l^3 < 1/2$  to easily obtain larger mixing angles for small  $\delta Y \simeq 0.1$ . This condition is very interesting as it is the same as in the quark sector, where  $c_q^3 \lesssim 1/2$  is needed to obtain a large top quark mass, which could be a hint of an additional family symmetry among the  $SU(2)$  doublets of the third family. The particular values used in the scan were  $c_l^3 = 0.41$ ,  $(\delta Y^\nu)_{13} = 0.008$  and  $(\delta Y^\nu)_{23} = 0.13$ .

In the charged lepton sector and the up- and down-quark sectors, the massless states are also lifted by the flavor symmetry breaking, leaving a suppression proportional to  $\delta Y$ . In addition, the exponential dependence on the symmetry breaking parameters  $\delta c_f^i$  creates a hierarchy among all the masses. The charged fermion masses are given by the diagonal elements of Eq. (5.15), multiplied by the appropriate diagonal elements of the Yukawa matrix. For the approximate  $c$  parameter and  $Y$  dependence of third generation we can write in general

$$\begin{aligned} m_t &\sim v y_u^0, \\ m_{b,\tau} &\sim v y_{b,\tau}^0 f(c_{L_{b,\tau}}^0 + \delta c_{L_{b,\tau}}) f(-c_{R_{b,\tau}}^0 - \delta c_{R_{b,\tau}}), \end{aligned} \quad (5.33)$$

where the last equation can be approximated as<sup>8</sup>

$$m_{b,\tau} \sim m_{b,\tau}^0 \epsilon^{(\delta c_q^{b,\tau} - \delta c_u^{b,\tau} - 1)}. \quad (5.34)$$

Here we have used  $m_{b,\tau}^0 = v y_{b,\tau}^0 \epsilon^{(c_q^{b,\tau 0} - c_u^{b,\tau 0} - 1)}$  for the 0-th order masses, which are the usual mass formulas in the RS formulation. We have also noted that for the top quark we have<sup>9</sup>  $\epsilon^{(\delta c_q^3 - \delta c_u^3 - 1)} \sim 1$ .

In contrast to the heavy fermions (corresponding to the heavy eigenvalues), the lighter fermion masses (electron, muon, up, charm, down and strange), are massless in the flavor symmetry limit. It is only after the flavor symmetry breaking that these fermions acquire masses, and therefore their masses are directly proportional to the generic size of the perturbations in the

<sup>8</sup>This approximation works better in the RS limit. Also see Appendix D for asymptotic expansions of the function  $f(c)$ .

<sup>9</sup>Assuming that  $c_q^{3 0}, c_u^{3 0} < \frac{1}{2}$  and  $c_d^{3 0}, c_e^{3 0}, c_l^{3 0} > \frac{1}{2}$ .

Yukawa matrix,  $\delta Y$ . Using Eq. (5.15) again, we can approximate their masses

$$m_{f_i} \sim v \delta Y_F f(c_q^{i0} + \delta c_q^i) f(-c_u^{i0} - \delta c_u^i), \quad (5.35)$$

which can be further expressed as

$$m_{f_i} \sim \delta Y_F m_{f_i}^0 \epsilon^{(\delta c_q^i + \delta c_u^i)}, \quad (5.36)$$

where the index  $i$  runs over  $u, c, d, s, e, \mu$  and the 0-th order mass is given by  $m_{f_i}^0 = v \epsilon^{(c_q^{i0} + c_u^{i0} - 1)}$ . In all of the mass formulas given, by approximating the actual mass eigenvalues by the diagonal elements of the mass matrix, we are implicitly assuming that the  $c$  parameters are in order (e.g.  $|c_u^1| > |c_u^2| > |c_u^3|$ ). For the case where one of the  $c$  parameters is not such ordered (e.g.  $|c_u^2| < |c_u^3|$ ), one can still use the above formulas but with appropriate indices (here for instance, consider the elements  $m_{f_{21}}$  and  $m_{f_{12}}$  instead of  $m_{f_{11}}$  and  $m_{f_{22}}$  in Eq. (5.21)). In numerical results, as we required to satisfy all the SM constraints, such cases have occurred.

In all the above considerations,  $\delta Y_F$  denotes the generic size of the perturbations. This model can naturally produce the SM mass hierarchy by fixing the different  $\delta c^i$  within the constraint  $|\delta c^i| \lesssim 0.1$ . This is due to exponential dependence of these parameters and typical hierarchies between generations of fermions in SM ( $\epsilon^{\mathcal{O}(0.1)} \simeq 10^{-1.5}$ )<sup>10</sup>. This implies that the typical sizes of the perturbation parameters,  $\delta c_f$  or  $\delta Y$  are fixed by SM bounds to  $\simeq 0.1$ . For the mixing angles in this scenario, consider the  $V_{us}$ ,  $V_{ub}$ , and  $V_{cb}$  elements of the CKM matrix. From Eq. (5.24) we know that for these elements, in general we have

$$V_{ij} \sim (Y_F)_{ij} \frac{f(c_q^i)}{f(c_q^j)}.$$

This easily produces the observed hierarchy in the mixing angles. For the special case of RS the CKM entries can be further simplified

$$V_{us} \sim \epsilon^{(\delta c_q^1 - \delta c_q^2)}, \quad V_{cb} \sim \delta Y \epsilon^{(\delta c_q^2 - \delta c_q^3)}, \quad V_{ub} \sim \delta Y \epsilon^{(\delta c_q^1 - \delta c_q^3)}. \quad (5.37)$$

These equations must be compared with the 0-th order CKM matrix given by Eq. (5.30). The two angles  $V_{cb}$  and  $V_{ub}$  are lifted from zero by an amount proportional to the Yukawa perturbations  $\delta Y \sim 0.1$  and an exponential of order  $\epsilon^{\delta c}$ , which imposes yet another constraint on the possible values of these perturbations, since they must produce the experimentally

---

<sup>10</sup>Here naturally means that randomly chosen  $\delta Y$  and  $\delta c$  parameters naturally produce a SM-like 4D effective theory.

well known ratio  $V_{cb}/V_{us}$ . One can check that, assuming an ordering  $\delta c_q^1 > \delta c_q^2 > \delta c_q^3$ , yields the correct order of magnitude. In contrast to  $V_{cb}$  and  $V_{ub}$ , the 0-th order Cabibbo angle in Eq. (5.30) is of  $\mathcal{O}(1)$ , suppressed after the symmetry breaking by exactly the expected amount  $V_{us} \sim V_{ub}/V_{cb}$ .

In Table 5.1 we show a numerical example of an  $S_3$  symmetric set of 0-th order bulk mass parameters (many other points with the same symmetry in the parameter space are possible), which with a small perturbation of order  $\delta c \simeq \delta Y \simeq 10\%$  can be used to produce the SM from the modified- $AdS_5$  scenario<sup>11</sup>. For this specific point we have taken the value of the warp exponent at the IR brane,  $A(y_1)$  to be exactly 35. With this assignment, there is only one more free parameter of the model left to completely fix the metric. This parameter can be either  $\nu$ , or the position of the singularity,  $y_s$ . Therefore one has the freedom to choose the amount of departure from the pure  $AdS_5$ . For the point presented in Table 5.1, we took  $\nu \simeq 1.1$ . The value of the dimension of the Higgs field operator  $a$  is chosen to be 2.05, to fix the position of the plateau shown in Fig. 5.3 and hence fix the neutrino masses to the correct value. With this starting point, the SM is then easily reproduced by breaking the symmetry by adding the perturbations  $\delta c^i$ -s and  $(\delta Y)_{ij}$ -s to lift the degeneracies of the symmetric scenario. At this stage one can go on and “fix” the  $(\delta Y)_{ij} \lesssim 0.1$  and  $\delta c^i \lesssim 0.1$  parameters to produce the SM masses, angles and phases by systematically using the approximate formulas in this section up to any order of precision consistent with the SM. In general the sensitivity to the precise values of the 5D Yukawa couplings,  $(\delta Y)_{ij}$ , is minimal and randomly chosen matrices with  $(\delta Y)_{ij} \lesssim 0.1$  can produce all the required SM features.

$f$	$q$	$u$	$d$	$l$	$\nu$	$e$
$c_f^1{}^0$	0.55	0.55	0.62	0.55	5.00	0.65
$c_f^3{}^0$	0.41	0.41	0.62	0.41	3.00	0.65

Table 5.1: A point for democratic symmetry in the localization parameters allowed space (out of many possible points) in the 0-th order 5D fermion  $c$ -parameter space, consistent with all the experimental and model constraints. For this point, we have set all the 0-th order Yukawa coefficients to be universal,  $y_u^0 = y_d^0 = y_\nu^0 = y_e^0 = 4.4$ , and the Higgs localization parameter to  $a = 2.1$ . The modified- $AdS_5$  metric parameters are  $\nu = 1.1$ ,  $y_1 = 2.8 \times 10^{-17}$ , and  $A(y_1) = 35$ .

<sup>11</sup>A similar point for the pure  $AdS_5$  is presented in [3] which we do not repeat here.

## 5.4 Conclusion

In this work, we have provided a framework in which all of the fermions are treated on equal footing, including neutrinos, and the where SM fermion flavor structure can still emerge naturally out of a slightly broken universal flavor symmetry. All the matter fields must be in the bulk and in particular the Higgs field should be as delocalized as possible from the IR boundary. In particular we have explored a warped scenario in which the metric is modified from the usual  $AdS_5$  background. This setup has the advantage of allowing lower KK masses ( $\sim 1\text{-}2$  TeV) while still safe from precision electroweak tests and flavor bounds. In our case the modified metric presents a further advantage as the neutrino mass generation in our framework is more natural. This is due to a numerical accident by which the neutrino masses generated in the  $AdS_5$  background are too small (at most  $\sim 10^{-4}$  eV ). Within the modified metric setup, neutrino masses can be up to two orders of magnitude greater, in the same qualitative region of parameter space, which we called the neutrino plateau, where the effective 4D neutrino masses do not have any exponential dependence on the bulk mass parameters  $c_i$  (in contrast with quarks and charged leptons).

Once the flavor symmetry is slightly broken, the SM flavor structure emerges thanks to the inherent features of warped space models. The wave function profiles of light quarks and charged leptons are exponentially sensitive to the symmetry violating terms and this results in masses and mixings controlled by the small flavor violating terms. In the neutrino sector, the wave functions are not exponentially sensitive to flavor violation parameters, due to the Higgs being highly delocalized, and thus the symmetry is mostly preserved. The observed structure of neutrino masses and mixings is generated mainly out of the original flavor symmetry. The de-localization of the Higgs in the bulk is thus an essential ingredient in our setup. Still, there is a source of tension in models with an  $AdS_5$  metric background, in which in order to produce the correct Dirac neutrino masses, too much Higgs delocalization is required. This Higgs does not generically solve the hierarchy problem (the original motivation of these models) unless some degree of fine-tuning is re-introduced. These tensions disappear when we use a modified- $AdS_5$  geometry so that our flavor setup can be successfully implemented. This becomes an added benefit of these promising modified metric scenarios, in which low KK masses are consistent with precision electroweak and flavor tests.

For illustration, we chose a simple example in which symmetries can provide an implementation for this mechanism. In this example, namely flavor democracy, the 5D Yukawa couplings for the fermions are invariant under  $S_3 \times S_3$  while the 5D fermion bulk mass matrices are

invariant under  $S_3$  family permutation invariance. As we saw in the example, the symmetries are broken with small terms and this is enough to generate the full flavor structure of the SM. Also, one could imagine other symmetries in the 5D scenario, where different predictions and correlations appear in the implementation, making this framework a very promising novel laboratory for studying fermion flavor symmetries.

# Chapter 6

## Conclusions and Outlook

In this thesis we investigated the phenomenological consequences of models with one spacial warped extra dimension. These models are physically important as they address the gauge and flavor hierarchy problem, while at the same time being generically consistent with the SM. Another aspect of these models that is particularly relevant is that, from a 4 dimensional effective theory point of view, these models predict the existence of additional resonances well within the reach of the LHC.

First, in the context of pure  $AdS_5$  models with all the SM fields, including the Higgs field, allowed to propagate in the bulk of the extra dimension, we addressed the Higgs phenomenology of a model with a single fermion field, though we expect the complete model will produce generically the same results. Our result was that, with Yukawa matrix mixings and phases all order one, and randomly chosen, the couplings of the Higgs fields to the fermions, gluons and photons can be significantly shifted from the values obtained by the SM. These shifts can be either enhancing or suppressing, depending on the phases of the fields involved. We also showed that the effect of the heavier KK modes decouples fast enough so that considering an effective field theory with only the first few KK modes approaches the result of considering the full infinite tower of KK modes. In this effective field theory approach, as the Higgs becomes more and more localized towards the IR brane, one needs to consider all relevant operators, and in particular, the effect of a certain higher derivative operator can be significant. We also showed that our results are more predictive for the case of the Higgs in the bulk, as the effect the mentioned higher derivative operator is small while the the effects due to only the normal 5D Yukawa terms are aligned, which results in all KK modes contributions to add up, an enhancement in the Higgs boson production caused by a single

fermion family, though for the case of 3 generations, this prediction would not be as robust, due to the flavor phases and mixings.

We then generalized these results to the case of (more general) modified  $AdS_5$  metrics. We showed that just as in the pure  $AdS_5$  case, the existence of a tower of KK fermions for each of the SM color charged particles, in these models can lead to significant enhancements in the total Higgs production rate at the LHC. We saw that as the Higgs production rate depends crucially on the coupling of the KK fermions with the Higgs profile in the bulk, the results depend on the profile of these fields along the extra dimension. Therefore the shifts in the Higgs production rate compared to the SM are reduced as the KK fermions become heavier or the Higgs becomes more delocalized away from the IR brane. This is achieved by a lower  $a$  parameter for the Higgs profile. If everything else kept identical, in the case of modified  $AdS_5$  scenarios, the overlap between the fermion and Higgs fields is suppressed relative to the pure  $AdS_5$  case. This is due to the fact that relative to the pure RS, the fermion fields are localized more towards the IR brane as compared to the Higgs field profile. As a result, for lower KK masses, as low as  $\sim 2$  TeV only the modified  $AdS_5$  appears to be consistent with the experimental results at the LHC.

In the last part, we shifted our analyses to neutrino phenomenology. We proposed a general unified scenario for the flavor structure of the SM arising from the 5D bulk scenario. We showed that if the 5D theory obeyed a symmetry in the flavor sector, the warped extra dimensions produce a framework in which this symmetry is completely washed out in the case of the quarks and charged leptons, leading to the correct hierarchical structure of the quark, charged lepton masses and mixing (the CKM matrix). However the same symmetry is almost intact in the case of neutrinos, resulting in consistent neutrino masses and mixings (the PMNS matrix), and therefore provides a very natural and simple explanation for this contrast within the SM flavor structure. This drastic difference within the flavor sector in the warped extra dimension scenarios is due to the existence of plateau for large values of the fermion localization (bulk mass) parameter,  $c$ . It was shown that for these values of  $c$  the position of this plateau is dominantly determined by the Higgs localization parameter,  $a$ , and depends only mildly on the  $c$  parameter. Therefore a small symmetry breaking in the 5D parameters, while producing a large effect in the quark and charged lepton sectors, has little or no effect on the neutrino sector. For these models both the pure  $AdS_5$  and modified scenarios were considered. As the mass of the neutrinos in this framework depends crucially on the position of the neutrino plateau, which itself depends on the Higgs localization parameter,  $a$ , and not the fermion bulk mass terms, there are some tensions which arise in the pure  $AdS_5$  case.

There, the neutrino mass data requires an  $a$  parameter as low as  $a = 1.8$ , which can only be achieved with significant fine tuning of some other 5D Higgs profile parameters in order to suppress the other branch of the Higgs profile (the one which decays towards the IR brane). We saw that these tensions can be alleviated in the case of the modified  $AdS_5$  geometries, as in these scenarios the position of the neutrino plateau is more consistent with the neutrino data.

In conclusion, warped extra dimensions offer a very interesting framework for the beyond the standard model physics. But the research into the phenomenology of these models is far from complete. The material in this thesis inspires future research in this area. For example in the case of the model proposed for the neutrinos other symmetries are possible and are under current speculation. Understanding the general framework of these symmetry breakings in the 5D context is also a very interesting problem, which we are currently working on.

For the Higgs production rate, a full, realistic three generation treatment of the model as well as evaluation of the production rate through other interesting channels (for example  $H \rightarrow \gamma\gamma$ ) would be an important project, especially as more and more data are expected through the next run at the LHC. This project is also being considered.

We are also currently working on collider signals for modified  $AdS_5$  models at the LHC.

# Bibliography

- [1] M. Frank, N. Pourtolami, and M. Toharia, “Higgs Bosons in Warped Space, from the Bulk to the Brane,” *Phys.Rev.*, vol. D87, no. 9, p. 096003, 2013, hep-ph/1301.7692.
- [2] M. Frank, N. Pourtolami, and M. Toharia, “Higgs Production in General 5D Warped Models,” *Phys.Rev.*, vol. D89, p. 016012, 2014, hep-ph/1311.1824.
- [3] M. Frank, C. Hamzaoui, N. Pourtolami, and M. Toharia, “Unified Flavor Symmetry from warped dimensions,” *Phys.Lett. B*, vol. 742, p. 178, 2015, hep-ph/1406.2331.
- [4] M. Frank, C. Hamzaoui, N. Pourtolami, and M. Toharia, “Fermion Masses and Mixings in General Warped Extra Dimensional Models,” *in progress.*, 2015.
- [5] S. Weinberg, *The Quantum Theory of Fields Vol. I and II*. New York, NY: Cambridge University Press, 1995.
- [6] P. A. M. Dirac, *The Principles of Quantum Mechanics*. Oxford, UK: Oxford University Press, forth edition ed., 1958.
- [7] C. M. Bender and K. A. Milton, “Nonperturbative calculation of symmetry breaking in quantum field theory,” *Phys.Rev.*, vol. D55, pp. 3255–3259, 1997, hep-th/9608048.
- [8] C. M. Bender and S. Boettcher, “Real Spectra in Non-Hermitian Hamiltonians Having PT Symmetry,” *Physical Review Letters*, vol. 80, pp. 5243–5246, June 1998, physics/9712001.
- [9] P. Dorey, C. Dunning, and R. Tateo, “Supersymmetry and the spontaneous breakdown of PT symmetry,” *J.Phys.*, vol. A34, p. L391, 2001, hep-th/0104119.
- [10] P. Dorey, C. Dunning, and R. Tateo, “Spectral equivalences, Bethe Ansatz equations, and reality properties in PT-symmetric quantum mechanics,” *J.Phys.*, vol. A34, pp. 5679–5704, 2001, hep-th/0103051.

- [11] C. M. Bender, D. C. Brody, and H. F. Jones, “Complex extension of quantum mechanics,” *eConf*, vol. C0306234, pp. 617–628, 2003, quant-ph/0208076.
- [12] C. M. Bender, D. C. Brody, and H. F. Jones, “Scalar quantum field theory with cubic interaction,” *Phys.Rev.Lett.*, vol. 93, p. 251601, 2004, hep-th/0402011.
- [13] C. M. Bender, D. C. Brody, and H. F. Jones, “Extension of PT symmetric quantum mechanics to quantum field theory with cubic interaction,” *Phys.Rev.*, vol. D70, p. 025001, 2004, hep-th/0402183.
- [14] K. A. Milton, “Anomalies in PT symmetric quantum field theory,” *Czech.J.Phys.*, vol. 54, pp. 85–91, 2004, hep-th/0308035.
- [15] K. A. Milton, E. Abalo, P. Parashar, N. Pourtolami, and J. Wagner, “PT-Symmetric Quantum Electrodynamics and Unitarity,” *Phil.Trans.Roy.Soc.Lond.*, vol. A371, p. 20120057, 2013, hep-th/1204.5235.
- [16] E. P. Wigner, *Gruppentheorie und ihre Anwendung auf die Quantenmechanik der Atom-spektren*. New York, NY: Academic Press, Inc (English translation), 1931.
- [17] G. Aad *et al.*, “Observation of a new particle in the search for the Standard Model Higgs boson with the ATLAS detector at the LHC,” *Phys.Lett.*, vol. B716, pp. 1–29, 2012, hep-ex/1207.7214.
- [18] S. Chatrchyan *et al.*, “Observation of a new boson at a mass of 125 GeV with the CMS experiment at the LHC,” *Phys.Lett.*, vol. B716, pp. 30–61, 2012, hep-ex/1207.7235.
- [19] N. Cabibbo, “Unitary Symmetry and Leptonic Decays,” *Phys.Rev.Lett.*, vol. 10, pp. 531–533, 1963.
- [20] M. Kobayashi and T. Maskawa, “CP Violation in the Renormalizable Theory of Weak Interaction,” *Prog.Theor.Phys.*, vol. 49, pp. 652–657, 1973.
- [21] L. Wolfenstein, “Parametrization of the Kobayashi-Maskawa Matrix,” *Phys.Rev.Lett.*, vol. 51, p. 1945, 1983.
- [22] A. J. Buras, M. E. Lautenbacher, and G. Ostermaier, “Waiting for the top quark mass,  $K^+ \rightarrow \pi^+ \nu \bar{\nu}$ ,  $B_s^0 - \bar{B}_s^0$  mixing and CP asymmetries in  $B$  decays,” *Phys.Rev.*, vol. D50, pp. 3433–3446, 1994, hep-ph/9403384.
- [23] J. Charles *et al.*, “CP violation and the CKM matrix: Assessing the impact of the asymmetric  $B$  factories,” *Eur.Phys.J.*, vol. C41, pp. 1–131, 2005, hep-ph/0406184.

- [24] K. Olive *et al.*, “Review of Particle Physics,” *Chin.Phys.*, vol. C38, p. 090001, 2014.
- [25] J. Beringer *et al.*, “Review of Particle Physics (RPP),” *Phys.Rev.*, vol. D86, p. 010001, 2012.
- [26] B. W. Lee, C. Quigg, and H. Thacker, “Weak Interactions at Very High-Energies: The Role of the Higgs Boson Mass,” *Phys.Rev.*, vol. D16, p. 1519, 1977.
- [27] J. M. Cornwall, D. N. Levin, and G. Tiktopoulos, “Derivation of Gauge Invariance from High-Energy Unitarity Bounds on the s Matrix,” *Phys.Rev.*, vol. D10, p. 1145, 1974.
- [28] C. Vayonakis, “Born Helicity Amplitudes and Cross-Sections in Nonabelian Gauge Theories,” *Lett.Nuovo Cim.*, vol. 17, p. 383, 1976.
- [29] M. S. Chanowitz and M. K. Gaillard, “The TeV Physics of Strongly Interacting W’s and Z’s,” *Nucl.Phys.*, vol. B261, p. 379, 1985.
- [30] T. Gherghetta, “TASI Lectures on a Holographic View of Beyond the Standard Model Physics,” 2010, hep-ph/1008.2570.
- [31] N. Arkani-Hamed, S. Dimopoulos, and G. Dvali, “The Hierarchy problem and new dimensions at a millimeter,” *Phys.Lett.*, vol. B429, pp. 263–272, 1998, hep-ph/9803315.
- [32] L. Randall and R. Sundrum, “A Large mass hierarchy from a small extra dimension,” *Phys.Rev.Lett.*, vol. 83, pp. 3370–3373, 1999, hep-ph/9905221.
- [33] L. Randall and R. Sundrum, “An Alternative to compactification,” *Phys.Rev.Lett.*, vol. 83, pp. 4690–4693, 1999, hep-th/9906064.
- [34] H. Davoudiasl, J. Hewett, and T. Rizzo, “Bulk gauge fields in the Randall-Sundrum model,” *Phys.Lett.*, vol. B473, pp. 43–49, 2000, hep-ph/9911262.
- [35] A. Pomarol, “Gauge bosons in a five-dimensional theory with localized gravity,” *Phys.Lett.*, vol. B486, pp. 153–157, 2000, hep-ph/9911294.
- [36] S. Chang, J. Hisano, H. Nakano, N. Okada, and M. Yamaguchi, “Bulk standard model in the Randall-Sundrum background,” *Phys.Rev.*, vol. D62, p. 084025, 2000, hep-ph/9912498.
- [37] K. Agashe, G. Perez, and A. Soni, “Flavor structure of warped extra dimension models,” *Phys.Rev.*, vol. D71, p. 016002, 2005, hep-ph/0408134.

- [38] K. Agashe, G. Perez, and A. Soni, “B-factory signals for a warped extra dimension,” *Phys.Rev.Lett.*, vol. 93, p. 201804, 2004, hep-ph/0406101.
- [39] S. J. Huber and Q. Shafi, “Neutrino oscillations and rare processes in models with a small extra dimension,” *Phys.Lett.*, vol. B512, pp. 365–372, 2001, hep-ph/0104293.
- [40] S. J. Huber and Q. Shafi, “Majorana neutrinos in a warped 5-D standard model,” *Phys.Lett.*, vol. B544, pp. 295–306, 2002, hep-ph/0205327.
- [41] S. J. Huber and Q. Shafi, “Seesaw mechanism in warped geometry,” *Phys.Lett.*, vol. B583, pp. 293–303, 2004, hep-ph/0309252.
- [42] T. Appelquist, B. A. Dobrescu, E. Ponton, and H.-U. Yee, “Neutrinos vis-a-vis the six-dimensional standard model,” *Phys.Rev.*, vol. D65, p. 105019, 2002, hep-ph/0201131.
- [43] T. Gherghetta, “Dirac neutrino masses with Planck scale lepton number violation,” *Phys.Rev.Lett.*, vol. 92, p. 161601, 2004, hep-ph/0312392.
- [44] G. Moreau and J. Silva-Marcos, “Neutrinos in warped extra dimensions,” *JHEP*, vol. 0601, p. 048, 2006, hep-ph/0507145.
- [45] G. Moreau, “Realistic neutrino masses from multi-brane extensions of the Randall-Sundrum model?,” *Eur.Phys.J.*, vol. C40, pp. 539–554, 2005, hep-ph/0407177.
- [46] S. Chang, C. Kim, and M. Yamaguchi, “Hierarchical mass structure of fermions in warped extra dimension,” *Phys.Rev.*, vol. D73, p. 033002, 2006, hep-ph/0511099.
- [47] C. Csaki, A. Falkowski, and A. Weiler, “The Flavor of the Composite Pseudo-Goldstone Higgs,” *JHEP*, vol. 0809, p. 008, 2008, hep-ph/0804.1954.
- [48] A. L. Fitzpatrick, G. Perez, and L. Randall, “Flavor anarchy in a Randall-Sundrum model with 5D minimal flavor violation and a low Kaluza-Klein scale,” *Phys.Rev.Lett.*, vol. 100, p. 171604, 2008, hep-ph/0710.1869.
- [49] M. Blanke, A. J. Buras, B. Duling, S. Gori, and A. Weiler, “ $\Delta F=2$  Observables and Fine-Tuning in a Warped Extra Dimension with Custodial Protection,” *JHEP*, vol. 0903, p. 001, 2009, hep-ph/0809.1073.
- [50] M. Blanke, A. J. Buras, B. Duling, K. Gemmler, and S. Gori, “Rare K and B Decays in a Warped Extra Dimension with Custodial Protection,” *JHEP*, vol. 0903, p. 108, 2009, hep-ph/0812.3803.

- [51] M. E. Albrecht, M. Blanke, A. J. Buras, B. Duling, and K. Gemmler, “Electroweak and Flavour Structure of a Warped Extra Dimension with Custodial Protection,” *JHEP*, vol. 0909, p. 064, 2009, hep-ph/0903.2415.
- [52] M. Bauer, S. Casagrande, L. Grunder, U. Haisch, and M. Neubert, “Little Randall-Sundrum models:  $\epsilon(K)$  strikes again,” *Phys.Rev.*, vol. D79, p. 076001, 2009, hep-ph/0811.3678.
- [53] M. Bauer, S. Casagrande, U. Haisch, and M. Neubert, “Flavor Physics in the Randall-Sundrum Model: II. Tree-Level Weak-Interaction Processes,” *JHEP*, vol. 1009, p. 017, 2010, hep-ph/0912.1625.
- [54] G. Cacciapaglia, C. Csaki, J. Galloway, G. Marandella, J. Terning, *et al.*, “A GIM Mechanism from Extra Dimensions,” *JHEP*, vol. 0804, p. 006, 2008, hep-ph/0709.1714.
- [55] J. Santiago, “Minimal Flavor Protection: A New Flavor Paradigm in Warped Models,” *JHEP*, vol. 0812, p. 046, 2008, hep-ph/0806.1230.
- [56] C. Csaki, G. Perez, Z. Surujon, and A. Weiler, “Flavor Alignment via Shining in RS,” *Phys.Rev.*, vol. D81, p. 075025, 2010, hep-ph/0907.0474.
- [57] M.-C. Chen, K. Mahanthappa, and F. Yu, “A Viable Randall-Sundrum Model for Quarks and Leptons with T-prime Family Symmetry,” *Phys.Rev.*, vol. D81, p. 036004, 2010, hep-ph/0907.3963.
- [58] M.-C. Chen and H.-B. Yu, “Minimal Flavor Violation in the Lepton Sector of the Randall-Sundrum Model,” *Phys.Lett.*, vol. B672, pp. 253–256, 2009, hep-ph/0804.2503.
- [59] G. Perez and L. Randall, “Natural Neutrino Masses and Mixings from Warped Geometry,” *JHEP*, vol. 0901, p. 077, 2009, hep-ph/0805.4652.
- [60] C. Csaki, C. Delaunay, C. Grojean, and Y. Grossman, “A Model of Lepton Masses from a Warped Extra Dimension,” *JHEP*, vol. 0810, p. 055, 2008, hep-ph/0806.0356.
- [61] F. del Aguila, A. Carmona, and J. Santiago, “Neutrino Masses from an A4 Symmetry in Holographic Composite Higgs Models,” *JHEP*, vol. 1008, p. 127, 2010, hep-ph/1001.5151.
- [62] C. Csaki, A. Falkowski, and A. Weiler, “A Simple Flavor Protection for RS,” *Phys.Rev.*, vol. D80, p. 016001, 2009, hep-ph/0806.3757.

- [63] J. A. Cabrer, G. von Gersdorff, and M. Quiros, “Soft-Wall Stabilization,” *New J.Phys.*, vol. 12, p. 075012, 2010, hep-ph/0907.5361.
- [64] J. A. Cabrer, G. von Gersdorff, and M. Quiros, “Improving Naturalness in Warped Models with a Heavy Bulk Higgs Boson,” *Phys.Rev.*, vol. D84, p. 035024, 2011, hep-ph/1104.3149.
- [65] J. A. Cabrer, G. von Gersdorff, and M. Quiros, “Suppressing Electroweak Precision Observables in 5D Warped Models,” *JHEP*, vol. 1105, p. 083, 2011, hep-ph/1103.1388.
- [66] A. Carmona, E. Ponton, and J. Santiago, “Phenomenology of Non-Custodial Warped Models,” *JHEP*, vol. 1110, p. 137, 2011, hep-ph/1107.1500.
- [67] R. Contino, Y. Nomura, and A. Pomarol, “Higgs as a holographic pseudoGoldstone boson,” *Nucl.Phys.*, vol. B671, pp. 148–174, 2003, hep-ph/0306259.
- [68] K. Agashe, R. Contino, and A. Pomarol, “The Minimal composite Higgs model,” *Nucl.Phys.*, vol. B719, pp. 165–187, 2005, hep-ph/0412089.
- [69] G. Giudice, C. Grojean, A. Pomarol, and R. Rattazzi, “The Strongly-Interacting Light Higgs,” *JHEP*, vol. 0706, p. 045, 2007, hep-ph/0703164.
- [70] I. Low, R. Rattazzi, and A. Vichi, “Theoretical Constraints on the Higgs Effective Couplings,” *JHEP*, vol. 1004, p. 126, 2010, hep-ph/0907.5413.
- [71] K. Agashe, A. Azatov, and L. Zhu, “Flavor Violation Tests of Warped/Composite SM in the Two-Site Approach,” *Phys.Rev.*, vol. D79, p. 056006, 2009, hep-ph/0810.1016.
- [72] B. Lillie, “Collider phenomenology of Higgs bosons in left-right symmetric Randall-Sundrum models,” *JHEP*, vol. 0602, p. 019, 2006, hep-ph/0505074.
- [73] A. Falkowski, “Pseudo-goldstone Higgs production via gluon fusion,” *Phys.Rev.*, vol. D77, p. 055018, 2008, hep-ph/0711.0828.
- [74] A. Djouadi and G. Moreau, “Higgs production at the LHC in warped extra-dimensional models,” *Phys.Lett.*, vol. B660, pp. 67–71, 2008, hep-ph/0707.3800.
- [75] C. Bouchart and G. Moreau, “Higgs boson phenomenology and VEV shift in the RS scenario,” *Phys.Rev.*, vol. D80, p. 095022, 2009, hep-ph/0909.4812.
- [76] G. Cacciapaglia, A. Deandrea, and J. Llodra-Perez, “Higgs  $\rightarrow$  Gamma Gamma beyond the Standard Model,” *JHEP*, vol. 0906, p. 054, 2009, hep-ph/0901.0927.

- [77] A. Azatov, M. Toharia, and L. Zhu, “Higgs Production from Gluon Fusion in Warped Extra Dimensions,” *Phys.Rev.*, vol. D82, p. 056004, 2010, hep-ph/1006.5939.
- [78] S. Casagrande, F. Goertz, U. Haisch, M. Neubert, and T. Pfoh, “Flavor Physics in the Randall-Sundrum Model: I. Theoretical Setup and Electroweak Precision Tests,” *JHEP*, vol. 0810, p. 094, 2008, hep-ph/0807.4937.
- [79] M. Carena, S. Casagrande, F. Goertz, U. Haisch, and M. Neubert, “Higgs Production in a Warped Extra Dimension,” *JHEP*, vol. 1208, p. 156, 2012, hep-ph/1204.0008.
- [80] A. Azatov, M. Toharia, and L. Zhu, “Higgs Mediated FCNC’s in Warped Extra Dimensions,” *Phys.Rev.*, vol. D80, p. 035016, 2009, hep-ph/0906.1990.
- [81] G. Cacciapaglia, C. Csaki, G. Marandella, and J. Terning, “The Gaugephobic Higgs,” *JHEP*, vol. 0702, p. 036, 2007, hep-ph/0611358.
- [82] K. Agashe, A. E. Blechman, and F. Petriello, “Probing the Randall-Sundrum geometric origin of flavor with lepton flavor violation,” *Phys.Rev.*, vol. D74, p. 053011, 2006, hep-ph/0606021.
- [83] J. Gunion, H. Haber, G. Kane, and S. Dawson, *The Higgs Hunters Guide*. Boulder, CO: Westview Press, 2nd edition ed., 2000.
- [84] A. Azatov. private communication.
- [85] Y. Grossman and M. Neubert, “Neutrino masses and mixings in nonfactorizable geometry,” *Phys.Lett.*, vol. B474, pp. 361–371, 2000, hep-ph/9912408.
- [86] T. Gherghetta and A. Pomarol, “Bulk fields and supersymmetry in a slice of AdS,” *Nucl.Phys.*, vol. B586, pp. 141–162, 2000, hep-ph/0003129.
- [87] H. Davoudiasl, J. Hewett, and T. Rizzo, “Experimental probes of localized gravity: On and off the wall,” *Phys.Rev.*, vol. D63, p. 075004, 2001, hep-ph/0006041.
- [88] M. S. Carena, A. Delgado, E. Ponton, T. M. Tait, and C. Wagner, “Precision electroweak data and unification of couplings in warped extra dimensions,” *Phys.Rev.*, vol. D68, p. 035010, 2003, hep-ph/0305188.
- [89] M. S. Carena, A. Delgado, E. Ponton, T. M. Tait, and C. Wagner, “Warped fermions and precision tests,” *Phys.Rev.*, vol. D71, p. 015010, 2005, hep-ph/0410344.

- [90] A. Delgado and A. Falkowski, “Electroweak observables in a general 5D background,” *JHEP*, vol. 0705, p. 097, 2007, hep-ph/0702234.
- [91] S. J. Huber, “Flavor violation and warped geometry,” *Nucl.Phys.*, vol. B666, pp. 269–288, 2003, hep-ph/0303183.
- [92] K. Agashe, R. Contino, L. Da Rold, and A. Pomarol, “A Custodial symmetry for Zb anti-b,” *Phys.Lett.*, vol. B641, pp. 62–66, 2006, hep-ph/0605341.
- [93] K. Agashe, A. Delgado, M. J. May, and R. Sundrum, “RS1, custodial isospin and precision tests,” *JHEP*, vol. 0308, p. 050, 2003, hep-ph/0308036.
- [94] J. A. Cabrer, G. von Gersdorff, and M. Quiros, “Warped Electroweak Breaking Without Custodial Symmetry,” *Phys.Lett.*, vol. B697, pp. 208–214, 2011, hep-ph/1011.2205.
- [95] J. A. Cabrer, G. von Gersdorff, and M. Quiros, “Flavor Phenomenology in General 5D Warped Spaces,” *JHEP*, vol. 1201, p. 033, 2012, hep-ph/1110.3324.
- [96] S. Mert Aybat and J. Santiago, “Bulk Fermions in Warped Models with a Soft Wall,” *Phys.Rev.*, vol. D80, p. 035005, 2009, hep-ph/0905.3032.
- [97] A. Delgado and D. Diego, “Fermion Mass Hierarchy from the Soft Wall,” *Phys.Rev.*, vol. D80, p. 024030, 2009, hep-ph/0905.1095.
- [98] J. de Blas, A. Delgado, B. Ostdiek, and A. de la Puente, “LHC Signals of Non-Custodial Warped 5D Models,” *Phys.Rev.*, vol. D86, p. 015028, 2012, hep-ph/1206.0699.
- [99] S. Casagrande, F. Goertz, U. Haisch, M. Neubert, and T. Pfoh, “The Custodial Randall-Sundrum Model: From Precision Tests to Higgs Physics,” *JHEP*, vol. 1009, p. 014, 2010, hep-ph/1005.4315.
- [100] K. Agashe. private communication.
- [101] K. Agashe and R. Contino, “Composite Higgs-Mediated FCNC,” *Phys.Rev.*, vol. D80, p. 075016, 2009, hep-ph/0906.1542.
- [102] W. D. Goldberger and M. B. Wise, “Modulus stabilization with bulk fields,” *Phys.Rev.Lett.*, vol. 83, pp. 4922–4925, 1999, hep-ph/9907447.
- [103] W. D. Goldberger and M. B. Wise, “Phenomenology of a stabilized modulus,” *Phys.Lett.*, vol. B475, pp. 275–279, 2000, hep-ph/9911457.

- [104] S. S. Gubser, “Curvature singularities: The Good, the bad, and the naked,” *Adv.Theor.Math.Phys.*, vol. 4, pp. 679–745, 2000, hep-th/0002160.
- [105] F. An *et al.*, “Observation of electron-antineutrino disappearance at Daya Bay,” *Phys.Rev.Lett.*, vol. 108, p. 171803, 2012, hep-ex/1203.1669.
- [106] F. An *et al.*, “Improved Measurement of Electron Antineutrino Disappearance at Daya Bay,” *Chin.Phys.*, vol. C37, p. 011001, 2013, hep-ex/1210.6327.
- [107] K. Abe *et al.*, “Indication of Electron Neutrino Appearance from an Accelerator-produced Off-axis Muon Neutrino Beam,” *Phys.Rev.Lett.*, vol. 107, p. 041801, 2011, hep-ex/1106.2822.
- [108] K. Abe *et al.*, “Precise Measurement of the Neutrino Mixing Parameter  $\theta_{23}$  from Muon Neutrino Disappearance in an Off-Axis Beam,” *Phys.Rev.Lett.*, vol. 112, no. 18, p. 181801, 2014, hep-ex/1403.1532.
- [109] P. Adamson *et al.*, “Measurement of the neutrino mass splitting and flavor mixing by MINOS,” *Phys.Rev.Lett.*, vol. 106, p. 181801, 2011, hep-ex/1103.0340.
- [110] P. Adamson *et al.*, “Combined analysis of  $\nu_\mu$  disappearance and  $\nu_\mu \rightarrow \nu_e$  appearance in MINOS using accelerator and atmospheric neutrinos,” *Phys.Rev.Lett.*, vol. 112, p. 191801, 2014, hep-ex/1403.0867.
- [111] J. Ahn *et al.*, “Observation of Reactor Electron Antineutrino Disappearance in the RENO Experiment,” *Phys.Rev.Lett.*, vol. 108, p. 191802, 2012, hep-ex/1204.0626.
- [112] Y. Abe *et al.*, “Reactor electron antineutrino disappearance in the Double Chooz experiment,” *Phys.Rev.*, vol. D86, p. 052008, 2012, hep-ex/1207.6632.
- [113] Y. Abe *et al.*, “Improved measurements of the neutrino mixing angle  $\theta_{13}$  with the Double Chooz detector,” *JHEP*, vol. 1410, p. 86, 2014, hep-ex/1406.7763.
- [114] P. Minkowski, “ $\mu \rightarrow e$  gamma at a Rate of One Out of 1-Billion Muon Decays?,” *Phys.Lett.*, vol. B67, p. 421, 1977.
- [115] M. Gell-Mann, P. Ramond, and R. Slansky, *Supergravity: Proceedings Of The Supergravity Workshop At Stony Brook*. New York: Elsevier Science Ltd, 2nd edition ed., 1979.
- [116] T. Yanagida, *Proceedings of the Workshop on the Unified Theory and the Baryon Number in the Universe*. Tsukuba, Japan: KEK, 1979.

- [117] J. Gunion, H. Haber, G. Kane, and S. Dawson, *Proceedings of the 1979 Cargese Summer Institute on Quarks and Leptons*. New York: Plenum Press, 1980.
- [118] R. N. Mohapatra and G. Senjanovic, “Neutrino Mass and Spontaneous Parity Violation,” *Phys.Rev.Lett.*, vol. 44, p. 912, 1980.
- [119] J. Schechter and J. Valle, “Neutrino Masses in SU(2) x U(1) Theories,” *Phys.Rev.*, vol. D22, p. 2227, 1980.
- [120] G. Lazarides, Q. Shafi, and C. Wetterich, “Proton Lifetime and Fermion Masses in an SO(10) Model,” *Nucl.Phys.*, vol. B181, pp. 287–300, 1981.
- [121] P. H. Frampton, S. L. Glashow, and D. Marfatia, “Zeroes of the neutrino mass matrix,” *Phys.Lett.*, vol. B536, pp. 79–82, 2002, hep-ph/0201008.
- [122] L. Lavoura, “Zeros of the inverted neutrino mass matrix,” *Phys.Lett.*, vol. B609, pp. 317–322, 2005, hep-ph/0411232.
- [123] S. Dev, S. Verma, S. Gupta, and R. Gautam, “Neutrino Mass Matrices with a Texture Zero and a Vanishing Minor,” *Phys.Rev.*, vol. D81, p. 053010, 2010, hep-ph/1003.1006.
- [124] C. Lam, “Determining Horizontal Symmetry from Neutrino Mixing,” *Phys.Rev.Lett.*, vol. 101, p. 121602, 2008, hep-ph/0804.2622.
- [125] C. Lam, “The Unique Horizontal Symmetry of Leptons,” *Phys.Rev.*, vol. D78, p. 073015, 2008, hep-ph/0809.1185.
- [126] W. Grimus, L. Lavoura, and P. Ludl, “Is S(4) the horizontal symmetry of tri-bimaximal lepton mixing?,” *J.Phys.*, vol. G36, p. 115007, 2009, hep-ph/0906.2689.
- [127] S.-F. Ge, D. A. Dicus, and W. W. Repko, “Z<sub>2</sub> Symmetry Prediction for the Leptonic Dirac CP Phase,” *Phys.Lett.*, vol. B702, pp. 220–223, 2011, hep-ph/1104.0602.
- [128] H.-J. He and F.-R. Yin, “Common Origin of  $\mu-\tau$  and CP Breaking in Neutrino Seesaw, Baryon Asymmetry, and Hidden Flavor Symmetry,” *Phys.Rev.*, vol. D84, p. 033009, 2011, hep-ph/1104.2654.
- [129] R. d. A. Toorop, F. Feruglio, and C. Hagedorn, “Discrete Flavour Symmetries in Light of T2K,” *Phys.Lett.*, vol. B703, pp. 447–451, 2011, hep-ph/1107.3486.

- [130] S.-F. Ge, D. A. Dicus, and W. W. Repko, “Residual Symmetries for Neutrino Mixing with a Large  $\theta_{13}$  and Nearly Maximal  $\delta_D$ ,” *Phys.Rev.Lett.*, vol. 108, p. 041801, 2012, hep-ph/1108.0964.
- [131] R. de Adelhart Toorop, F. Feruglio, and C. Hagedorn, “Finite Modular Groups and Lepton Mixing,” *Nucl.Phys.*, vol. B858, pp. 437–467, 2012, hep-ph/1112.1340.
- [132] H.-J. He and X.-J. Xu, “Octahedral Symmetry with Geometrical Breaking: New Prediction for Neutrino Mixing Angle  $\theta_{13}$  and CP Violation,” *Phys.Rev.*, vol. D86, p. 111301, 2012, hep-ph/1203.2908.
- [133] D. Hernandez and A. Y. Smirnov, “Lepton mixing and discrete symmetries,” *Phys.Rev.*, vol. D86, p. 053014, 2012, hep-ph/1204.0445.
- [134] C. Lam, “Finite Symmetry of Leptonic Mass Matrices,” *Phys.Rev.*, vol. D87, p. 013001, 2013, hep-ph/1208.5527.
- [135] D. Hernandez and A. Y. Smirnov, “Discrete symmetries and model-independent patterns of lepton mixing,” *Phys.Rev.*, vol. D87, no. 5, p. 053005, 2013, hep-ph/1212.2149.
- [136] M. Holthausen, K. S. Lim, and M. Lindner, “Lepton Mixing Patterns from a Scan of Finite Discrete Groups,” *Phys.Lett.*, vol. B721, pp. 61–67, 2013, hep-ph/1212.2411.
- [137] B. Hu, “Neutrino Mixing and Discrete Symmetries,” *Phys.Rev.*, vol. D87, no. 3, p. 033002, 2013, hep-ph/1212.2819.
- [138] D. Hernandez and A. Y. Smirnov, “Relating neutrino masses and mixings by discrete symmetries,” *Phys.Rev.*, vol. D88, no. 9, p. 093007, 2013, hep-ph/1304.7738.
- [139] S. F. King, T. Neder, and A. J. Stuart, “Lepton mixing predictions from  $\Delta(6n^2)$  family Symmetry,” *Phys.Lett.*, vol. B726, pp. 312–315, 2013, hep-ph/1305.3200.
- [140] C. Hagedorn, A. Meroni, and L. Vitale, “Mixing patterns from the groups  $\Sigma(n\phi)$ ,” *J.Phys.*, vol. A47, p. 055201, 2014, hep-ph/1307.5308.
- [141] L. Lavoura and P. O. Ludl, “Residual  $\mathbb{Z}_2 \times \mathbb{Z}_2$  symmetries and lepton mixing,” *Phys.Lett.*, vol. B731, pp. 331–336, 2014, hep-ph/1401.5036.
- [142] P. Harrison, D. Perkins, and W. Scott, “A Redetermination of the neutrino mass squared difference in tri - maximal mixing with terrestrial matter effects,” *Phys.Lett.*, vol. B458, pp. 79–92, 1999, hep-ph/hep-ph/9904297.

- [143] P. Harrison, D. Perkins, and W. Scott, “Tri-bimaximal mixing and the neutrino oscillation data,” *Phys.Lett.*, vol. B530, p. 167, 2002, hep-ph/0202074.
- [144] Z.-z. Xing, “Nearly tri bimaximal neutrino mixing and CP violation,” *Phys.Lett.*, vol. B533, pp. 85–93, 2002, hep-ph/0204049.
- [145] P. Harrison and W. Scott, “Symmetries and generalizations of tri - bimaximal neutrino mixing,” *Phys.Lett.*, vol. B535, pp. 163–169, 2002, hep-ph/0203209.
- [146] P. Harrison and W. Scott, “Permutation symmetry, tri - bimaximal neutrino mixing and the S3 group characters,” *Phys.Lett.*, vol. B557, p. 76, 2003, hep-ph/0302025.
- [147] X. G. He and A. Zee, “Some simple mixing and mass matrices for neutrinos,” *Phys.Lett.*, vol. B560, pp. 87–90, 2003, hep-ph/0301092.
- [148] F. Vissani, “A Study of the scenario with nearly degenerate Majorana neutrinos,” 1997, hep-ph/9708483.
- [149] V. D. Barger, S. Pakvasa, T. J. Weiler, and K. Whisnant, “Bimaximal mixing of three neutrinos,” *Phys.Lett.*, vol. B437, pp. 107–116, 1998, hep-ph/9806387.
- [150] A. J. Baltz, A. S. Goldhaber, and M. Goldhaber, “The Solar neutrino puzzle: An Oscillation solution with maximal neutrino mixing,” *Phys.Rev.Lett.*, vol. 81, pp. 5730–5733, 1998, hep-ph/9806540.
- [151] I. Stancu and D. V. a. Ahluwalia, “L / E flatness of the electron - like event ratio in Super-Kamiokande and a degeneracy in neutrino masses,” *Phys.Lett.*, vol. B460, pp. 431–436, 1999, hep-ph/9903408.
- [152] H. Georgi and S. Glashow, “Neutrinos on earth and in the heavens,” *Phys.Rev.*, vol. D61, p. 097301, 2000, hep-ph/9808293.
- [153] N. Li and B.-Q. Ma, “A New parametrization of the neutrino mixing matrix,” *Phys.Lett.*, vol. B600, pp. 248–254, 2004, hep-ph/0408235.
- [154] H. Fritzsch and Z.-Z. Xing, “Lepton mass hierarchy and neutrino oscillations,” *Phys.Lett.*, vol. B372, pp. 265–270, 1996, hep-ph/9509389.
- [155] H. Fritzsch and Z.-z. Xing, “Large leptonic flavor mixing and the mass spectrum of leptons,” *Phys.Lett.*, vol. B440, pp. 313–318, 1998, hep-ph/9808272.

- [156] H. Fritzsch and Z.-z. Xing, “Maximal neutrino mixing and maximal CP violation,” *Phys.Rev.*, vol. D61, p. 073016, 2000, hep-ph/9909304.
- [157] Y. Zhang, X. Zhang, and B.-Q. Ma, “Quark-lepton complementarity and self-complementarity in different schemes,” *Phys.Rev.*, vol. D86, p. 093019, 2012, hep-ph/1211.3198.
- [158] X. Zhang, Y.-j. Zheng, and B.-Q. Ma, “Quark-lepton complementarity revisited,” *Phys.Rev.*, vol. D85, p. 097301, 2012, hep-ph/1203.1563.
- [159] G.-N. Li, H.-H. Lin, and X.-G. He, “Comment on Reparametrization Invariance of Quark-Lepton Complementarity,” *Phys.Lett.*, vol. B711, pp. 57–61, 2012, hep-ph/1112.2371.
- [160] S. K. Kang, “Revisiting the Quark-Lepton Complementarity and Triminimal Parametrization of Neutrino Mixing Matrix,” *Phys.Rev.*, vol. D83, p. 097301, 2011, hep-ph/1104.1969.
- [161] Y. Ahn, H.-Y. Cheng, and S. Oh, “Quark-lepton complementarity and tribimaximal neutrino mixing from discrete symmetry,” *Phys.Rev.*, vol. D83, p. 076012, 2011, hep-ph/1102.0879.
- [162] Y. Shimizu and R. Takahashi, “Deviations from Tri-Bimaximality and Quark-Lepton Complementarity,” *Europhys.Lett.*, vol. 93, p. 61001, 2011, hep-ph/1009.5504.
- [163] K. M. Patel, “An SO(10)XS4 Model of Quark-Lepton Complementarity,” *Phys.Lett.*, vol. B695, pp. 225–230, 2011, hep-ph/1008.5061.
- [164] J. Barranco, F. Gonzalez Canales, and A. Mondragon, “Universal Mass Texture, CP violation and Quark-Lepton Complementarity,” *Phys.Rev.*, vol. D82, p. 073010, 2010, hep-ph/1004.3781.
- [165] Y.-j. Zheng, “Dependence of the Quark-Lepton Complementarity on Parametrizations of the CKM and PMNS Matrices,” *Phys.Rev.*, vol. D81, p. 073009, 2010, hep-ph/1002.0919.
- [166] Z.-z. Xing, “Right Unitarity Triangles, Stable CP-violating Phases and Approximate Quark-Lepton Complementarity,” *Phys.Lett.*, vol. B679, pp. 111–117, 2009, hep-ph/0904.3172.

- [167] P. H. Frampton and S. Matsuzaki, “Strong Incompatibility of Tribimaximal Mixing with Quark-Lepton Complementarity,” *Mod.Phys.Lett.*, vol. A24, pp. 429–430, 2009, hep-ph/0807.4785.
- [168] W. Rodejohann and K. A. Hochmuth, “Lepton flavor violation, leptogenesis and neutrino mixing in quark-lepton complementarity scenarios,” *Int.J.Mod.Phys.*, vol. A22, pp. 5875–5888, 2007.
- [169] F. Plentinger, G. Seidl, and W. Winter, “The Seesaw mechanism in quark-lepton complementarity,” *Phys.Rev.*, vol. D76, p. 113003, 2007, hep-ph/0707.2379.
- [170] M. Picariello, B. C. Chauhan, J. Pulido, and E. Torrente-Lujan, “Predictions from non trivial quark-lepton complementarity,” *Int.J.Mod.Phys.*, vol. A22, pp. 5860–5874, 2007, hep-ph/0706.2332.
- [171] G. Burdman, “Constraints on the bulk standard model in the Randall-Sundrum scenario,” *Phys.Rev.*, vol. D66, p. 076003, 2002, hep-ph/0205329.
- [172] G. Burdman, “Flavor violation in warped extra dimensions and CP asymmetries in B decays,” *Phys.Lett.*, vol. B590, pp. 86–94, 2004, hep-ph/0310144.
- [173] K. Agashe, T. Okui, and R. Sundrum, “A Common Origin for Neutrino Anarchy and Charged Hierarchies,” *Phys.Rev.Lett.*, vol. 102, p. 101801, 2009, hep-ph/0810.1277.
- [174] A. Carmona and J. Santiago, “The Effective Lagrangian for Bulk Fermions in Models with Extra Dimensions,” *JHEP*, vol. 1201, p. 100, 2012, hep-ph/1110.5651.
- [175] M. Quiros, “Higgs Bosons in Extra Dimensions,” 2013, hep-ph/1311.2824.
- [176] H. Harari, H. Haut, and J. Weyers, “Quark Masses and Cabibbo Angles,” *Phys.Lett.*, vol. B78, p. 459, 1978.
- [177] S. Pakvasa and H. Sugawara, “Discrete Symmetry and Cabibbo Angle,” *Phys.Lett.*, vol. B73, p. 61, 1978.
- [178] S. Pakvasa and H. Sugawara, “Mass of the t Quark in SU(2) x U(1),” *Phys.Lett.*, vol. B82, p. 105, 1979.
- [179] E. Derman and H.-S. Tsao, “SU(2) X U(1) X S(n) Flavor Dynamics and a Bound on the Number of Flavors,” *Phys.Rev.*, vol. D20, p. 1207, 1979.

- [180] Y. Yamanaka, H. Sugawara, and S. Pakvasa, “Permutation Symmetries and the Fermion Mass Matrix,” *Phys.Rev.*, vol. D25, p. 1895, 1982.
- [181] K. A. Milton, E. Abalo, P. Parashar, N. Pourtolami, I. Brevik, *et al.*, “Repulsive Casimir and Casimir-Polder Forces,” *J.Phys.*, vol. A45, p. 374006, 2012, hep-th/1202.6415.
- [182] K. Milton, E. Abalo, P. Parashar, N. Pourtolami, I. Brevik, *et al.*, “Repulsive Casimir Effects,” *Int.J.Mod.Phys.*, vol. A27, p. 1260014, 2012, hep-th/1111.5367.
- [183] K. A. Milton, P. Parashar, N. Pourtolami, and I. Brevik, “Casimir-Polder repulsion: Polarizable atoms, cylinders, spheres, and ellipsoids,” *Phys.Rev.*, vol. D85, p. 025008, 2012, hep-th/1111.4224.
- [184] K. A. Milton, E. Abalo, P. Parashar, N. Pourtolami, I. Brevik, *et al.*, “Casimir-Polder repulsion near edges: wedge apex and a screen with an aperture,” *Phys.Rev.*, vol. A83, p. 062507, 2011, hep-th/1103.4386.

# Appendix A

## Analytical Results for Bulk Higgs Gluon Fusion

From equation (3.39) the shift defined as  $\frac{\Delta}{mv_4} \equiv \frac{1}{v_4} - \frac{Y}{m}$ , can be also derived from

$$\frac{\Delta}{mv_4} = \frac{v_4}{Y_{qu}^u} \sum_{i,j} \frac{Y_{qU_j}^u Y_{U_j Q_i}^{u*} Y_{Q_i u}^u}{M_{Q_i} M_{U_j}}. \quad (\text{A.1})$$

Therefore simply replacing the second Yukawa coupling with the Yukawa coupling of the Higher derivative operator,  $Y^R$  will give

$$\frac{\Delta^R}{mv_4} = \frac{v_4}{Y_{qu}^u} \sum_{i,j} \frac{Y_{qU_j}^u Y_{U_j Q_i}^{Ru*} Y_{Q_i u}^u}{M_{Q_i} M_{U_j}}. \quad (\text{A.2})$$

Here, we present explicit analytic expressions for the  $hgg$  production and also the Yukawa coupling-mass shifts by performing the infinite sums over the KK modes. We also include the result given in reference [80] for the shift due to the usual Yukawa term,  $Y_d \bar{Q} H U$ , for completeness.<sup>1</sup> To summarize, we have

$$\begin{aligned} c_{hgg} &= \frac{2m_d^2}{v_4} R'^2 \frac{2 + c_u - c_q + \beta}{(1 - 2c_q)(1 + 2c_u)} \left[ \frac{(1 - \epsilon^{1-2c_q})(1 - \epsilon^{1+2c_u})}{4 + 2\beta} - \frac{1 - \epsilon^{1-2c_q}}{5 + 2c_u + 2\beta} - \frac{1 - \epsilon^{1+2c_u}}{5 - 2c_q + 2\beta} \right. \\ &\quad + \frac{\epsilon^{1-2c_q}}{4 + 2\beta} (1 - \epsilon^{1+2c_u}) + \frac{\epsilon^{1+2c_u}}{4 + 2\beta} (1 - \epsilon^{1-2c_q}) + \frac{\epsilon^{2-2c_q+2c_u}}{2 - c_u + c_q + \beta} - \frac{\epsilon^{-2c_q+1}}{3 + c_u + c_q + \beta} \\ &\quad \left. - \frac{\epsilon^{1+2c_u}}{3 - c_u - c_q + \beta} + \frac{1}{4 + c_u - c_q + \beta} \right] + \frac{y_t^{RS}}{m_t} A_{1/2}(\tau_t) + \frac{\Delta_2^t}{m_t v_4}, \end{aligned} \quad (\text{A.3})$$

<sup>1</sup>We have reproduced this result using the equation (A.2), and our results match the one given in the text of [80]. Note however that there are a few typos in the eq. A1 of their appendix.

for the  $hgg$  production and

$$\begin{aligned}
 \frac{\Delta_1^d}{mv_4} &= \frac{2m_d^2}{v_4} R'^2 \frac{2+c_u-c_q+\beta}{(1-2c_q)(1+2c_u)} \left[ \frac{(1-\epsilon^{1-2c_q})(1-\epsilon^{1+2c_u})}{6+c_u-c_q+3\beta} - \frac{1-\epsilon^{1-2c_q}}{5+2c_u+2\beta} - \frac{1-\epsilon^{1+2c_u}}{5-2c_q+2\beta} \right. \\
 &+ \frac{\epsilon^{1-2c_q}}{4+2\beta}(1-\epsilon^{1+2c_u}) + \frac{\epsilon^{1+2c_u}}{4+2\beta}(1-\epsilon^{1-2c_q}) + \frac{\epsilon^{2-2c_q+2c_u}}{2-c_u+c_q+\beta} - \frac{\epsilon^{-2c_q+1}}{3+c_u+c_q+\beta} \\
 &\left. - \frac{\epsilon^{1+2c_u}}{3-c_u-c_q+\beta} + \frac{1}{4+c_u-c_q+\beta} \right], \tag{A.4}
 \end{aligned}$$

for the shifted Yukawa coupling. Also, there is a misalignment due to the kinetic term [80], which as discussed in the text, is only important for the case of the third generation quarks. We do not repeat that result here. For the higher derivative term the shift is:

$$\begin{aligned}
 \frac{\Delta_R^d}{mv_4} &= 2 \frac{Y'_R}{\Lambda^2} \frac{m_d^2}{v_4} \frac{2+c_u-c_q+\beta}{(1+2c_u)(1-2c_q)} \left[ \frac{(4-c_q+\beta)(4+c_u+\beta)}{6+3\beta+c_u-c_q} (1-\epsilon^{1-2c_q})(1-\epsilon^{1+2c_u}) \right. \\
 &- \frac{(3-c_q)(4-c_q+\beta)}{5+2\beta-2c_q} (1-\epsilon^{1+2c_u}) - \frac{(3+c_u)(4+c_u+\beta)}{5+2\beta+2c_u} (1-\epsilon^{1-2c_q}) \\
 &+ \frac{(2+c_q)(4-c_q+\beta)}{4+2\beta} \epsilon^{1-2c_q} (1-\epsilon^{1+2c_u}) + \frac{(2-c_u)(4+c_u+\beta)}{4+2\beta} \epsilon^{1+2c_u} (1-\epsilon^{1-2c_q}) \\
 &+ \frac{(2+c_q)(2-c_u)}{2+c_q-c_u+\beta} \epsilon^{2-2c_q+2c_u} - \frac{(3-c_q)(2-c_u)}{3-c_u-c_q+\beta} \epsilon^{1+2c_u} - \frac{(2+c_q)(3+c_u)}{3+c_u+c_q+\beta} \epsilon^{1-2c_q} \\
 &\left. + \frac{(3-c_q)(3+c_u)}{4+c_u-c_q+\beta} \right].
 \end{aligned}$$

# Appendix B

## Bulk to Brane Limit

We summarize the matching prescription for operators containing Higgs field for the case where the Higgs boson is localized on the brane. As explained in Section 3.2, these prescriptions insures that the 5D bulk Higgs scenario transitions smoothly to a brane-localized Higgs case. The brane prescription for the Higgs associates a delta function to the Higgs normalization integral

$$\int_R^{R'} \left(\frac{R}{z}\right)^3 dz [h_\beta(z)]^2 = 1.$$

As the  $HH$ , rather than  $H$  field, is associated with a  $\delta$  function, one must include a  $\beta$  dependence to the bulk Higgs fields to be able to match operators, in the limit  $\beta \rightarrow \infty$  to the brane ones. The conversion is:

$$\begin{aligned} H &\rightarrow \sqrt{\beta}, \\ HH &\rightarrow HH, \\ HHH &\rightarrow \frac{1}{\sqrt{\beta}} HHH, \end{aligned}$$

for matching brane to bulk in the appropriate limit.

So for the shift, we have contributions from  $Y_2$  and  $Y_R$ . As we are dealing with an effective theory, we look at the effect of summing over a finite number of modes, let's say 3 to 5.

For the case of brane Higgs, the contributions for a finite number of modes for  $Y_2$  give exactly 0 (because of boundary values on the brane). This confirms the work of [75]. However, we must add higher order operators  $Y_R$ , which give a significant result (converging to a constant

for  $\beta \rightarrow 1000$  and anything beyond). The result obtained by summing over a finite number of modes in the brane on the  $Y_R$  contribution must be compared with the result in the paper by [80] for the infinite sum of  $Y_2$  on the brane.

For bulk Higgs, the shift contribution from a finite number of modes on the  $Y_2$  contribution is no longer 0. However, adding to this the  $Y_R$  contribution, we notice that the  $Y_R$  contribution for bulk Higgs is much smaller (two orders of magnitude) than the corresponding one in the brane. This is a clear indication that higher order corrections are much more important for the brane Higgs case than for the bulk.

# Appendix C

## Infinite Sums in Modified $AdS_5$

In this appendix we show how to obtain the infinite sums in Eq. (3.41). Using the equations of motion for the fermion field profiles before the electroweak symmetry breaking, from the  $S_{matter}$  one gets

$$\partial_y \hat{\psi}_L + M_\psi(y) \hat{\psi}_L = e^{A(y)} m_n \hat{\psi}_R,$$

$$-\partial_y \hat{\psi}_R + M_\psi(y) \hat{\psi}_R = e^{A(y)} m_n \hat{\psi}_L,$$

and using the definition (4.11) we obtain

$$m_n \hat{\psi}_R - e^{-A-Q} \partial_y (\hat{\psi}_L e^Q) = 0, \quad (C.1)$$

$$m_n \hat{\psi}_L + e^{-A+Q} \partial_y (\hat{\psi}_R e^{-Q}) = 0, \quad (C.2)$$

where the hatted functions are defined as  $\hat{\psi} \equiv e^{-2A} \psi$ . We now multiply the first equation by  $e^{A+Q}$  and the second by  $e^{A-Q}$ . Integrating from 0 to some arbitrary value,  $y'$ , gives,

$$\int_0^{y'} e^{A+Q} \hat{\psi}_R = \frac{1}{m_n} \hat{\psi}_L(y') e^{Q(y')}, \quad (C.3)$$

$$\int_0^{y'} e^{A-Q} \hat{\psi}_L = -\frac{1}{m_n} \hat{\psi}_R(y') e^{-Q(y')}, \quad (C.4)$$

where we have imposed Dirichlet boundary conditions,  $\hat{\psi}_L(0) = 0$  on the first equation, and  $\hat{\psi}_R(0) = 0$  on the second one. Multiplying these equations by  $\hat{\psi}_R(y'')$  and  $\hat{\psi}_L(y'')$  and performing a summation over all of the KK modes we obtain

$$\int_0^{y'} e^{A+Q} \sum_{n=1}^{\infty} \hat{\psi}_R^{(n)}(y'') \hat{\psi}_R^{(n)}(y) = e^{Q(y')} \sum_{n=1}^{\infty} \frac{\hat{\psi}_R^{(n)}(y'') \hat{\psi}_L^{(n)}(y')}{m_n}, \quad (C.5)$$

$$\int_0^{y'} e^{A-Q} \sum_{n=1}^{\infty} \hat{\psi}_L^{(n)}(y'') \hat{\psi}_L^{(n)}(y) = -e^{-Q(y')} \sum_{n=1}^{\infty} \frac{\hat{\psi}_L^{(n)}(y'') \hat{\psi}_R^{(n)}(y')}{m_n}. \quad (\text{C.6})$$

Now using the completeness of the Sturm-Liouville system as<sup>1</sup>

$$\sum_{n=0}^{\infty} \hat{\psi}^{(n)}(y) \hat{\psi}^{(n)}(y') = e^{-A} \delta(y - y'), \quad (\text{C.7})$$

we obtain the sums

$$\sum_{n=1}^{\infty} \frac{\hat{\psi}_R^{(n)}(y'') \hat{\psi}_L^{(n)}(y')}{m_n} = e^{-Q(y')} \int_0^{y'} e^{A+Q} \left[ e^{-A} \delta(y'' - y) - \hat{\psi}_R^{(0)}(y'') \hat{\psi}_R^{(0)}(y) \right], \quad (\text{C.8})$$

$$\sum_{n=1}^{\infty} \frac{\hat{\psi}_L^{(n)}(y'') \hat{\psi}_R^{(n)}(y')}{m_n} = -e^{Q(y')} \int_0^{y'} e^{A-Q} \left[ e^{-A} \delta(y'' - y) - \hat{\psi}_L^{(0)}(y'') \hat{\psi}_L^{(0)}(y) \right]. \quad (\text{C.9})$$

Finally performing the  $\delta$ -function integrals and using the normalized zero modes ( $y_1$  being the position of the IR brane)

$$\hat{\psi}_L^{(0)}(y) = \frac{e^{-Q(y)}}{\left(\int_0^{y_1} e^{A-2Q}\right)^{\frac{1}{2}}}, \quad \hat{\psi}_R^{(0)}(y) = \frac{e^{Q(y)}}{\left(\int_0^{y_1} e^{A+2Q}\right)^{\frac{1}{2}}}, \quad (\text{C.10})$$

we get

$$\sum_{n=1}^{\infty} \frac{\hat{\psi}_R^{(n)}(y'') \hat{\psi}_L^{(n)}(y')}{m_n} = e^{Q(y'')-Q(y')} \left[ \theta(y' - y'') - \frac{\int_0^{y'} e^{A-2Q}}{\int_0^{y_1} e^{A-2Q}} \right], \quad (\text{C.11})$$

$$\sum_{n=1}^{\infty} \frac{\hat{\psi}_L^{(n)}(y'') \hat{\psi}_R^{(n)}(y')}{m_n} = -e^{Q(y')-Q(y'')} \left[ \theta(y' - y'') - \frac{\int_0^{y'} e^{A+2Q}}{\int_0^{y_1} e^{A+2Q}} \right]. \quad (\text{C.12})$$

---

<sup>1</sup>Note that here we are working with the hatted functions  $\hat{\psi} \equiv e^{-2A}\psi$ .

# Appendix D

## Explicit Expressions for the Field Profiles

In this appendix we present the explicit expressions mentioned in the text. The fermion profiles are given by

$$q_L^{0,i}(y) = q_0^i e^{(2-c_q^i)A(y)} \quad (\text{D.1})$$

$$u_R^{0,i} = u_0^i e^{(c_u^i+2)A(y)} \quad (\text{D.2})$$

while the Higgs profile is

$$h(y) = h_0 e^{aky} \quad (\text{D.3})$$

with

$$q_0^i = \sqrt{k} \epsilon^{\frac{1}{2}-c_q^i} f(c_q^i) \equiv \sqrt{k} \mathfrak{f}(c_q^i) \quad (\text{D.4})$$

$$u_0^i = \sqrt{k} \epsilon^{\frac{1}{2}+c_u^i} f(-c_u^i) \equiv \sqrt{k} \mathfrak{f}(-c_u^i) \quad (\text{D.5})$$

and

$$h_0 \equiv \sqrt{k} e^{-(a-1)ky_s} \mathfrak{h}_0 \quad (\text{D.6})$$

$$\mathfrak{h}_0 = \frac{1}{\sqrt{ky_s(2(a-1)ky_s)^{-\frac{2}{\nu^2}-1} \left( \Gamma\left(1 + \frac{2}{\nu^2}, 2(a-1)k(y_s - y_1)\right) - \Gamma\left(1 + \frac{2}{\nu^2}, 2(a-1)ky_s\right) \right)}}$$

where

$$\epsilon = e^{-A(y)} = e^{-ky_1} \left(1 - \frac{y_1}{y_s}\right)^{\frac{1}{\nu^2}}. \quad (\text{D.7})$$

We have also defined

$$\mathfrak{f}(c) \equiv \epsilon^{\frac{1}{2}-c} f(c) \quad (\text{D.8})$$

where the function  $f(c)$  is defined as

$$f(c) \equiv \frac{\epsilon^{c-\frac{1}{2}}}{\sqrt{k y_s e^{(1-2c)k y_s} ((1-2c)k y_s)^{\frac{1-2c}{\nu^2}-1} \left( \Gamma\left(1 - \frac{1-2c}{\nu^2}, (1-2c)k(y_s - y_1)\right) - \Gamma\left(1 - \frac{1-2c}{\nu^2}, (1-2c)k y_s\right) \right)}}.$$

Note that the Higgs and the fermion profiles are defined differently. This is due to the specific Higgs potential we have considered. We can now write down the most general form for the Yukawa couplings as

$$y_{ij}^u = \tilde{Y}_{ij}^u h_0 f(c_q^i) f(-c_u^j) \quad (\text{D.9})$$

where the  $\tilde{Y}_{ij}^u$ s are related to the 5D Yukawa couplings via the equation

$$\tilde{Y}_{ij}^u \equiv Y_{ij}^u \sqrt{k} \epsilon^{1-c_q+c_u} y_s e^{k y_s (a-c_q^i+c_u^j)} (k y_s (a-c_q^i+c_u^j))^{\frac{c_u^j-c_q^i}{\nu^2}-1} \left( \Gamma\left(\frac{c_q^i-c_u^j}{\nu^2}+1, (a-c_q^i+c_u^j)k(y_s-y_1)\right) - \Gamma\left(\frac{c_q^i-c_u^j}{\nu^2}+1, (a-c_q^i+c_u^j)k y_s\right) \right) \quad (\text{D.10})$$

Before switching to RS let us use the asymptotic expansion of the incomplete gamma function

$$\Gamma(a, z) \sim z^{a-1} e^{-z} \left( 1 + \frac{a-1}{z} + \frac{(a-1)(a-2)}{z^2} + \mathcal{O}(z^{-3}) \right), \quad (\text{D.11})$$

and up to the first order  $\mathcal{O}(z^{a-1})$  with  $\epsilon$  defined as in (D.7) we get the following asymptotic behavior

$$f(c) \sim \sqrt{\frac{1-2c}{1-\epsilon^{1-2c}}} \quad (\text{D.12})$$

$$h_0 \sim \sqrt{\frac{2(1-a)}{1-e^{2ak y_1} \epsilon^2}} \quad (\text{D.13})$$

$$\tilde{Y}_{ij}^u \sim \frac{e^{ak y_1} \epsilon^{c_q-c_u} - 1}{a-c_q^i+c_u^j} Y_{ij}^u \quad (\text{D.14})$$

keeping the  $\mathcal{O}(z^{a-2})$  term not only gives a much better approximation for the top and neutrino plateaux, it also gives an intuitive picture of these functions:

$$f(c) \sim \epsilon^{c-\frac{1}{2}} \sqrt{\frac{(1-2c)ky_s\nu^2}{ky_s\nu^2(\epsilon^{2c-1}-1) - \epsilon^{2c-1} + \left(\frac{y_s}{y_s-y_1}\right)}} \quad (\text{D.15})$$

$$h_0 \sim \epsilon^{-1}e^{-aky_1} \sqrt{\frac{2(1-a)^2 ky_s\nu^2}{ky_s\nu^2(1-a)(\epsilon^{-2}e^{-2aky_1}-1) - \epsilon^{-2}e^{-2aky_1} + \left(\frac{y_s}{y_s-y_1}\right)}}. \quad (\text{D.16})$$

From these formulas one can see that taking the limits  $\nu \rightarrow \infty$  and  $y_s \rightarrow \infty$  we arrive at the RS

$$f^{RS}(c) = \sqrt{\frac{1-2c}{1-\epsilon^{1-2c}}} \equiv \epsilon^{c-\frac{1}{2}} f^{RS}(c) \quad (\text{D.17})$$

$$h_0^{RS} = e^{(1-a)ky_1} \sqrt{\frac{2(1-a)}{\epsilon^{2(a-1)}-1}} \quad (\text{D.18})$$

$$\tilde{Y}_{ij}^{RS,u} \equiv \frac{\epsilon^{-(a-c_q^i+c_u^j)}-1}{a-c_q^i+c_u^j} Y_{ij}^{RS,u} \quad (\text{D.19})$$

$$\epsilon \equiv e^{-ky_1} \quad (\text{D.20})$$

$$y_{ij}^{RS,u} = \tilde{Y}_{ij}^{RS,u} h_0^{RS} f^{RS}(c_q^i) f^{RS}(-c_u^j) \quad (\text{D.21})$$

# Additional Works

In this section some extra research work conducted at the University of Oklahoma is presented [15, 181, 182, 183, 184]. For this section I am specially grateful to my supervisor at the University of Oklahoma professor Kimball A. Milton. I would also wish to thank my collaborators in that university, Dr. E. K. Abalo, Dr. Prachi Parashar and Dr. Jef Wagner. I would also like to thank professor Iver Brevik and Dr. Simen Å. Ellingsen.

**Casimir-Polder repulsion near edges: Wedge apex and a screen with an aperture**Kimball A. Milton,<sup>\*</sup> E. K. Abalo,<sup>†</sup> Prachi Parashar,<sup>‡</sup> and Nima Pourtolami<sup>§</sup>*Homer L. Dodge Department of Physics and Astronomy, University of Oklahoma, Norman, Oklahoma 73019-2061, USA*Iver Brevik<sup>||</sup> and Simen Å. Ellingsen<sup>¶</sup>*Department of Energy and Process Engineering, Norwegian University of Science and Technology, N-7491 Trondheim, Norway*

(Received 22 March 2011; published 13 June 2011)

Although repulsive effects have been predicted for quantum vacuum forces between bodies with nontrivial electromagnetic properties, such as between a perfect electric conductor and a perfect magnetic conductor, realistic repulsion seems difficult to achieve. Repulsion is possible if the medium between the bodies has a permittivity in value intermediate to those of the two bodies, but this may not be a useful configuration. Here, inspired by recent numerical work, we initiate analytic calculations of the Casimir-Polder interaction between an atom with anisotropic polarizability and a plate with an aperture. In particular, for a semi-infinite plate, and, more generally, for a wedge, the problem is exactly solvable, and for sufficiently large anisotropy, Casimir-Polder repulsion is indeed possible, in agreement with the previous numerical studies. In order to achieve repulsion, what is needed is a sufficiently sharp edge (not so very sharp, in fact) so that the directions of polarizability of the conductor and the atom are roughly normal to each other. The machinery for carrying out the calculation with a finite aperture is presented. As a motivation for the quantum calculation, we carry out the corresponding classical analysis for the force between a dipole and a metallic sheet with a circular aperture, when the dipole is on the symmetry axis and oriented in the same direction.

DOI: [10.1103/PhysRevA.83.062507](https://doi.org/10.1103/PhysRevA.83.062507)

PACS number(s): 31.30.jh, 42.50.Lc, 32.10.Dk, 03.50.De

**I. INTRODUCTION**

There has been increasing interest in utilizing the quantum vacuum force or the Casimir effect in nanotechnology employing mesoscopic objects [1]. Although the original Casimir effect, between parallel conducting or dielectric plates separated by vacuum [2,3], always gives an attractive force between the plates, introducing a material (liquid) with an intermediate value of the dielectric constant can result in repulsion [4], which has now been observed [5]; for precursors, see [6–10]. [The first experimental test of the Lifshitz theory with an intermediate liquid (helium) was that of Sabisky and Anderson [11]; application of the Lifshitz theory to the melting of water ice was considered by Elbaum and Schick [12].] A recent experiment involving air bubbles in a liquid with boundary walls is described in Ref. [13]. However, this type of repulsion is unlikely to have many applications in building devices.

There are well-known repulsive quantum forces in vacuum. The first example was found by Boyer [14]. He computed the self-stress of a perfectly conducting spherical shell due to quantum electrodynamic field fluctuations and found a repulsive result, but the meaning of such a self-energy is extremely obscure. He later found [15] a more observable effect, that the force between a perfect electrically conducting plane ( $\epsilon$ , the permittivity, goes to infinity) and a parallel perfect magnetic conducting plane ( $\mu$ , the permeability, goes

to infinity) is repulsive. This, again, may be a difficult situation to approximately replicate in practice, because the unusual magnetic properties must persist over a wide frequency range.

There has been extensive interest in designing metamaterials that could give rise to Casimir repulsion by simulating a magnetic response [16–21]. Despite some early optimism, the conclusion seems to have transpired that repulsion is impossible between metamaterials made from dielectric and metallic components [22–24]. For recent attempts combining dielectric and magnetic setups, see Refs. [25–27].

Several years ago there was an interesting suggestion by Sopova and Ford [28] that the force between a small dielectric sphere and a dielectric wall was oscillatory, so there were a number of repulsive regimes. However, this effect was canceled by plasmon modes leaving the usual attractive result [29]. Earlier Ford had suggested [30] that the frequency response of materials might be manipulated in order to achieve repulsion, but this was proved to be impossible [31].

Thus it was extremely interesting when Levin *et al.* showed examples of repulsion between conducting objects, in particular between an elongated cylinder above a conducting plane with a circular aperture [32]. (An analytic counterpart is given in [33].) They first gave examples of repulsive forces between arrays of electric dipoles, and an electric dipole and a conducting plane with an aperture cut out. Then they turned to quantum vacuum forces between conducting objects, computed by quite impressive “brute force” finite-difference time-domain and boundary-element methods.

The purpose of the present paper is to try to understand these phenomena analytically. We first show, in Sec. II, that there is no repulsion possible in the weak coupling regime, where because the materials are dilute one may sum Casimir-Polder interactions between atoms [34]. However, there is repulsion in classical electrostatics between a system of three dipoles

<sup>\*</sup> milton@nhn.ou.edu<sup>†</sup> abalo@nhn.ou.edu<sup>‡</sup> prachi@nhn.ou.edu<sup>§</sup> nimap@ou.edu<sup>||</sup> iver.h.brevik@ntnu.no<sup>¶</sup> simen.a.ellingsen@ntnu.no

(Sec. III) and between a fixed dipole and a conducting plane with an aperture, which we discuss in Sec. IV, both in two and three dimensions. This is an interesting pedagogical problem, for it involves mixed coupled integral equations, like those for an electrified disk, or a plane with an aperture with different constant electric fields at large distances above and below the punctured plane [35]. These problems exhibit closed form solutions, and clearly exhibit repulsion when the dipole is directly above the aperture and is sufficiently close. In Sec. V we turn to the real problem, that of the Casimir-Polder force between an anisotropic polarizable atom and a punctured dielectric plane. Because solving the integral equations arising for the Green's dyadic for the plate with aperture is rather complicated, in Sec. VI we content ourselves with computing the Casimir-Polder interaction between a polarizable atom and a perfectly conducting wedge. When the opening angle of the wedge approaches  $2\pi$ , this describes the interaction between an atom and a semi-infinite conducting plane. We exhibit situations in which repulsive forces in certain directions can arise for anisotropic atoms, in qualitative agreement with numerical work [32]. In Appendix A we give another derivation of the Casimir-Polder energy formula for the wedge, based on a closed form for the Green's dyadic, and in Appendix B we give a classical calculation of a conducting ellipsoid above a conducting plate with a circular aperture in the presence of a background field.

A word about terminology: When we say "atom" we mean any microscopic particle which may be described by a polarizability tensor. Our calculations assume that we are in the retarded regime, so that static (frequency-independent) polarizabilities may be employed. Should lower frequency transitions dominate (which could occur with some molecules), so that the separations are in the nonretarded regime, electrostatic results are valid [but for a factor of  $1/2$ —See Eq. (4.15) below and Ref. [36]].

In this paper we set  $\hbar = c = 1$ , and all results are expressed in Gaussian units except that Heaviside-Lorentz units are used for Green's dyadics.

## II. WEAK COUPLING CALCULATION

### A. Scalar field

We first illustrate the ideas by considering the case of a massless scalar field in two dimensions. The quantum vacuum energy between two weakly coupled potentials  $V_1$  and  $V_2$  is

$$U_{12} = -\frac{1}{32\pi^2} \int (d\mathbf{r})(d\mathbf{r}') \frac{V_1(\mathbf{r})V_2(\mathbf{r}')}{|\mathbf{r} - \mathbf{r}'|^2}, \quad (2.1)$$

the scalar analog of the Casimir-Polder force between atoms. Here we consider the potentials as shown in Fig. 1, which represents a needle of length  $L$  on the symmetry axis a distance  $Z$  above a line with a gap of width  $a$ . The potentials are given by

$$V_1(x, z) = \lambda_1 \delta(x) \theta(z - Z + L/2) \theta(Z + L/2 - z), \quad (2.2a)$$

$$V_2(x, z) = \lambda_2 \delta(z) [\theta(x - a/2) + \theta(-x - a/2)]. \quad (2.2b)$$

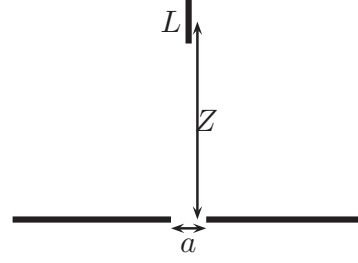


FIG. 1. Two-dimensional geometry of a needle of length  $L$  a distance  $Z$  above a line with a gap of width  $a$ .

This means that the interaction energy is

$$U_{12} = -\frac{\lambda_1 \lambda_2}{32\pi^2} \int_{Z-L/2}^{Z+L/2} dz \left\{ \int_{a/2}^{\infty} + \int_{-\infty}^{-a/2} \right\} dx \frac{1}{x^2 + z^2}. \quad (2.3)$$

To get the force on the needle, we simply have to integrate on  $x$ , and differentiate with respect to the limits of the  $z$  integral:

$$F = -\frac{\partial}{\partial Z} U_{12} = \frac{\lambda_1 \lambda_2}{8\pi^2 a} \left[ \frac{\arctan(2Z/a + L/a)}{2Z/a + L/a} - \frac{\arctan(2Z/a - L/a)}{2Z/a - L/a} \right], \quad (2.4)$$

which, because  $F < 0$ , always represents an attractive force between the punctured line and the needle. Note that although the force vanishes at  $Z = 0$ , the energy there, which represents the work done in bringing the needle in from infinity, is not zero.

### B. Electromagnetic field

Now we consider the quantum vacuum force between dilute dielectric media, which may be obtained from the Casimir-Polder potential between isotropic polarizable atoms [34],

$$U_{CP} = -\frac{23}{4\pi} \alpha_1 \alpha_2 \frac{1}{r^7}, \quad (2.5)$$

where  $r$  is the distance between the atoms. We might mention that Eq. (2.5) is in general valid in the retarded limit where the atomic polarizability can be regarded as constant. (For more details, see the review [37].) The result is applicable provided that the atom-plate separation is much greater than the atomic transition wavelength (typically some hundreds of nanometers for ground-state atoms). The media have dielectric constants  $\epsilon_i = 1 + 4\pi N_i \alpha_i$ , where  $N_i$  represents the density of atoms of type  $i$ . Specifically, we consider a three-dimensional configuration, in which an atom of isotropic polarizability  $\alpha$  is placed on the symmetry axis a distance  $Z$  above a dielectric plate of thickness  $t$  with a circular hole in the middle, as shown in Fig. 2.

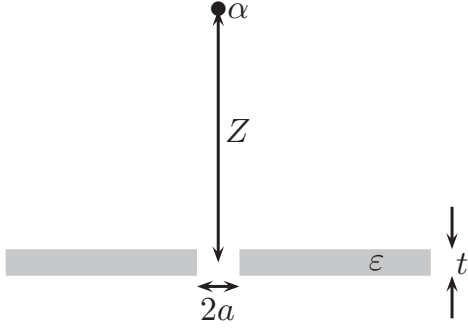


FIG. 2. Three-dimensional geometry of a polarizable atom a distance  $Z$  above a dielectric slab with a circular aperture of radius  $a$ .

The quantum interaction energy is

$$\begin{aligned}
 U &= -\frac{23}{(4\pi)^2} \alpha(\epsilon - 1) \int_{\text{slab}} (d\mathbf{r}) \frac{1}{[(z - Z)^2 + r_{\perp}^2]^{7/2}} \\
 &= -\frac{23}{60\pi a^4} \alpha(\epsilon - 1) \left[ \frac{(t + 2Z)[6a^2 + (t + 2Z)^2]}{[4a^2 + (t + 2Z)^2]^{3/2}} \right. \\
 &\quad \left. + (Z \rightarrow -Z) \right]. \tag{2.6}
 \end{aligned}$$

It is easy to see that the force  $F = -\partial U / \partial Z$  is always negative (i.e., attractive).

A more favorable case for possible repulsion would be an anisotropic atom. It is easy to derive the appropriate generalization of the Casimir-Polder potential in this case, starting from the weak-coupling multiple scattering formula [38],

$$U_{12} = \frac{i}{2} \text{Tr} \Gamma_0 V_1 \Gamma_0 V_2, \tag{2.7}$$

where the free Green's dyadic is ( $\zeta = -i\omega$ ),

$$\Gamma_0(\mathbf{r}, \mathbf{r}') = (\nabla \nabla - \mathbf{1} \zeta^2) \frac{e^{-|\zeta| |\mathbf{r} - \mathbf{r}'|}}{4\pi |\mathbf{r} - \mathbf{r}'|}. \tag{2.8}$$

Following the procedure given in Ref. [38], we find for an isotropic medium facing an anisotropic atom,

$$\begin{aligned}
 U &= \frac{\epsilon - 1}{32\pi^2} \int_{\text{slab}} (d\mathbf{r}) \frac{1}{|\mathbf{r} - \mathbf{R}|^7} \\
 &\quad \times \left[ 13 \text{tr} \alpha + 7 \frac{(\mathbf{r} - \mathbf{R}) \cdot \alpha \cdot (\mathbf{r} - \mathbf{R})}{(\mathbf{r} - \mathbf{R})^2} \right], \tag{2.9}
 \end{aligned}$$

where  $\mathbf{R} = (0, 0, Z)$  is the position of the atom, relative to the center of the aperture. This may be easily checked to reduce to the usual Casimir-Polder result (2.5) when  $\alpha = \alpha \mathbf{1}$ .

Let us consider the extreme case when only  $\alpha_{zz}$  is significant. Then the integrals may be easily carried out, with the result,

$$\begin{aligned}
 U &= \frac{\alpha_{zz}(\epsilon - 1)}{60\pi a^4} \left[ \frac{t + 2Z}{[4 + (t + 2Z)^2]^{5/2}} [156a^4 + 70a^2(t + 2Z)^2 \right. \\
 &\quad \left. + 7(t + 2Z)^4] + (Z \rightarrow -Z) \right]. \tag{2.10}
 \end{aligned}$$

This, again, always gives rise to an attractive force.

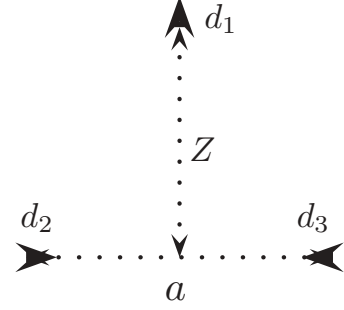


FIG. 3. Configuration of three dipoles, two of which are antiparallel, and one perpendicular to the other two.

An interesting special case is when the aperture is small compared to the thickness of the dielectric. Then the energy is a step function,

$$U = -\frac{7}{30\pi a^4} \alpha_{zz}(\epsilon - 1) \theta(t - 2|Z|), \quad a \ll t, \tag{2.11}$$

which gives rise to a  $\delta$ -function force just when the atom enters and exits the aperture. If the aperture is very large compared to the thickness of the slab,  $t \ll a$ , the energy and force are proportional to the thickness of the slab,

$$U = -\frac{1}{80\pi a^4} \alpha_{zz}(\epsilon - 1) \frac{13a^2 + 18Z^2}{(a^2 + Z^2)^{7/2}} a^4 t. \tag{2.12}$$

### III. CLASSICAL DIPOLE INTERACTION

It is possible to achieve a repulsive force between a configuration of fixed dipoles. Consider the situation illustrated in Fig. 3. Here we have two dipoles, of strength  $d_2$  and  $d_3$  lying along the  $x$  axis, separated by a distance  $a$ . A third dipole of strength  $d_1$  lies along the  $z$  axis. If the two parallel dipoles are oppositely directed and of equal strength,

$$\mathbf{d}_2 = -\mathbf{d}_3 = d_2 \hat{\mathbf{x}}, \tag{3.1}$$

and are equally distant from the  $z$  axis, and the dipole on the  $z$  axis is directed along that axis,

$$\mathbf{d}_1 = d_1 \hat{\mathbf{z}}, \tag{3.2}$$

the force on that dipole is along the  $z$  axis:

$$F_z = 3ad_1 d_2 \frac{a^2/4 - 4Z^2}{(Z^2 + a^2/4)^{7/2}}, \tag{3.3}$$

which changes sign at  $Z = a/4$ ; that is, for distances  $Z$  larger than this, the force is attractive (in the  $-z$  direction) while for shorter distances the force is repulsive (in the  $+z$  direction). Evidently, by symmetry, the dipole-dipole energy vanishes at  $z = 0$ . Consistent with Earnshaw's theorem, the point where the force vanishes is an unstable point with respect to deviations in the  $x$  direction.

In view of this self-evident finding, it might seem surprising that the interaction between a polarizable atom and a dilute medium (made up of polarizable atoms) studied in Sec. II B failed to exhibit a repulsive regime, but this is because the medium is isotropic.

#### IV. CLASSICAL INTERACTION BETWEEN A DIPOLE AND A CONDUCTING PLANE WITH AN APERTURE

In this section, we consider the interaction between a dipole and a perfectly conducting plane containing an aperture. We first consider two dimensions. (As above, we denote the Cartesian coordinates by  $x$  and  $z$  for uniformity with the three-dimensional situation.)

##### A. Dipole above aperture in a conducting line

If we use the Green's function which vanishes on the entire line  $z = 0$ ,

$$G(\mathbf{r}, \mathbf{r}') = -\ln[(x - x')^2 + (z - z')^2] + \ln[(x - x')^2 + (z + z')^2], \quad (4.1)$$

so

$$G(x, 0; x', z') = 0, \quad (4.2)$$

we can calculate the electrostatic potential at any point above the  $z = 0$  plane to be

$$\begin{aligned} \phi(\mathbf{r}) &= \int_{z>0} (d\mathbf{r}') G(\mathbf{r}, \mathbf{r}') \rho(\mathbf{r}') \\ &+ \frac{1}{4\pi} \int_{\text{ap}} dS' \frac{\partial}{\partial z'} G(\mathbf{r}, \mathbf{r}') \Big|_{z'=0} \phi(\mathbf{r}'), \end{aligned} \quad (4.3)$$

where the volume integral is over the charge density of the dipole,

$$\rho(\mathbf{r}) = -\mathbf{d} \cdot \nabla \delta(\mathbf{r} - \mathbf{R}), \quad \mathbf{R} = (0, Z). \quad (4.4)$$

The surface integral extends only over the aperture because the potential vanishes on the conducting sheet. If we choose  $\mathbf{d}$  to point along the  $z$  axis we easily find

$$\begin{aligned} \phi(x, z > 0) &= 2d \left[ \frac{z - Z}{x^2 + (z - Z)^2} + \frac{z + Z}{x^2 + (z + Z)^2} \right] \\ &+ \frac{1}{\pi} \int_{-a/2}^{a/2} dx' \frac{z}{(x - x')^2 + z^2} \phi(x', 0), \end{aligned} \quad (4.5)$$

where  $a$  is the width of the aperture.

Now the free Green's function in two dimensions is

$$\begin{aligned} G_0(\mathbf{r}, \mathbf{r}') &= 4\pi \int \frac{(d\mathbf{k})}{(2\pi)^2} \frac{e^{ik_x(x-x')} e^{ik_z(z-z')}}{k_x^2 + k_z^2} \\ &= \int_{-\infty}^{\infty} dk_x \frac{1}{|k_x|} e^{ik_x(x-x')} e^{-|k_x||z-z'|}. \end{aligned} \quad (4.6)$$

Then the surface integral in Eq. (4.5) is

$$\int_{-\infty}^{\infty} \frac{dk_x}{2\pi} e^{ik_x x} e^{-|k_x|z} \tilde{\phi}(k_x), \quad (4.7)$$

in terms of the Fourier transform of the field,

$$\begin{aligned} \tilde{\phi}(k_x) &= \int_{-\infty}^{\infty} dx' e^{-ik_x x'} \phi(x', 0) \\ &= 2 \int_0^{a/2} dx' \cos k_x x' \phi(x', 0), \end{aligned} \quad (4.8)$$

since  $\phi(x, 0)$  must be an even function for the geometry considered. Thus we conclude

$$\begin{aligned} \phi(x, z > 0) &= 2d \left[ \frac{z - Z}{x^2 + (z - Z)^2} + \frac{z + Z}{x^2 + (z + Z)^2} \right] \\ &+ \frac{1}{\pi} \int_0^{\infty} dk \cos kx e^{-kz} \tilde{\phi}(k). \end{aligned} \quad (4.9)$$

This becomes an identity as  $z \rightarrow 0$ .

The electric field in the aperture is

$$\begin{aligned} E_z(x, z = 0+) &= -\frac{\partial}{\partial z} \phi(x, z) \Big|_{z=0+} \\ &= -4d \frac{x^2 - Z^2}{(x^2 + Z^2)^2} + \frac{1}{\pi} \int_0^{\infty} dk k \cos kx \tilde{\phi}(k). \end{aligned} \quad (4.10)$$

On the other side of the aperture, there is no charge density, so for  $z < 0$  the potential is

$$\phi(x, z < 0) = \frac{1}{\pi} \int_0^{\infty} dk \cos kx e^{kz} \tilde{\phi}(k), \quad (4.11)$$

so the  $z$  component of the electric field in the aperture is

$$\begin{aligned} E_z(x, z = 0-) &= -\frac{\partial}{\partial z} \phi(x, z) \Big|_{z=0-} \\ &= -\frac{1}{\pi} \int_0^{\infty} dk k \cos kx \tilde{\phi}(k). \end{aligned} \quad (4.12)$$

Because we require that the electric field be continuous in the aperture, and the potential vanish on the conductor, we obtain the two coupled integral equations for this problem,

$$\begin{aligned} 4d \frac{x^2 - Z^2}{(x^2 + Z^2)^2} &= \frac{2}{\pi} \int_0^{\infty} dk k \cos kx \tilde{\phi}(k), \\ 0 < |x| < a/2, \end{aligned} \quad (4.13a)$$

$$0 = \int_0^{\infty} dk \cos kx \tilde{\phi}(k), \quad |x| > a/2. \quad (4.13b)$$

In fact, these equations have a simple solution [39]:

$$\tilde{\phi}(k) = -\frac{4Zd\pi}{a} \int_0^1 dx x \frac{J_0(kax/2)}{(x^2 + 4Z^2/a^2)^{3/2}}. \quad (4.14)$$

From this, we can work out the energy of the system from

$$U = -\frac{1}{2} d E_z(0, Z) = \frac{1}{2} d \frac{\partial \phi}{\partial z} \Big|_{z=Z, x=0}, \quad (4.15)$$

where the factor of 1/2 comes from the fact that this must be the energy required to assemble the system. In computing this energy we must, of course, drop the self-energy of the dipole due to its own field. We are then left with

$$\begin{aligned} U_{\text{int}} &= -\frac{d^2}{4Z^2} - \frac{d}{2\pi} \int_0^{\infty} dk k e^{-kZ} \tilde{\phi}(k) \\ &= -\frac{d^2}{4Z^2} + Z^2 d^2 \left(\frac{2}{a}\right)^4 \int_0^1 \frac{1}{2} dx^2 \frac{1}{(x^2 + 4Z^2/a^2)^3} \\ &= -\frac{4Z^2 d^2}{(a^2 + 4Z^2)^2}, \end{aligned} \quad (4.16)$$

where to get the second line we used the derivative of Eq. (4.17). This is exactly two times larger that the result

quoted in Ref. [32].<sup>1</sup> Since this vanishes at  $Z = 0$  and  $Z = \infty$ , the force must change from attractive to repulsive, which happens at  $Z = a/2$ .

### B. Three-dimensional aperture interacting with dipole

It is quite straightforward to repeat the above calculation in three dimensions. Again we are considering a dipole, polarized on the symmetry axis, a distance  $Z$  above a circular aperture of radius  $a$  in a conducting plate.

The free three-dimensional Green's function in cylindrical coordinates has the representation,

$$\frac{1}{\sqrt{\rho^2 + z^2}} = \int_0^\infty dk J_0(k\rho) e^{-k|z|}, \quad (4.17)$$

and so if we follow the above procedure we find for the potential above the plate,

$$\begin{aligned} \phi(\mathbf{r}_\perp, z > 0) = d \left[ \frac{z - Z}{[r_\perp^2 + (z - Z)^2]^{3/2}} + \frac{z + Z}{[r_\perp^2 + (z + Z)^2]^{3/2}} \right] \\ + \int_0^\infty dk k e^{-kz} J_0(kr_\perp) \Phi(k), \end{aligned} \quad (4.18)$$

where the Bessel transform of the potential in the aperture is

$$\Phi(k) = \int_0^\infty d\rho \rho J_0(k\rho) \phi(\rho, 0). \quad (4.19)$$

Thus the integral equations resulting from the continuity of the  $z$  component of the electric field in the aperture and the vanishing of the potential on the conductor are

$$d \frac{r_\perp^2 - 2Z^2}{[r_\perp^2 + Z^2]^{5/2}} = \int_0^\infty dk k^2 J_0(kr_\perp) \Phi(k), \quad r_\perp < a, \quad (4.20a)$$

$$0 = \int_0^\infty dk k J_0(kr_\perp) \Phi(k), \quad r_\perp > a. \quad (4.20b)$$

The solution to these equations is given in Titchmarsh's book [40], and after a bit of manipulation we obtain

$$\Phi(k) = -\left(\frac{2ka}{\pi}\right)^{1/2} \frac{d}{ka} \int_0^1 dx x^{3/2} J_{1/2}(xka) \frac{2Z/a}{(x^2 + Z^2/a^2)^2}. \quad (4.21)$$

Then the energy (4.15) may be easily evaluated using

$$\int_0^\infty dk k^{3/2} e^{-kZ} J_{1/2}(kax) = 2\sqrt{\frac{2xa}{\pi}} \frac{Z}{(x^2a^2 + Z^2)^2}. \quad (4.22)$$

The energy can again be expressed in closed form:

$$\begin{aligned} U = -\frac{d^2}{8Z^3} + \frac{d^2}{4\pi Z^3} \left[ \arctan \frac{a}{Z} \right. \\ \left. + \frac{Z}{a} \frac{1 + 8/3(Z/a)^2 - (Z/a)^4}{(1 + Z^2/a^2)^3} \right]. \end{aligned} \quad (4.23)$$

<sup>1</sup>This is not the factor of 1/2 in Eq. (4.15). It is not possible to trace the origin of the discrepancy, since the authors of that reference quote the result without details.

This is always negative, but vanishes at infinity and at zero:

$$Z \rightarrow 0: \quad U \rightarrow -\frac{4}{5\pi} d^2 \frac{Z^2}{a^5}. \quad (4.24)$$

This means that for some value of  $Z \sim a$  the force changes from attractive to repulsive. Numerically, we find that the force changes sign at  $Z = 0.742358a$ .

The reason why the energy vanishes when the dipole is centered in the aperture is clear: Then the electric field lines are perpendicular to the conducting sheet on the surface, and the sheet could be removed without changing the field configuration.

Our goal is to analytically find the quantum (Casimir) analog of this classical repulsion.

### V. STRONG COUPLING—FORCE BETWEEN AN ATOM AND A PUNCTURED PLANE DIELECTRIC

Now we turn to the real problem. Our starting point is the general expression for the vacuum energy [38]:

$$U = \frac{i}{2} \text{Tr} \ln \Gamma \Gamma_0^{-1}, \quad (5.1)$$

where  $\Gamma$  is the full Green's dyadic for the problem, and  $\Gamma_0^{-1}$  is the inverse of the free Green's dyadic (2.8), namely,

$$\Gamma_0^{-1} = \frac{1}{\omega^2} \nabla \times \nabla \times -\mathbf{1}. \quad (5.2)$$

In the presence of a potential  $\mathbf{V}$ , the full Green's dyadic has the symbolic form,

$$\Gamma = (\mathbf{1} - \Gamma_0 \mathbf{V})^{-1} \Gamma_0. \quad (5.3)$$

Here we are thinking of the interaction between a dielectric medium, characterized by an isotropic permittivity, so  $V_1 = \varepsilon - 1$ , and a polarizable atom, represented by a polarizability dyadic, as shown in Fig. 2,

$$\mathbf{V}_2 = 4\pi \alpha \delta(\mathbf{r} - \mathbf{R}), \quad (5.4)$$

where  $\mathbf{R}$  is the position of the dipole. We are only interested in a single interaction with the latter potential, so we have for the interaction energy,

$$\begin{aligned} U_{12} = \text{Tr} \mathbf{V}_2 \frac{\delta}{\delta V_1} \left[ -\frac{i}{2} \ln(1 - \Gamma_0 V_1) \right] \\ = \frac{i}{2} \text{Tr}(\Gamma_1 - \Gamma_0) \mathbf{V}_2, \end{aligned} \quad (5.5)$$

where we have used Eq. (5.3) for the potential  $V_1$  describing the dielectric slab plus aperture and we have subtracted the term that represents the self-energy of the atom with its own field. This subtraction happens automatically if we start from the "TGTG" form,

$$\begin{aligned} U_{12} = -\frac{i}{2} \text{Tr} \ln(\mathbf{1} - \Gamma_1 \mathbf{V}_1 \Gamma_2 \mathbf{V}_2) \\ \approx \frac{i}{2} \text{Tr} \Gamma_1 \mathbf{V}_1 \Gamma_0 \mathbf{V}_2 = \frac{i}{2} \text{Tr}(\Gamma_1 - \Gamma_0) \mathbf{V}_2, \end{aligned} \quad (5.6)$$

because  $\mathbf{V}_2$  is weak. This implies the Casimir-Polder expression for the interaction between the polarizable atom and the

dielectric,

$$U_{\text{CP}} = - \int_{-\infty}^{\infty} d\zeta \operatorname{tr} \boldsymbol{\alpha} \cdot (\boldsymbol{\Gamma} - \boldsymbol{\Gamma}_0)(Z, Z). \quad (5.7)$$

We could also derive this result from the formula for the force on a dielectric body in an inhomogeneous electric field [36],

$$\mathbf{F} = - \frac{1}{8\pi} \int (d\mathbf{r}) E^2(\mathbf{r}) \nabla \varepsilon, \quad (5.8)$$

which classically says that a dielectric body experiences a force pushing it into the region of the stronger field. This implies the interaction energy,

$$U = - \frac{1}{2} \alpha E^2(\mathbf{0}, Z), \quad (5.9)$$

and when we make the quantum-field-theoretic replacement,

$$\frac{1}{4\pi} \langle \mathbf{E}(\mathbf{r}) \mathbf{E}(\mathbf{r}') \rangle \rightarrow \frac{1}{i} \boldsymbol{\Gamma}(\mathbf{r}, \mathbf{r}') = \frac{1}{i} \int \frac{d\omega}{2\pi} \boldsymbol{\Gamma}(\mathbf{r}, \mathbf{r}'; \omega), \quad (5.10)$$

we recover the static isotropic version of Eq. (5.7) after the self-energy is subtracted.

### A. No aperture

When the aperture is not present, we are considering the well-studied case of a dielectric slab, of thickness  $t$ , interacting with a polarizable atom. Because the Green's dyadic in this situation, denoted  $\boldsymbol{\Gamma}^{(0)}$ , then possesses translational invariance in the  $x$ - $y$  plane, we can express it in terms of a reduced Green's dyadic,

$$\boldsymbol{\Gamma}^{(0)}(\mathbf{r}, \mathbf{r}') = \int \frac{(d\mathbf{k}_{\perp})}{(2\pi)^2} e^{i\mathbf{k}_{\perp} \cdot (\mathbf{r} - \mathbf{r}')_{\perp}} \mathbf{g}(z, z'; k_{\perp}). \quad (5.11)$$

$$\begin{aligned} U &= -\alpha \int_{-\infty}^{\infty} d\zeta \int \frac{(d\mathbf{k}_{\perp})}{(2\pi)^2} [-\zeta^2 R^H + (2k^2 + \zeta^2) R^E] \frac{1}{2\kappa} e^{-\kappa(2Z-t)} \\ &= -\frac{\alpha}{4\pi} \int_0^{\infty} d\zeta \int dk_{\perp}^2 \frac{1}{\kappa} e^{-2\kappa(Z-t/2)} \left\{ (\varepsilon - 1) \zeta^4 \frac{e^{2\kappa' t} - 1}{(\kappa + \kappa')^2 e^{2\kappa' t} - (\kappa - \kappa')^2} \right. \\ &\quad \left. + \frac{\varepsilon - 1}{\varepsilon} (2k^2 + \zeta^2) \left[ k^2 \left( 1 + \frac{1}{\varepsilon} \right) + \zeta^2 \right] \frac{e^{2\kappa' t} - 1}{(\kappa + \kappa'/\varepsilon)^2 e^{2\kappa' t} - (\kappa - \kappa'/\varepsilon)^2} \right\}. \end{aligned} \quad (5.17)$$

This is precisely the result found, for example, by Zhou and Spruch [41].

### B. Integral equations for Green's dyadic

We now specialize to the case where the plane  $z = 0$  consists of a perfectly conducting screen with a circular aperture of radius  $a$  at the origin. The Green's dyadic satisfies the differential equation,

$$\left( \frac{1}{\omega^2} \nabla \times \nabla \times - \mathbf{1} \right) \cdot \boldsymbol{\Gamma}(\mathbf{r} - \mathbf{r}') = \mathbf{1} \delta(\mathbf{r} - \mathbf{r}'), \quad (5.18)$$

subject to the boundary conditions,

$$\hat{\mathbf{z}} \times \boldsymbol{\Gamma}(\mathbf{r}, \mathbf{r}')|_{|\mathbf{r}_{\perp}| > a, z=0} = 0, \quad (5.19)$$

In the case of an isotropic atom, the trace of the Green's dyadic occurs, which is for the reduced Green's dyadic,

$$\operatorname{tr} \mathbf{g}(Z, Z) = -\zeta^2 g^H(Z, Z) + \left( \frac{\partial}{\partial Z} \frac{\partial}{\partial Z'} + k_{\perp}^2 \right) g^E(Z, Z') \Big|_{Z'=Z}, \quad (5.12)$$

in terms of the transverse electric (H) and transverse magnetic (E) Green's functions. These subtracted quantities are for  $z, z'$  above the dielectric,

$$g^{H,E}(z, z') - g_0^{H,E}(z, z') = \frac{1}{2\kappa} R^{H,E} e^{-\kappa(z+z'-t)}, \quad (5.13)$$

in terms of the reflection coefficients,

$$R^H = \frac{\kappa - \kappa'}{\kappa + \kappa'} + 4 \frac{\kappa \kappa'}{\kappa'^2 - \kappa^2} \frac{1}{D}, \quad (5.14a)$$

$$R^E = \frac{\kappa - \bar{\kappa}'}{\kappa + \bar{\kappa}'} + 4 \frac{\kappa \bar{\kappa}'}{\bar{\kappa}'^2 - \kappa^2} \frac{1}{\bar{D}}, \quad (5.14b)$$

where

$$\kappa^2 = k_{\perp}^2 + \zeta^2, \quad \kappa'^2 = k_{\perp}^2 + \varepsilon \zeta^2, \quad \bar{\kappa}' = \kappa' / \varepsilon, \quad (5.15)$$

and

$$D = \left( \frac{\kappa + \kappa'}{\kappa - \kappa'} \right)^2 e^{2\kappa' t} - 1, \quad (5.16)$$

with  $\bar{D}$  obtained from this by replacing  $\kappa'$  by  $\bar{\kappa}'$  except in the exponent. These results are rather trivially obtained by multiple scattering arguments.

Now the interaction energy is

which just states that the tangential components of the electric field must vanish on the conductor. Following Levine and Schwinger [42] we introduce auxiliary electric and magnetic Green's dyadics  $\boldsymbol{\Gamma}^{(1,2)}(\mathbf{r}, \mathbf{r}')$  which satisfy the same differential equation (5.18) but with the boundary conditions satisfied on the entire  $z = 0$  plane:

$$\hat{\mathbf{z}} \times \boldsymbol{\Gamma}^{(1)}(\mathbf{r}, \mathbf{r}')|_{z=0} = 0, \quad \hat{\mathbf{z}} \times [\nabla \times \boldsymbol{\Gamma}^{(2)}(\mathbf{r}, \mathbf{r}')]|_{z=0} = 0. \quad (5.20)$$

These can be constructed in terms of the free Green's dyadic  $\boldsymbol{\Gamma}_0$ , subject only to outgoing boundary conditions at infinity, as given in Eq. (2.8),

$$\boldsymbol{\Gamma}_0(\mathbf{r}, \mathbf{r}') = (\mathbf{1}\omega^2 + \nabla \nabla) G(|\mathbf{r} - \mathbf{r}'|), \quad (5.21)$$

expressed in turn in terms of the Helmholtz Green's function,

$$G(R) = \frac{e^{i|\omega|R}}{4\pi R}. \quad (5.22)$$

We can write, after the Euclidean rotation  $|\omega| \rightarrow i\zeta$ , the free Green's dyadic in the explicit form ( $\mathbf{R} = \mathbf{r} - \mathbf{r}'$ ),

$$\begin{aligned} \Gamma_0(\mathbf{r}, \mathbf{r}') = & -\frac{G(R)}{R^2} \left[ \mathbf{1}(1 + \zeta R + \zeta^2 R^2) \right. \\ & \left. - \frac{\mathbf{R}\mathbf{R}}{R^2}(3 + 3\zeta R + \zeta^2 R^2) \right]. \end{aligned} \quad (5.23)$$

In terms of this last dyadic, the auxiliary Green's dyadics have the form,

$$\begin{aligned} z, z' > 0: \quad \Gamma^{(1),(2)}(\mathbf{r}, \mathbf{r}') \\ = \Gamma^{(0)}(\mathbf{r}, \mathbf{r}') \mp \Gamma^{(0)}(\mathbf{r}, \mathbf{r}' - 2\hat{\mathbf{z}}z') \cdot (\mathbf{1} - 2\hat{\mathbf{z}}\hat{\mathbf{z}}). \end{aligned} \quad (5.24)$$

Now using Green's second identity, it is easy to prove

$$\nabla \times \Gamma^{(2)}(\mathbf{r}, \mathbf{r}') = [\nabla' \times \Gamma^{(1)}]^T(\mathbf{r}', \mathbf{r}), \quad (5.25a)$$

$$\Gamma^{(1),(2)}(\mathbf{r}, \mathbf{r}') = [\Gamma^{(1),(2)}]^T(\mathbf{r}', \mathbf{r}), \quad (5.25b)$$

where  $T$  signifies transposition. In the same way we may derive the integral equations for the Green's dyadic for the screen with the aperture,

$$\begin{aligned} z, z' > 0: \quad \Gamma(\mathbf{r}, \mathbf{r}') \\ = \Gamma^{(1)}(\mathbf{r}, \mathbf{r}') - \frac{1}{\zeta^2} \int_{\text{ap}} dS'' \nabla \times \Gamma_+^{(2)}(\mathbf{r}, \mathbf{r}'') \cdot \hat{\mathbf{z}} \times \Gamma(\mathbf{r}'', \mathbf{r}'), \end{aligned} \quad (5.26a)$$

$$\begin{aligned} z < 0 < z': \quad \Gamma(\mathbf{r}, \mathbf{r}') \\ = -\frac{1}{\zeta^2} \int_{\text{ap}} dS'' \nabla \times \Gamma_-^{(2)}(\mathbf{r}, \mathbf{r}'') \cdot \hat{\mathbf{z}} \times \Gamma(\mathbf{r}'', \mathbf{r}'), \end{aligned} \quad (5.26b)$$

where the  $\pm$  subscripts on  $\Gamma^{(2)}$  indicate that the Green's function is defined in the domain above or below the  $z = 0$  plane. The continuity of the  $z$  component of the electric field in the aperture then leads to the integral equation:

$$\begin{aligned} \hat{\mathbf{z}} \cdot \Gamma^{(1)}(\mathbf{r}, \mathbf{r}')|_{z \rightarrow 0+} \\ = \frac{1}{\zeta^2} \int_{\text{ap}} dS'' \hat{\mathbf{z}} \cdot \nabla \times (\Gamma_+^{(2)} + \Gamma_-^{(2)})(\mathbf{r}, \mathbf{r}'') \cdot \hat{\mathbf{z}} \times \Gamma(\mathbf{r}'', \mathbf{r}'). \end{aligned} \quad (5.27)$$

The system of integral equations defining the Green's dyadic is rather more complicated than that describing the corresponding (classical) static potential problem, so we will defer the discussion of strategies for its solution to a subsequent publication. We will here turn to a situation that can be solved exactly.

## VI. CASIMIR-POLDER FORCE BETWEEN ATOM AND A CONDUCTING WEDGE

The interaction between a polarizable atom and a perfectly conducting half plane is a special case of the vacuum interaction between such an atom and a conducting wedge. For the case of an isotropic atom, this was considered by Brevik *et al.* [43]. (This followed on earlier work by Brevik

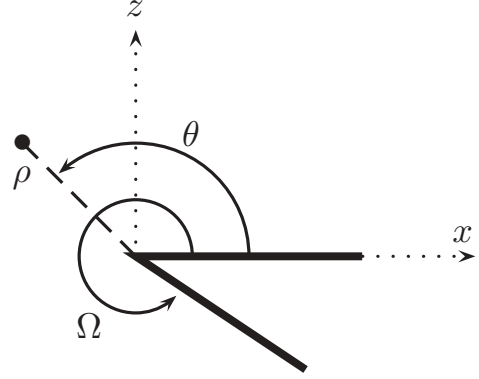


FIG. 4. Polarizable atom, located at polar coordinates  $\rho, \theta$ , within a conducting wedge with dihedral angle  $\Omega$ .

and Lygren [44] and DeRaad and Milton [45].) In terms of the opening dihedral angle of the wedge  $\Omega$ , which we describe in terms of the variable  $p = \pi/\Omega$ , the electromagnetic Green's dyadic has the form (here the translational direction is denoted by  $y$ , and one plane of the wedge lies in the  $z = 0$  plane, the other intersecting the  $xy$  plane on the line  $\theta = \Omega$ —see Fig. 4,

$$\begin{aligned} \Gamma(\mathbf{r}, \mathbf{r}') = 2p \sum_{m=0}^{\infty} \int \frac{dk}{2\pi} \left[ -\mathcal{M}\mathcal{M}'^* (\nabla_{\perp}^2 - k^2) \frac{1}{\omega^2} F_{mp}(\rho, \rho') \right. \\ \times \frac{\cos mp\theta \cos mp\theta'}{\pi} e^{ik(x-x')} + \mathcal{N}\mathcal{N}'^* \frac{1}{\omega} G_{mp}(\rho, \rho') \\ \left. \times \frac{\sin mp\theta \sin mp\theta'}{\pi} e^{ik(x-x')} \right]. \end{aligned} \quad (6.1)$$

The first term here refers to TE (H) modes, the second to TM (E) modes. The prime on the summation sign means that the  $m = 0$  term is counted with half weight. In the polar coordinates in the  $xz$  plane,  $\rho$  and  $\theta$ , the H and E mode operators are

$$\mathcal{M} = \hat{\rho} \frac{\partial}{\rho \partial \theta} - \hat{\theta} \frac{\partial}{\partial \rho}, \quad (6.2a)$$

$$\mathcal{N} = ik \left( \hat{\rho} \frac{\partial}{\partial \rho} + \hat{\theta} \frac{\partial}{\rho \partial \theta} \right) - \hat{\mathbf{y}} \nabla_{\perp}^2, \quad (6.2b)$$

where the transverse Laplacian is

$$\nabla_{\perp}^2 = \frac{1}{\rho} \frac{\partial}{\partial \rho} \rho \frac{\partial}{\partial \rho} + \frac{1}{\rho^2} \frac{\partial^2}{\partial \theta^2}. \quad (6.3)$$

In this situation, the boundaries are entirely in planes of constant  $\theta$ , so the radial Green's functions are equal to the free Green's function,

$$\begin{aligned} \frac{1}{\omega^2} F_{mp}(\rho, \rho') = \frac{1}{\omega} G_{mp}(\rho, \rho') \\ = -\frac{i\pi}{2\lambda^2} J_{mp}(\lambda\rho_{<}) H_{mp}^{(1)}(\lambda\rho_{>}), \end{aligned} \quad (6.4)$$

with  $\lambda^2 = \omega^2 - k^2$ . We will immediately make the Euclidean rotation,  $\omega \rightarrow i\zeta$ , where  $\lambda \rightarrow i\kappa$ ,  $\kappa^2 = \zeta^2 + k^2$ , so the free Green's functions become  $-\kappa^{-2} I_{mp}(\kappa\rho_{<}) K_{mp}(\kappa\rho_{>})$ .

We start by considering the most favorable case for CP repulsion, where the atom is only polarizable in the  $z$  direction, that is, only  $\alpha_{zz} \neq 0$ . In the static limit, then the only

component of the Green's dyadic that contributes is

$$\int \frac{d\xi}{2\pi} \Gamma_{zz} = \frac{2p}{4\pi^3} \int dk d\xi \left\{ [\xi^2 \sin^2 \theta \sin^2 mp\theta - k^2 \cos^2 \theta \cos^2 mp\theta] \frac{m^2 p^2}{\kappa^2 \rho_{<} \rho_{>}} I_{mp}(\kappa \rho_{<}) K_{mp}(\kappa \rho_{>}) - [k^2 \sin^2 \theta \sin^2 mp\theta - \xi^2 \cos^2 \theta \cos^2 mp\theta] I'_{mp}(\kappa \rho_{<}) K'_{mp}(\kappa \rho_{>}) \right\}. \quad (6.5)$$

Here we note that the off diagonal  $\rho$ - $\theta$  terms in  $\Gamma$  cancel. We have regulated the result by point-splitting in the radial coordinate. At the end of the calculation, the limit  $\rho_{<} \rightarrow \rho_{>} = \rho$  is to be taken.

Now the integral over the Bessel functions is given by

$$\int_0^\infty dk \kappa I_\nu(\kappa \rho_{<}) K_\nu(\kappa \rho_{>}) = \frac{z^\nu}{\rho_{>}^2 (1 - \xi^2)}, \quad (6.6)$$

where  $\xi = \rho_{<}/\rho_{>}$ . After that the  $m$  sum is easily carried out by summing a geometrical series. Care must also be taken with the  $m = 0$  term in the cosine series. The result of a straightforward calculation leads to

$$\int \frac{d\xi}{2\pi} \Gamma_{zz} = -\frac{\cos 2\theta}{\pi^2 \rho^4} \frac{1}{(\xi - 1)^4} + \text{finite}, \quad (6.7)$$

where the divergent term, as  $\xi \rightarrow 1$ , may, through a similar calculation, be shown to be that corresponding to the vacuum in the absence of the wedge, that is, that obtained from the free Green's dyadic. Therefore, we must subtract this term off, leaving for the static Casimir energy (5.7):

$$U_{\text{CP}}^{zz} = -\frac{\alpha_{zz}(0)}{8\pi} \frac{1}{\rho^4 \sin^4 p\theta} \left[ p^4 - \frac{2}{3} p^2 (p^2 - 1) \sin^2 p\theta + \frac{(p^2 - 1)(p^2 + 11)}{45} \sin^4 p\theta \cos 2\theta \right]. \quad (6.8)$$

This result is derived by another method in Appendix A.

A small check of this result is that as  $\theta \rightarrow 0$  (or  $\theta \rightarrow \Omega$ ) we recover the expected Casimir-Polder result for an atom above an infinite plane:

$$U_{\text{CP}}^{zz} \rightarrow -\frac{\alpha_{zz}(0)}{8\pi Z^4}, \quad (6.9)$$

in terms of the distance of the atom above the plane,  $Z = \rho\theta$ . This limit is also obtained when  $p \rightarrow 1$ , for when  $\Omega = \pi$  we are describing a perfectly conducting infinite plane.

A very similar calculation gives the result for an isotropic atom,  $\alpha = \alpha \mathbf{1}$ , which was first given in Ref. [43]:

$$U_{\text{CP}} = -\frac{3\alpha(0)}{8\pi \rho^4 \sin^4 p\theta} \left[ p^4 - \frac{2}{3} p^2 (p^2 - 1) \sin^2 p\theta - \frac{1}{3} \frac{1}{45} (p^2 - 1)(p^2 + 11) \sin^4 p\theta \right]. \quad (6.10)$$

Note that this is not three times  $U_{\text{CP}}^{zz}$  in Eq. (6.8) because the  $\cos 2\theta$  factor in the last term in the latter is replaced by  $-1/3$  here. This case was reconsidered recently, for example, in Ref. [46].

### A. Repulsion by a conducting half plane

Let us consider the special case  $p = 1/2$ , that is  $\Omega = 2\pi$ , the case of a semi-infinite conducting plane. This was the situation considered, for anisotropic atoms, in recent papers by Eberlein and Zietal [47–49]. Note that in such a case, for the completely anisotropic atom,  $U_{\text{CP}}^{zz} = 0$  at  $\theta = \pi/2$ , that is, there is no force on the dipole when it is polarized perpendicular to the half sheet and directly above the edge, as observed in Refs. [48,49].

Consider a particle free to move along a line parallel to the  $z$  axis, a distance  $X$  to the left of the semi-infinite plane; see Fig. 5. The half plane  $x < 0, z = 0$  constitutes an aperture of infinite width. With  $X$  fixed, we can describe the trajectory by  $u = X/\rho = -\cos \theta$ , in which the variable ranges from 0 to 1. The polar angle is given by

$$\sin^2 \frac{\theta}{2} = \frac{1+u}{2}. \quad (6.11)$$

The energy for an isotropic atom is given by

$$U_{\text{CP}} = -\frac{\alpha(0)}{32\pi} \frac{1}{X^4} V(u), \quad (6.12)$$

where

$$V(u) = 3u^4 \left[ \frac{1}{(1+u)^2} + \frac{1}{u+1} + \frac{1}{4} \right]. \quad (6.13)$$

The energy for the completely anisotropic atom is

$$V_{zz} = \frac{1}{3} V(u) + \frac{u^4}{2} (1 - 3u^2). \quad (6.14)$$

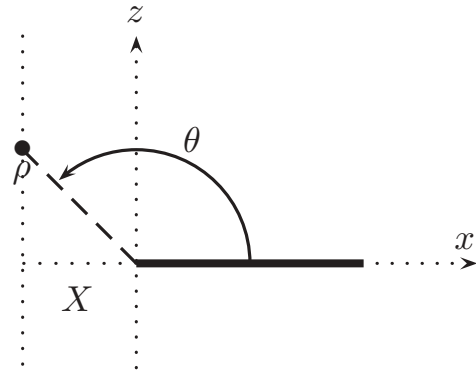


FIG. 5. Polarizable atom, above a half conducting plane, free to move on a line perpendicular to the plane but a distance  $X$  to the left of the plane.

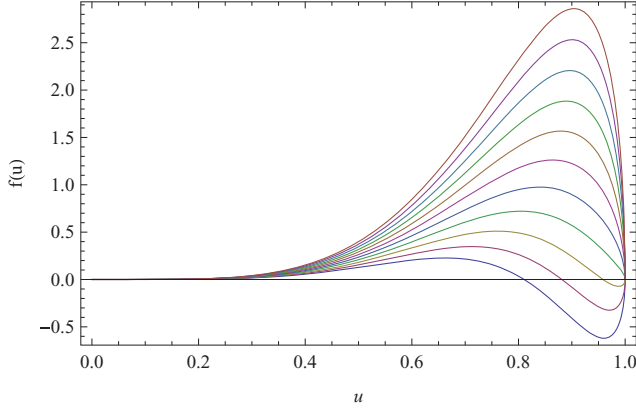


FIG. 6. (Color online) The  $z$  component of the force between an anisotropic atom (with ratio of transverse to longitudinal polarizabilities  $\gamma$ ) and a semi-infinite perfectly conducting plane,  $z = 0$ ,  $x > 0$ .  $F_z = -\alpha_{zz}/(32\pi X^5)f(u)$  in terms of the variable  $u = X/\rho = -\cos\theta$ . Here the atom lies on the line  $y = 0$ ,  $x = -X$ , and  $\rho$  is the distance from the edge of the plane and the atom. Here,  $f > 0$  corresponds to an attractive force on the  $z$  direction, and  $f < 0$  corresponds to a repulsive force. The different curves correspond to different values of  $\gamma$ ,  $\gamma = 0$  to 1 by steps of 0.1, from bottom to top. For  $\gamma < 1/4$  a repulsive regime always occurs when the atom is sufficiently close to the plane of the conductor.

If we consider instead a cylindrically symmetric polarizable atom in which

$$\alpha = \alpha_{zz}\hat{z}\hat{z} + \gamma\alpha_{zz}(\hat{x}\hat{x} + \hat{y}\hat{y}) = \alpha_{zz}(1 - \gamma)\hat{z}\hat{z} + \gamma\alpha_{zz}\mathbf{1}, \quad (6.15)$$

where  $\gamma$  is the ratio of the transverse polarizability to the longitudinal polarizability of the atom, then the effective potential is

$$(1 - \gamma)V_{zz} + \gamma V, \quad (6.16)$$

and the  $z$  component of the force on the atom is

$$F_z^\gamma = -\frac{\alpha_{zz}(0)}{32\pi} \frac{1}{X^5} u^2 \sqrt{1 - u^2} \frac{d}{du} \times \left[ \frac{1}{2} u^4 (1 - \gamma)(1 - 3u^2) + \frac{1}{3} (1 + 2\gamma)V(u) \right], \quad (6.17)$$

where  $V$  is given by Eq. (6.13). Note that the energy (6.16), or the quantity in square brackets in Eq. (6.17), only vanishes at  $u = 1$  (the plane of the conductor) when  $\gamma = 0$ . Thus, the argument given in Ref. [32] applies only for the completely anisotropic case.

The force is plotted in Figs. 6 and 7. It will be seen that if  $\gamma$  is sufficiently small, when the atom is sufficiently close to the plane of the plate the  $z$  component of the force is repulsive rather than attractive. The critical value of  $\gamma$  is  $\gamma_c = 1/4$ . This is a completely analytic exact analog of the numerical calculations shown in Ref. [32], where the interaction was considered between a conducting plane with an aperture (circular hole or slit), and a conducting cylindrical or ellipsoidal object. Our calculation demonstrates that three-body effects are not required to exhibit Casimir-Polder repulsion.

It is interesting to observe that the same critical value of  $\gamma$  occurs for the nonretarded regime of a circular aperture,

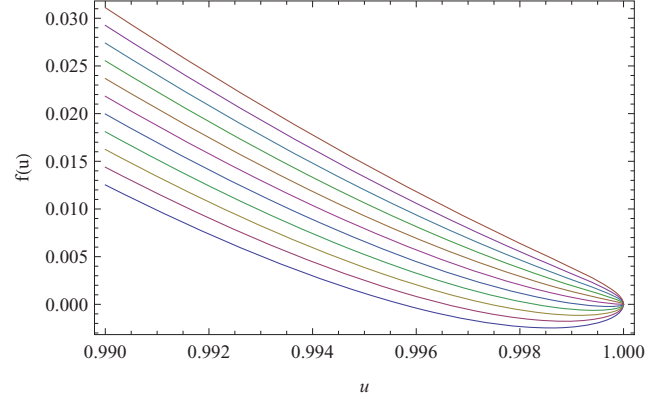


FIG. 7. (Color online) Same as Fig. 6. The region close to the plane,  $1 \geq u \geq 0.99$ , with  $\gamma$  near the critical value of  $1/4$ . Here from bottom to top are shown the results for values of  $\gamma$  from 0.245 to 0.255 by steps of 0.001.

as follows from a simple computation based on the result of Ref. [49]. For example, applying the result there for an atom with polarizability given by Eq. (6.15) placed a distance  $Z$  along the symmetry axis of a circular aperture of radius  $a$  in a conducting plane gives an energy,

$$U = -\frac{1}{16\pi^2} \int_{-\infty}^{\infty} d\zeta \alpha_{zz}(\zeta) \times \frac{1}{Z^3} \left\{ (1 + \gamma) \left( \frac{\pi}{2} + \arctan \frac{Z^2 - a^2}{2aZ} \right) + \frac{2aZ}{(Z^2 + a^2)^3} \times \left[ (1 + \gamma)(Z^4 - a^4) - \frac{8}{3}(1 - \gamma)a^2 Z^2 \right] \right\}. \quad (6.18)$$

It is easy to see that this has a minimum for  $z > 0$ , and hence there is a repulsive force close to the aperture, provided  $\gamma < \gamma_c = 1/4$ .

## B. Repulsion by a wedge

It is very easy to generalize the above result for a wedge,  $p > 1/2$ ; that is, we want to consider a strongly anisotropic atom, with only  $\alpha_{zz}$  significant, to the left of a wedge of the opening angle,

$$\beta = 2\pi - \Omega, \quad (6.19)$$

as shown in Fig. 8. We want the  $z$  axis to be perpendicular to the symmetry axis of the wedge so the relation between the polar angle of the atom and the angle to the symmetry line is

$$\phi = \theta + \beta/2, \quad (6.20)$$

where, as before,  $\theta$  is the angle relative to the top surface of the wedge. Then, it is obvious that the formula for the Casimir-Polder energy (6.8) is changed only by the replacement of  $\cos 2\theta$  by  $\cos 2\phi$ , with no change in  $\sin p\theta$ . Now we can ask how the region of repulsion depends on the wedge angle  $\beta$ .

Write for an atom on the line  $x = -X$ ,

$$U_{\text{CP}}^{zz} = -\frac{\alpha_{zz}(0)}{8\pi X^4} V(\phi), \quad (6.21)$$

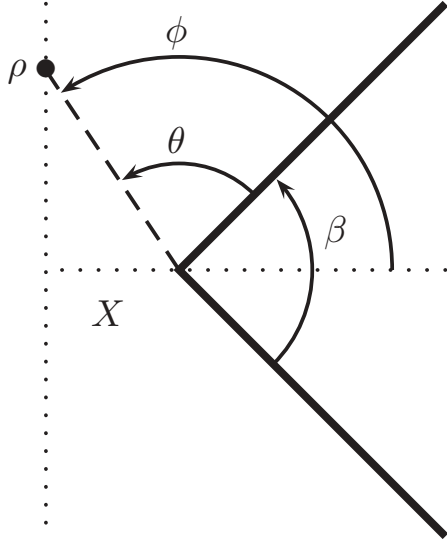


FIG. 8. A polarizable atom outside a perfectly conducting wedge of interior angle  $\beta$ . The atom is located at polar angles  $\rho$ ,  $\phi$  relative to the symmetry plane of the wedge.

where

$$V(\phi) = \cos^4 \phi \left[ \frac{p^4}{\sin^4 \left( \frac{\pi}{2} \frac{\phi - \beta/2}{\pi - \beta/2} \right)} - \frac{2}{3} \frac{p^2(p^2 - 1)}{\sin^2 \left( \frac{\pi}{2} \frac{\phi - \beta/2}{\pi - \beta/2} \right)} + \frac{1}{45} (p^2 - 1)(p^2 + 11) \cos 2\phi \right]. \quad (6.22)$$

At the point of closest approach,

$$V(\pi) = \frac{1}{45} (4p^2 - 1)(4p^2 + 11), \quad (6.23)$$

so the potential vanishes at that point only for the half-plane case,  $p = 1/2$ . The force in the  $z$  direction is

$$F_z = -\frac{\alpha_{zz}}{8\pi} \frac{1}{X^5} f(\phi), \quad (6.24a)$$

$$f(\phi) = \cos^2 \phi \frac{\partial V(\phi)}{\partial \phi}. \quad (6.24b)$$

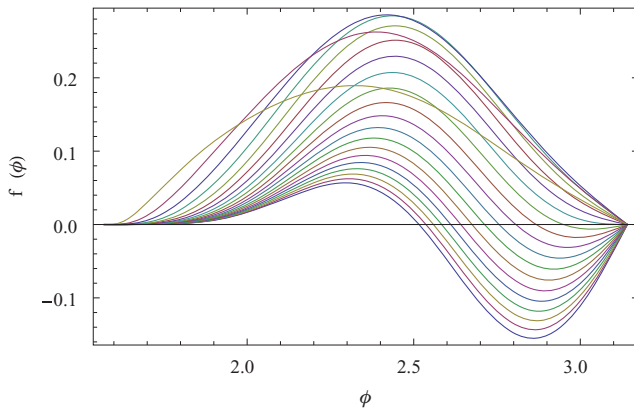


FIG. 9. (Color online) The  $z$  component of the force on a completely anisotropic atom moving on a line perpendicular to a wedge. The different curves are for various values of  $\beta$  from 0 to  $\pi$  by steps of  $\pi/20$ , from bottom up. The last few values of  $\beta$  have a markedly different character from the others.

Figure 9 shows the force as a function of  $\phi$  for fixed  $X$ . It will be seen that the force has a repulsive region for angles close enough to the apex of the wedge, provided that the wedge angle is not too large. The critical angle is actually rather large,  $\beta_c = 1.87795$ , or about  $108^\circ$ . For larger angles, the  $z$  component of the force exhibits only attraction. Of course, the force is zero for  $\beta = \pi$  because then the geometry is translationally invariant in the  $z$  direction.

## VII. CONCLUSIONS

This paper may be thought of as a counterpart to Ref. [32]. While that reference proceeded on the basis of numerical calculations, we have used analytic approaches. After some examples indicating that Casimir-Polder attraction is typical, and always seems to occur in weak coupling, we demonstrate that the quantum-vacuum Casimir-Polder interaction for a sufficiently anisotropic atom above a conducting half plane can exhibit regimes of repulsive forces for motion confined to certain specified directions. This directly translates into repulsion between such an atom and a plane with an aperture for motion along a line perpendicular to the plane. More complete analysis of that case will be presented elsewhere.

Recently, Ref. [49] appeared, which demonstrates in the *nonretarded* (van der Waals) regime, repulsion could occur between an anisotropically polarizable atom and a conducting plate with an aperture. The critical value of the anisotropy is the same as found here.

Perhaps most remarkable here is that not only can we achieve repulsion with a half plane, but also with a wedge geometry, even when the interior angle of the wedge is greater than  $90^\circ$ . This indicates that while anisotropy in both the atom and the conductor must be present for repulsion, the anisotropy in the latter need not be too extreme, and that repulsion in other geometries may be readily achievable. Three-body forces are not required, nor is a high degree of symmetry, as was present in Refs. [32,49].

## ACKNOWLEDGMENTS

We thank the US Department of Energy and the US National Science Foundation for partial support of this research. The support of the ESF Casimir Network is also acknowledged. S.Å.E. thanks Stefan Buhman, Stefan Scheel, and Alexander McCauley for discussions. P.P. acknowledges the hospitality of the University of Zaragoza.

## APPENDIX A: DERIVATION OF ANISOTROPIC WEDGE CP FORCE FROM CLOSED-FORM GREEN'S FUNCTION

Many years ago Lukosz gave a closed form for the Green's functions for a perfectly conducting wedge [50]. The four-dimensional Euclidean Green's dyadic has the closed form,

$$\mathbf{\Gamma}(\tau - \tau', y - y', \rho, \rho', \phi, \phi') = -\mathbf{M}\mathbf{M}'G^H + \mathbf{N}\mathbf{N}'G^E, \quad (A1)$$

where the transverse differential operators are [cf. Eq. (6.2)]

$$\mathbf{M} = \hat{\rho} \frac{1}{\rho} \frac{\partial}{\partial \phi} - \hat{\phi} \frac{\partial}{\partial \rho} \equiv \mathcal{M}, \quad \mathbf{N} = \hat{\rho} \frac{\partial}{\partial \rho} + \hat{\phi} \frac{1}{\rho} \frac{\partial}{\partial \phi}, \quad (A2)$$

where there is an additional contribution to  $\mathbf{N}$  in the  $y$  direction. This Green's dyadic is the frequency Fourier transform of that discussed in Sec. VI. Here the E (TM) and H (TE) Green's functions have the form,

$$G^{\text{H,E}} = \chi(y, \rho, \tau; y', \rho', \tau'; \phi - \phi') \pm \chi(y, \rho, \tau; y', \rho', \tau'; \phi + \phi' - \Omega), \quad (\text{A3})$$

for a wedge of dihedral angle  $\Omega$ , with  $\phi \in [-\Omega/2, \Omega/2]$ . Here

$$\chi(y, \rho, \tau; y', \rho', \tau'; \psi) = \frac{1}{8\pi\Omega\rho\rho' \sinh v \cosh(\pi v/\Omega) - \cos(\pi\psi/\Omega)}, \quad (\text{A4})$$

where

$$\sinh \frac{v}{2} = \frac{1}{2} \left[ \frac{(\tau - \tau')^2 + (y - y')^2 + (\rho - \rho')^2}{\rho\rho'} \right]^{1/2}. \quad (\text{A5})$$

For the interaction with an atom possessing only an  $\alpha_{zz}$  polarizability, we need

$$\begin{aligned} \Gamma_{zz} = & \cos(\phi + \phi') \left( \frac{1}{\rho\rho'} \frac{\partial}{\partial\phi} \frac{\partial}{\partial\phi'} - \frac{\partial}{\partial\rho} \frac{\partial}{\partial\rho'} \right) \chi(\phi - \phi') \\ & + 2 \left( \sin\phi \cos\phi' \frac{1}{\rho} \frac{\partial}{\partial\phi} \frac{\partial}{\partial\rho'} + \sin\phi' \cos\phi \frac{1}{\rho'} \frac{\partial}{\partial\phi'} \frac{\partial}{\partial\rho} \right) \\ & \times \chi(\phi - \phi') - \cos(\phi - \phi') \\ & \times \left( \frac{1}{\rho\rho'} \frac{\partial}{\partial\phi} \frac{\partial}{\partial\phi'} + \frac{\partial}{\partial\rho} \frac{\partial}{\partial\rho'} \right) \chi(\phi + \phi' - \Omega). \end{aligned} \quad (\text{A6})$$

Here, we have suppressed all the arguments in  $\chi$  except for the angular ones. For our application here, we are interested in the coincidence limit, so from the outset we can set  $\tau = \tau'$  and  $x = x'$ . Then,

$$\sinh \frac{v}{2} = \frac{1}{2} \frac{1 - \xi}{\sqrt{\xi}}, \quad \xi = \frac{\rho_{<}}{\rho_{>}}, \quad (\text{A7})$$

which implies

$$v = -\ln \xi. \quad (\text{A8})$$

Now we expand first in  $\phi - \phi'$ , then after the differentiations set  $\phi = \phi'$ , and then expand in  $v$ , that is, in  $1 - \xi$ . We immediately note that the mixed derivative term in Eq. (A6) does not contribute, because there is no linear term in  $\phi - \phi'$ . The result of a straightforward calculation is

$$\begin{aligned} \Gamma_{zz} = & -\frac{\cos 2\theta}{16\pi^2\rho^4} \left\{ \frac{16}{(1 - \xi)^4} - \frac{1}{45}(p^2 - 1)(p^2 + 11) \right\} \\ & + \frac{1}{16\pi^2\rho^4} \left\{ \frac{p^4}{\sin^4 p\theta} - \frac{2}{3} \frac{p^2(p^2 - 1)}{\sin^2 p\theta} \right\}, \end{aligned} \quad (\text{A9})$$

where  $p = \pi/\Omega$ , and we have switched to the angle from the ‘‘upper’’ plate,  $\theta = \phi + \Omega/2$ , which is chosen to run from 0 to  $\Omega$ . The first term in Eq. (A9) corresponds to the  $\chi(\phi - \phi')$  contribution, and the second to the  $\cos(\phi + \phi' - \Omega)$  contribution. Note, the divergent term (as  $\xi \rightarrow 1$ ) is precisely

the vacuum term given in Eq. (6.7), and should be subtracted off, and the rest, when multiplied by  $-2\pi\alpha_{zz}$ , coincides with Eq. (6.8).

## APPENDIX B: ELECTROSTATIC ASPECTS: CONDUCTING ELLIPSOID OUTSIDE A CONDUCTING PLATE WITH A CIRCULAR HOLE

Consider a conducting uncharged solid ellipsoid with semi-axes  $c > a > b$ , centered at  $X = Y = Z = 0$ . The ellipsoid is orientated such that the major semiaxis  $c$  lies along the  $Z$  axis. To describe the electrostatic potential  $\phi$  in the external region, one can make use of ellipsoidal coordinates  $\xi, \eta, \zeta$ , corresponding to solutions for  $u$  of the cubic equation,

$$\frac{Z^2}{c^2 + u} + \frac{X^2}{a^2 + u} + \frac{Y^2}{b^2 + u} = 1. \quad (\text{B1})$$

The coordinate intervals are

$$\infty > \xi \geq -b^2, \quad -b^2 \geq \eta \geq -a^2, \quad -a^2 \geq \zeta \geq -c^2. \quad (\text{B2})$$

The relationships between the ellipsoidal and the Cartesian coordinates are given in Ref. [51] and will not be reproduced here. We shall, however, need the line element,

$$dl^2 = h_1^2 d\xi^2 + h_2^2 d\eta^2 + h_3^2 d\zeta^2, \quad (\text{B3})$$

where

$$h_1 = \frac{1}{2R_\xi} \sqrt{(\xi - \eta)(\xi - \zeta)}, \quad h_2 = \frac{1}{2R_\eta} \sqrt{(\eta - \zeta)(\eta - \xi)}, \quad (\text{B4})$$

$$h_3 = \frac{1}{2R_\zeta} \sqrt{(\zeta - \xi)(\zeta - \eta)}, \quad R_u^2 = (u + c^2)(u + a^2)(u + b^2), \quad (\text{B5})$$

with  $u = \xi, \eta, \zeta$ .

In the following we assume axial symmetry around the  $Z$  axis. Then  $a \rightarrow b$ ,  $\eta \rightarrow -b^2$ , and the equation for the surface of the ellipsoid becomes

$$\frac{Z^2}{c^2} + \frac{R^2}{b^2} = 1, \quad (\text{B6})$$

with  $R^2 = X^2 + Y^2$ . We now have

$$Z = \pm \left[ \frac{(\xi + c^2)(\zeta + c^2)}{c^2 - b^2} \right]^{1/2}, \quad R = \left[ \frac{(\xi + b^2)(\zeta + b^2)}{b^2 - c^2} \right]^{1/2}. \quad (\text{B7})$$

The ellipsoidal coordinates  $\xi, \eta, \zeta$  reduce in the case of axisymmetry to so-called prolate spheroidal coordinates  $\xi$  and  $\zeta$ , lying in the intervals,

$$\infty > \xi \geq -b^2, \quad -b^2 \geq \zeta \geq -c^2. \quad (\text{B8})$$

Surfaces of constant  $\xi$  and  $\zeta$  are prolate spheroids and hyperboloids of revolution, the surfaces intersecting orthogonally. On the  $Z$  axis ( $R = 0$ ) one has  $\zeta = -b^2, Z = \pm\sqrt{\xi + c^2}$ ,

whereas in the  $XY$  plane ( $Z = 0$ ) one has  $\zeta = -c^2, R = \sqrt{\xi + b^2}$ . On the surface of the ellipsoid,  $\xi = 0$ .

In free space outside the ellipsoid the Laplace equation reads

$$\nabla^2 \phi \equiv \frac{4}{\zeta - \xi} \left[ \frac{R_\xi}{\xi + b^2} \frac{\partial}{\partial \xi} \left( R_\xi \frac{\partial \phi}{\partial \xi} \right) - \frac{R_\zeta}{\zeta + b^2} \frac{\partial}{\partial \zeta} \left( R_\zeta \frac{\partial \phi}{\partial \zeta} \right) \right] = 0. \quad (\text{B9})$$

Assume now that the ellipsoid is placed in an external potential  $\phi_0$ , axisymmetric with respect to the  $Z$  axis so that  $\phi_0 = \phi_0(\xi, \zeta)$ . We write the resulting potential  $\phi$  in the form,

$$\phi(\xi, \zeta) = \phi_0(\xi, \zeta)[1 + F(\xi)], \quad (\text{B10})$$

so that  $\phi_0 F$  is the perturbation of the external field. As the boundary condition  $\xi = 0$  on the surface has to hold for all values of  $\zeta$ , it is natural to make the ansatz that  $F$  depends on  $\xi$  only.

Inserting Eq. (B10) into Eq. (B9) we find that the terms containing  $F$  as a factor sum up to zero, the reason being the validity of Eq. (B9) also when  $\phi$  is replaced by  $\phi_0$ . The remaining terms containing  $F'(\xi)$  and  $F''(\xi)$  yield the equation,

$$\frac{d^2 F}{d\xi^2} + \frac{dF}{d\xi} \frac{d}{d\xi} \ln(R_\xi \phi_0^2) = 0. \quad (\text{B11})$$

When integrating this equation, in order to preserve the validity of the ansatz  $F = F(\xi)$ , the coordinate  $\zeta$  in  $\phi_0$  has to be regarded as a parameter. The integration thus has to extend from  $\xi = 0$  (the surface) in the outward direction, along a line on the hyperboloid  $\zeta = \text{constant}$ .

The solution of Eq. (B11) can be written as

$$F = A \int_\xi^\infty \frac{d\xi}{R_\xi \phi_0^2}, \quad (\text{B12})$$

where the constant  $A$  is determined from the condition  $F(0) = -1$  on the ellipsoid surface. That means

$$\phi = \phi_0 \left[ 1 - \frac{\int_\xi^\infty \frac{d\xi}{R_\xi \phi_0^2}}{\int_0^\infty \frac{d\xi}{R_\xi \phi_0^2}} \right]. \quad (\text{B13})$$

We now specify the form of  $\phi_0$ , as the potential from a grounded conducting plate lying in the  $xy$  plane, when far from the plate there are constant electric fields, directed normal to the plate, having different values on either side. In the plate there is a circular opening with radius  $a$  (this radius is not to be confused with the semiaxis  $a$  mentioned above). The center of the opening is at position  $x = y = z = 0$ . It is known (Ref. [35], Sec. 3.13) that on the  $z$  axis,

$$\phi_0(z) = \Phi_{00} \left[ 1 - \frac{|z|}{a} \arctan \frac{a}{|z|} \right], \quad (\text{B14})$$

where  $\Phi_{00}$  is a constant. At the origin,  $\phi_0 = \Phi_{00}$ . At infinity,  $|z| \rightarrow \infty, \phi_0 \rightarrow 0$ .

The center of the vertically oriented ellipsoid is at position  $z = z_0$ . Thus  $z = z_0 + Z$ . We will assume that the ellipsoid

is so slender that the variation of  $\phi_0$  in the transverse  $x$  and  $y$  directions can be neglected. Thus we adopt the expression (B14) in the external field region of interest,  $\phi_0 = \phi_0(\xi, \zeta)$ ,  $\xi$  and  $\zeta$  being restricted to the same intervals (B8) as before.

We consider now the upper half of the ellipsoid,  $z \geq z_0$  or  $Z \geq 0$ . The nonperturbed potential, called  $\phi_{0+}$ , is then

$$\phi_{0+} = \Phi_{00} \left[ 1 - \frac{z_0 + \sqrt{\xi + c^2}}{a} \arctan \frac{a}{z_0 + \sqrt{\xi + c^2}} \right]. \quad (\text{B15})$$

Thus the potential  $\phi_+$  in Eq. (B13) can be found numerically, inserting  $\phi_{0+}$  together with  $R_\xi = (\xi + b^2)\sqrt{\xi + c^2}$ . [In practice the following expansion can here be useful [52]:

$$\frac{1}{x} \arctan x = 1 + \sum_{k=1}^8 a_{2k} x^{2k} + O(10^{-8}), \quad 0 \leq x \leq 1, \quad (\text{B16})$$

with coefficients  $a_{2k}$  of order unity or less.]

The induced surface charge density  $\sigma_+$  on the ellipsoid is

$$\sigma_+ = - \left[ \frac{\epsilon_0}{h_1} \frac{\partial \phi_+}{\partial \xi} \right]_{\xi=0} = - \left[ \frac{2\epsilon_0 bc}{\sqrt{-\zeta}} \frac{\partial \phi_+}{\partial \xi} \right]_{\xi=0}, \quad (\text{B17})$$

since on the surface  $h_1 = (b/2R_\xi)\sqrt{-\zeta} = (1/2bc)\sqrt{-\zeta}$ . In view of the relationships between the ellipsoidal and Cartesian coordinates this can be reexpressed as

$$\sigma_+ = -2\epsilon_0 \left[ \frac{Z^2}{c^4} + \frac{R^2}{b^4} \right]^{-1/2} \left[ \frac{\partial \phi_+}{\partial \xi} \right]_{\xi=0}. \quad (\text{B18})$$

From Eq. (B13) it follows that the derivative  $[\partial \phi_{0+}/\partial \xi]_{\xi=0}$  does not contribute to  $\sigma_+$  [recall that  $F(0) = -1$ ]. The remaining term is

$$\left[ \frac{\partial \phi_+}{\partial \xi} \right]_{\xi=0} = \frac{1}{b^2 c} \frac{1}{[\phi_{0+}]_{\xi=0}} \left[ \int_0^\infty \frac{d\xi}{R_\xi \phi_{0+}^2} \right]^{-1}. \quad (\text{B19})$$

Thus for  $z \geq z_0$  we get as solution,

$$\sigma_+ = \frac{\sigma_{0+}}{c} \left[ \frac{Z^2}{c^4} + \frac{R^2}{b^4} \right]^{-1/2}, \quad (\text{B20})$$

where  $\sigma_{0+}$  is the constant,

$$\sigma_{0+} = - \frac{2\epsilon_0}{b^2} \frac{1}{\Phi_{00}} \left[ \int_0^\infty \frac{d\xi}{R_\xi \phi_{0+}^2} \right]^{-1} \quad (\text{B21})$$

(recall again that  $a$  is the radius of the hole). The dependence of  $\sigma_+$  on the coordinates  $Z$  and  $R$  in Eq. (B20) is actually the same as for a charged ellipsoid in free space [51]. The surface force density on the ellipsoid is  $(\sigma^2/2\epsilon_0)\mathbf{n}$ ,  $\mathbf{n}$  being the outward normal. The slope of the tangent to the surface is  $dZ/dR = -(c^2/b^2)R/Z$ ; the slope of  $\mathbf{n}$  is accordingly  $(b^2/c^2)Z/R$ . Denoting this as  $\tan \theta$ , we get, when going over to ellipsoidal coordinates,

$$\tan \theta = \frac{b}{c} \left[ \frac{\xi + c^2}{-\xi - b^2} \right]^{1/2}. \quad (\text{B22})$$

The component of  $\mathbf{n}$  along the  $Z$  axis is, then,

$$n_Z = \sin \theta = \frac{b}{\sqrt{c^2 - b^2}} \left[ \frac{\zeta + c^2}{-\zeta} \right]^{1/2}, \quad (\text{B23})$$

and we can now find the total vertical force  $F_{Z+}$  on the upper half of the ellipsoid by integrating over the actual surface. The line element along the meridian is

$$h_3 d\zeta = \frac{1}{2} \left[ \frac{\zeta}{(\zeta + b^2)(\zeta + c^2)} \right]^{1/2} d\zeta, \quad (\text{B24})$$

and the surface element  $dA$  becomes

$$dA = 2\pi R h_3 d\zeta = \frac{\pi b}{\sqrt{c^2 - b^2}} \left[ \frac{-\zeta}{\zeta + c^2} \right]^{1/2} d\zeta. \quad (\text{B25})$$

As  $\sigma_+$  in Eq. (B20) can be reexpressed as

$$\sigma_+ = \sigma_{0+} \frac{b}{\sqrt{-\zeta}}, \quad (\text{B26})$$

we can calculate  $F_{Z+}$  as

$$\begin{aligned} F_{Z+} &= \int_{Z \geq 0} \frac{\sigma_+^2}{2\epsilon_0} n_Z dA = \frac{\sigma_{0+}^2}{2\epsilon_0} \frac{\pi b^4}{c^2 - b^2} \int_{b^2}^{c^2} \frac{d(-\zeta)}{(-\zeta)} \\ &= \frac{\sigma_{0+}^2}{\epsilon_0} \frac{\pi b^4}{c^2 - b^2} \ln \frac{c}{b}. \end{aligned} \quad (\text{B27})$$

The expression is positive as expected; the force is acting upward. The only dependence on the position  $z_0$  lies in  $\sigma_{0+}$ , as  $\sigma_{0+} = \sigma_{0+}(z_0)$  according to Eq. (B21).

The lower half of the ellipsoid,  $Z < 0$ , can be treated in an analogous way. A complicating element is here the presence of the conducting plate in the  $xy$  plane, for radii  $\rho \geq a$ . It means that we can no longer extend the integration over  $\xi$  in the solution (B12) to infinity in a straightforward way. We observe that the undisturbed potential in the  $xy$  plane can be written as

$$\phi_0(\rho, 0) = \begin{cases} \Phi_{00} \sqrt{1 - \rho^2/a^2}, & \rho \leq a \\ 0, & \rho > a, \end{cases} \quad (\text{B28})$$

where  $\rho^2 = x^2 + y^2$ ,  $\Phi_{00}$  being the potential at the center.

Our approach will be based on the following two assumptions:

(1) The  $\xi$  integration will be terminated on the  $xy$  plane, this implying that the effect of the perturbation is assumed to be small at that level. This approximation is expected to be good except when the distance between the lower end of the ellipsoid and the plane is small.

(2) Secondly, the integration over  $\xi$  will be assumed to run over trajectories lying close to the  $z$  axis, corresponding to  $\zeta = -b^2$ . This assumption simplifies the mathematical analysis. It is supported by physical considerations also, since when the ellipsoid is slender the hyperboloids  $\zeta = \text{constant}$  emerging from the surface of the ellipsoid near its lower end become concentrated in the vicinity of the  $z$  axis.

As according to Eq. (B7) the plane position  $z = 0$  in general corresponds to

$$z_0 = \left[ \frac{(\xi + c^2)(\zeta + c^2)}{c^2 - b^2} \right]^{1/2}, \quad (\text{B29})$$

our approximations imply that the  $\xi$  integration is terminated at

$$\xi_{\text{plane}} = z_0^2 - c^2, \quad (\text{B30})$$

that is, the same constant for the whole lower half of the ellipsoid.

As solution for the perturbed potential we thus get

$$\phi_- = \phi_{0-} \left[ 1 - \frac{\int_{\xi}^{\xi_{\text{plane}}} \frac{d\xi}{R_{\xi} \phi_{0-}^2}}{\int_0^{\xi_{\text{plane}}} \frac{d\xi}{R_{\xi} \phi_{0-}^2}} \right], \quad (\text{B31})$$

where

$$\phi_{0-} = \Phi_{00} \left[ 1 - \frac{z_0 - \sqrt{\xi + c^2}}{a} \arctan \frac{a}{z_0 - \sqrt{\xi + c^2}} \right]. \quad (\text{B32})$$

The force  $F_{Z-}$  on the lower half can now be calculated. As before,  $R_{\xi} = (\xi + b^2)\sqrt{\xi + c^2}$ . Equation (B26) becomes replaced by

$$\sigma_- = \sigma_{0-} \frac{b}{\sqrt{-\zeta}}, \quad (\text{B33})$$

where now

$$\sigma_{0-} = -\frac{2\epsilon_0}{b^2} \frac{1}{\Phi_{00}} \left[ \int_0^{\xi_{\text{plane}}} \frac{d\xi}{R_{\xi} \phi_{0-}^2} \right]^{-1}. \quad (\text{B34})$$

The total force on the ellipsoid becomes

$$F_Z = F_{Z+} + F_{Z-} = \frac{\sigma_{0+}^2 - \sigma_{0-}^2}{\epsilon_0} \frac{\pi b^4}{c^2 - b^2} \ln \frac{c}{b}, \quad (\text{B35})$$

which can be rewritten as

$$\begin{aligned} F_Z &= \frac{4\pi\epsilon_0}{\Phi_{00}^2} \frac{1}{c^2 - b^2} \left\{ \frac{\left[ \int_0^{\infty} \frac{d\xi}{R_{\xi} \phi_{0+}^2} \right]^{-2}}{\left[ 1 - \frac{z_0+c}{a} \arctan \frac{a}{z_0+c} \right]^2} \right. \\ &\quad \left. - \frac{\left[ \int_0^{\xi_{\text{plane}}} \frac{d\xi}{R_{\xi} \phi_{0-}^2} \right]^{-2}}{\left[ 1 - \frac{z_0-c}{a} \arctan \frac{a}{z_0-c} \right]^2} \right\} \ln \frac{c}{b}. \end{aligned} \quad (\text{B36})$$

In the limiting case of a sphere,  $b \rightarrow c$ , the expression becomes somewhat simpler,

$$\begin{aligned} F_Z &= \frac{2\pi\epsilon_0}{\Phi_{00}^2} \frac{1}{c^2} \left\{ \frac{\left[ \int_0^{\infty} \frac{d\xi}{(\xi+c^2)^{3/2} \phi_{0+}^2} \right]^{-2}}{\left[ 1 - \frac{z_0+c}{a} \arctan \frac{a}{z_0+c} \right]^2} \right. \\ &\quad \left. - \frac{\left[ \int_0^{\xi_{\text{plane}}} \frac{d\xi}{(\xi+c^2)^{3/2} \phi_{0-}^2} \right]^{-2}}{\left[ 1 - \frac{z_0-c}{a} \arctan \frac{a}{z_0-c} \right]^2} \right\}. \end{aligned} \quad (\text{B37})$$

We have made some numerical checks of these expressions (using MAPLE). They indicate that there is no change in the sign of the force for various input parameters for the geometry. The force is attractive, as expected. It turns out that the dependence on the upper integration limit  $\xi_{\text{plane}} = z_0^2 - c^2$  is weak, as anticipated above.

- [1] A. W. Rodriguez, A. P. McCauley, D. Woolf, F. Capasso, J. D. Joannopoulos, and S. G. Johnson, *Phys. Rev. Lett.* **104**, 160402 (2010).
- [2] H. B. G. Casimir, Proc. Kon. Ned. Wetensch. **51**, 793 (1948).
- [3] E. M. Lifshitz, Zh. Eksp. Teor. Fiz. **29**, 94 (1956) [*Sov. Phys. JETP* **2**, 73 (1956)].
- [4] I. D. Dzyaloshinskii, E. M. Lifshitz, and L. P. Pitaevskii, *Usp. Fiz. Nauk* **73**, 381 (1961) [*Sov. Phys. Usp.* **4**, 153 (1961)].
- [5] J. Munday, F. Capasso, and V. A. Perseghian, *Nature (London)* **457**, 170 (2009).
- [6] A. Milling, P. Mulvaney, and I. Larson, *J. Colloid Interface Sci.* **180**, 460 (1996).
- [7] A. Meurk, P. F. Luckham, and L. Bergstrom, *Langmuir* **13**, 3896 (1997).
- [8] S. Lee and W. M. Sigmund, *J. Colloid Interface Sci.* **243**, 365 (2001).
- [9] S. Lee and W. M. Sigmund, *J. Colloids Surf. A* **204**, 43 (2002).
- [10] A. A. Feiler, L. Bergström, and M. W. Rutland, *Langmuir* **24**, 2274 (2008).
- [11] E. S. Sabisky and C. H. Anderson, *Phys. Rev. A* **7**, 790 (1973).
- [12] M. Elbaum and M. Schick, *Phys. Rev. Lett.* **66**, 1713 (1991).
- [13] R. F. Tabor, R. Manica, D. Y. C. Chan, F. Grieser, and R. R. Dagastine, *Phys. Rev. Lett.* **106**, 064501 (2011).
- [14] T. H. Boyer, *Phys. Rev.* **174**, 1764 (1968).
- [15] T. H. Boyer, *Phys. Rev. A* **9**, 2078 (1974).
- [16] C. Henkel and K. Joulain, *Europhys. Lett.* **72**, 929 (2005).
- [17] I. G. Pirozhenko and A. Lambrecht, *J. Phys. A* **41**, 164015 (2008).
- [18] F. S. S. Rosa, D. A. R. Dalvit, and P. W. Milonni, *Phys. Rev. Lett.* **100**, 183602 (2008).
- [19] F. S. S. Rosa, D. A. R. Dalvit, and P. W. Milonni, *Phys. Rev. A* **78**, 032117 (2008).
- [20] R. Zhao, J. Zhou, Th. Koschny, E. N. Economou, and C. M. Soukoulis, *Phys. Rev. Lett.* **103**, 103602 (2009).
- [21] M. G. Silveirinha and S. I. Maslovski, *Phys. Rev. Lett.* **105**, 189301 (2010); R. Zhao, J. Zhou, Th. Koschny, E. N. Economou, and C. M. Soukoulis, *ibid.* **105**, 189302 (2010).
- [22] V. Yannopoulos and N. V. Vitanov, *Phys. Rev. Lett.* **103**, 120401 (2009).
- [23] M. G. Silveirinha and S. I. Maslovski, *Phys. Rev. A* **82**, 052508 (2010).
- [24] A. P. McCauley, R. Zhao, M. T. Homer Reid, A. W. Rodriguez, J. Zhou, F. S. S. Rosa, J. D. Joannopoulos, D. A. R. Dalvit, C. M. Soukoulis, and S. G. Johnson, *Phys. Rev. B* **82**, 165108 (2010).
- [25] S. I. Maslovski and M. G. Silveirinha, *Phys. Rev. A* **83**, 022508 (2011).
- [26] R. Zeng and Y. Yang, *Phys. Rev. A* **83**, 012517 (2011).
- [27] A. G. Grushin and A. Cortijo, *Phys. Rev. Lett.* **106**, 020403 (2011).
- [28] V. Sopova and L. H. Ford, *Phys. Rev. A* **70**, 062109 (2004).
- [29] L. H. Ford, *J. Phys. A* **39**, 6365 (2006).
- [30] L. H. Ford, *Phys. Rev. A* **48**, 2962 (1993).
- [31] C. Genet, A. Lambrecht, and S. Reynaud, *Phys. Rev. A* **67**, 043811 (2003).
- [32] M. Levin, A. P. McCauley, A. W. Rodriguez, M. T. Homer Reid, and S. G. Johnson, *Phys. Rev. Lett.* **105**, 090403 (2010).
- [33] M. F. Maghrebi, *Phys. Rev. D* **83**, 045004 (2011).
- [34] H. B. G. Casimir and D. Polder, *Phys. Rev.* **73**, 360 (1948).
- [35] J. D. Jackson, *Classical Electrodynamics* (Wiley, New York, 1999).
- [36] J. Schwinger, L. L. DeRaad Jr., K. A. Milton, and W.-y. Tsai, *Classical Electrodynamics* (Perseus/Westview, New York, 1998).
- [37] S. Y. Buhmann and D.-G. Welsch, *Prog. Quantum Electron.* **31**, 51 (2007).
- [38] K. A. Milton, P. Parashar, and J. Wagner, in *The Casimir Effect and Cosmology*, edited by S. D. Odintsov, E. Elizalde, and O. B. Gorbunova (Tomsk State Pedagogical University, Tomsk, 2009), pp. 107–116, e-print [arXiv:0811.0128](https://arxiv.org/abs/0811.0128).
- [39] A. D. Khanzhov, *Inzherero-Fizicheskia Zhurnal* **11**, 658 (1966) [*J. Eng. Phys. Thermophys.* **11**, 370 (1966)].
- [40] E. C. Titchmarsh, *Theory of Fourier Integrals* (Oxford University Press, Oxford, 1948).
- [41] F. Zhou and L. Spruch, *Phys. Rev. A* **52**, 297 (1995).
- [42] H. Levine and J. Schwinger, *Commun. Pure Appl. Math.* **III** **4**, 355 (1950), reprinted in K. A. Milton and J. Schwinger, *Electromagnetic Radiation: Variational Methods, Waveguides, and Accelerators* (Springer, Berlin, 2006), p. 543.
- [43] I. Brevik, M. Lygren, and V. N. Marachevsky, *Ann. Phys. (NY)* **267**, 134 (1998).
- [44] I. Brevik and M. Lygren, *Ann. Phys. (NY)* **251**, 157 (1996).
- [45] L. L. DeRaad Jr., and K. A. Milton, *Ann. Phys. (NY)* **136**, 229 (1981).
- [46] T. N. C. Mendez, F. S. S. Rosa, A. Tenório, and C. Farina, *J. Phys. A: Math. Theor.* **41**, 164020 (2008).
- [47] C. Eberlein and R. Zietal, *Phys. Rev. A* **75**, 032516 (2007).
- [48] C. Eberlein and R. Zietal, *Phys. Rev. A* **80**, 012504 (2009).
- [49] C. Eberlein and R. Zietal, e-print [arXiv:1103.2381](https://arxiv.org/abs/1103.2381).
- [50] W. Lukosz, *Z. Phys.* **262**, 327 (1971).
- [51] L. D. Landau and E. M. Lifshitz, in *Electrodynamics of Continuous Media* (Pergamon, Oxford, 1960), Sec. IV, p. 20ff.
- [52] M. Abramowitz and I. A. Stegun (editors), in *Handbook of Mathematical Functions with Formulas, Graphs, and Mathematical Tables*, National Bureau of Standards Applied Mathematics Series (US Government Printing Office, Washington, DC, 1964), formula 4.4.49.

**Casimir-Polder repulsion: Polarizable atoms, cylinders, spheres, and ellipsoids**Kimball A. Milton,<sup>\*</sup> Prachi Parashar,<sup>†</sup> and Nima Pourtolami<sup>‡</sup>*Homer L. Dodge Department of Physics and Astronomy, University of Oklahoma, Norman, Oklahoma 73019-2061, USA*Iver Brevik<sup>§</sup>*Department of Energy and Process Engineering, Norwegian University of Science and Technology, N-7491 Trondheim, Norway*  
(Received 17 November 2011; published 18 January 2012)

Recently, the topic of Casimir repulsion has received a great deal of attention, largely because of the possibility of technological application. The general subject has a long history, going back to the self-repulsion of a conducting spherical shell and the repulsion between a perfect electric conductor and a perfect magnetic conductor. Recently, it has been observed that repulsion can be achieved between ordinary conducting bodies, provided sufficient anisotropy is present. For example, an anisotropic polarizable atom can be repelled near an aperture in a conducting plate. Here, we provide new examples of this effect, including the repulsion on such an atom moving on a trajectory nonintersecting a conducting cylinder; in contrast, such repulsion does not occur outside a sphere. Classically, repulsion does occur between a conducting ellipsoid placed in a uniform electric field and an electric dipole. The Casimir-Polder force between an anisotropic atom and an anisotropic dielectric semispace does not exhibit repulsion. The general systematics of repulsion are becoming clear.

DOI: [10.1103/PhysRevD.85.025008](https://doi.org/10.1103/PhysRevD.85.025008)

PACS numbers: 42.50.Lc, 03.50.De, 12.20.-m, 32.10.Dk

**I. INTRODUCTION**

Although known since the time of Lifshitz's work on the subject [1], repulsive Casimir forces have recently received serious scrutiny [2]. Experimental confirmation of the repulsion that occurs when dielectric surfaces are separated by a liquid with an intermediate value of the dielectric constant has appeared [3], although this seems devoid of much practical application. The context of our work is the considerable interest in utilizing the quantum vacuum force or the Casimir effect in nanotechnology employing mesoscopic objects [4].

The first repulsive Casimir stress in vacuum was found by Boyer [5], who discovered the surprising fact that the Casimir self-energy of a perfectly conducting spherical shell is positive. (This has become somewhat less mysterious since the phenomenon is part of a general pattern [6–9].) Boyer later observed that a perfect electrical conductor and a perfect magnetic conductor repel [10], but this also seems beyond reach since the unusual electrical properties must be exhibited over a wide frequency range. The analogous effect for metamaterials also seem impracticable [11].

Thus, it was a significant advance when Levin *et al.* showed examples of repulsion between conducting objects, in particular, between an elongated cylinder above a conducting plane with a circular aperture [2] (see also Ref. [12]). They computed the quantum vacuum forces between conducting objects by using impressive numerical

finite-difference time-domain and boundary-element methods.

We subsequently showed [13] that repulsive Casimir-Polder (CP) forces between anisotropic atoms and a conducting half-plane, and even between such an atom and a conducting wedge of rather large opening angle, could be achieved. Of course, we must be careful to explain what we mean by repulsion: the total force on the atom is attractive, but the component of the force perpendicular to the symmetry axis of the conductor changes sign when the atom is sufficiently close to that axis. This is the only component that survives in the case of an aperture in a plane, so our analytic calculation provided a counterpart to the numerical work of Ref. [2].

In this paper, we give further examples. After demonstrating, in Sec. II, that Casimir-Polder repulsion between two atoms requires that both be sufficiently anisotropic, we show in Sec. III that the force between one such atom and a conducting cylinder is repulsive for motion confined to a perpendicular line not intersecting with the cylinder, provided the line is sufficiently far from the cylinder. The analogous effect does not occur for a spherical conductor (Sec. IV), as one might suspect, since at large distances such a sphere looks like an isotropic atom. The classical interaction between a dipole and a conducting ellipsoid polarized by an external field is examined in Sec. V, which, as expected, yields a repulsive region. In contrast, in Sec. VI, we examine the Casimir-Polder interaction of an anisotropic atom with an anisotropic dielectric half-space, but this fails to reveal any repulsive regime.

In this paper, we set  $\hbar = c = 1$ , and all results are expressed in Gaussian units except that Heaviside-Lorentz units are used for Green's dyadics.

<sup>\*</sup>milton@nhn.ou.edu<sup>†</sup>prachi@nhn.ou.edu<sup>‡</sup>nimap@ou.edu<sup>§</sup>iver.h.brevik@ntnu.no

## II. CASIMIR-POLDER REPULSION BETWEEN ATOMS

The interaction between two polarizable atoms described by general polarizabilities  $\alpha_{1,2}$  with the relative separation vector given by  $\mathbf{r}$  is [14,15]

$$U_{\text{CP}} = -\frac{1}{4\pi r^7} \left[ \frac{13}{2} \text{Tr} \alpha_1 \cdot \alpha_2 - 28 \text{Tr}(\alpha_1 \cdot \hat{\mathbf{r}})(\alpha_2 \cdot \hat{\mathbf{r}}) + \frac{63}{2} (\hat{\mathbf{r}} \cdot \alpha_1 \cdot \hat{\mathbf{r}})(\hat{\mathbf{r}} \cdot \alpha_2 \cdot \hat{\mathbf{r}}) \right]. \quad (2.1)$$

This formula is easily re-derived by the multiple-scattering technique as explained in Ref. [16]. This reduces in the isotropic case  $\alpha_i = \alpha_i \mathbf{1}$  to the usual Casimir-Polder energy  $U_{\text{CP}} = -\frac{23}{4\pi r^7} \alpha_1 \alpha_2$ . Suppose the two atoms are only polarizable in perpendicular directions,  $\alpha_1 = \alpha_1 \hat{\mathbf{z}} \hat{\mathbf{z}}$ ,  $\alpha_2 = \alpha_2 \hat{\mathbf{x}} \hat{\mathbf{x}}$ . Choosing atom 2 to be at the origin, we obtain the configuration shown in Fig. 1. Then, in terms of the polar angle  $\cos\theta = z/r$ , the  $z$ -component of the force on atom 1 is

$$F_z = -\frac{63}{8\pi} \frac{\alpha_1 \alpha_2}{x^8} \sin^{10}\theta \cos\theta (9 - 11 \sin^2\theta). \quad (2.2)$$

In this paper, we are considering motion for fixed  $x = r \sin\theta$  in the  $y = 0$ -plane. Evidently, the force is attractive at large distances, vanishing as  $\theta \rightarrow 0$ ; it must change sign at small values of  $z$  for fixed  $x$  since the energy also vanishes as  $\theta \rightarrow \pi/2$ . The force component in the  $z$ -direction vanishes when  $\sin\theta = 3/\sqrt{11}$  or  $\theta = 1.130$  or  $25^\circ$  from the  $x$ -axis.<sup>1</sup>

No repulsion occurs if one of the atoms is isotropically polarizable. If both have cylindrically symmetric anisotropies, but with respect to perpendicular axes,

$$\begin{aligned} \alpha_1 &= (1 - \gamma_1) \alpha_1 \hat{\mathbf{z}} \hat{\mathbf{z}} + \gamma_1 \alpha_1 \mathbf{1}, \\ \alpha_2 &= (1 - \gamma_2) \alpha_2 \hat{\mathbf{x}} \hat{\mathbf{x}} + \gamma_2 \alpha_2 \mathbf{1}, \end{aligned} \quad (2.3)$$

it is easy to check that if both are sufficiently anisotropic, repulsion occurs. For example, if  $\gamma_1 = \gamma_2$  repulsion in the  $z$ -direction takes place close to the plane  $z = 0$  if  $\gamma \leq 0.26$ .

## III. REPULSION OF AN ATOM BY A CONDUCTING CYLINDER

Now we turn to the Casimir-Polder interaction between a polarizable body (“atom”) and a macroscopic body. That interaction is generally given by

<sup>1</sup>After the first version of this paper was prepared, Ref. [17] appeared, which rederived these results, and then went on to extend the calculation to Casimir-Polder repulsion by an anisotropic dilute dielectric sheet with a circular aperture. The authors quite correctly point out that the statement that no repulsion is possible in the weak-coupling regime, in Ref. [13], is erroneous.

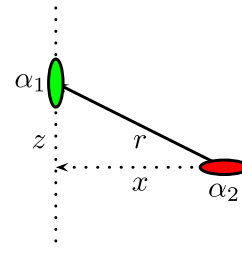


FIG. 1 (color online). Casimir-Polder interaction between two atoms of polarizability  $\alpha_1$  and  $\alpha_2$  separated by a distance  $r$ . Atom 1 is predominantly polarizable in the  $z$  direction, while atom 2 is predominantly polarizable in the  $x$  direction. The force on atom 1 in the  $z$  direction becomes repulsive when sufficiently close to the polarization axis of atom 2, provided both atoms are sufficiently anisotropic.

$$E_{\text{CP}} = - \int_{-\infty}^{\infty} d\zeta \text{tr} \alpha \cdot \Gamma(\mathbf{r}, \mathbf{r}), \quad (3.1)$$

where  $\mathbf{r}$  is the position of the atom and  $\zeta$  is the imaginary frequency, in terms of the polarizability of the atom  $\alpha$  and the Green’s dyadic due to the macroscopic body, which for a body characterized by a permittivity  $\varepsilon$  satisfies the differential equation

$$\left( \frac{1}{\omega^2} \nabla \times \nabla \times - \mathbf{1} \varepsilon(\mathbf{r}) \right) \cdot \Gamma(\mathbf{r}, \mathbf{r}') = \mathbf{1} \delta(\mathbf{r} - \mathbf{r}'). \quad (3.2)$$

In this paper, except for Sec. VI, we will consider perfect conducting boundaries  $S$  immersed in vacuum. In this case, we need to solve this equation with  $\varepsilon = 1$  for  $\Gamma$ , subject to the boundary conditions  $\hat{\mathbf{n}} \times \Gamma(\mathbf{r}, \mathbf{r}')|_{\mathbf{r} \in S} = 0$ , where  $\hat{\mathbf{n}}$  is the normal to the surface of the conductor, which just states that the tangential components of the electric field must vanish on the conductor.

Let us henceforth assume that the polarizability has negligible frequency dependence (static approximation) and, in order to maximize the repulsive effect, the atom is only polarizable in the  $z$ -direction, the direction of the trajectory (assumed not to intersect the cylinder), in which case the quantity we need to compute for a conducting cylinder of radius  $a$  is given by [18]

$$\begin{aligned} & \int_{-\infty}^{\infty} \frac{d\zeta}{2\pi} \Gamma_{zz}(r, \theta) \\ &= \sum_{m=-\infty}^{\infty} \int_0^{\infty} \frac{d\kappa}{(2\pi)^3} \frac{\pi}{2a} \frac{1}{K_m(\kappa a) K'_m(\kappa a)} \left\{ \frac{m^2}{r^2} K_m^2(\kappa r) \right. \\ & \quad \left. + \kappa^2 K_m'^2(\kappa r) - \cos 2\theta \kappa a [I_m(\kappa a) K_m(\kappa a)]' \right. \\ & \quad \left. \times \left( -\frac{m^2}{r^2} K_m^2(\kappa r) + \kappa^2 K_m'^2(\kappa r) \right) \right\}. \end{aligned} \quad (3.3)$$

The geometry we are considering is illustrated in Fig. 2. Greater insight is provided by giving the transverse electric (TE) and transverse magnetic (TM) contributions to the CP energy

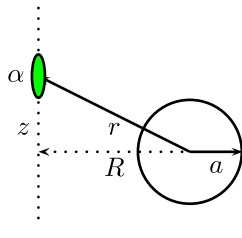


FIG. 2 (color online). Interaction between an anisotropically polarizable atom and a conducting cylinder of radius  $a$ . The force on the atom along a line which does not intersect the cylinder is considered. If the atom is only polarizable in that direction and the line lies sufficiently far from the cylinder, the force component along the line changes sign near the point of closest approach.

$$E_{\text{CP}}^{\text{TE}} = -\frac{\alpha_{zz}}{4\pi} \sum_{m=-\infty}^{\infty} \int_0^{\infty} d\kappa \kappa \frac{I_m^l(\kappa a)}{K_m^l(\kappa a)} \times \left[ \frac{\cos^2\theta}{r^2} m^2 K_m^2(\kappa r) + \kappa^2 \sin^2\theta K_m^{\prime 2}(\kappa r) \right], \quad (3.4a)$$

$$E_{\text{CP}}^{\text{TM}} = \frac{\alpha_{zz}}{4\pi} \sum_{m=-\infty}^{\infty} \int_0^{\infty} d\kappa \kappa \frac{I_m(\kappa a)}{K_m(\kappa a)} \times \left[ \frac{\sin^2\theta}{r^2} m^2 K_m^2(\kappa r) + \kappa^2 \cos^2\theta K_m^{\prime 2}(\kappa r) \right]. \quad (3.4b)$$

The distance of the atom from the center of the cylinder is  $r = R/\sin\theta$ , where  $R$  is the distance of closest approach and  $\theta$  is the polar angle, which ranges from 0 when the atom is at infinity to  $\pi/2$  where the atom is closest to the cylinder.

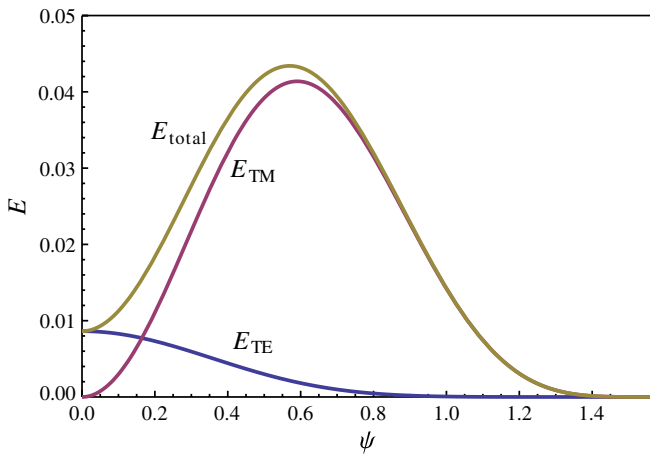


FIG. 3 (color online).  $m = 0$  contributions to the Casimir-Polder energy between an anisotropic atom and a conducting cylinder. The (generally) lowest curve (blue) is the TE contribution, the second (magenta) is the TM contribution, and the top curve (yellow) is the total CP energy. In this case, the distance of closest approach of the atom is taken to be 10 times the radius of the cylinder. The energy  $E$  is plotted as a function of  $\psi = \pi/2 - \theta$ .

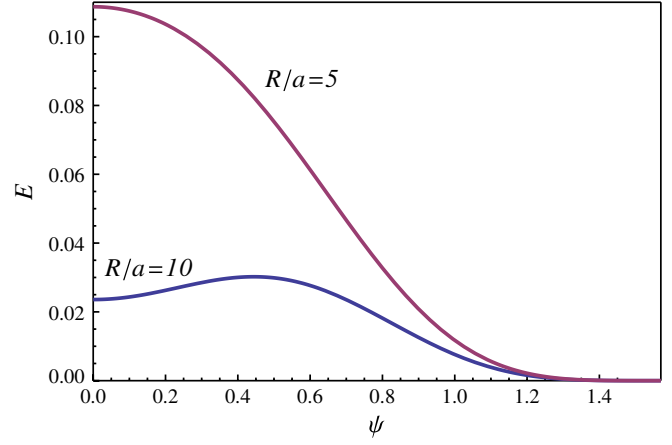


FIG. 4 (color online). The CP energy between an anisotropic atom and a conducting cylinder. Plotted is the total CP energy, the upper curve for the distance of closest approach  $R$  being 5 times the cylinder radius  $a$ , the lower curve for the distance of closest approach 10 times the radius. The curves move up slightly as more  $m$  terms are included, but have completely converged by the time  $m = 3$  is included. Repulsion is clearly observed when  $R/a = 10$ , but not for  $R/a = 5$ .

At large distances, the CP force is dominated by the  $m = 0$ -term in the energy sum. Figure 3 shows that for  $m = 0$  the TM mode dominates except near the position of closest approach, where only the TE mode is nonzero. This indicates that there is a region of repulsion near  $\theta = \pi/2$  since the total energy has a minimum for small  $\psi = \pi/2 - \theta$ . This effect is partially washed out by including higher  $m$ -modes as seen in Fig. 4, which shows the effect of including the first five  $m$ -values. But the repulsion goes away if the line of motion passes too close to the cylinder. Numerically, we have found that to have repulsion close to the plane of closest approach requires that  $a/R < 0.15$ .

#### IV. CP INTERACTION BETWEEN ATOM AND CONDUCTING SPHERE

It is straightforward to derive the TE and TM contributions for the interaction between a completely anisotropic atom and a conducting sphere as

$$E^{\text{TM}} = \frac{\alpha_{zz}}{2\pi R^4} \cos^4\theta \sum_{l=1}^{\infty} (2l+1) \int_0^{\infty} dx g_l(x), \quad (4.1a)$$

$$E^{\text{TE}} = \frac{\alpha_{zz}}{4\pi R^4} \cos^6\theta \sum_{l=1}^{\infty} (2l+1) \int_0^{\infty} dx f_l(x), \quad (4.1b)$$

where

$$g_l(x) = x \frac{s_l'(x a \cos\theta/R)}{e_l'(x a \cos\theta/R)} \left[ \frac{1}{2} \cos^2\theta e_l^{\prime 2}(x) + \frac{l(l+1) \sin^2\theta e_l^2(x)}{x^2} \right], \quad (4.2a)$$

$$f_l(x) = x \frac{s_l(x a \cos\theta/R)}{e_l(x a \cos\theta/R)} e_l^2(x), \quad (4.2b)$$

in terms of the modified Riccati-Bessel functions are

$$s_l(x) = \sqrt{\frac{\pi x}{2}} I_{l+1/2}(x), \quad e_l(x) = \sqrt{\frac{2x}{\pi}} K_{l+1/2}(x). \quad (4.3)$$

We expect, in the case of a sphere, not to see Casimir repulsion at large distances. The reason is that far from the sphere it appears to be an isotropic atom, which (as we have seen above) will not give a repulsive force on another completely anisotropic atom. Indeed, far from the sphere we can replace the Bessel functions of argument  $xa/r$  by their leading small argument approximations and easily find

$$E^{\text{TM}} \sim \frac{\alpha_{zz} a^3}{4\pi r^7} (13 + 7\sin^2\theta), \quad a/r \rightarrow 0. \quad (4.4a)$$

The TE mode contributes

$$E^{\text{TE}} \sim \frac{\alpha_{zz} a^3}{4\pi r^7} \frac{7}{4} \cos^2\theta, \quad a/r \rightarrow 0. \quad (4.4b)$$

We see here the expected isotropic electric polarizability of a conducting sphere  $\alpha_{\text{sp},E} = \mathbf{1}a^3$ . We note that the TM result (4.4a) coincides with the result obtained from Eq. (2.1). The TE contribution is, in fact, the coupling between the electric polarizability of the atom and the magnetic polarizability of the sphere  $\alpha_{\text{sp},M} = -\frac{a^3}{2} \mathbf{1}$  [19].

To see this, we first remind the reader of the CP interaction between isotropic atoms possessing both electric and magnetic polarizabilities [20],

$$U_{\text{CP}} = -\frac{23}{4\pi r^7} (\alpha_1^E \alpha_2^E + \alpha_1^M \alpha_2^M) + \frac{7}{4\pi r^7} (\alpha_1^E \alpha_2^M + \alpha_1^M \alpha_2^E). \quad (4.5)$$

When the atoms are not isotropic it is easy to deduce the generalization of this, using the methods described in Ref. [16], starting from the multiple-scattering coupling term between electric and magnetic dyadics,

$$\begin{aligned} E_{\text{em}} &= -\frac{i}{2} \text{Tr} \ln(1 + \Phi_0 \mathbf{T}_1^E \cdot \Phi_0 \mathbf{T}_2^M) \\ &\approx -\frac{i}{2} \text{Tr} \Phi_0 \cdot \mathbf{V}_1^E \Phi_0 \cdot \mathbf{V}_2^M, \end{aligned} \quad (4.6)$$

where the last form reflects weak coupling; we are considering the interaction between one object having purely electric susceptibility and a second object having purely magnetic susceptibility, so

$$\mathbf{V}_1^E = 4\pi \alpha_1^E \delta(\mathbf{r} - \mathbf{r}_1), \quad \mathbf{V}_2^M = 4\pi \alpha_2^M \delta(\mathbf{r} - \mathbf{r}_2). \quad (4.7)$$

This formula is expressed in terms of the magnetic Green's dyadic ( $\mathbf{R} = \mathbf{r}_1 - \mathbf{r}_2$ ),

$$\Phi_0 = -\frac{\zeta^2}{4\pi R^3} \mathbf{R} \times \mathbf{1} (|\zeta|R + 1) e^{-|\zeta|R}. \quad (4.8)$$

Then, an immediate calculation yields the electric-magnetic CP interaction

$$U_{\text{CP,EM}} = \frac{7}{8\pi R^7} \text{tr}(\hat{\mathbf{R}} \times \alpha^E)(\hat{\mathbf{R}} \times \alpha^M), \quad (4.9)$$

which, indeed, for isotropic polarizabilities gives the second term in Eq. (4.5). The result (4.4b) is now an immediate consequence for a conducting sphere interacting with an atom only polarizable in the  $z$ -direction.

Evidently, no repulsion can occur in this CP limit where the conducting sphere is regarded as an isotropically polarizable atom. In fact, numerical evaluation shows no repulsion occurs at any separation distance between the sphere and the atom.

## V. ELECTROSTATIC FORCE BETWEEN A CONDUCTING ELLIPSOID AND A DIPOLE

In this section we return, for heuristic reasons, to the electrostatic situation of the interaction between a fixed dipole and a conducting body, which has been given considerable attention lately [2,13,21]. Here, we consider the interaction between a perfectly conducting ellipsoid polarized by a constant electric field and a fixed dipole. The polarization of the ellipsoid by the dipole is neglected at this stage. This is a much simpler calculation than the more interesting one of the interaction between a dipole and an ellipsoid, but we justify the inclusion of the details of the simpler calculation because it allows us to approach the complexity of the full calculation. Elsewhere, we will present that calculation and the corresponding quantum Casimir-Polder calculation, building on the work of Ref. [22].

### A. Ellipsoidal coordinates

Consider a conducting uncharged solid ellipsoid with semiaxes  $a > b > c$  centered at the origin  $x = y = z = 0$ . The semiaxis  $c$  lies along the  $z$ -axis. The electrostatic potential  $\phi$  in the external region can be described in terms of ellipsoidal coordinates  $\xi, \eta, \zeta$ , corresponding to solutions for  $u$  of the cubic equation

$$\frac{x^2}{a^2 + u} + \frac{y^2}{b^2 + u} + \frac{z^2}{c^2 + u} = 1. \quad (5.1)$$

The coordinate intervals are in general

$$\infty > \xi \geq -c^2, \quad -c^2 \geq \eta \geq -b^2, \quad -b^2 \geq \zeta \geq -a^2. \quad (5.2)$$

We will henceforth assume axial symmetry around the  $z$ -axis. In that case,  $b \rightarrow a$ ,  $\zeta \rightarrow -a^2$ , and the ellipsoidal coordinates  $\xi, \eta, \zeta$  reduce to oblate spheroidal coordinates  $\xi$  and  $\eta$  restricted to the intervals

$$\infty > \xi \geq -c^2, \quad -c^2 \geq \eta \geq -a^2. \quad (5.3)$$

If  $\rho = \sqrt{x^2 + y^2}$  denotes the horizontal radius in the plane  $z = \text{constant}$ , the cubic Eq. (5.1) reduces to the quadratic equation

$$u^2 - (\rho^2 - a^2 - c^2 + z^2)u - (\rho^2 - a^2)c^2 - z^2a^2 = 0 \quad (5.4)$$

for  $u = (\xi, \eta)$ . The solution for  $u = \xi$  corresponds to the positive square root

$$\xi = \frac{1}{2}(\rho^2 - a^2 - c^2 + z^2) + \frac{1}{2}\sqrt{(\rho^2 - a^2 + c^2)^2 + z^2(2\rho^2 + 2a^2 - 2c^2 + z^2)}. \quad (5.5)$$

At the surface of the ellipsoid  $\xi = 0$ , whereas in the external region  $\xi > 0$ . Note that in the  $xy$ -plane ( $z = 0$ ) the expression for  $\xi$  simplifies to  $\xi = \rho^2 - a^2$  when  $\rho > a$ . The solution for  $u = \eta$  corresponds to the same expression (5.5) but with the negative square root.

Surfaces of constant  $\xi$  and  $\eta$  are oblate spheroids and hyperboloids of revolution, the surfaces intersecting orthogonally. On the symmetry axis  $\rho = 0$ , one has  $\xi = -c^2 + z^2$ ,  $\eta = -a^2$ . The relations between  $\xi$ ,  $\eta$  and  $z$ ,  $\rho$  are

$$z = \pm \sqrt{\frac{(\xi + c^2)(\eta + c^2)}{c^2 - a^2}}, \quad \rho = \sqrt{\frac{(\xi + a^2)(\eta + a^2)}{a^2 - c^2}}. \quad (5.6)$$

We will henceforth only be concerned with the half-space  $z \geq 0$ .

## B. Ellipsoid situated in a uniform electric field

Assume now that the ellipsoid is placed in a uniform electric field  $\mathbf{E}_0$ , directed along the  $z$ -axis. We take the electrostatic potential  $\phi$  to be zero on the ellipsoid surface. With quantities  $R_\xi$  and  $R_\eta$  defined as

$$R_\xi = (\xi + a^2)\sqrt{\xi + c^2}, \quad R_\eta = (\eta + a^2)\sqrt{\eta + c^2}, \quad (5.7)$$

Laplace's equation in the external region  $\xi \geq 0$  can be written as

$$\nabla^2 \phi \equiv \frac{4}{\xi - \eta} \left[ \frac{R_\xi}{\xi + a^2} \frac{\partial}{\partial \xi} \left( R_\xi \frac{\partial \phi}{\partial \xi} \right) - \frac{R_\eta}{\eta + a^2} \frac{\partial}{\partial \eta} \left( R_\eta \frac{\partial \phi}{\partial \eta} \right) \right] = 0. \quad (5.8)$$

The potential due solely to  $\mathbf{E}_0$  is

$$\phi_0 = -E_0 z, \quad (5.9)$$

and we write the full potential  $\phi$  in the form

$$\phi = \phi_0 [1 + F(\xi)] \quad (5.10)$$

so that  $\phi_0 F$  denotes the modification due to the ellipsoid. The boundary condition at the surface is  $F(0) = -1$ .

Inserting Eq. (5.10) into Eq. (5.8), we find the following equation for  $F$ :

$$\frac{d^2 F}{d\xi^2} + \frac{dF}{d\xi} \frac{d}{d\xi} \ln[R_\xi(\xi + c^2)] = 0. \quad (5.11)$$

The solution can be written as

$$\phi = \phi_0 \left[ 1 - \frac{\int_\xi^\infty \frac{ds}{(s+c^2)R_s}}{\int_0^\infty \frac{ds}{(s+c^2)R_s}} \right]. \quad (5.12)$$

We can also express the solution in terms of the incomplete beta function, defined as

$$B_x(\alpha, \beta) = \int_0^x t^{\alpha-1} (1-t)^{\beta-1} dt. \quad (5.13)$$

Some manipulation yields

$$\int_\xi^\infty \frac{ds}{(s+c^2)R_s} = \frac{1}{(a^2 - c^2)^{3/2}} B_{(a^2 - c^2)/(\xi + a^2)} \left( \frac{3}{2}, -\frac{1}{2} \right), \quad (5.14)$$

and so we can write the final answer for the potential as

$$\phi = \phi_0 \left[ 1 - \frac{B_{(a^2 - c^2)/(\xi + a^2)} \left( \frac{3}{2}, -\frac{1}{2} \right)}{B_{1 - c^2/a^2} \left( \frac{3}{2}, -\frac{1}{2} \right)} \right]. \quad (5.15)$$

For small values of  $x$ , the following expansion may be useful:

$$B_x(\alpha, \beta) = \frac{x^\alpha}{\alpha} (1-x)^\beta \left[ 1 + \sum_{n=0}^{\infty} \frac{B(\alpha+1, n+1)}{B(\alpha+\beta, n+1)} x^{n+1} \right], \quad (5.16)$$

where  $B(\alpha, \beta) = \Gamma(\alpha)\Gamma(\beta)/\Gamma(\alpha+\beta)$  is the complete beta function. In our case, the limit  $x \ll 1$  corresponds to the minor semiaxis  $c$  being only slightly less than the major semiaxis  $a$ .

In the following, we shall need the expression for the  $z$ -component of the electric field,  $E_z = -\partial\phi/\partial z$ , at an arbitrary point  $(\rho, z)$  in the exterior region. Here, it is convenient to first differentiate the relation (5.4) ( $u = \xi$ ) with respect to  $z$ , keeping  $\rho$  constant, in order to obtain

$$\left( \frac{\partial \xi}{\partial z} \right)_\rho = \frac{2(\xi + a^2)}{\xi - \eta} \sqrt{\frac{(\xi + c^2)(\eta + c^2)}{c^2 - a^2}}. \quad (5.17)$$

With  $x = (a^2 - c^2)/(\xi + a^2)$ , we have

$$\begin{aligned} \frac{\partial B_x \left( \frac{3}{2}, -\frac{1}{2} \right)}{\partial z} &= \frac{\partial \xi}{\partial z} \frac{\partial x}{\partial \xi} \frac{\partial B_x \left( \frac{3}{2}, -\frac{1}{2} \right)}{\partial x} \\ &= 2 \frac{(a^2 - c^2)}{(\xi + c^2)(\xi - \eta)} (-\eta - c^2)^{1/2}. \end{aligned} \quad (5.18)$$

Then, from Eq. (5.15),

$$E_z = E_0 \left[ 1 - \frac{B_{(a^2-c^2)/(\xi+a^2)}(\frac{3}{2}, -\frac{1}{2})}{B_{1-c^2/a^2}(\frac{3}{2}, -\frac{1}{2})} - \frac{2(a^2-c^2)^{1/2}(\xi+c^2)^{-1/2}(\eta+c^2)}{B_{1-c^2/a^2}(\frac{3}{2}, -\frac{1}{2})} \frac{1}{\xi-\eta} \right]. \quad (5.19)$$

For large values of  $z$  and arbitrary  $\rho$  the influence from the ellipsoid must evidently fade away,  $E_z \rightarrow E_0$ .

In the  $xy$ -plane, where  $z=0$ ,  $\xi+a^2=\rho^2$ ,  $\eta+c^2=0$ , we have

$$E_z(z=0) = E_0 \left[ 1 - \frac{B_{(a^2-c^2)/\rho^2}(\frac{3}{2}, -\frac{1}{2})}{B_{1-c^2/a^2}(\frac{3}{2}, -\frac{1}{2})} \right]. \quad (5.20)$$

When  $\rho=a$  (on the surface), then  $E_z(z=0)=0$  as expected.

### C. Force on a dipole

Assume now that a dipole  $\mathbf{p} = p_z \hat{\mathbf{z}}$  is situated at rest in the position  $(\rho, z)$ . The dipole is taken to be polarized in the  $z$ -direction only. The value of  $z (\geq 0)$  is arbitrary, whereas the value of  $\rho$  is assumed constant. Thus, writing  $\rho = a + L$ ,  $L$  is the constant horizontal distance between the dipole and the edge of the ellipsoid, the force  $F_z$  on the dipole is

$$F_z = \nabla_z(\mathbf{p} \cdot \mathbf{E}) = p_z \frac{\partial E_z}{\partial z}. \quad (5.21)$$

Note that we are ignoring the polarization of the ellipsoid by the field of the dipole; the ellipsoid acquires a dipole moment only because of the applied external field. Thus, we have to differentiate the expression (5.19) with respect to  $z$ . Performing the calculation along the same lines as above, we obtain

$$F_z = \frac{6p_z E_0}{B_{1-c^2/a^2}(\frac{3}{2}, -\frac{1}{2})} \frac{(a^2-c^2)\sqrt{-\eta-c^2}}{(\xi+c^2)(\xi-\eta)} \times \left[ 1 - \frac{(\xi+a^2)(-\eta-c^2)}{(a^2-c^2)(\xi-\eta)} + \frac{2}{3} \frac{(\xi+c^2)(\eta+c^2)(\xi+\eta+2a^2)}{(a^2-c^2)(\xi-\eta)^2} \right]. \quad (5.22)$$

At  $z=0$ , the force vanishes as it should, since  $\eta+c^2=0$ .

Note that the force vanishes if  $c/a \rightarrow 0$ , that is, for a disk, because the integral representing the incomplete beta function diverges in the limit. (It is not to be interpreted as its analytic continuation.) This is not surprising, for in the limit of a disk, the electric field is just  $\mathbf{E}_0$ , the applied constant field. This is because inserting a perfectly conducting sheet perpendicular to the field line has no effect on the boundary conditions. See also the discussion in Chap. 4 of Ref. [23].

As a small check, we consider the limit of a sphere,  $c^2 \rightarrow a^2$ . Then, according to Eq. (5.16), we have

$$B_{1-c^2/a^2}\left(\frac{3}{2}, -\frac{1}{2}\right) \rightarrow \frac{2}{3} a^{-3} (a^2 - c^2)^{3/2} \quad (5.23)$$

and

$$\xi \approx \rho^2 + z^2 - c^2, \quad \eta = -c^2 - \frac{\delta^2 z^2}{\rho^2 + z^2}, \quad (5.24)$$

in terms of the ultimately vanishing quantity  $\delta^2 = a^2 - c^2$ . Then, we immediately obtain

$$F_z = 3p_z E_0 \frac{a^3 z}{(\rho^2 + z^2)^{7/2}} (3\rho^2 - 2z^2). \quad (5.25)$$

This result also follows immediately from the dipole-dipole interaction energy

$$U = -\frac{1}{r^5} (3\mathbf{r} \cdot \mathbf{p}_1 \mathbf{r} \cdot \mathbf{p}_2 - r^2 \mathbf{p}_1 \cdot \mathbf{p}_2) \quad (5.26)$$

when we take

$$\mathbf{p}_1 = p_z \hat{\mathbf{z}}, \quad \mathbf{p}_2 = a^3 E_0 \hat{\mathbf{z}}. \quad (5.27)$$

The force on the sphere (5.25) is attractive at large distance because the dipoles become essentially coaxial; the force on the sphere is repulsive at small distance because the case of parallel dipoles in a plane is approached in that situation.

The same features hold for a general ellipsoid. For short distances,  $z^2 \ll \rho^2 - a^2 + c^2$ , we have

$$\xi = \rho^2 - a^2 + O(z^2), \quad (5.28)$$

$$\eta = -c^2 - \frac{z^2(a^2 - c^2)}{\rho^2 - a^2 + c^2} + O(z^4),$$

and then the force is repulsive,

$$z \rightarrow 0: F_z = \frac{6p_z E_0}{B_{1-c^2/a^2}(\frac{3}{2}, -\frac{1}{2})} \frac{z(a^2 - c^2)^{3/2}}{(\rho^2 - a^2 + c^2)^{5/2}}, \quad (5.29)$$

which reduces in the spherical case to

$$c \rightarrow a: F_z = \frac{9p_z E_0 a^3 z}{\rho^5}, \quad (5.30)$$

which agrees with Eq. (5.25). And in the large distance limit, where  $\xi \approx z^2$ ,  $\eta \approx -a^2$ , the force, in general, is attractive,

$$z \rightarrow \infty: F_z = -\frac{4p_z E_0 (a^2 - c^2)^{3/2}}{B_{1-c^2/a^2}(\frac{3}{2}, -\frac{1}{2})} \frac{1}{z^4}, \quad (5.31)$$

which again has the expected limit

$$c \rightarrow a: F_z = -\frac{6p_z E_0 a^3}{z^4}. \quad (5.32)$$

## VI. INTERACTION OF ANISOTROPIC ATOM WITH ANISOTROPIC DIELECTRIC

In view of the considerations of Sec. II, we might hope that repulsion could be achieved if an anisotropic atom were placed above an anisotropic dielectric medium. Consider such an atom with polarizability only in the  $z$ -direction,  $\boldsymbol{\alpha} = \alpha \hat{\mathbf{z}} \hat{\mathbf{z}}$ , a distance  $a$  above a dielectric with different permittivities in the  $z$ -direction, and the transverse directions

$$\boldsymbol{\varepsilon} = \text{diag}(\varepsilon_{\perp}, \varepsilon_{\perp}, \varepsilon_{\parallel}). \quad (6.1)$$

We will assume (see below) that  $\varepsilon_{\perp}, \varepsilon_{\parallel} > 1$ . The Casimir-Polder interaction is

$$E_{\text{CP}} = -\alpha \int_{-\infty}^{\infty} d\zeta (\Gamma_{zz} - \Gamma_{zz}^0)(\mathbf{R}, \mathbf{R}), \quad (6.2)$$

where the atom is located at  $\mathbf{R} = (0, 0, a)$ . Here, we have subtracted the free-space contribution. We can write the Green's dyadic in terms of a transverse Fourier transform

$$\boldsymbol{\Gamma}(\mathbf{r}, \mathbf{r}') = \int \frac{(d\mathbf{k}_{\perp})}{(2\pi)^2} e^{i\mathbf{k}_{\perp} \cdot (\mathbf{r} - \mathbf{r}')_{\perp}} \boldsymbol{\gamma}(z, z'), \quad (6.3)$$

where (assuming that  $\mathbf{k}_{\perp}$  lies in the  $+x$  direction)

$$\boldsymbol{\gamma}(z, z') = \begin{pmatrix} \frac{1}{\varepsilon_{\perp}} \frac{\partial}{\partial z} \frac{1}{\varepsilon'_{\perp}} \frac{\partial}{\partial z'} g^H & 0 & \frac{ik_{\perp}}{\varepsilon_{\perp} \varepsilon'_{\parallel}} \frac{\partial}{\partial z} g^H \\ 0 & -\zeta^2 g^E & 0 \\ -\frac{ik_{\perp}}{\varepsilon'_{\perp} \varepsilon_{\parallel}} \frac{\partial}{\partial z'} g^H & 0 & \frac{k_{\perp}^2}{\varepsilon_{\parallel} \varepsilon'_{\parallel}} g^H \end{pmatrix}. \quad (6.4)$$

We have followed Ref. [24] and used the notation  $\varepsilon = \varepsilon(z)$ ,  $\varepsilon' = \varepsilon(z')$ . Here, we have omitted  $\delta$ -function terms that do not contribute in the point-splitting limit. The transverse electric and transverse magnetic Green's functions satisfy the differential equations

$$\left( -\frac{\partial^2}{\partial z^2} + k_{\perp}^2 - \omega^2 \varepsilon_{\perp} \right) g^E(z, z') = \delta(z - z'), \quad (6.5a)$$

$$\left( -\frac{\partial}{\partial z} \frac{1}{\varepsilon_{\perp}} \frac{\partial}{\partial z} + \frac{k_{\perp}^2}{\varepsilon_{\parallel}} - \omega^2 \right) g^H(z, z') = \delta(z - z'). \quad (6.5b)$$

It is rather straightforward to solve these equations and find the Casimir-Polder energy

$$E_{\text{CP}} = \frac{\alpha}{4\pi^2} \int_{-\infty}^{\infty} d\zeta \int (d\mathbf{k}_{\perp}) \frac{k_{\perp}^2}{2\kappa} \frac{\bar{\kappa} - \kappa}{\bar{\kappa} + \kappa} e^{-2\kappa a}, \quad (6.6)$$

where  $\kappa^2 = k_{\perp}^2 - \omega^2$ ,  $\bar{\kappa} = \sqrt{(k_{\perp}^2 - \omega^2 \varepsilon_{\parallel})/\varepsilon_{\perp} \varepsilon_{\parallel}}$ . Checks of this result are

$$\varepsilon_{\perp} \rightarrow \infty: E_{\text{CP}} \rightarrow -\frac{\alpha}{8\pi a^4}, \quad (6.7)$$

one-third of the usual Casimir-Polder interaction of an isotropic atom with a perfect conducting plate. This is what we would have for such an anisotropic atom above a isotropic conducting plate because taking  $\varepsilon_{\perp} \rightarrow \infty$

imposes the usual boundary condition that the tangential components of  $\mathbf{E}$  vanish on the surface. In the other limit, we have no such simple correspondence,

$$\varepsilon_{\parallel} \rightarrow \infty: E_{\text{CP}} \rightarrow \frac{\alpha}{8\pi a^4} \left( 1 + \frac{3}{2} \sqrt{\varepsilon_{\perp}} - 3\varepsilon_{\perp} + 3\sqrt{\varepsilon_{\perp}}(\varepsilon_{\perp} - 1) \ln \frac{\sqrt{\varepsilon_{\perp} + 1}}{\sqrt{\varepsilon_{\perp}}} \right), \quad (6.8)$$

where the quantity in parentheses varies between  $-1/2$  for  $\varepsilon_{\perp} = 1$  and  $-1$  as  $\varepsilon_{\perp} \rightarrow \infty$ .

We can check that, in all cases, if we ignore dispersion, Eq. (6.6) yields an attractive result:  $E_{\text{CP}}$  scales like  $a^{-4}$  times a numerical integral, which is always negative because  $\bar{\kappa}^2 - \kappa^2 < 0$ . Repulsion does not occur in this case because there is no breaking of translational invariance in the transverse direction.

In fact, the electromagnetic force density in an anisotropic nonmagnetic medium is (see Ref. [25], Eq. (1.2a))

$$\mathbf{f} = -\frac{1}{8\pi} E_i E_k \nabla \varepsilon_{ik}. \quad (6.9)$$

Assume that the single air-medium interface is flat, lying in the  $xy$ -plane. Then, the only nonvanishing component of the gradient  $\nabla \varepsilon_{ik}$  is the vertical component  $\partial_z \varepsilon_{ik}$ . If the principal coordinate axes for  $\varepsilon_{ij}$  coincide with the  $x, y, z$  axes, then the surface force density  $\int f_z dz$  (which is subsequently to be integrated across the surface  $z = 0$ ) is directed upwards because  $\varepsilon_{\parallel, \perp} > 1$ . The surface force acts in the direction of the optically thinner medium. Now, momentum conservation of the total system asserts that the force on a dipole above the surface acts in the downward direction. The dipole force has to be attractive.

That  $\varepsilon > 1$  for an isotropic medium is a thermodynamical result. For an anisotropic medium, oriented such that the coordinate axes fall together with the crystallographic axes, one must analogously have  $\varepsilon_{\parallel, \perp} > 1$ . See, for instance, Sec. 14 in Ref. [26].

Note the contrast with the force on a dipole outside a conducting wedge, studied in Ref. [13]. In the latter case, the normal surface force on the inclined (lower) surface has a vertical ( $z$ ) component that is downward directed. Thus, momentum conservation for the total system no longer forbids the force on the dipole to be repulsive.

## VII. CONCLUSIONS

Earlier, we observed that Casimir-Polder repulsion along a direction perpendicular to the symmetry axis of a semi-infinite planar conductor or a conducting wedge and an anisotropically polarizable atom could be achieved in the region close to the conductor [13]. Here, we have shown that anisotropically polarizable atoms can also repel in this sense, provided they are sufficiently anisotropic and have perpendicular principal axes. We further show that such an atom may be repelled by a conducting cylinder

provided, at closest approach, it is sufficiently far from the cylinder, whereas no such phenomenon occurs for a sphere and an anisotropic atom. We further discussed a new example of classical repulsion by considering a polarized ellipsoid interacting with a dipole. On the other hand, a system of an anisotropically polarizable atom interacting via fluctuation forces with an anisotropic dielectric half-space does not exhibit repulsion. Apparently, spatial anisotropy is also required for repulsion between electric bodies.

## ACKNOWLEDGMENTS

We thank the U.S. Department of Energy, and the U.S. National Science Foundation, for partial support of this research. The support of the European Science Foundation Casimir Network is also acknowledged. P.P. acknowledges the hospitality of the University of Zaragoza. We thank E. K. Abalo for collaborative discussions. We also thank K. V. Shajesh and M. Schaden for useful correspondence.

- 
- [1] I. D. Dzyaloshinskii, E. M. Lifshitz, and L. P. Pitaevskii, *Adv. Phys.* **10**, 165 (1961); [*Sov. Phys. Usp.*, **4**, 153 (1961)].
  - [2] M. Levin, A. P. McCauley, A. W. Rodriguez, M. T. Homer Reid, and S. G. Johnson, *Phys. Rev. Lett.* **105**, 090403 (2010).
  - [3] J. Munday, F. Capasso, and V. A. Persegian, *Nature (London)* **457**, 170 (2009).
  - [4] A. W. Rodriguez, A. P. McCauley, D. Woolf, F. Capasso, J. D. Joannopoulos, and S. G. Johnson, *Phys. Rev. Lett.* **104**, No. 16, 160402 (2010).
  - [5] T. H. Boyer, *Phys. Rev.* **174**, 1764 (1968).
  - [6] C. M. Bender and K. A. Milton, *Phys. Rev. D* **50**, 6547 (1994).
  - [7] K. A. Milton, *Phys. Rev. D* **55**, 4940 (1997).
  - [8] E. K. Abalo, K. A. Milton, and L. Kaplan, *Phys. Rev. D* **82**, 125007 (2010).
  - [9] E. K. Abalo, K. A. Milton, and L. Kaplan, Quantum Field Theory under the Influence of External Conditions, 2011 (to appear in the proceedings).
  - [10] T. H. Boyer, *Phys. Rev. A* **9**, 2078 (1974).
  - [11] A. P. McCauley, Rongkuo Zhao, M. T. Homer Reid, A. W. Rodriguez, J. Zhou, F. S. S. Rosa, J. D. Joannopoulos, D. A. R. Dalvit, C. M. Soukoulis, and S. G. Johnson, *Phys. Rev. B* **82**, 165108 (2010).
  - [12] M. F. Maghrebi, *Phys. Rev. D* **83**, 045004 (2011).
  - [13] K. A. Milton, E. K. Abalo, P. Parashar, N. Pourtolami, I. Brevik, and S. Å. Ellingsen, *Phys. Rev. A* **83**, 062507 (2011).
  - [14] D. P. Craig and E. A. Power, *Chem. Phys. Lett.* **3**, 195 (1969).
  - [15] D. P. Craig and E. A. Power, *Int. J. Quantum Chem.* **3**, 903 (1969).
  - [16] K. A. Milton, P. Parashar, and J. Wagner, in *The Casimir Effect and Cosmology*, edited by S. D. Odintsov, E. Elizalde, and O. B. Gorbunova, (Tomsk State Pedagogical University, Tomsk, Russia, 2009), in Honor of Iver Brevik, pp. 107–116.
  - [17] K. V. Shajesh and M. Schaden, *Physical Review A* (to be published).
  - [18] V. B. Bezerra, E. R. B. de Mello, G. L. Klimchitskaya, V. M. Mostepanenko, and A. A. Saharian, *Eur. Phys. J. C* **71**, 1614 (2011).
  - [19] J. Schwinger, L. L. DeRaad, Jr., K. A. Milton, and W.-y. Tsai, *Classical Electrodynamics* (Perseus/Westview, New York, 1998).
  - [20] G. Feinberg and J. Sucher, *J. Chem. Phys.* **48**, 3333 (1968).
  - [21] M. Levin and S. Johnson, *Am. J. Phys.* **79**, 843 (2011).
  - [22] N. Graham, A. Shpunt, T. Emig, S. J. Rahi, R. L. Jaffe, and M. Kardar, *Phys. Rev. D* **83**, 125007 (2011).
  - [23] K. A. Milton and J. Schwinger, *Electromagnetic Radiation: Variational Methods, Waveguides and Accelerators* (Springer, Berlin, 2006).
  - [24] J. Schwinger, L. L. DeRaad, Jr., and K. A. Milton, *Ann. Phys. (N.Y.)* **115**, 1 (1978).
  - [25] I. Brevik, *Phys. Rep.* **52**, 133 (1979).
  - [26] L. D. Landau and E. M. Lifshitz, *Electrodynamics of Continuous Media* (Pergamon, Oxford, 1984).